Studies on the Performance of a Short Haul Optical Link for Broadband Indoor and Outdoor Wireless Communications

Thesis Submitted

by

Sachin Mohanrao Kale

Doctor of Philosophy (Engineering)

Department of Electronics & Telecommunication Engineering

Faculty Council of Engineering and Technology

Jadavpur University, Kolkata, India– 700032

March - 2016

JADAVPUR UNIVERSITY

KOLKATA – 700 032, INDIA

CERTIFICATE FROM THE SUPERVISOR

This is to certify that the thesis entitled "STUDIES ON THE PERFORMANCE OF A SHORT HAUL OPTICAL LINK FOR BROADBAND INDOOR AND OUTDOOR WIRELESS COMMUNICATIONS" submitted by Shri Sachin Mohanrao Kale , who got his name registered on 13.03.2009 for the award of Ph. D. (Engg.) degree of Jadavpur University is absolutely based upon his own work under the supervision of Prof. (Dr) Asim Kar that neither his thesis nor any part of the thesis has been submitted for any degree/diploma or any other academic award anywhere before.

Asim Kar 15/09/2022

Signature of the Supervisor

Date with Office Seal

Professor
Electronics & Tele-communication
Engineering Department
Jadavpur University
Kolkata-700 032

J A D A V P U R U N I V E R S I T Y

KOLKATA – 700 032, INDIA

Title of the Thesis:

STUDIES ON THE PERFORMANCE OF A SHORT HAUL OPTICAL LINK FOR BROADBAND INDOOR AND OUTDOOR WIRELESS COMMUNICATIONS

Name, Designation & Institution of the Supervisor

[1] Prof. (Dr) Asim Kar

Professor, Department of Electronics and Telecommunication Engineering

Jadavpur University, Kolkata

List of Publications:

[A] International Journal Publications:

[1] Sachin M Kale, Asim Kar, "Mitigation of scintillation in FSO using aperture averaging of partially coherent input Gaussian optical beam", International Journal of Signal and Imaging Systems Engineering, (2014), Volume 7: No. 1, pp: 21–29.

[B] National conference proceeding publications:

[1] Sachin M Kale, Asim Kar "Development of a FSO link to connect institute LAN" , Proceeding of National Conference on Wireless Communication And Its Social Need (WCSN-2010) , January 07-08, 2010, Institution of Engineer, Kolkata, pp:25-27.

[2] Sachin M Kale, Asim Kar, "Propagation Characteristics of FSO Link Using Partially Coherent Gaussian Optical Beam", ,Proceeding of National Conference on IEEE CASCOM Student Paper Conference September 17-18, 2010,Jadavpur University, Kolkata, pp :10-16.

[3] Sachin M Kale, Asim Kar "A Study on the Atmospheric Effects on Optical Wireless Link for Short Haul Communication", Proceeding National Conference on Advances in Wireless Cellular Telecommunication: Technologies & Services. ICEIT 2011, Delhi, India, 14-15 April 2011.pp:25-31

[C] International conference proceeding publications:

[1] Sachin M Kale, Asim Kar, "Mitigation of Scintillation in FSO Using Aperture Averaging of Partially Coherent Input Gaussian Optical Beam", Proceeding of International Conference on Electronics Engineering, January 7-9,2011, NIT Roulkela , India, pp :20-16

[2] Sachin M Kale, Asim Kar "Performance Improvement of FSO System Through Aperture Averaging of Partially Coherent Beam" Proceeding of the International Conference on Information, Signal and Communication (ICISE), February 7-9, 2011, A.D. Patel Institute of Technology, New V. V. Nagar, Gujarat, India, pp: 509-513

[3] Sachin M Kale, Asim Kar, "Comparison of the BER Performance of Coherent and Spatially Partially Coherent Light Beams In Optical Wireless Systems", Proceedings of International conference on Electronic Communication Engineering, 5-6 January 2011, IEM, Kolkata,pp:40-46

List of Patents: Nil

List of presentation in National/International Conference/Seminar:

[1] Sachin M Kale, Asim Kar "Development of a FSO link to connect institute LAN" , Proceeding of National Conference on Wireless Communication And Its Social Need (WCSN-2010) , January 07-08, 2010, Institution of Engineer, Kolkata.

[2] Sachin M Kale, Asim Kar, “Propagation Characteristics of FSO Link Using Partially Coherent Gaussian Optical Beam”, ,Proceeding of National Conference on IEEE CASCOM Student Paper Conference September 17-18, 2010,Jadavpur University, Kolkata.

[3] Sachin M Kale, Asim Kar “A Study on the Atmospheric Effects on Optical Wireless Link for Short Haul Communication”, Proceeding National Conference on Advances in Wireless Cellular Telecommunication: Technologies & Services. ICEIT 2011, 14-15 April 2011, Delhi, India.

[4] Sachin M Kale, Asim Kar, “Mitigation of Scintillation in FSO Using Aperture Averaging of Partially Coherent Input Gaussian Optical Beam”, Proceeding of International Conference on Electronics Engineering, January 7-9,2011, NIT Roulkela , India.

[5] Sachin M Kale, Asim Kar, “Comparison of the BER Performance of Coherent and Spatially Partially Coherent Light Beams In Optical Wireless Systems”, Proceedings of International conference on Electronic Communication Engineering, 5-6 January 2011, IEM, Kolkata.

PREFACE

In today's scenario, communications using electronic wireless systems is the ultimate desirable technology for any type of information transmission between two locations. We feel good and convenient to use Blue tooth or Zigbee type very short distance indoor wireless RF communication links or many other wireless remote control systems in our daily life. Similarly, we are using standard wireless microwave broadband outdoor communications links with repeaters for our PSTN, Internet technologies and other switching networks and systems for long distance transmission of information.

Although we have our standards in the design of hardware systems, as well as we have various systems for communication, but as days passes we find that the global demand for bandwidth continues to accelerate. It is felt that copper/coaxial cables and RF cellular/microwave mobile and Internet technologies with such limitations as limited bandwidth, congested spectrum, security issues, expensive licensing and high cost of installation and accessibility to all, cannot meet the upcoming needs.

A communication system would automatically deny services to its users whenever there is shortage of bandwidth. Similarly, when we plan to transmit broadband signals such as digital real time video, we need high speed broadband transmission networks. But presently we have limited availability of total RF bandwidth resources divided for specific purposes. With time the problems due to shortage of bandwidth has aggravated. We therefore have to depend on development of new generations of wireless communication technology.

Presently, the smart phones are making a pressing demand for much higher bandwidth availability for mobile access. Along with this, the new concepts of “Internet of Things” and technology for “cloud computing” are gaining popularity. All such new progress and developments in communication technologies will bring lot of change in our society and our day-to-day life. New developments all over the world for breakthrough in technologies via research are very much under way because International Communication Consortium (ICC) agencies are planning to introduce the 5G –the fifth generation technology by 2022. The ultimate plan and objectives are to give the facilities to access any information from anywhere to any other place in this global earth.

In developing the broadband mobile communication technology, the greatest challenge we are facing today is the technology for the “Last Mile” for access to the networks. In order to obtain higher bandwidth in microwave transmission range, we need to shift the carrier frequencies to much higher frequencies such as millimeter wave frequencies in the 30 GHz to 300 GHz bands. The 60 GHz band became attractive to scientists during the last decade and plenty of research have been made and a new technology termed “Microwave Photonics” have emerged where we are able to merge the two technologies (i) microwave and (ii) Photonics technologies to take best of the benefits of their combinations.

Things are also taking new directions because the low cost electronic component technologies for 60GHz operation are not yet been available in the market. Scientists are simultaneously developing an alternative to 60 GHz millimeter wave technology using optical carrier frequencies and total optical technology named as “Optical Wireless Communication” (OWC) Technology.

Knowing the high bandwidth capability of optical wireless systems, scientists for the past decade is trying to use it for applications as the Last Mile wireless solutions of the mobile communication technology. This technology, like the microwave counterpart, is being developed for applications in both indoor and outdoor environments. Thus, ultimately we can have radio-over-fiber in the backbone network for high bandwidth signal transmission over long distance and then this broadband signal at the end can be sent wirelessly to the mobile user using the OWC technology. In future we would have either of the two options for the last mile. The last mile can be (i) millimeter wave system or (ii) optical wireless system or (iii) A Hybrid technology using any of them when needed for optimum operation of communication systems.

The available features of OWC are most promising and it can be an alternative to microwave technologies for indoor and outdoor applications. It is observed to offer flexible networking solutions that provide cost-effective, highly secure high-speed license-free wireless broadband connectivity for a number of applications, including voice and data, video and entertainment, enterprise connectivity, disaster recovery, illumination and data communications, surveillance and many others. OWCs also referred to as free-space optical communication systems for outdoor applications and it will play a significant role as a complementary technology to the RF systems in future information superhighways.

The success of optical wireless technology in Inter-satellite links came in easily as the lightwave communication signals pass almost through the vacuum in free space where there is no atmospheric effects present (for GEO at height ~ 36000 km from earth surface) to disturb the propagation of optical wave. But as soon as we try to employ the same technology for high speed data transmission in free space near the surface of the earth, we find that the optical wireless communication link does not work satisfactorily as it was expected. The reason is that the atmospheric outdoor channel is a very complex and dynamic environment that can affect the characteristics of the propagating optical beam, thus resulting in optical losses and turbulence-induced amplitude and phase fluctuation. A number of theoretical models to characterize the statistical nature of the atmospheric channel have been developed during 1960's. Since the atmospheric effect can be weak, moderate or severe due to varying atmospheric turbulence conditions, due to presence of fog, snow, rain, and wind as well as thermally induced fluctuations of refractive index of air.

The requirement of the design of the OWC system for outdoor applications are really very challenging and requires more research in this area. Thus to design efficient outdoor optical wireless communication systems, it is imperative that the dynamic characteristics of the channel are well understood. In our present work we have decided to design and develop laboratory based free space optical communication links for detailed studies of their performances in the indoor and outdoor environments. We have planned also to prepare theoretical models on their practical performances. We have made the planning for procurement of necessary equipments and devices and we present here our findings of theoretical and experimental results.

ACKNOWLEDGEMENT

The insight of this thesis is certainly due to the contribution of several outstanding persons. I express my deep sense of gratitude to my Ph.D. (Engg.) thesis supervisor Prof.(Dr) Asim Kar, Professor, Electronics and Telecommunication Engineering Department, Jadavpur University for his constant guidance, helpful suggestions, continuous association, supports, encouragement and valuable advice at every aspect from the embryonic stage to the development stage of this research work. Without his constructive and timely advice, this thesis would have not been progressed as smoothly as it did towards its completion. I indeed owes to him for his valuable time, which he has spent for the present research work.

I gratefully acknowledges the co-operation and encouragement received from Head of the Department, Dr. Bhaskar Gupta, Dr. Iti Saha Misra and Non teaching faculty members of Electronics and Telecommunication Engineering Department, Jadavpur University during the course of the research work.

Thanks are extended to the All India Council for Technical Education (AICTE), New Delhi for providing QIP (Poly) fellowship to me. I extend my heartiest thanks to the Dr.S.K.Mahajan, Hon. Director, Department of Higher and Technical Education, Govt. of Maharashtra for permitting me to carry out my research work under QIP (Poly) scheme. I would also like to extend my sincere gratitude to Shri E.M. Choudhari , Principal, Government Polytechnic, Gadchiroli and Shri P.V.Sarode , Principal Government Polytechnic ,Pune, and all the faculty members of Government Polytechnic, Gadchiroli and Amravati. Thanks are also extended to Dr. Shri V. M. Mankar H.O.D. Electronics Engineering Government polytechnic, Amravati and

Shri. R. N. Shikari H.O.D. Electronics ,Government polytechnic, Gadchiroli for their cordial assistance and executive support.

My appreciation is also due to all fellow colleagues Vijay Rathod, Prasad Karande, Hemant Pardeshi, Sudansu Pati ,Prasanna Gadhari, Vijay Mankar, Vijay Gangapure , Praomod Wankhade and Jayanta Modak for their constant co-operation, useful assistance and support during this research work.

I wish to thank specially , Anuradha Kar for sharing her comments at a crucial moment of thesis writing.

Last ,but not the least, I would like to thank my parents, my wife, beloved son, elder brother, sister and all my family members for their constant encouragement and support in the pursuit of this research work. Without their understanding, none of this would be possible. I would extend my sincere gratitude especially to my wife for her cooperation and enthusiastic support during the entire period of this research work.

Finally, I thank all of them who contributed directly or indirectly to this research work and help me in making this research work a success.

(Mr. Sachin Mohanrao Kale)
Jadavpur University,
Kolkata (WB)

CONTENTS

LIST OF TABLES

LIST OF FIGURES

LIST OF SYMBOLS

Symbol	Name
A	Aperture averaging factor
BER	Bit Error Rate
C_n^2	Refractive Index Structure Parameter
C_T^2	Temperature Structure Parameter
c	Speed of Light
D_G	Diameter of Gaussian Lens
$erfc(x)$	Error Function
FSO	Free Space Optics
$H(x)$	Atmospheric Transfer Function
$I^0(r, L)$	Irradiance of beam in free space
$I \quad (r, L)$	Irradiance of Beam in Random Medium
k	Wave Number of Beam wave
L	Propagation Path Length
L_0	Outer Scale of Turbulence
l_0	Inner Scale of Turbulence
PDF	Probability density function
r_0	Atmospheric Coherence Width
SNR	Signal to Noise Ratio
$U_0(r, z)$	Complex Amplitude of the field in free space
$U \quad (r, z)$	Complex Amplitude of the field in Random Medium
W_0	Beam Radius at Transmitter
W	Beam Radius at Receiver

W_G	**Radius of Gaussian Lens**
α_0	**Complex Parameter at Transmitter**
α , β	**Parameters of the Gamma-Gamma Distribution**
Θ_0	**Beam Curvature parameter at transmitter**
Θ	**Beam Curvature parameter of the beam at receiver**
Θ_e, Λ_e	**Effective Beam parameter at Receiver**
Λ_0	**Fresnel Ratio of Beam at Transmitter**
Λ	**Fresnel Ratio of Beam at Receiverr**
λ	**Wavelength**
ϱ	**Coherence Radius**
σ^2	**Rytov Variance**
σ_I^2	**Scintillation Index**
$\sigma_{Inx}^2, \sigma_{Iny}^2$	**Large scale and Small scale Irradiance variances**
$\Psi(r, L)$	**Complex Phase perturbations of Rytov approximation**
Ω	**Focusing Parameter**
$< >$	**Ensemble Average**

CHAPTER 1

Introduction

The 'birth' of optical wireless communications by Bell

"I have heard articulate speech produced by sunlight. I have heard a ray of the sun laugh and cough and sing!"

Alexander Graham Bell, February 1879.

These were the words of Alexander Graham Bell that expressed his idea of the use of light for communications. The photo-phone, invented by Bell in 1880, is considered to be the precursor of optical wireless communications (OWCP) **[1-3]**. Moving forward to the present-day scenario it is observed that wireless data rates have doubled every eighteen months over the last three decades and are quickly approaching the capacity of wired communication systems **[4-7]**. Even further explosion of data traffic is predicted.

The demand for higher data rate and higher bandwidth in wireless communication systems is becoming more day by day as more people are using smart phones for data, voice and Internet access and the demand for much higher bandwidth is arising due to digital video transmission in wireless mobile systems **[8-10]**. According to Cisco's estimates predicted in February 2011, the 2010 mobile data traffic growth rate was higher than anticipated. The global mobile data traffic grew 2.6-fold in 2010, nearly tripling for the third year in a row.

Furthermore, according to Cisco's estimates published in February 2013, the global mobile data traffic grew 70% in 2012, and it reached 885 petabytes (PB) per month at the end of 2012, up from 520 PB per month at the end of 2011. The overall mobile data traffic is expected to grow to 11.2 exa-bytes (EB) per month by 2017, a 13-fold increase over 2012 **[11-14]**. Following this trend, wireless Terabit-per-second (Tbps) links are expected to become a reality within the next five to ten years **[15-18]**.

Advanced physical layer solutions and more importantly, new spectral bands will be required to support these extremely high data rates.

There are several reasons that motivate the use of the THz as well as optical frequency bands for ultra-broadband communication networks. Firstly wireless technologies below 0.1 THz (100 GHz) are not able to support Tbps links **[19-21]**. On one hand, advanced digital modulations, e.g., Orthogonal Frequency Division Multiplexing (OFDM), and sophisticated communication schemes, such as Multiple Input Multiple Output (MIMO) systems, is being used to achieve a very high spectral efficiency at frequencies below 5 GHz **[22,23]**. For example, in Long- Term Evolution Advanced (LTE-A) networks, peak data rates in the order of 1 Gbps are possible when using a four-by-four MIMO scheme over a 100 MHz aggregated bandwidth. On the other hand, millimeter wave (mm-Wave) communication systems, such as those at 60 GHz, can support data rates in the order of 10 Gbps within one meter. The path to further improve the data rate involves the development of more complex transceiver architectures able to implement physical layer solutions with much higher spectral efficiency. However, the usable bandwidth is still limited to less than 7 GHz, which effectively imposes an upper bound on the data rates **[24,25]** .

Global plans for fifth generation (5G) wireless systems have already started, which is expected to have major focus on higher system spectral efficiency, data rates, network capacity, scalability and reliability of communications, as well as lower battery consumption, cost, and so on **[26,27]**. Considering the above development plans, 5G technology should be significantly different from current communication technology standards. As a matter of fact, the traditional radio frequency (RF)-based wireless communication has arrived at a bottleneck to meet these needs. First, there is a shortage of RF spectra: most of them have been allocated and the bandwidth of each allocation is limited. Second, various exploitations of RF frequency utilization have been studied for decades, and the potential to exploit more is limited. Third, although the low-power integrated circuit (IC) innovations helped improve power consumption, it is still severe in RF communication **[28,29]**.

Researchers are now vigorously searching for new wireless alternatives to RF. Increasing attentions are now given to explore frequencies beyond the microwave range to millimeter wave and terahertz frequency bands of the electromagnetic spectrum **[30,31]**. The same optical terahertz frequency bands (visible and near-infrared frequencies) used in fibre optic communications is now also explored for applications in unguided optical wireless communication. Visible light communications (VLC), also known as Li-Fi, wireless technology offers such an option and has gained increasing attention **[32,33]**. While the current RF networks serve outdoor users or users in fast moving vehicles, VLC can serve indoor environment communications in future 5G systems because of these factors: 1) There is no interference between the indoor user and the outdoor user at all due to different spectra 2) Because there is no interference, an RF base station can transmit with low power 3) Scarce wireless link resources are used most efficiently.

Optical wireless communication (OWC) enables wireless connectivity using infrared, visible or ultraviolet bands **[34,35]**. With its powerful features such as high bandwidth, low cost and operation in an unregulated spectrum, OWC can be, a powerful alternative to and complementary to the existing wireless technologies. It is one of the most promising current areas of research with significant potentials for high-impact results. Two such important new areas of applications include (i) Body Area Network (BAN) **[36,37]** and (ii) Underwater Optical Wireless Communication **[38]** .

FSO (free space optics) communication is a technology that can potentially solve the incompatibility problems between RF and optical technologies. FSO can address a diverse array of connectivity needs in optical networks such as in metropolitan area networks (MANs) as FSO communications can be used to extend the existing MAN rings **[39]**. Further, FSO is also an excellent candidate for the last-mile connectivity having the attractive properties such as high-directivity of the optical beam, high power efficiency and spatial isolation from other potential interferers and large fractional-bandwidth coupled with high optical gain permitting very high data rate transmission **[40]** .

1.2 Objective of This Thesis Work

Looking at the excellent future prospects of wireless optical technology for many areas of applications in our modern society, we planned to utilize our experience in, past concepts and culture in fiber optic communication technology for the new generation in optical wireless technology. We have the required laboratory infrastructure including optical trans-receiver systems, various test and measurement systems, required passive optical devices, the optical sources and detectors to work in the UV, Visible and Near IR regions for designing and arranging Indoor and Outdoor optical wireless system set ups.

This thesis is a combination of theoretical and experimental works done for studying the detailed performance of an optical wireless communication system for short distance broadband information transfer. This work is envisioned to address the challenges and requirements of the upcoming fourth and fifth generation (5G) wireless systems for communication and networking. Another key aspect of the study is to estimate how closely the optical wireless technology can act as a parallel or alternative to existing radio frequency (RF) technologies for short distance communications.

In our work, we first identified the problems associated with transmission of optical beam in atmosphere for terrestrial communications. We started with the studies of atmospheric turbulence and scintillation effects on the propagation of optical beam in laboratory environment. For this purpose, a multipath folded optic transmission system has been designed to get experimental results for comparison with the theoretical propositions. The complete automated optical system is versatile. Varieties of experiments could be performed for studying controlled temperature induced scintillation effects, and simultaneously studying different techniques for mitigation of the beam divergence, beam wander and random intensity fluctuations due to turbulence. In spite of these studies, one major objectives of our work using a multipath optical cell was to measure some important statistical scintillation parameters (such as Rytov Variance) of the channel due to atmospheric turbulence **[41]**. These statistical parameters were used to determine the BER of bit patterns travelling from transmitter to receiver inside the channel. Because of the stochastic nature of atmospheric turbulence, we have used Kolmogorov model of turbulence to calculate various statistical parameters of the channel and finally to get the time varying Impulse response of the atmospheric channel prevailing within the laboratory **[42]** .

This thesis is organized as follows- the course of development of free space optical wireless principles and corresponding growth in optical components is described in Chapter II. This chapter also present the fundamental aspects of the atmospheric turbulence theory and computational techniques for assessing the effects of turbulence on communication parameters. The design and construction of the folded optics multipath measurement set up for studying the effects of atmospheric turbulence (scintillation) on short haul optical links is described in Chapter III. The experimental setup developed inside our laboratory for the generation of atmospheric turbulence and measurements of turbulence effects on digital data bits is made in Chapter IV and Chapter V describes the simulation studies on aperture averaging techniques to mitigate the effects of scintillation due to the random variations of the refractive index structure parameter. The development of an visible light communication system using LED lights for indoor optical propagation channel is described in Chapter VI. Results, discussions and major claims from the thesis work are presented in Chapter VII followed by the Conclusion section respectively.

References

[1] Bell A. G. ”Selenium and the photophone”, Nature, pp 500–503, Sept. 23, 1880.

[2] ”Photophone by Alexander Graham Bell and Charles Sumner Tainter”, [The Alexander Graham Bell Family Papers, Library of Congress], April 1880.

[3] Carson M.K., Alexander Graham Bell, ” Giving Voice to the World”, Sterling Publishing Co., New York, 2007.

[4] Tse D. and Viswanath P.” Fundamentals of Wireless Communication”, New York, Cambridge University Press, 2005.

[5] Jeff Foerster, ”Ultra-wideband Technology for Short-Range, High-Rate Wireless Communications”, Intel Labs, 2001.

[6] IEEE Communication Magazine: 100 years of Communications Progress vol.22, No.5, May 1984.

[7] Le Nguyen Binh , ” Advanced Digital Optical Communications”, Second Edition, CRC Press, 2008

[8] Leiner B.M. “ A Brief History of the Internet” http://www.isoc.org/internet-history/brief.html, May 1997, Accessed on June 2010.

[9] Marvin K. Simon and Mohamed-Slim Alouini,” Digital Communications Over Fading Channels” Wiley, 2nd edition, 2005.

[10] Jakes W. C., Journal of Microwave Mobile Communications. —New York, Wiley, 1974.

[11] Cisco Unified Communications Overview: http://www.cisco.com/c/en/us/td/docs/voice_ipcomm, Accessed on May 2011.

[12] Anwar M. Mousa, “Prospective of Fifth Generation Mobile Communications”, International Jr. of Next-Generation Networks (IJNGN) Vol.4, No.3, September 2012.

[13] Benny Bing,”High-Speed Wireless ATM and LANs”, Artech House Mobile Communications Library, Artech House Publishers, Unabridged edition, 31 January 2000.

[14] Gagliardi R. M. and S. Karp, “Optical Communications”, John Wiley & Sons, New York,1976.

[15] James E. Katz, “Handbook of Mobile Communication Studies”, The MIT Press, 2008.

[16] Baines S. "The next billion mobile users, http://networks.silicon.com/mobile.2005", Accessed on May 2011.

[17] Castells M. "The Internet Galaxy: Reflections on the Internet, Business and Society", Oxford University Press, 2001.

[18] Castells, M., J. L. Qiu, M. Fernandez-Ardeand A. Sey. "Mobile Communication and Society: A Global Perspective".Cambridge, The MIT Press, 2007.

[19] Ian F. Akyildiz ," Terahertz band: Next frontier for wireless communications", Elsevier, Journal of Physical Communication, Vol-12, pp-16-32, 2014.

[20] Cherry S., "Edholm's law of bandwidth", IEEE Spectrum, Vol.41 (7), pp.58–60,2004.

[21] M. Koch, X. C. Zhang, Eisele, A. Krotkus (Eds.), "Terahertz communications: a 2020 vision ", NATO Security through Science Series, vol. 19, Springer, pp. 325–338, 2007.

[22] Piesiewicz R., T. Kleine-Ostmann, N. Krumbholz, D. Mittleman, M. Koch, J. Schoebel, T. Kurner,"Short-range ultra-broadband terahertz communications: concepts and perspectives" , IEEE Antennas Propag. Mag. Vol. 49 (6), pp.24–39, 2007.

[23] Kleine-Ostmann T., Nagatsuma T." A review on terahertz communication research, Infrared Millim". Terahertz Waves, Vol. 32, pp 143–171,2011.

[24] Glushko B., Kin D., A. Shar, "Gigabit optical wireless communication system for personal area networking", Opt. Mem. Neural Network. Vol.22 (2), pp 73–80, 2013.

[25] Rappaport T., Murdock J., Gutierre F." State of the art in 60-GHz integrated circuits and systems for wireless communications", Proc. IEEE Vol.99 (8), pp 1390–1436, 2011.

[26] Li X., J. Vucic, V. Jungnickel, J. Armstrong."On the capacity of intensity-modulated direct-detection systems and the information rate of a OFDM for indoor optical wireless applications", IEEE Trans. Commun. Vol.60(3),pp 799–809, 2012.

[27] Azhar A.H., Tran A., D. O'Brien." A gigabit/s indoor wireless transmission using MIMO-OFDM visible light communications", IEEE Photonics Technol. Lett. Vol.25 (2), pp 171-174, 2013.

[28] Ciaramella E., Arimoto Y., Contestabile G., M. Presi, A. D'Errico, V. Guarino, M. Matsumoto." 1.28 terabit/s (32 × 40 Gbit/s) wdm transmission system for

free space optical communications", IEEE J. Sel. Areas Commun. Vol.27 (9) ,pp 1639–1645, 2009.

[29] IEEE 802.15 WPAN Study Group 100 Gbit/s Wireless (SG100G). http://www.ieee802.org/15/pub/SG100G.html. Accessed on May 2011.

[30] Akyildiz I.F., Jornet J.M., "Electromagnetic wireless nanosensor networks", Nano Commun. Netw. Elsevier J. 1(1). pp 3–19, 2010.

[31] Akyildiz I.F., J.M. Jornet, "The internet of nano-things", IEEE Wireless Communication Mag. Vol.17 (6), pp 58–63,2010.

[32] Akyildiz I.F., Gutierrez-Estevez D.M., Balakrishnan R., Chavarria Reyes E., "LTE-advanced and the evolution to beyond 4G (B4G) systems", Phys. Communication, Elsevier, 2014.

[33] Sebastian Anthony."255Tbps: World's fastest network could carry all of the internet's traffic on a single fiber", October 27, 2014.

[34] Jian Wang, "Terabit free-space data transmission employing orbital angular momentum multiplexing", Nature Photonics, Vol.6,pp.488–496, 2012.

[35] Chan V.W.S.," Free-Space Optical Communications ,"Technology (Invited Paper), Volume 24, Issue 12, pp.4750-4762, Dec. 2006.

[36] Lin H.S.," Communication Model for the Turbulent Atmosphere," Ph.D. Thesis Case Western Reserve Univ, 1973.

[37] Strohbehn J.W.," Laser Beam Propagation in the Atmosphere", New York: Springer-Verlag, 1978.

[38] Tse D. and P. Viswanath," Fundamentals of Wireless Communication", New York, Cambridge University Press, 2005.

[39] Abdulsalam Ghalib Alkholidi and Khaleel Saeed Altowij, "Free Space Optical Communications—Theory and Practices", Contemporary Issues in Wireless Communications, 2014.

[40] Zimu Zhou. "LiFi: Line-Of-Sight Identification with WiFi", IEEE Infocom, May-2014.

[41] Aria Nosratinia," Cooperative Communication in Wireless Networks", IEEE Communications Magazine, pp-74-80, October 2004.

[42] Lawrence R.S. and J.W. Strohbehn." A Survey of Clear-Air Propagation Effects Relevant to Optical Communications", Proceedings of the IEEE, vol. 58, n. 10, pp. 1523-1545, October 1970.

CHAPTER 2

Optical Links and Networks for Free Space Communication- A Review and Theory

2.1 Introduction

In this chapter, principles and technologies for free space optical communication links are described. These links are developed for providing last mile communication facilities for high-speed broadband data transfer outdoor system and the short-range indoor system. Both OFSO (outdoor free space optics) and IFSO(indoor free space optics) systems are presented in detail in terms of key requirements, major technological developments, difficulties faced by researcher in initial stages and the impact of atmospheric effects on the optical channel and remedy measures undertaken to mitigate these effects.

Since the properties of the channel would ultimately bring a limit to the performance of optical link, effective measures are to be taken at both transmitter and receiver positions to maintain a desired level of performance. This chapter also highlighting the comprehensive treatment of the evaluation of parameters needed for analyzing system performance. The significance of probability density function of irradiance fluctuations due to turbulence use to analysis link performance is explained. Starting from Kolmogorov theory of weak and strong atmospheric turbulence, the necessary expressions relating refractive index structure parameter, scintillation index for coherent and partially coherent beam, signal to noise ratio and bit error rate are presented.

2.2 OFSO Links (Outdoor Free Space Optical Communication Links)

It has been more than 20 years since optical wireless (OW) was proposed as an alternative broadband technology for wireless data transmission applications. The underlying concept of FSO is utilize optical beams to carry a high-speed data through the atmosphere or vacuum. As a result, optical link architectures are very similar to optical fiber communication point-to-point links, with the exception that no optical fibers are deployed as a transmission medium [1].

FSO is also very similar to RF wireless, but radio waves are replaced with optical frequency carriers and antennas with free-space optical transceivers. Fiber-optic communication is a method of transmitting information from one place to another by sending pulses of light through an optical fiber using light as an electromagnetic carrier wave. Because of its advantages over electrical transmission-such as high bandwidth and low electromagnetic interference, optical fibers have largely replaced copper wire communications in core networks. However the deployment cost of fiber optic systems is significantly higher, which easily reach $1M/mile in urban areas [2].

Optical wireless communication (OWC)is an effective high bandwidth optical communication technology serving commercial point–to-point links in terrestrial last mile applications, such as air-to-air, satellite-to submarine, air- to- satellite, and satellite-to satellite links. OWC has several attractive characteristics such as simple optical frontends, high bandwidth, high linearity and signal-to-noise ratios, spectrally efficient modulation for high data throughput, support of multi-user communication and no electromagnetic interference (EMI) with existing radio systems. OWC systems operating in the visible band (390–750 nm) has potential application areas including wireless local area networks, wireless personal area networks and vehicular networks.

Terrestrial point-to-point OWC system, also known as the free space optical (FSO) system. It operates at the near IR frequencies (750–1600 nm) and typically use laser transmitters to offer a cost-effective protocol-transparent link with high data rates, i.e., 10 Gbit/s per wavelength. That equals metro fiber optic systems and is significantly higher than the 1.25 Gb/s Ethernet provided by competing RF wireless systems.

FSO applications span over a wide range including several distinct markets, namely: last mile high bandwidth internet connectivity, the temporary high bandwidth data links, the mobile telephony backhaul (4G), satellite links as well as the various applications where the optical fibers cannot be used. For mobile wireless applications high speed data transmission can be enabled using 10 Gbps optical source and receiver using dense wavelength division multiplexing (DWDM) technology. These systems can be used simultaneously to transmit digital signal and direct RF signal transmission e.g. WiFi (IEEE 802.11), WiMAX (IEEE 802.16), ZigBee (IEEE 802.15.4), cellular based 3G signals etc.

Advanced radio on FSO (RO-FSO) systems have also been developed which are capable of transferring multiple wireless signals using WDM FSO channel. Main advantage of RO-FSO system is that it can provide heterogeneous wireless services quickly and effectively.

2.3 Developments of optical wireless communication systems

In 1960 [1], wireless laser technology was first proposed to establish communication link between transmitter and receiver. However, this technology experienced a lot off difficulties while implementing it in the operational system. A common problem was non-availability of reliable components like laser sources, detectors, high speed modulators and demodulators, high speed electronic circuit and effective pointing arrangements.

In the next decade (1970s) [2], gas laser and flash lamp pumped solid state lasers were used in the transmitter section, but these sources undergo a large number of problems like short lifetime, size, weight and power requirements.

In 1976, first fiber optic cable system was developed for transmission of communication signal employing 0.8μm multimode fiber for maximum bit rate of 1 or 2 Mbps. As fiber optic cable is a guided optical communication, it became more popular than optical wireless communication systems in a short time.

In 1980s, the semiconductor laser diode was developed. Since these lasers were very small in size and highly efficient, they showed potential for longer distance communication.

The next major technological breakthrough was the development of AlGaAs quantum well material structure for high power semiconductor lasers. InGaAs active regions in AlGaAs layer structure resulted in several key benefits i.e. higher gain, lower threshold current operation, higher efficiency, extension of the emission wavelength to longer wavelengths and higher reliability.

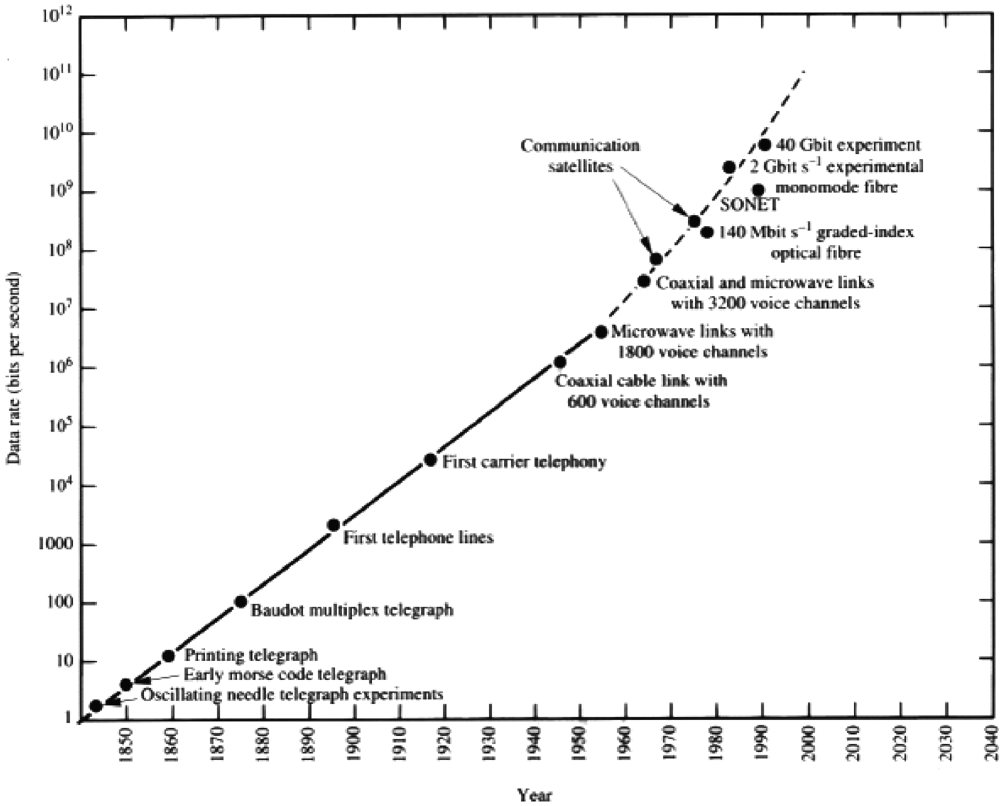

Fig. 2.3.1: Roadmap of data rate with information technology.

Since the 1960s, the discovery of semiconductor laser diode caused the fast development of FSO and wider possibilities for the communications involving beams propagating over long-distance communication in atmosphere. Several OFSO link designs have been proposed using different techniques to get high performance. Fig. 2.3.1 shows development in the data rate of communication channel since 1950 and Fig. 2.3.2 shows categorization of OWC applications based on the transmission range [3].

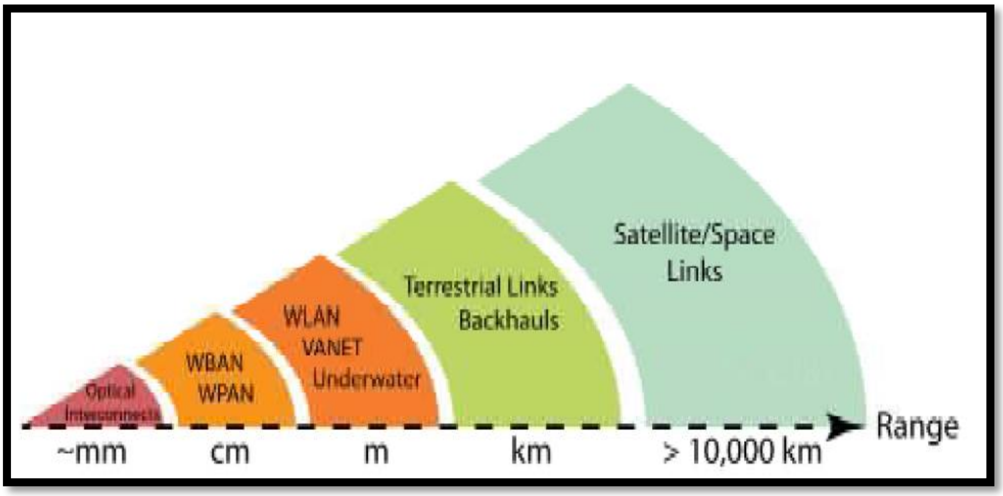

Fig. 2.3.2:Categorization of OWC applications based on the transmission range.

Lot of FSO demonstrations were recorded during 1960 to 1970 [4]. Some of these included the transmission of television signal over 48 km distance using laser diode by researchers working in the MIT. In 1960s (NASA) started performing preliminary experiments for Gemini 7 module at Goddard space center [5].

In 1963 [6], a group of researchers working in the North American Aviation department demonstrated a first TV-over-laser link to send TV signals. In 1968, the first experiment about FSO transmission of 12 phone channels along 4km was demonstrated in Rome (Italy) by researchers of Institution P.T.

Introduction of semiconductor light source working at room temperature by Alferov in 1970, was crucial for a further development of integrated and low cost

FSO systems. The first laser link to handle commercial traffic was built in Japan by Nippon electric company around 1970.

Between 1994 and 1996, first demonstration of a bidirectional space to ground laser link between the ETS-VI satellite and the Communications Research Laboratory in Koganey (Tokyo) was accomplished. After 2001, FSO short range links are used as an alternative to the RF links for the last mile broad band applications in LAN, MAN and WAN access networks.

Several researchers and companies have suggested the idea of hybrid RF/FSO communication system as a solution to the link availability and reliability problem. Low data rate RF channel acts as a backup link to ensure a minimum data communication when the main FSO link is down. However, these solutions are not efficient in terms of bandwidth utilization. In 2007, Vangala and Nik proposed a novel LDPC coding method that optimally achieved the capacity of the combined FSO and RF channels and provided 99.9% reliabilities in the FSO link.

Active and Passive Optical wireless Communication systems

Active optical communication typically uses an active-steered onboard laser-diode based transmitter to send a collimated laser beam to a base station. This system contains a semiconductor laser, a collimating lens and a beam-steering micro-mirror. Active optical communication is suitable for peer-to-peer communication when the application requires but one of the disadvantages of the active transmitter is its relatively high-power consumption.

A passive optical communication approach employs a micro-fabricated corner cube retro-reflector (CCR). The CCR reflects any incident ray of light within a certain range of angles centered about the cube’s diagonal back to the source. If one of the mirrors in CCR is misaligned, the CCR would not be able to reflect signal back to the source. An electrostatic actuator in the CCR deflects one of the mirrors, and it leads to the modulation of the incident ray of light at kilohertz rates. Since the dust mote does not need to emit any light, it consumes very little power. Therefore, passive optical transmission can be performed in the smart dust system since dust motes can modulate the optical signal without having to supply any optical power [7,8].

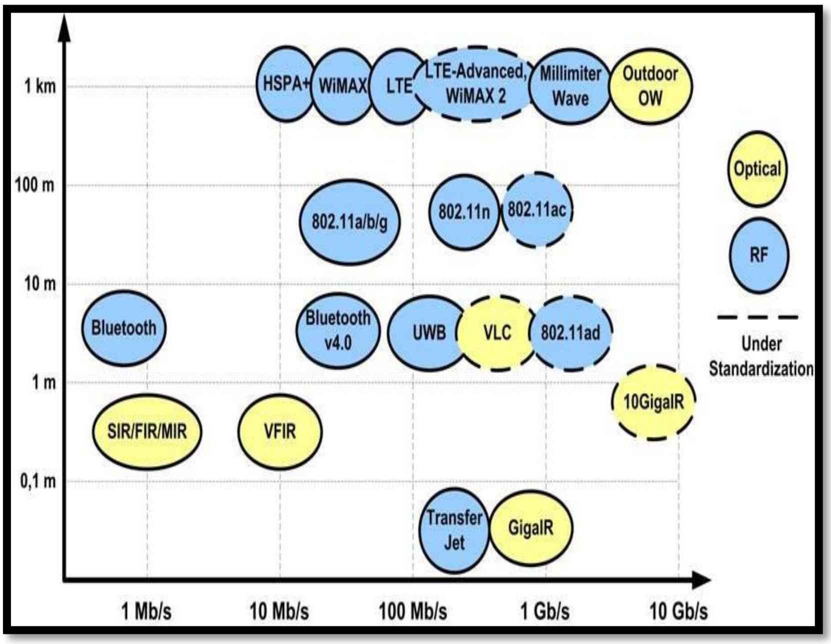

Fig. 2.3.3 :RF and OW technologies* standards with data rates

Figure 2.3.3 summarizes the development of latest commercial RF and OW technologies, as well as technologies under standardization by major agencies like IEEE, 3GPP, Bluetooth and IrDA.

In this figure, technologies are presented with respect to their area of coverage ranging from a few centimeters in personal communications to over 1 km in outdoor communications, and the data rates attained by them including low rate legacy links under 1 Mb/s (Bluetooth and older IrDA systems) . It clearly shows that outdoor free space optical link will be the best alternative for 10 Gb/sand above high-speed data rate communication network.

2.4 Optical Communication Networks using Free Space Optics (OFSO)

The block diagram representing the principles of operation of an outdoor and indoor free space short haul optical link is shown in Fig 2.4.1. The diagram shows an optical transmitter and an optical receiver exchanging information through the optical communication channel. The baseband transmission bit stream is an input to the modulator, turning the direct bias current ON and OFF to modulate the laser diode or LED source. Some of the most popular modulation schemes used for OFSO system are OOK (On-Off-Keying) and subcarrier modulation [9].

The modulated beam is then passed through a collimating lens that forms the beam into parallel ray propagating through the atmosphere. At the receiver end, the information is recovered (down-converted from an optical into an electrical signal) using a technique called direct detection (DD), in which the photo-detector generates an electrical signal according to the instantaneous power of the received optical signal [10].

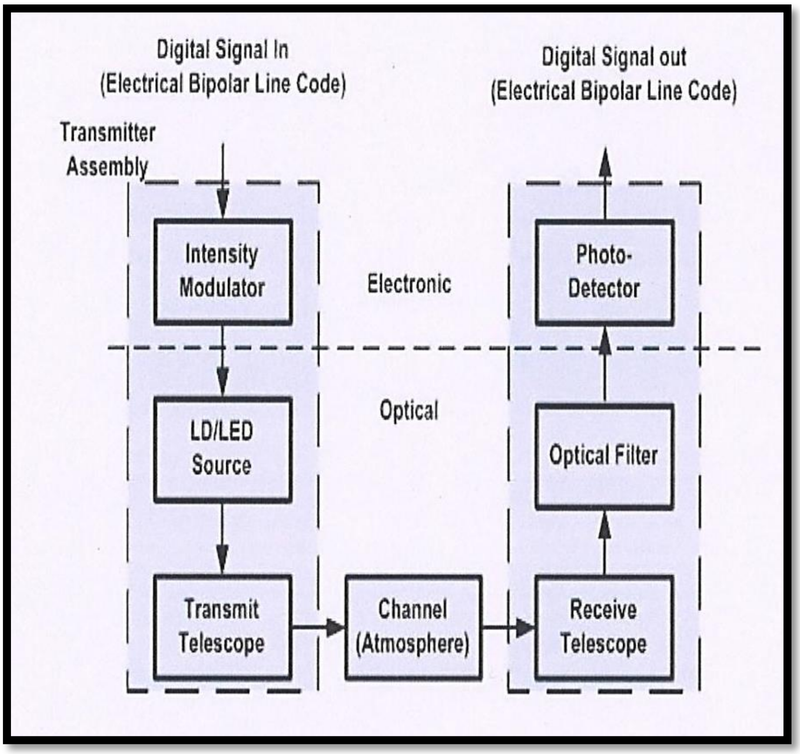

Fig.2.4.1: Short haul free space optical link

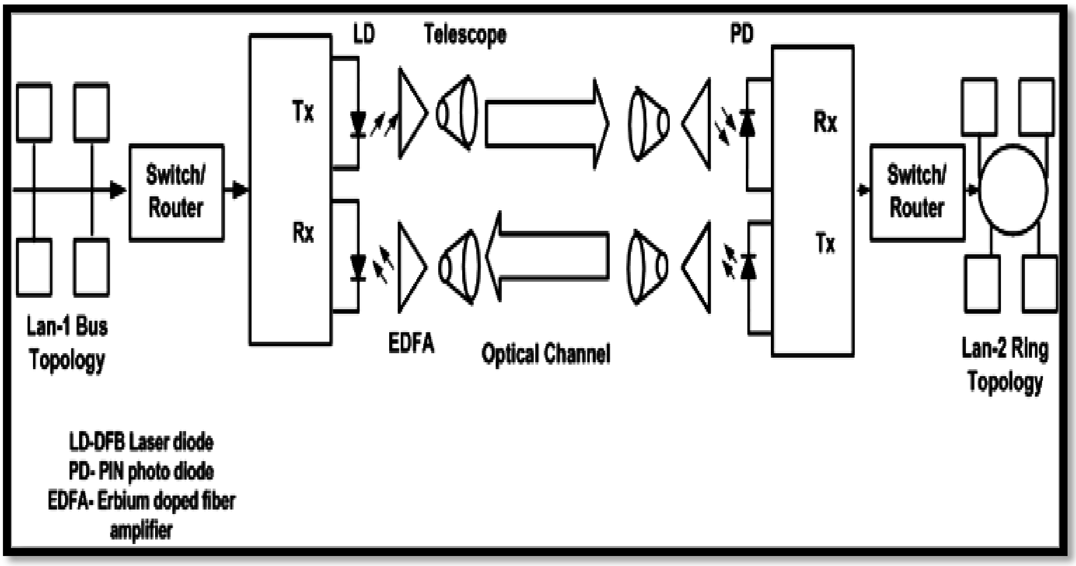

Fig. 2.4.2: The horizontal connection between an Ethernet bus LAN and ring topology LAN

The schematic diagram of the overall total LAN to LAN is shown in Fig.2.4.2. The diagram shows the horizontal connection between an Ethernet Bus LAN and a Ring topology LAN at the sites of two campuses being bridged by the FSO communication link. Optical telescope has been used as optical transmitting and receiving antennas on both the sides of trans-receiver system facing atmospheric channel.

The optical transmitter has been designed using single mode distributed feedback [DFB] semiconductor laser operating at 1550nm wavelength with power output of 5mw. A binary level PPM modulation is used due to its average high power efficiency in combination with convolution coding techniques. The optical receiver has been designed using high speed PIN photodiode. The EDFA amplifiers are used with optical power gain of 20dBm. The overall optical transmitter –receiver system has been designed to work at data rate of 100-Mbps having bit error rate at least 10^{-7}.

The situation for OFSO with respect to IFSO links differs in the length of the communication channel and the type of transmitting source being used. For outdoor applications, single mode semiconductor lasers diodes are used as transmitters, while for indoor LEDs are used [11].

Lasers are attractive for outdoor applications due to their high-power output and high-speed modulation capabilities for broadband communication. LEDs are mostly used in indoor environment where small power and reasonable bandwidth from the source is desirable. So far as the channel length is concerned indoor channel is generally few meters in length while the outdoor channel can be up to few kilometers in length. However, the characteristics of the atmospheric channel for OFSO and IFSO largely differ. The outdoor channel characteristics are very random in nature due to the temperature effects such as scintillation, fog attenuation, smoke, rain etc. [11,12].

A broadband Line of Sight (LOS) FSO link can be used as short haul communication link to connect two private LANs located at two different sites at an aerial distance within 1 km away from each other as shown in Fig.2.4.2 . ",The optical communication link would connect the two LANs via a switch/router to serve two major purposes",. First, it provides inter operation between any two computers in the two LANs utilizing the necessary medium access control (MAC) protocol.

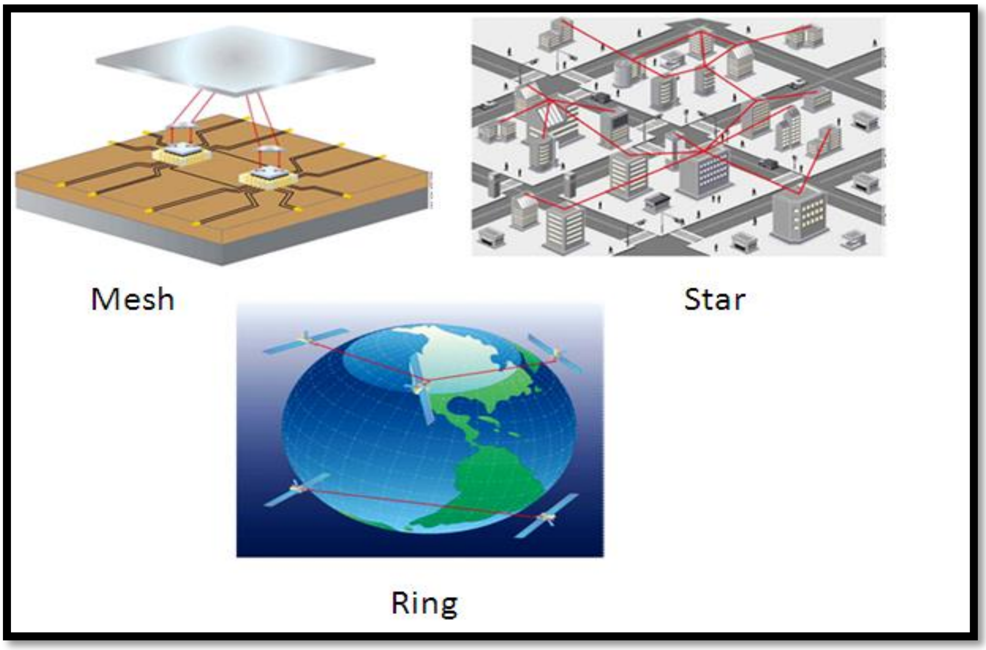

Fig.2.4.3: Applications of FSO communication system

Secondly, the two LAN will have Internet connectivity through Internet Service Providers (ISPs) either independently or jointly. Additionally, the FSO connectivity can be freely utilized to have data-voice integration for real time communication within the combined private LAN networks. The available high bandwidth of the FSO link can also be used for multimedia communication and video-conferencing between the administrative staffs and other members connected to the LANs.

The FSO link will act as a bridge to provide high-capacity connectivity to maintain privacy, reduce cost, reduce time of installation and have no dependence on Government regulatory body. Important applications of FSO using different topologies [13] are shown in Fig. 2.4.3.

2.5 An OFSO Transceiver Model

Fig. 2.5.1(a) [13] shows the Light-Pointe's Flight Apex and its internal structure in Fig. 2.5.1(b) [13], one of the highest bandwidth commercially available OFSO products today. It uses lasers at a frequency of almost 200 Terahertz to achieve full-duplex speeds of 2.5 Gbps for distances up to 1km. Here, fiber optic cables are used to carry transmitted and received optical signals collected by lens. Incoming signal is collected by the receiving aperture and then focused on the photo-detector followed by data processing unit. The outgoing signal is first given to the laser source and then to the transmitter aperture.

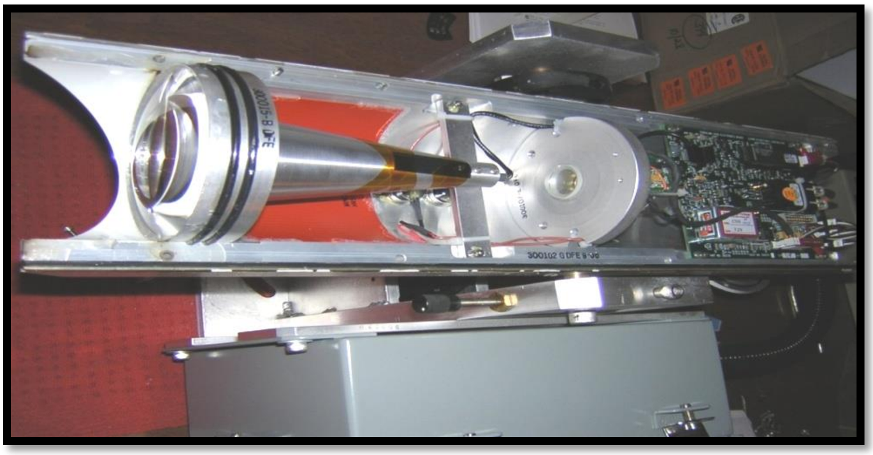

Fig.2.5.1 (a):Light pointe's flight apex

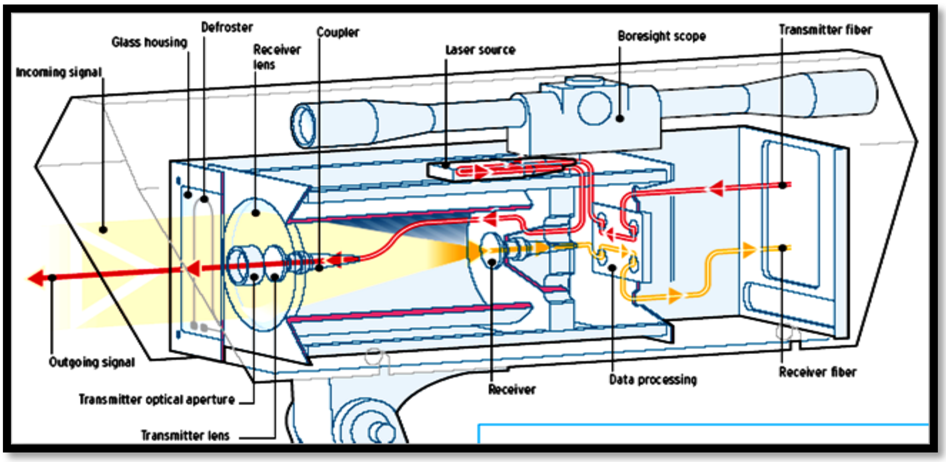

Fig. 2.5.1 (b): Internal structure of light pointe's flight apex

The Lawrence Livermore National Laboratory (LLNL) demonstrated an FSO link of the data speed (2.5 Gbps) over a distance of 28 km. With the help of wavelength division multiplexing (WDM), the LLNL had previously managed to scale the capacity of an FSO link to 20 Gbps.

Initial Challenges in OFSO systems

In spite of early developments in the techniques to build OFSO and IFSO communication system, the usefulness and practicability of these systems was questionable for many reasons some of which are given below:

1. After 1970, the discovery of fiber optic cable was adequate to handle the demand of bandwidth for high-speed data communication.
2. Considerable research and development were required to improve the reliability and availability of optical wireless link for system performance.
3. The atmospheric effects such as fog, rain, smoke and turbulence due to temperature variation would always influence the OFSO.
4. The use of these systems in indoor and outdoor communication required accurate pointing and tracking optical system which were not developed or available.

However with the rapid development and maturity of optoelectronic devices in recent years (2001-2015), OFSO and IFSO have emerged as a commercially viable alternative to RF frequency and millimeter wave links. For long-distance high-speed data communication fiber optic cables were previously in use but, in situations where they are practically unreachable or infeasible, OFSO or IFSO link can be used as an alternative communication technology.

2.6 IFSO (Indoor Free Space Optical Links) Systems

The purpose of an IFSO system is to build a wireless optical communication link between a base station tower fitted over the ceiling inside a room with number of users within the room. Since the atmosphere inside the room is undisturbed i.e. not affected by atmospheric effects such as wind flow, fog, snow, rain, scintillation etc, the channel characteristics is not similar as in OFSO. However, "line of sight signal may be blocked by the roaming users inside the room and therefore an alternative arrangement using diffusing optics is used for uniform illumination inside the room",.

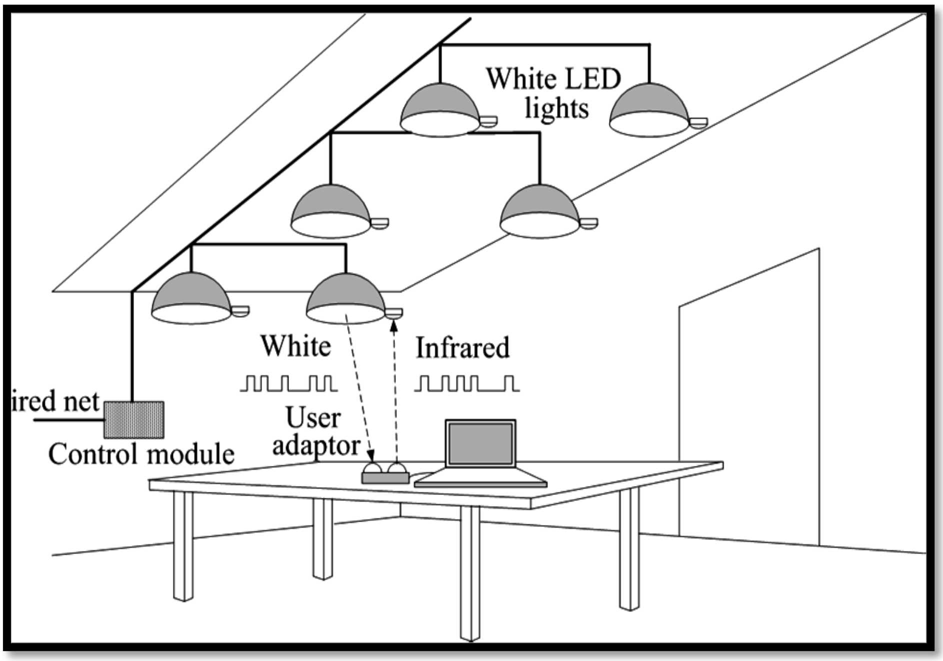

Fig.2.6.1: LED-based duplex channel optical wireless communication system

The block diagram represents the principle of operation of LED based duplex channel wireless communication link employing white LED lights and infrared LEDs for indoor internet access as shown in Fig 2.6.1. The diagram shows white LEDs acting as optical transmitters and photodiodes as optical receivers [16]. The white light LED will act as source for illumination as well as for communication with the user inside the room. The downlink comprises of white lights from LED which is modulated by signals from the wired net. A PIN photo-detector is used to detect these incoming modulated signals. The uplink section comprises an infrared LED and a photo-detector to detect downlink signals. Both links adopt intensity modulation with direct detection (IM/DD) techniques. On-off keying (OOK) is one of the preferred modulation techniques employed in IFSO communication due to its good bandwidth efficiency and ease of implementation [14].

LEDs present wider emission beams than laser diode, which makes them the preferred option of the indoor non-directed and the hybrid configurations. In addition, they are generally considered safer to eyes, which mean that they can be used at higher emission powers than laser diodes. Further, they are more robust and cheaper than laser diode, which favors their use for indoor applications [15].

Other important features of LEDs include lower sensitivity to temperature variations (compared to laser) and simplicity of the driver circuit associated with them. Laser diodes, on the other hand, require more complex driver circuits and are more sensitive to temperature fluctuations [15-17]. Despite of these limitations, laser diodes can be modulated at higher speeds than LEDs, which makes them the only option in applications that require a very high data rate. Moreover, the fact that their emission beams are very narrow means that they can be used over longer distances, which favors their use in directed-LOS outdoors links for high-speed data communication.

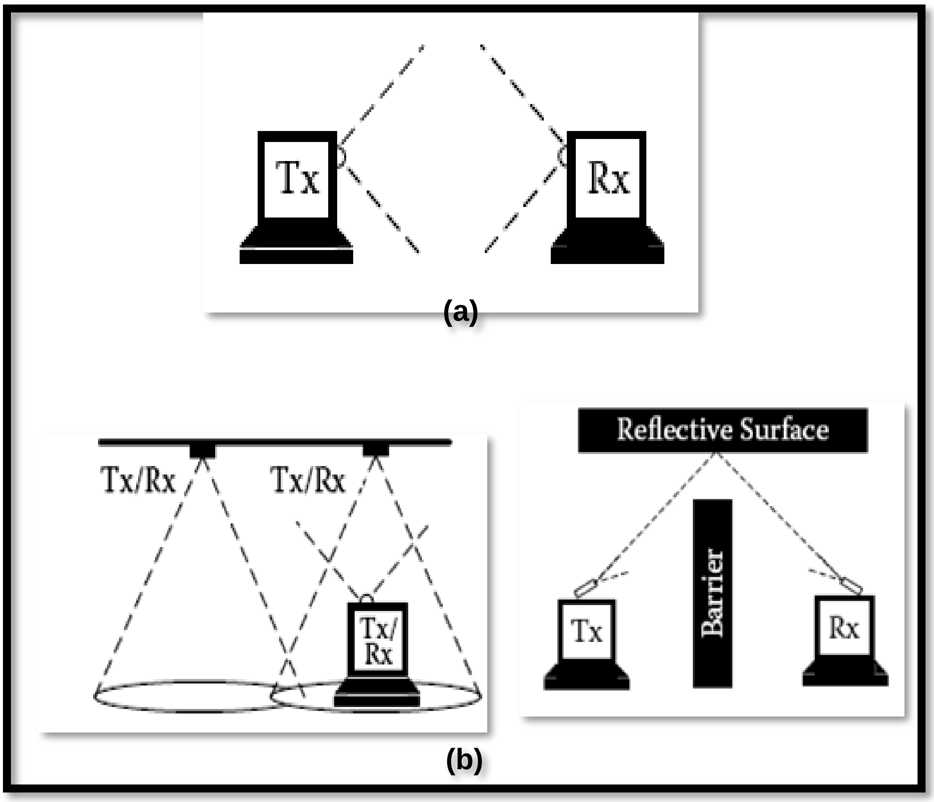

Fig2.6.2: (a) line of sight topology (b) different configurations of IFSO (cellular and directed non-line of sight)

The different configurations of IFSO wireless systems are illustrated in Figure 2.6.2(a) and (b) [16]. In LOS (Line of sight) topology, the transmitter and the receiver are in direct view of each other, without any object obstructing the path between them. Non-LOS systems may have obstacles blocking the direct path between transmitter and receiver. Therefore, these configurations rely on the use of reflective surfaces to create an alternative path for the communication link.

A special case of the directed LOS configuration is the cellular topology. Here, each optical satellite creates spots or cell energy with minimum overlap between each other and communicate with group of mobile or computer terminals through optical beam. The main advantage of this topology is that the information signal is received after a single reflection only, which minimizes multipath dispersion and the possibility of an obstacle is removed.

2.7 IFSO Transceiver Model

Fig. 2.7.1:LED display as (a)light audio transmitter(b) indoor parking light(c) conference room.

The commercial use of LED display as a light audio transmitter is shown in above Fig2.7.1. Any illumination system making use of high brightness visible LEDs can be used as a short-range information beacon. In this system the audio signal having small amplitude is first amplified by an audio amplifier and is then fed to the voltage control oscillator (VCO). The VCO is used to modulate the incoming audio signal variations from audio amplifier and generate the frequency modulated (FM) modulate signal. The FM modulated signal is transmitted by switching the LEDs 'ON' and 'OFF'. The frequency of the switching is high enough such that the perceivable light appears to be constantly illuminated to the human eye. The photo detector is used to detect light signal from the transmitter and convert the signal into an electrical signal. However, the main drawback of LED based IFSO is that they are suitable only for short range because the photo-detector current is proportional to receive power. Usually intensity modulation with direct detection method is used for transmission and reception of indoor communication signals. The signal to noise ratio (SNR) depends on the received optical power and noise arising from sunlight, incandescent lighting and fluorescent lighting.

2.8 Atmospheric Turbulence

The atmosphere is a fluid comprising various species of gaseous substances, suspended water vapor and dust particles. Atmospheric turbulence is the disturbance that may occur in the characteristic properties of the fluidic atmosphere due to external effects such as random temperature fluctuations or random change in the flowing conditions of air. The properties of the atmosphere such as: refractive index, opacity and the visibility conditions are largely affected when atmospheric conditions are disturbed by random motion of the air molecules due to the turbulence of the medium caused by temperature variations and wind velocity change.

An optical or infrared wave passing through a turbulent atmosphere can face serious obstructions to its propagation through the medium. First, the coherence properties of the optical beam may be partially or totally lost and the information it carries may be fully or partially affected. Fading of the optical wave may occur due to multiple reflections or refractions in the atmospheric medium, random fluctuations of the intensity and the phase of the propagating optical wave will be observed when the optical beam will ultimately reach the receiver of light at the end of the optical path.

The amount of fluctuations in intensity and phase of the travelling beam will depend on the strength of the turbulence in atmosphere. Thus, there can be (i) weak, (ii) moderate and (iii) strong turbulence conditions are created in the atmosphere by the strength of the air flow velocity or temperature rise. ",The random fluctuation of the refractive index of the atmosphere can affect the propagating beam to different degrees and as a result the fluctuating conditions can be described and represented properly only when proper statistical distribution functions are assumed for the above three types of turbulences",.

Rytov, Kolmogorov ,Andrew & Philips , Fante [18-19] and many other scientists have studied in great details about the propagation properties of the atmosphere and the type of statistical distributions that fit well with the type of turbulence observed in the atmosphere.

From their studies and observations, the log-normal distribution [20] is seen to be fitting very well with weak turbulence while the gamma-gamma statistical distributions fits well for moderate to strong turbulences [21-23]. However, there remains still scope of improving the statistical methods of analysis because in many cases it has been observed that these statistical variations do not always tally well with the observed performances of the optical transmission systems.

The main purpose of this chapter is also to study theoretically the effect of atmospheric turbulence on the propagation of a monochromatic optical beam in a laboratory condition. Since the arrangement for artificial creation of turbulence inside a laboratory can only create weak turbulence, we were able to work only under the weak turbulent conditions. Rytov in his work suggested that the Log-Normal Distributions fits very well with the weak turbulence conditions in the atmosphere. Many research works have been published on weak turbulence conditions and it has been found that the Rytov method is now a standard procedure for weak turbulence analysis.

2.9 Refractive index fluctuation with atmospheric temperature.

When optical beam propagating through atmospheric turbulence it undergo multiple refraction by turbulence eddies. Due to this refraction optical coherence breaks up into different pieces moving randomly in different path toward the receiver. When a portion of wave reaches a receiver, irradiance fluctuations are occurred due to addition and subtraction of optical wave-front called fading.

The theory of irradiance fluctuations has been extensively developed by Rytov. He represents the strength of irradiance fluctuations as a function of refractive index structure parameter and varies as a logarithm of the amplitude and phase therefore it is called the log-amplitude fluctuations.

We used these theories to illustrate different turbulence parameters like scintillation index and refractive index structure parameter C_n^2 for coherent and partially coherent optical beam propagation.

Clear air turbulence phenomena affect the propagation of an optical beam because the refractive index randomly varies in space and time. Mainly, random variation of the refractive index of air depends on the air mixing due to temperature variation in the atmosphere. In-fact, sunlight incident upon the earth's surface causes heating of the earth's surface and the air in its proximity.

This sheet or region of warmed air becomes less dense and rises to combine with the cooler air of the above layers, which causes air temperature to vary randomly (from point to point). Because the atmospheric refractive index depends on air temperature and density, it varies in a random fashion in space and time, and this variation is the origin of clear air turbulence. To describe clear air turbulence, one should consider the atmosphere as a fluid that is in continuous flow [24-25]. A fluid flow at small velocity is first characterized by a smooth laminar phase. In fluid dynamics, a figure of merit of the fluid flow is the Reynolds number (Re), which is the ratio between fluid inertial forces and viscous forces.

$$\mathrm{Re} = V_c l / V_k \tag{2.1}$$

where V_c & l are the characteristic velocity scale and length given in m/s and m, respectively. V_k is the kinematics viscosity given in m^2/s

The laminar flow of the fluid is stable only when the Reynolds number does not exceed a certain critical value ($R_e \approx 2300$). When the Reynolds number exceeds the critical value (e.g., by increasing flow velocity), motion becomes unstable and the flow changes from laminar to a more chaotic, turbulent state. To describe this turbulent state, Kolmogorov developed a theory based on the hypothesis that kinetic energy associated with larger eddies is redistributed without loss to eddy of decreasing size, until they are finally dissipated by viscosity. [26]

The structure of the turbulence according to this theory is depicted in Figure 2.9.1. The scale of the turbulence can be divided into three ranges: input range, dissipation range, and inertial sub-range. The input range, where the energy is injected in the turbulence, is characterized by eddies of size greater than the outer scale of turbulence $\left(L_0\right)$.

The turbulence in this range greatly depends on local atmospheric conditions. The dissipation range is characterized by eddies of size smaller than the inner scale of turbulence $(l_0 << L_0)$. In this case, turbulent eddies disappear, the remaining energy is dissipated as heat, and energy loss from eddies (due to viscosity) dominates [27,28].

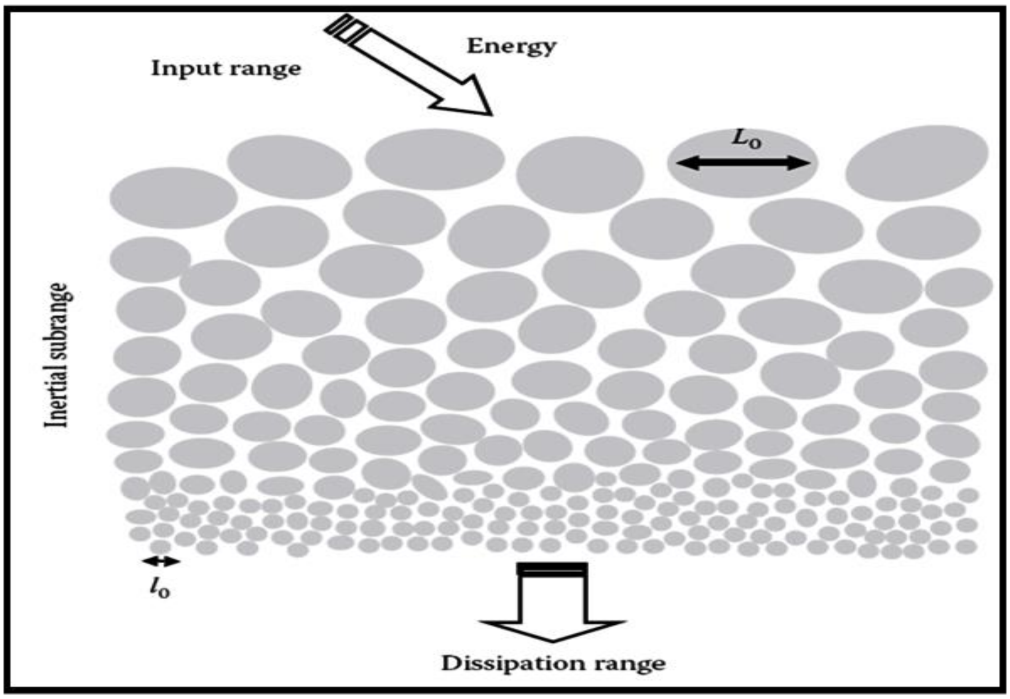

Fig 2.9.1 : Structure of the turbulence with small and large eddies.

The inertial sub-range is at the core to the -Kolmogorov theory, here the turbulence energy is transferred from larger eddies size L_0 down to smaller eddies of size l_0. These eddies form regions of different refractive indices.

In the visible and near infrared regions of spectrum, these index of refraction fluctuations are caused almost exclusively by temperature fluctuations; whereas in the far infrared region, humidity fluctuations may also contribute.

The atmospheric refractive index at optical frequency depends on the four quantities optical wavelength, atmospheric temperature, atmospheric pressure and specific humidity. For optical frequency humidity over dry land generally contribute less than 1% to the refractive index fluctuation and it is typically ignored. The refractive index of air can be written in the form [29]

$$\eta = \langle \eta \rangle + \Delta\eta \quad (2.2)$$

Where $\langle \eta \rangle$ represents average value of refractive index and $\langle \Delta\eta \rangle$ random deviation from this average value.

The refractive index of air at optical frequency can found from following equation [30,31].

$$\Delta\eta = \frac{77.6\times10^{-6}P}{T}\left(1 + \frac{7.52\times10^{-3}}{\lambda^2}\right) \quad (2.3)$$

Where,

P- is the atmospheric pressure

T- is the temperature in Kelvin

λ- is the wavelength in Microns

Let $\eta(\rho1)$and $\eta(\rho2)$ be values of the refractive index at the vector location $\rho1$ and $\rho2$ respectively. We can describe fluctuations in the refractive index using the refractive index structure function define as

$$D_n(\rho_1, \rho_2) = \langle |\eta(\rho_1) - \eta(\rho_2)| \rangle \quad (2.4)$$

$\langle . \rangle$ - represents statistical averaging.

ρ_1, ρ_2- Vector location

The refractive index structure function is describe by the kolmogorov as

$$D_n(\rho_1, \rho_2) = C_n^2 \rho^{\frac{2}{3}},\ l_0 \ll \rho \ll L_0 \quad (2.5)$$

Where, C_n^2 is the proportionality constant called refractive index structure parameter given by

$$C_n^2 = \left(79 \times 10^{-6}\frac{P}{T^2}\right) C_T^2 \quad (2.6)$$

C_T^2 is the temperature structure constant.

P- is the atmospheric pressure in millibars.

2.10 Wave equations incorporate the effects of atmospheric turbulence using Maxwell's Equations.

We start by considering the Maxwell's equations describing the Wave equation for the modulated optical carrier and then we can incorporate the effects of atmospheric effects through the variations of the properties of the medium such as μ, ϵ, η [32,33].

In turbulent medium, the relative dielectric constant ε_r or the index of refraction η varies from point to point and at a different instant of time. The dielectric constant ε_r described by a random function of position (r) and time as

$$\varepsilon_r = \varepsilon_r(r,t) = \eta^2(r,t) \tag{2.7}$$

Where r- Transverse position of observation point, t- time

If ε_r is a function of r only and independent of time then above equation becomes

$$\varepsilon_r = \varepsilon_r(r) = \eta^2(r) \tag{2.8}$$

Now Maxwell's equation for the medium given in equation (2.7) is given by

$$\nabla \times E(r) = i\omega\mu_0 H(r) \tag{2.9}$$

$$\nabla \times H(r) = -i\omega\varepsilon_0\varepsilon_r(r)E(r) \tag{2.10}$$

Where μ_0 is the permeability of the medium .

ε_0 is the permittivity of free space.

ω is the angular frequency and E, H represents electric and magnetic fields. [34]

Combining these two equations, we obtain

$$\nabla^2 E(r) + \omega^2\mu_0\varepsilon_0\varepsilon_r(r)E - \nabla\left(\frac{\nabla\varepsilon_r}{\varepsilon_r}.E\right) = 0 \tag{2.11}$$

In terms of refractive index η, we write

$$\nabla^2 E(r) + K_0^2 \eta^2 E(r) - 2\nabla\left(\frac{\nabla\eta}{\eta}.E\right) = 0 \qquad (2.12)$$

Where K_0 is spectrum wave number.

We now consider the wave propagation in the direction of X-axis. The Y-component of the electric field is $U(r) = E_y(r)$ satisfies

$$\left(\nabla^2 + K_0^2\eta^2\right)U(r) = 0 \qquad (2.13)$$

The index of refraction η fluctuates about the average value $\langle\eta\rangle$, and thus using the wave number for the average $K^2 = K_0^2\langle\eta_0\rangle^2$ we can write

$$\left[\nabla^2 + K^2(1+\eta_1)^2\right]U(r) = 0 \qquad (2.14)$$

Where η_0 represents index of refraction without fluctuations η_1 represents the fluctuations of the index of refraction. For Weak fluctuation, i.e. for small η_1 the solution is given by Rytov equation and U can be written as [35]

$$U = U_0 + U_1 + U_2 + U_3 + --- \qquad (2.15)$$

or

$$U = \exp\left(\psi_0 + \psi_1 + \psi_2 + \psi_3 + ----\right) \qquad (2.16)$$

$$U(r) = \exp^{\psi(r)}$$

Or

$$U(r,L) = U_0(r,L)\exp\left[\psi(r,L)\right] \qquad (2.17)$$

where ψ is the complex phase perturbation and $U_0(r,L)$ is a reference field with definite amplitude and phase. Real part of the equation (2.17) represents the fluctuations of the logarithm of the amplitude and therefore it is called the log-amplitude fluctuations while the imaginary part ψ represents the fluctuations of phase.

Now, let us consider a lowest order transverse electromagnetic (TEM) Gaussian beam wave [36] ($TEM_{0,0}$ wave) as shown in fig (2.10.1) . It is assumed that the transmitting aperture located at z=0 and the amplitude distribution is Gaussian with effective beam radius w_0.

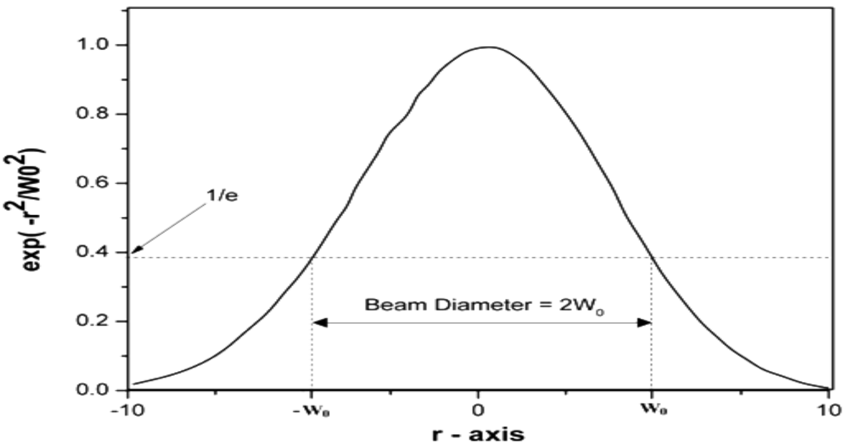

Fig 2.10.1: Amplitude profile of a Gaussian-beam wave

Here we consider atmosphere acts as a transfer function with optical signal X(s) acts as a input and Y(s) as the output signal fig 2.10.2. The output Y(s) in terms of transfer function is given by,

$$Y(s)=H(s)+X(s)$$

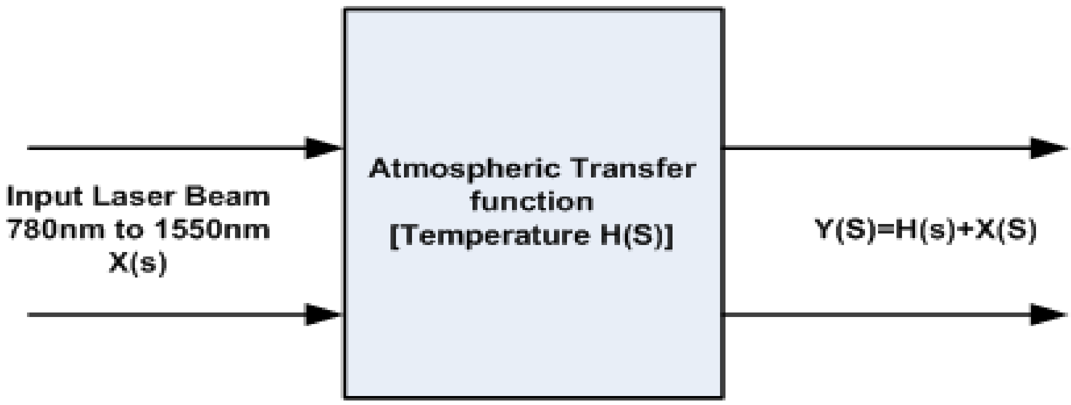

Fig 2.10.2: Transfer function

Where s is a parameter depends on amplitude and phase. A Gaussian laser beam propagating through the turbulence atmosphere to a receiver along horizontal path distance 'L' as shown in Fig.2.10.3

Now consider the optical field unit amplitude is applied as an input to the atmospheric transfer function box given by [37]

$$U(r,0)=\exp\left(-\frac{r^2}{w_0^2}\right) \text{ at } z=0 \tag{2.18}$$

Where, $r=\sqrt{x^2+y^2}$, w_0 is the initial beam size and x and y are the horizontal and vertical coordinator of the incident beam field from beam center respectively. The irradiance function of the beam at a distance L from the source can be express as

$$I(x,y,L)=\frac{w_0}{w^2}\exp\left[-\frac{2(x^2+y^2)}{w^2}\right] \tag{2.19}$$

where, w is the average beam size or radius at the receiver

Given by,

$$w=w_0\left[1+(\frac{2L}{kw_0})^2\right]^{1/2}\left[1+1.63\sigma^{12/5}\Lambda(L)\right]^{\frac{1}{2}} \tag{2.20}$$

where , k= $2\pi/\lambda$ is wave number, λ is the wavelength of the beam , σ^2 is the Rytov variance for plane wave and $\Lambda(L)$ is the fresnel ratio for vacuum propagation.

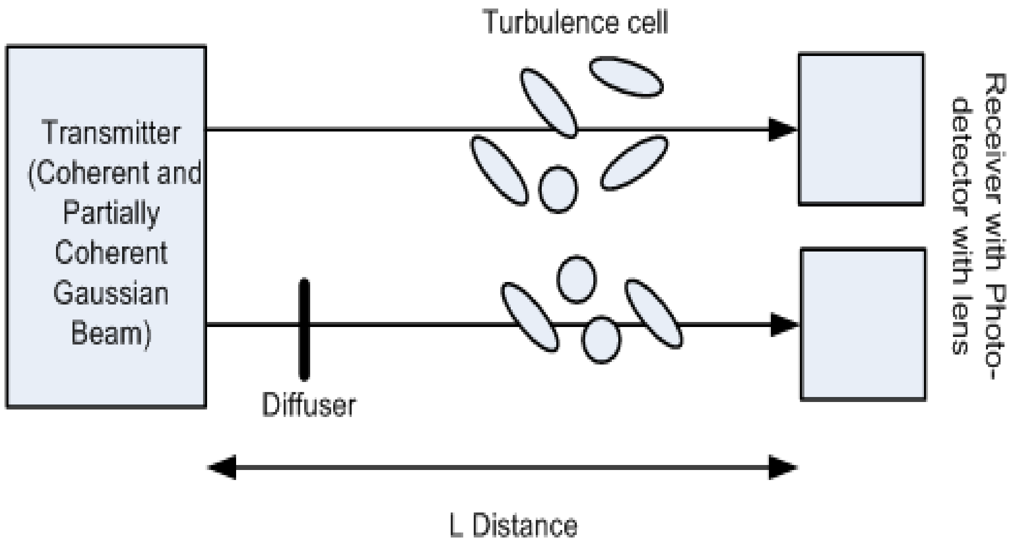

Fig 2.10.3: Propagation geometry of optical channel

Now, the intensity of the optical wave 'I' propagating through turbulent atmosphere is a random variable. The normalized variance of optical wave intensity at the output of a turbulence box is defined as,

$$\sigma^2 = \frac{\langle I^2 \rangle}{\langle I \rangle^2} - 1 \tag{2.21}$$

where, the angle bracket denotes an ensemble average σ^2 indicate the strength of irradiance fluctuations due to atmospheric temperature variations and proportional to Rytov variance, define as [37-38]

$$\sigma_R^2 = 1.23 C_n^2 k^{7/6} L^{11/6} \tag{2.22}$$

For weak fluctuation, it is less than 1 and for strong fluctuation it is greater than 1. C_n^2 is the refractive index structure constant that characterizes the strength of the index of refraction fluctuations.

2.11 Kolmogorov Approximation for Weak and Strong Turbulence

Using the Kolmogorov spectrum described by Andrews L.C., Phillips L.R. and standard extended Rytov theory the on axis scintillation index (i.e. for point receiver , D≈0) for weak turbulence (inner scale l=0, Outer scale L=∞) is given by.

$$\sigma_{I,w}^2 = 3.86\sigma^2 \left\{ 0.4\left[\left(1+2\Theta(L)\right)^2 + 4(\Lambda(L))^2 \right]^{5/12} \times \cos\left[\frac{5}{6}\tan^{-1}\left(\frac{1+2\Theta(L)}{2\Lambda(L)}\right) \right] - \frac{11}{6}(\Lambda(L))^{5/6} \right\} \tag{2.23}$$

The fresnel ratio $\Lambda(L)$ is the beam spread due to diffractions when propagate through the air and define as ,

$$\Lambda(L) = \frac{\Lambda_0(L)}{\Theta_0^2(L) + \Lambda_0^2(L)} \tag{2.24}$$

where $\Lambda_0(L) = \dfrac{2L}{kw_0^2}$ is the initial fresnel ratio.

$\Lambda(L)$ is associated with the beam curvature parameter,

$\Theta(L)$ is the phase curvature of the beam as it propagates in vacuum defined as.

$$\Theta(L) = \frac{\Theta_0(L)}{\Theta_0^2(L) + \Lambda_0^2(L)} \tag{2.25}$$

where $\Theta_0(L) = 1 - \frac{L}{F_0}$ is the initial phase curvature and for Gaussian beam $F_0 = \infty$

Hence $\Theta(L) = 1$

For moderate to strong turbulence, scintillation index is defined as

$$\sigma_{I,s}^2 = \exp\left(\frac{0.49\sigma_{I,w}^2}{\left[1 + 0.56(1+\Theta)\sigma_{I,w}^{\frac{12}{5}}\right]^{\frac{7}{6}}} + \frac{0.51\sigma_{I,w}^2}{\left(1 + 0.69\sigma_{I,w}^{12/5}\right)^{\frac{5}{6}}} \right) - 1 \tag{2.26}$$

2.12 Link Analysis

The overall system performance of a optical wireless communication is quantified using a link budget derived from the range equation, which combines atmospheric attenuation and geometrical aspects to calculate the received power. The system link calculation is carried out as shown in the following Fig.2.12.1.

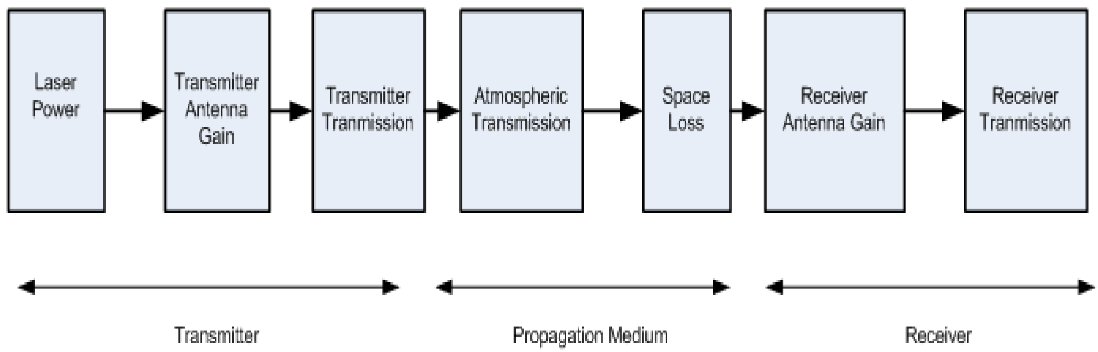

Fig 2.12.1 : Optical link calculation

",The receiver's sensitivity determines the amount of received optical power needed to achieve the required signal-to-noise ratio (SNR) for a given expected communication performance",.

Consider a laser transmitter antenna with gain G_T transmitting a total power P_T at the wavelength 'λ'. The signal power received at the communications detector can be expressed

$$P_{REC} = P_T G_T \tau_T \tau_{ATM} S G_R \tau_R \qquad (2.27)$$

Where τ_T is the transmitter optical efficiency, τ_{ATM} is the value of the atmospheric attenuation due to fog , rain at the laser transmitter wavelength, S is the free-space loss, G_R is the receiver antenna gain, and τ_R is the receiver optical efficiency. The transmitter gain, free-space loss, and receiver antenna gain are given by $G_T = \frac{16}{\theta^2}$ Where θ is transmitting divergence angle, $S = \left(\frac{\lambda}{4\pi L}\right)^2$ (L is the range), and $G_R = \left(\frac{\pi D}{\lambda}\right)^2$ (Dis receiver diameter).

Therefore above equation can be return as

$$P_{REC} = P_T G_T \tau_T \tau_{ATM} \left(\frac{\lambda}{4\pi L}\right)^2 \left(\frac{\pi D}{\lambda}\right)^2 \tau_R \qquad (2.28)$$

τ_{ATM} may be written in terms of the atmospheric attenuation factor αgiven by -10 log (τ_{ATM})/ L.

$$P_{REC} = P_T G_T \tau_T - \left(10^{\frac{-\alpha L}{10}} / L\right) \left(\frac{\lambda}{4\pi L}\right)^2 \left(\frac{\pi D}{\lambda}\right)^2 \tau_R \qquad (2.29)$$

Atmospheric attenuation :

For optical beam transmit through a rain rate of 155 mm/hr, specific attenuation exceeds 30 dB/km. It can cause more than 80 dB attenuation for 2.7 km link used in Prokes [38-39] . The specific attenuation of wireless optical link for rain rate of R mm/hr is given by

$$a_{spec} = 1.076 \times R^{0.67} \text{ [bB/ km]} \qquad (2.30)$$

and for microwave frequency , the relationship between specific attenuation and rain rate is given by

$$\gamma_R = kR^{\alpha} \qquad (2.31)$$

where k and α depends upon the frequency and microstructure of rain. The specific attenuation of different GHz link has been simulated by Koudelka and Kandus [40] for different rain rate and it is observed that rain attenuation of GHz links below 40 GHz is less than optical wireless link.

Snow Attenuation

Fog, rain and other precipitation causes the scattering of the light and the laser beam power is attenuated resulting in reduction of received single strength. If S is the snow rate in mm/hr then specific attenuation in dB/km is given by

$$a_{snow} = a.s^{b} \tag{2.32}$$

Where, a and b is constant given by

$$a = 5.42 \times 10^{-5}\lambda + 5.495, \quad b = 1.38 \tag{2.33}$$

In microwave region the attenuation due to dry snow is less than attenuation due to rain. However wet or watery snow gives attenuation comparable to that due to rain in microwave and millimeter wave region. The specific snow attenuation A in terms of snow rate 'R' for GHz link is given as

$$A = 0.00349 \times \frac{R^{16}}{\lambda^{4}} + 0.00224 \times \frac{R}{\lambda} \text{ (F.Nadeem and Kandus model)} \tag{2.34}$$

From above equations it is observed that as the wavelength becomes short specific attenuation A is increases. Therefore the attenuation due to snow is quit high for wireless optical communication in comparison to GHz frequency and the specific attenuation for optical wavelength is almost 8 or 9 times more than 100 GHz link . The effect of dry snow for GHz frequency i.e up to 60 GHz link is within acceptable range. The atmospheric conditions where the snow rate probably is very high can use frequency up to 60 GHz as a backup link. [41,42]

Fog attenuation:

Fog is composed of very fine water droplets of water (<100 μm), smoke, ice or combination of both suspended in the air . These droplets form when moist air is cooled below its dew point. The air becomes saturated and the water vapors contained in the air condense in the form of fine water droplets. The amount of light attenuation is proportional to number and size of fog . The specific attenuation is calculated using kruse and kim model. These models use variables such as visibility V [km] , wavelength λ [nm] and visibility reference at wavelength λ_0 [nm].

$$a_{spec} = \frac{10 \log V\%}{V[km]} \left(\frac{\lambda}{\lambda_0} \right)^{-q} [db/km] \tag{2.35}$$

q=1.6 if V>50 km; 1.3 if 6 km< V <50 km ; 0.58 $V^{1/3}$ if V < 6 km

Real time measurement of fog attenuation shown that [43] the effect of fog is significant when humidity increases above 85% while the temperature is decreasing. The attenuation coefficient is the sum of the absorption and the scattering coefficient from aerosols and molecular constituents of the atmosphere. The attenuation effects due to absorption can be minimized by the appropriate selection of wavelengths for transmission. The scattering effects depends on the size parameter (D_0) , such that $D_0 = \frac{2\pi r}{\lambda}$, where r is the size of the aerosol particle encountered during propagation. if $D_0 \langle\langle 1$ the scattering process is termed as Rayleigh scattering , $D_0 \approx 1$ then it is Mie scattering and for $D_0 \rangle\rangle 1$, the scattering process can then be described using geometrical scattering theory and Optical attenuation based on visibility range is given in following table 2.1

Table 2.1 Attenuation with Visibility

Description	**Visibility Range (m)**	**Attenuation (dB/km)**
Dense Fog	40-70	250-143
Thick Fog	70-250	143-40
Moderate Fog	250-500	40-20
Light Fog	500-1000	20-9.3

2.13 Scintillation Index Model for coherent optical beam

Above equations in section 2.11 described on-axis scintillation index for point receiver, where diameter $D\approx 0$. Now, let us define scintillation index for receiver detector having lens diameter '$D\neq 0$'). For that we assume Ω is the normalized receiver aperture define as

$\Omega=\dfrac{2L}{kW_G^2}$ where W_G^2 is the Gaussian lens radius.

Log irradiance due to large scale eddies is given as

$$\sigma_{\ln,x}^2(D)=\frac{0.49\left(\dfrac{\Omega-\Lambda_1}{\Omega+\Lambda_1}\right)\sigma_{I,s}^2}{\left[1+\dfrac{0.4\left(2-\bar{\Theta}_1\right)\left(\dfrac{\sigma_{I,s}}{\sigma}\right)^{\frac{12}{7}}}{\left(\Omega+\Lambda_1\right)\left(\dfrac{1}{3}-\dfrac{1}{2}\bar{\Theta}_1+\dfrac{1}{5}\bar{\Theta}_1^2\right)^{\frac{6}{7}}+0.56\left(1+\Theta_1\right)\sigma_{I,s}^{\frac{12}{5}}}\right]^{\frac{7}{6}}} \tag{2.36}$$

Log irradiance due to small scale eddies is given as

$$\sigma_{\ln,y}^2(D)=\frac{\left(0.51\sigma_{I,s}^2\right)/\left(1+0.69\sigma_{I,w}^{\frac{12}{5}}\right)^{\frac{5}{6}}}{1+\left[1.20\left(\dfrac{\sigma}{\sigma_{I,s}}\right)^{\frac{12}{5}}+0.83\sigma^{\frac{12}{5}}\right]/\left(\Omega+\Lambda_1\right)} \tag{2.37}$$

Therefore the total scintillation index for coherent optical beam is

$$\sigma_I^2(D)=\exp\left[\sigma_{\ln,x}^2(D)+\sigma_{\ln,y}(D)\right]-1 \tag{2.38}$$

2.14 Scintillation Index Model for Partially Coherent Beam

If a coherent beam passing through diffuser, the phase and amplitude between two random points in an optical beam wander by significant amount such that the correlation between them partially decreases define as partially coherent beam [44-46].

In this section we calculate the scintillation index caused by the combination of diffuser and atmospheric turbulence under weak and moderate to strong conditions with arrangement shown in Fig 2.14.1

In the presence of atmospheric effect, we need to take into account some scattering properties caused by the diffuser. Now speckle cells associated with diffuser acts as scattering center with the spatial correlation radius 'l_c' (cell size) of the diffuser surface produces a separate beam coherence center within the original beam source diameter. Hence, the diffuser acts as an array of independent scattering centers. The number of scattering centers is given by,

$$N_S = 1 + \frac{2w_0^2}{l_c^2} \quad (2.39)$$

The effect of diffuser on a optical beam at the receiver is characterized by replacing standard beam parameter Θ_1, Λ_1 by effective beam parameter $\Theta_{ed}, \Lambda_{ed}$ define in term of N_s as follows

$$\Lambda_{eff} = \frac{\Lambda_0 N_S}{\Theta_0^2 + \Lambda_0^2 N_S} \quad \text{and} \quad \Theta_{eff} = \frac{\Theta_0}{\Theta_0^2 + \Lambda_0^2 N_S} \qquad (2.40)$$

Expressions for partially coherent beam are derived as same as coherent beam equations except the input beam parameters are change due to diffuser located at the transmitter side with different diffuser correlation length lc= 0.1,0.001 .

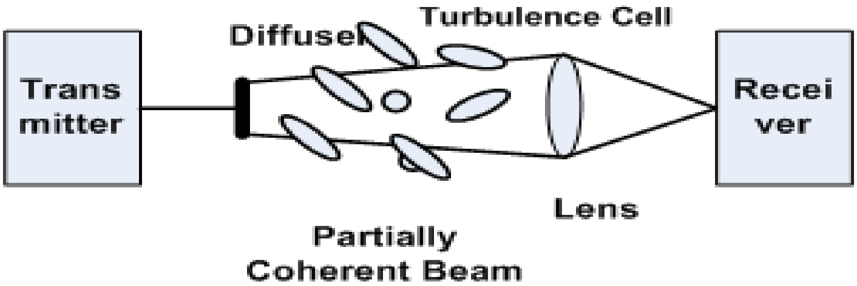

Fig. 2.14.1 : Model of partially coherent beam

Now for point receiver (D≈0) the output at atmospheric transfer box using the Kolmogorov spectrum and standard extended Rytov theory , the on axis scintillation index for weak turbulence (inner scale l=0, Outer scale L=∞) is given by

$$\sigma^2_{I,w} = 3.86\sigma^2 \left\{ \begin{matrix} 0.4\left[\left(1+2\Theta_{eff}(L)\right)^2 + 4(\Lambda_{eff}(L))^2\right]^{5/12} \\ \cos\left[\frac{5}{6}\tan^{-1}\left(\frac{1+2\Theta_{eff}(L)}{2\Lambda_{eff}(L)}\right)\right] \\ -\frac{11}{6}(\Lambda(L))^{5/6} \end{matrix} \right\} \tag{2.41}$$

Where, σ^2 indicate the strength of irradiance fluctuations and proportional to Rytov variance as $\sigma^2_R = 1.23C^2_n k^{7/6} L^{11/6}$

For weak fluctuation, it is less than 1 and for strong fluctuation it is greater than 1. C^2_n is the refractive index structure constant that characterizes the strength of the index of refraction fluctuations. For moderate to strong turbulence scintillation index is

$$\sigma^2_{I,s} = \exp\left\{ \frac{0.49\sigma^2_{I,w}}{\left[1+0.56\left(1+\Theta_{eff}\right)\sigma^{\frac{12}{5}}_{I,w}\right]^{\frac{7}{6}}} + \frac{0.51\sigma^2_{I,w}}{\left(1+0.69\sigma^{12/5}_{I,w}\right)^{\frac{5}{6}}} \right\} - 1 \tag{2.42}$$

Now, let us define scintillation index for receiver detector having lens diameter ‘D’. For that we assume Ω is the normalized receiver aperture define as

$$\Omega = \frac{2L}{kW^2_G} \text{ where , } W^2_G \text{ is the Gaussian lens radius.}$$

Log irradiance due to large scale eddies is given as

$$\sigma_{\mathrm{Pln,x}}^2(D)=\frac{0.49\left(\frac{\Omega-\Lambda_{\mathrm{eff}}}{\Omega+\Lambda_{\mathrm{eff}}}\right)\sigma_{\mathrm{PI,s}}^2}{\left[1+\frac{0.4\left(2-\bar{\Theta}_{\mathrm{eff}}\right)\left(\frac{\sigma_{\mathrm{PI,s}}}{\sigma}\right)^{\frac{12}{7}}}{\left(\Omega+\Lambda_{\mathrm{eff}}\right)\left(\frac{1}{3}-\frac{1}{2}\bar{\Theta}_{\mathrm{eff}}+\frac{1}{5}\bar{\Theta}_{\mathrm{eff}}^2\right)^{\frac{6}{7}}+0.56\left(1+\Theta_1\right)\sigma_{\mathrm{I,s}}^{\frac{12}{5}}}\right]^{\frac{7}{6}}} \tag{2.43}$$

& Log irradiance due to small scale eddies is given as

$$\sigma_{\mathrm{Pln,y}}^2(D)=\frac{\left(0.51\sigma_{\mathrm{PI,s}}^2\right)/\left(1+0.69\sigma_{\mathrm{PI,w}}^{\frac{12}{5}}\right)^{\frac{5}{6}}}{1+\left[1.20\left(\frac{\sigma}{\sigma_{\mathrm{PI,s}}}\right)^{\frac{12}{5}}+0.83\sigma^{\frac{12}{5}}\right]/\left(\Omega+\Lambda_{\mathrm{eff1}}\right)} \tag{2.44}$$

Therefore the total scintillation index is given by

$$\sigma_{\mathrm{P,I}}^2(D)=\exp\left[\sigma_{\mathrm{Pln,x}}^2(D)+\sigma_{\mathrm{Pln,y}}^2(D)\right]-1 \tag{2.45}$$

2.15 Signal to Noise Ratio and Bit Error Rate

In almost every area of measurements, the ultimate limit to detect-ability of a weak signal is set by noise or unwanted signals that obscure the desired signal. The same is true for free-space laser communications systems where the shot noise, background noise and thermal noise contribute to the total noise at the receiver [47]. The goal of a laser-com system for digital communication is to transmit the maximum number of bits per second over the maximum possible range with the fewest errors. Electrical data signals are converted to optical signals via a modulator. A "1" is transmitted as a pulse of light while a "0" has no light output. [48-50]

The number of "1's" and "O's" transmitted per second determines the speed of the link (bit rate). At the receiving end of the link, the optical signal is detected by an optical-to-electrical converter (e.g., a photo detector). A decision circuit then identifies the "1's" and "O's" in the signal, and thus recovers the information sent.

For digital communication system, information is sent over an optical link as digital symbols. This is accompanied by encoding the source information into binary symbols (bits) and transmitting the bits as some type of coded optical field, for example, by encoding on a bit-by-bit basis (binary encoding). Each bit is then sent individually by transmitting one of two optical fields to represent each bit. [51-52] We will consider only direct detection (DD) system in which the standard binary procedure is to pulse an optical source (e.g., a laser source) on or off depending on data bit. This encoding is referred to as on-off keying (OOK). At the receiver OOK decoding is based on a decision as to whether the pulse slot time has high enough field energy or not. The selected threshold determines the best performance in decoding the correct signal with the lowest probability of making a bit decision error and thus the bit error rate (BER) can be obtained. First, we define the output SNR in the absence of optical turbulence by the ratio of the detector signal current i_s to the root-mean-square (rms) noise current- σ_N, which yields

$$SNR_0 = \frac{i_s}{\sigma_N} = \sqrt{\frac{\eta P_s}{2hvB}}, \qquad i_s = \frac{\eta e P_s}{hv} \tag{2.46}$$

where , i_s - is signal current , P_s is the signal power in watts , B - filter bandwidth , η is the detector quantum efficiency in electrons/photon , e is electric charge in coulombs , h is the Planck's constant ($h = 6.63 * 10^{-34}$ joule-second) and v is optical frequency in hertz .

We use the most basic form of pulse modulation is on–off keying (OOK). Each bit symbol is transmitted by pulsing the source either on or off during each bit interval. Because of random noise, a transmitted 0 may be mistaken for a 1, which is denoted by $\Pr(1/0)$, and 1 may be mistaken for a 0, denoted by $\Pr(0/1)$. Assuming each symbol is equally likely to be sent, the BER is given by. [53]

$$\Pr(E) = \frac{1}{2}\Pr\left(\frac{1}{0}\right) + \frac{1}{2}\Pr\left(\frac{0}{1}\right) = \frac{1}{2}\operatorname{erfc}\left(\frac{SNR_0}{2\sqrt{2}}\right) \tag{2.47}$$

In the presence of atmospheric turbulence, the received signal exhibits additional power losses (refraction, diffraction [54-55] and random irradiance fluctuations. The output current from the detector is given by

$i = i_S + i_N$ and the variance

$$\sigma_{SN}^2 = \left\langle i_S^2 \right\rangle - \left\langle i_S \right\rangle^2 + \left\langle i_N^2 \right\rangle$$

$$= \left(\frac{\eta e}{hv}\right)^2 \left\langle \Delta P_S^2 \right\rangle + \frac{2\eta e^2 B \left\langle P_S \right\rangle}{hv} \tag{2.48}$$

Where ΔP_S – represents power fluctuations in the signal.

SNR at the output of the detector

$$\left\langle SNR \right\rangle = \frac{\left\langle i_S \right\rangle}{\sigma_{SN}} = \frac{\left\langle P_S \right\rangle}{\sqrt{\left\langle \Delta P_S^2 \right\rangle + \frac{2hvB\left\langle P_S \right\rangle}{\eta}}}$$

Rearranged as,

$$\left\langle SNR \right\rangle = \frac{SNR_0}{\sqrt{\left(\frac{Pso}{\left\langle Ps \right\rangle}\right) + \sigma_I^2\left(D\right) SNR_0^2}} \tag{2.49}$$

Where Pso is the signal power in the absence of atmospheric effects and $\sigma_I^2(D)$ is the irradiance flux variance on the photo detector. Angle bracket $\langle\ \rangle$ represent mean.

The power ratio $\frac{Pso}{\left\langle Ps \right\rangle}$ in above equation provides a measure of SNR deterioration caused by atmospheric induced beam spreading given by

$$\frac{Pso}{\langle Ps \rangle} = 1 + 1.63\sigma_R^{\frac{12}{5}} \Lambda_1 \tag{2.50}$$

In the presence of optical turbulence, the probability of error is given by

$$\Pr(E) = \langle BER \rangle = \frac{1}{2}\int_0^\infty p_I(u)\,\mathrm{erfc}\left(\frac{\langle SNR \rangle u}{2\sqrt{2}}\right)du \tag{2.51}$$

Where $p_I(u)$ is a gamma-gamma distribution with unit mean

$$p_I(u) = \frac{2(\alpha\beta)^{(\alpha+\beta)/2}}{\Gamma(\alpha)\Gamma(\beta)} u^{\frac{(\alpha+\beta)}{2}-1} K_{\alpha-\beta}\left(2\sqrt{\alpha\beta u}\right) \text{(for u>0)} \tag{2.52}$$

When aperture averaging effects are consider, parameters α and β for the gamma-gamma PDF are define as

$$\alpha = \frac{1}{\exp\left[\sigma_{\ln X}^2(D)\right] - 1},$$

$$\beta = \frac{1}{\exp\left[\sigma_{\ln Y}^2(D\ )\right] - 1} \tag{2.53}$$

2.16 Multipath Impulse response for laboratory generated free space optical channel.

Impulse response equation for No turbulence.

Source and Receiver Model:

Following G. feller [56] we model a optical source using a generalized Lambertain radiation pattern (fig 2.16.1) having uniaxial symmetry (independent of θ) denoted as $R(\emptyset,\theta)$ and define as the optical power per unit solid angle emitted from the source at position $(\emptyset,\theta)$.

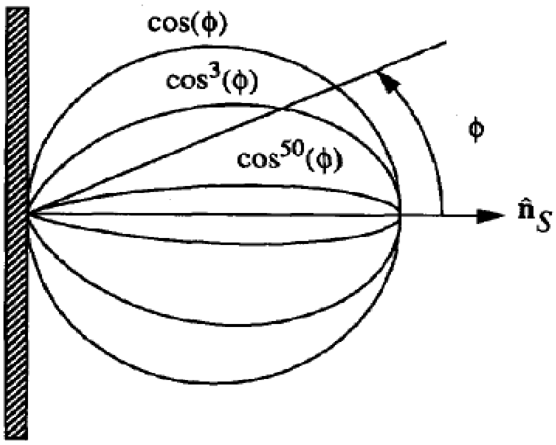

Fig 2.16.1. : **Generalized lambertain pattern**

$$R(\phi) = \frac{\eta+1}{2\pi} P_s cos^n(\phi), \text{ for } \phi \in \left(-\frac{\pi}{2}, \frac{\pi}{2}\right) \quad (2.54)$$

Here n is the mode number of the radiation lobe which specifies the directionality of the source.

The coefficient ($\frac{\eta+1}{2\pi}$)ensures that integrating $R(\emptyset)$ over the surface of a hemisphere results in the source power *Ps*. A mode of η = 1 corresponds to a traditional Lambertian source.

A point source S that emits a unit impulse of optical intensity at time zero is denoted by

$$S = \{r_s, \hat{\eta}_S, \eta\} \quad (2.55)$$

Where, $r_s$issource position, $\hat{\eta}_S$ is its orientation, and η in its mode number.

Similarly, a receiving element R with position, r_R , orientation $\hat{\eta}_R$,area $A_R$and field of view FOV will be denoted by

$$R = \{r_R, \hat{\eta}_R, A_R, FOV\} \quad (2.56)$$

The scalar angle FOV is defined such that a receiver only detects light whose angle of incidence (with respect to detector normal$\hat{\eta}_R$) is less than FOV. A limited field of view may be an inadvertent effects of detector packaging or it may be use intentionally to reduce unwanted reflection or noise.

Reflector Model

We make the simplifying assumption that all multiple reflectors are purely ideal Lambertian. The radiation intensity pattern R(∅) emitted by a differential element of an ideal reflector is dependent on the angle of the incident light. To model the reflection from a differential reflecting element with area dA and reflectivity ρ, first consider the element as a receiver with area dA and calculate the power dP it receives. Second, model the differential reflector as a source with total power P = ρdP and an ideal Lambertian radiation intensity pattern, as given by (2.54) with $n = 1$.

Line-of-Sight Impulse Response

Consider a source S and receiver *R*, as specified by (2.55) and (2.56), in an environment with no reflectors (Fig.2.16.2). If the distance *R* between a transmitter and receiver is large relative to the detector size, so that $R^2 >> A_R$, then the received irradiance is approximately constant over the surface of the detector. Furthermore, all of the signal energy will arrive at the receiver at approximately the same time. Thus, the impulse response for this simple system is approximately a delayed Dirac delta function

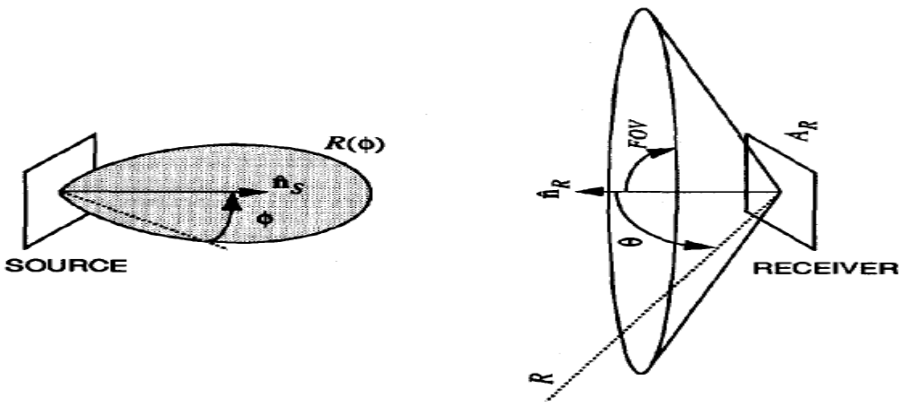

Fig.2.16.2 : Arrangement of source and detector without reflectors

$$h^{(0)}(t: s, R) \approx \frac{n+1}{2\pi} . cos^n(\emptyset) d\Omega rect\left(\frac{\theta}{FOV}\right) \delta\left(t - \frac{R}{c}\right) \quad (2.57)$$

Where,

$d\Omega$ is the solid angle subtended by receiver differential area

(assuming $A_R \ll R^2$)

$$d\Omega = cos(\theta)A_R/R^2 \tag{2.58}$$

R is the distance between the source and receiver

$$R = \|r_s - r_R\| \tag{2.59}$$

θ is the angle between $\widehat{n_R}$ and $r_s - r_R$

$$\cos(\theta)=\widehat{n_R}.r_s - r_R/R \tag{2.60}$$

$\emptyset$is the angle between $\widehat{n_s}.r_s - r_R/R$

The rectangular function is define by

$$rect(x) = \begin{cases} 1 & for|x| \le 1 \\ 0 & for|x| > 1 \end{cases} \tag{2.61}$$

A multiple bounce impulse response for proposed laboratory generated free space optical channel as shown in fig.2.16..3 .

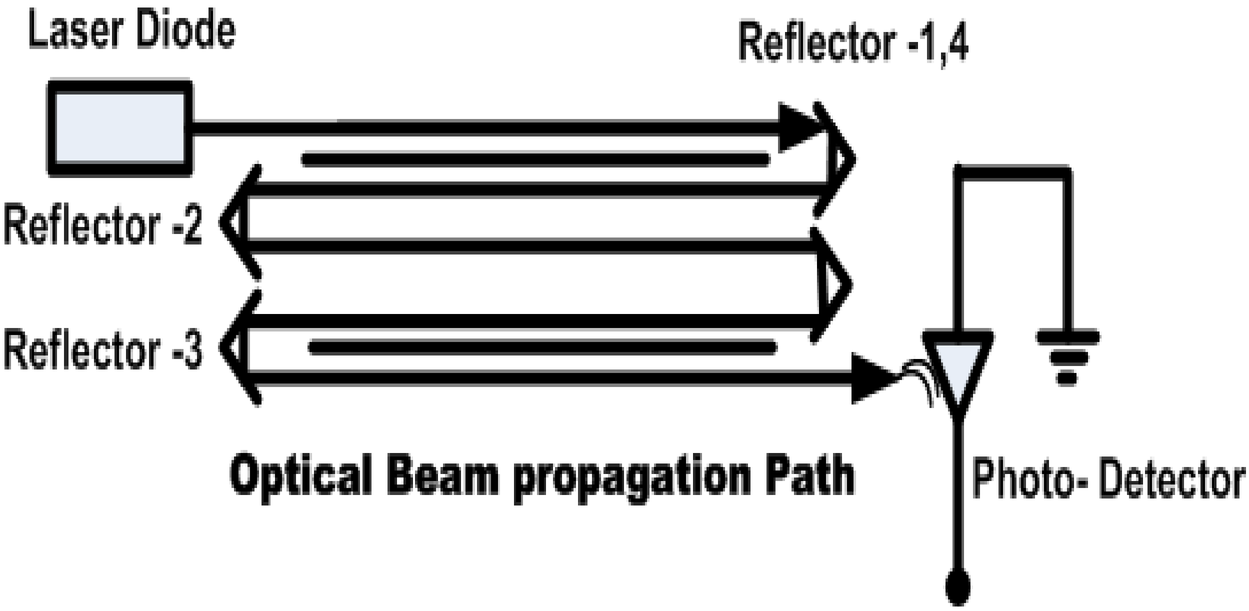

Fig. 2.16.3 : Laboratory generated free space optical channel

Given a optical source S and receiver R in a room with total 4 reflectors, optical beam from the source can reach the receiver after 8 of reflection (two from each reflector). Therefore impulse response can written as

$$h(t; S, R) = \sum_{k=0}^{8} h^{(k)}(t; S, R) \tag{2.62}$$

where,

$h^{(k)}(t)$ is the response of the light undergoing exactly 8 reflection ($k = 8$) and can be calculated as [57]

$$h(t;S,R) = \int_S h^{(0)}\left(t;,S,\left\{r,\hat{n},\frac{\pi}{2},d_r^2\right\}\right) \otimes h^{(k-1)}(t;\{r,\hat{n},1\},R) \qquad (2.63)$$

where the symbol $\otimes$ denotes convolution.

Substituting $h^{(0)}$ from equation (2.57) and performing convolution we get

$$h(t;S,R) = \frac{n+1}{2\pi}\int_S \frac{\rho_{r}\cos^{n}(\emptyset)\cos(\theta)}{R^2}\, rect\left(\frac{2\theta}{\pi}\right) h^{(k-1)}\left(t-\frac{R}{c};\{r,\hat{n},1\},R\right) d_r^2 \qquad (2.64)$$

Equation (2.63) can be calculated numerically by multiplying small reflecting surface of each reflector with area ΔA . Thus $h^{(k)}(t)$can be approximated by

$$h(t;S,R) = \frac{n+1}{2\pi}\sum_{k=1}^{8} \frac{\rho_{r}\cos^{n}(\emptyset)\cos(\theta)}{R^2}\, rect\left(\frac{2\theta}{\pi}\right) h^{(k-1)}\left(t-\frac{R}{c};\{r,\hat{n},1\},R\right) d_r^2 \qquad (2.65)$$

where ,

$\hat{n}$- is the normal to the surface S at position r, ρ_r-is the reflectivity at position r, R-Distance between source and detector.

Impulse response equation with turbulence.

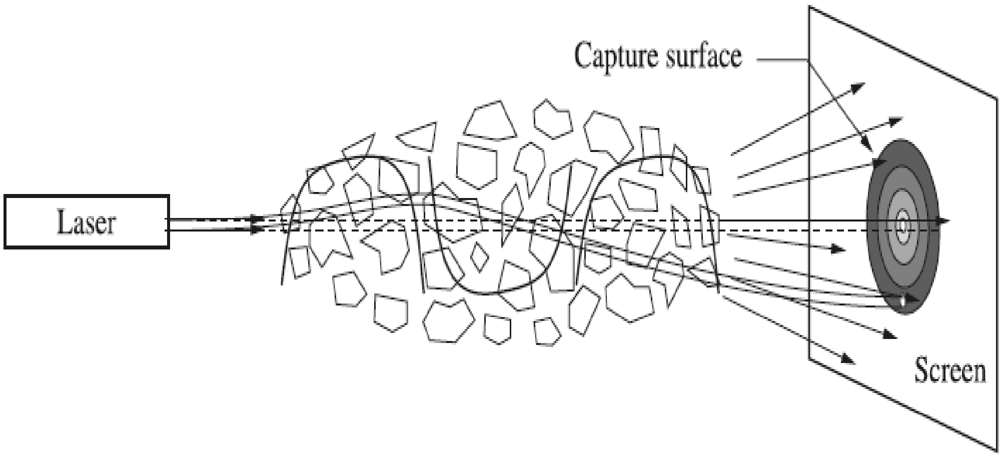

Fig. 2.16.4 :Effect of atmospheric turbulence on laser beam propagation

In order to evaluate the temporal spreading of the very short transmitted pulse, we need to know the transfer function characteristics of the atmospheric channel as shown in Fig.2.16.4 . This transfer function can actually be obtained from the convolution of $G_1\left(t-\frac{z}{c}\right)$with $G_2\left(t-\frac{z}{c}\right)$, where $G_1\left(t-\frac{z}{c}\right)$corresponds to the high-frequency component of the transfer function , and $G_2\left(t-\frac{z}{c}\right)$ corresponds to the low-frequency component. The reason for the separation of the G function into these two components comes from the fact that the output pulse can be expressed in terms of the two-frequency mutual coherence function (MCF), r, given by Ishimaru [58] The impulse response function of the random medium and the MCF is related by

r = r(ω_1, ω_2), where ω_1, ω_2 are low and high frequency component

The impulse response function of the random medium and MCF is related by

$$G(t-t') = \frac{1}{2\pi}\int_{-\infty}^{\infty} \mathrm{r}(\omega_d)\, e^{-i\omega_d(t-t^{-})} d\omega_d \tag{2.66}$$

Where ω_d represents the difference between angular frequency ω_1, ω_2

The instantaneous output power resulting from a given input pulse $P_i(t)$ is

$$P_o(t) = \int_{-\infty}^{\infty} P_i(t')\; G(t-t') d_t{}' \tag{2.67}$$

The impulse response along z direction is given by

$$G\left(t-\frac{z}{c}\right) = G_1\left(t-\frac{z}{c}\right) \otimes G_2\left(t-\frac{z}{c}\right) = \int_{-\infty}^{\infty} \quad G_1\left(t-\frac{z}{c}-t'\right) G_2(t') d_t{}' \tag{2.68}$$

Where,

$$G_1\left(t-\frac{z}{c}\right) = \frac{\pi}{4T_1}\sum_{n=0}^{\infty}(-1)^n(2n+1)exp\left\{-(2n+1)^2\frac{\pi^2}{16}\frac{\left(t-\frac{z}{c}\right)}{\pi}\right\}$$

$$T_1 = \left(\frac{1}{1.28c}\right) C_n^{\frac{12}{5}} k_0^{\frac{2}{5}} L^{\frac{11}{5}}$$

L is the propagation length with turbulence, $k_0 = \frac{2\pi}{\lambda}$ is the wave number of optical signal.

$$G_2\left(t-\frac{z}{c}\right) = \frac{1}{\sqrt{\pi T_2}} exp\left\{-\frac{\left(t-\frac{z}{c}\right)}{T_2^2}\right\}$$

Where $T_2 = \frac{1}{c}\ 1.2050 C_n L_0^{\frac{5}{6}} L^{\frac{1}{2}}$

L_0 is the outer scale size of turbulence. The parameters T_1 and T_2 were calculated for a given turbulence strength.2

2.17 Conclusion

A review of free space broadband optical communication systems is presented. The recent development in technology of optical sources such as laser and LED shows benefits of use of alternative communication systems. A line of sight terrestrial laser optical link has been discussed which is used for high speed data rate up to 2.5 Gbps for distances of up to 1km. White light LED is likely to be next generation of lamps due to high brightness, reliability, low consumption and long life span. An indoor optical wireless duplex channel communication system, as an access to the internet to different computer terminal has been discussed as a replacement of Wi-Fi or Wi-max technology. This chapter also presented an overview of the key turbulence theory that will be used throughout this dissertation. It also includes efficient computational techniques and correlation functions that are important in assessing the effects of turbulence in weak and strong conditions. The expressions for attenuation due to rain, fog and scintillation losses are given to identify the link parameters to improve overall performance. A fundamental analysis for visible light communication system using LED lights for indoor optical propagation channel is given in chapter 5. Statistical estimation and computation of communication parameters presented in this chapter will be useful in designing and optimizing laser-com systems performances that are consistent under all weather conditions.

References

[1] Davis C.C. "Fiber optic Technology and its role in the information revolution". Research paper, A James Clark school of engineering,davis/optfib.html. Accessed on May 2012.

[2] Henniger,H. and Wilfert O. "An introduction to free-space optical communications", Journal of Radio Engineering, Vol. 19. No 12. PP 203-212, 2010.

[3] Murat Uysal."Optical wireless communication an emerging technology" Springer International publication, Switzerland , 2016.

[4] Hemmati H., "Deep space communication", Wiley Inter Science Publication, 2006.

[5] Bates D.R., "Rayleigh scattering by air", Planetary space science, Vol. 32, PP 875-790. 1998 .

[6] Goodwin F. E.," A review of operational laser communication systems", Proceedings of IEEE, 58, PP 1746-1752.1994.

[7] Gagliardi R. M. and Karp S."Optical communication", John Wiley publication, 1995.

[8] Gowar J."Optical communication systems", Prentice Hall Publication , 1993.

[9] Jeganathan M. and Ionov,"Multi-gigabits per second optical wireless communication", White papers, www. freespaceoptics.com, Optical Crossing Accessed on June 2013.

[10] Kazaura K, Suzuki K." Performance evaluation of next generation free space optical communication system ", IEICE Transaction of Electronics,Vol. E90-C, PP 381-388, 2007

[11] Killinger D. "Free space optics for laser communication through the air", Optics and photonic news, PP 36-42,2002.

[12] Pratt W. K."Laser Communication Systems", John Wiley and Sons, 1969.

[13] Willebrand H. and Ghuman B.S." Free Space Optics: Enabling Optical Connectivity in today's N/W ", Indiana-pols, SAMS Publishing, 2002

[14] Light-points white paper series 2009: light point, Accessed on May 2010.

[15] Borah Deva K,"A review of communication-oriented optical wireless systems",EURASIP Journal on Wireless Communications and Networking,Sringer,pp.1-28,2012

[16] Mansour A., R. Mesleh, and M. Abaza, "New challenges in wireless and free space optical communications," Opt. Lasers Eng., vol. 89, pp. 95–108, 2017.

[17] Sachin M, Asim Kar "Development of a FSO link to connect institute LAN" , Proceeding of National Conference on Wireless Communication And Its Social Need (WCSN-2010) , Institution of Engineer, Kolkata, pp:25-27, January 07-08, 2010.

[18] Larry C. Andrews , Ronald L. Phillips ,"Laser beam propagation through random media", II Ed SPIE press ,USA, 2005

[19] Fante R.W.," Electromagnetic beam propagation in turbulent media", Proc IEEE , vol.63 pp.1669-1692.1975.

[20] Sengupta M. K., D. Nandini, "A comparative study of scintillation Analysis over Two Line -of-Sight Paths at 6.7 Ghz and 7.6 GHz," IEEE Transaction Antenna propagations, vol -3, no. 4, pp. 620–624, 1983.

[21] Lawrence R. S. and Strohbehn J. W., "A Survey of Clear-Air Propagation Effects Relevant to Optical Communications," proceeding IEEE, vol. 58, no. 10, 1970.

[22] Dabberdt W. F. and Johnson W. B., "Analysis of Multi wavelength Observations of Optical Scintillation," Applied Optics, vol. 12, no. 7, pp. 1544–1548, 1973.

[23] Berman G. P., Bishop A. R., Chernobrod B. M., Nguyen D. C., and Gorshkov V. N., "Suppression of intensity fluctuations in free space high-speed optical communication", Optics communication, pp 264-270, 2007.

[24] Buck A. L., "Effects of the Atmosphere on Laser Beam Propagation," Applied Optics, vol. 6, no. 4, pp. 703–708, 1967.

[25] Andrews L.C. and Phillips L.R.," Laser Beam Propagation through Random Medium", Second Edition, SPIE Press, Bellingham, Washington, USA,2005

[26] Andrews, L.C., Phillips, R.L. and Hopen, C.Y. "Aperture averaging of optical scintillations: power fluctuations and the temporal spectrum", Waves in Random and complex media, Vol. 10. Issue 1, pp 53-70, 2000.

[27] Henniger H. and Wilfert, O.,"An introduction to free-space optical communications", Journal of Radio Engineering , Vol. 19. No 12. pp 203-212, 2010.

[28] Zhu X. and Kahn J. M., "Free-Space Optical Communication Through Atmospheric Turbulence Channels," IEEE Trans. Communication, vol. 50, no. 8, pp. 1293–1300, 2002.

[29] Andrews L.C., Phillips R.L., Hopen C.Y. and Al-Habash, M.A. ,"Theory of optical scintillation', Journal of Opt. Soc. of America, Vol. 16, No. 6. Pp. 1417-1429, 1999.

[30] Andrews L.C., Phillips L.R. and Hopen, C.Y. ," Laser Scintillation with Applications", SPIE Press, Bellingham, Washington, USA, 2001.

[31] Ghassemlooy Z., W. O. Popoola, E. Leitgeb, and E. Building, "Free-Space Optical Communication Using Subcarrier Modulation in Gamma-Gamma Atmospheric Turbulence," Ict. 2007, vol. 01, pp. 156–160, 2007.

[32] Muhammad S. S., Köhldorfer P., and Leitgeb E., "Channel Modeling for Terrestrial Free Space Optical Links," Ict. 2005, no. 05, pp. 407–410, 2005.

[33] Perlot N., "Turbulence-induced probability in coherent optical communication through the atmosphere," Applied Optics, vol. 46, no. 29, pp. 7218–7226, 2007.

[34] Kiasaleh K., "Scintillation index of a multi-wavelength beam in turbulent atmosphere," Journal of Optical Society of America., vol. 21, no. 8, pp. 1452–1454, 2004.

[35] Goodman, J.W. ,"Statistical Properties of Laser Speckle Patterns in Laser Speckle and Related Phenomena, Springer-Verlag, Berlin,1999.

[36] Rui-Zhong, "Scintillation Index of Optical wave propagating in turbulent atmosphere," Chinese Phys., vol. 18, no. 2, pp. 581–587, 2009.

[37] Lee I. E., Z. Ghassemlooy W. P. Ng, and S. Rajbhandari, "Fundamental Analysis of Hybrid Free Space Optical and Radio Frequency Communication Systems," PG Net, pp. 342–348, 2011.

[38] Gaussian C., Tem C., "Gaussian Beam Propagation," www.mellesgriot.com, pp. 2–5. Accessed on May 2012.

[39] Prokes A., "Atmospheric effects on availability of free space optics systems," Opt. Eng., vol. 48, no.-4,pp. 1–10, June-2009.

[40] Nadeem F. , Leitgeb E., Koudelka O., Javornic T.. Kandus G.," Comparing the rain effects on hybrid network using optical wireless and GHz links". IEEE International Conference on Emerging Technologies, 2008

[41] Taylor C. A., "Two-Beam Interference with Partially Coherent Light," Journal of Optical society America, vol. 47, no. 10, pp. 895–902, 1957.

[42] "Atmospheric propagation effects relevant to optical communication," TDA Progressive Report, vol. 6, no. 1988, pp. 180–190, 1988..

[43] Leeb W. R., "Degradation of signal to noise ratio in optical free space data links due to background illumination," Applied Optics ,vol. 28, no. 15, pp. 3443–3449, 1989.

[44] Lee E. J., Member S., and Chan V. W. S., "Part 1: Optical Communication Over the Clear Turbulent Atmospheric Channel Using Diversity," IEEE Journal Selected areas in Communication, vol. 22, no. 9, pp. 1896–1906, 2004.

[45] Webb W. E. and Marino J. T., "Threshold detection in an on-off binary communications channel with atmospheric scintillation," Applied Optics, vol. 14, no. 6, pp. 1413–1417, 1975.

[46] Bara J. and Rubio J. A., "Averaging of collected- power fluctuations by a multiaperture receiver system ," Socity of Photo-Optical Instrum. Eng., vol. 35, no. 10, pp. 2775–2778, 1996.

[47] Applicata O., "Performance analysis of bit error rate for free space optical communication with tip-tilt compensation based on gamma – gamma distribution," Applied Optics., vol. 4, no. 3, pp. 1–13, 2009. based on spectral encoding of a partially coherent beam," Opt. Commun., vol. 280, pp. 264–270, 2007.

[48] Kim I. I., Mcarthur B., Korevaar E., R. Street, and S. Diego, "Comparison of laser beam propagation at 785 nm and 1550 nm in fog and haze for optical wireless communications," Optical Access Communcation,vol-1, 2000.

[49] Tiffany J. L., A. L. F. S. O. Systems, and U. Im, "Achievable Information Rate for Outdoor Free Space Optical Communication with Intensity Modulation and Direct Detection," Globecom IEEE, pp. 2654–2658, 2003.

[50] Tsiftsis T. A., Sandalidis H. G., Karagiannidis G. K., and S. Member, "Optical Wireless Links with Spatial Diversity over Strong Atmospheric Turbulence Channels," IEEE Trans. Wirel. Commun., vol. 8, no. 2, pp. 951–957, 2009.

[51] Weyrauch, T. and Vorontso, M.A. ,"Free-Space Laser Communications With Adaptive Optics Atmospheric Compensation Experiments", Journal of optical and fiber communication research ,Vol-1, No-4, pp 355-379,2004.

[52] Zeinab, H. and Fadlullah J. "MIMO Free space optical communication in turbid and turbulent atmosphere", Journal of Communications, Vol. 4, No. 8. pp 524-532, 2009

[53] Djordjevic I. B., "LDPC-coded MIMO optical communication over the atmospheric turbulence channel using Q -ary pulse-position modulation," Opt. Express, vol. 15, no. 16, pp. 10026–10032, 2007.

[54] Ghassemlooy Z., Popoola ,"Optical Wireless Communications: System and Channel Modelling with Matlab". CRC Press, Boca Raton, 2013

[55] Sachin M Kale, Asim Kar "A Study on the Atmospheric Effects on Optical Wireless Link for Short Haul Communication", Proceeding National Conference on Advances in Wireless Cellular Telecommunication: Technologies & Services. ICEIT 2011, Delhi, India, pp:25-31, 14-15 April 2011.

[56] Gfeller F.R. , H.R. Muller and P. Veitiger," Infrared communication for in-house aodications." IEEE COMPCON Proc. Washinpton, D.C., PP 132-138. 1978.

[57] John R. Barry, Joseph M. Kahn, William J. Krause, Edward A. Lee, and David G. Messerschmitt ,"Simulation of Multipath Impulse Response for Indoor Wireless Optical Channels", Journal on Selected Areas in Communication, vol.11,no. 3, 1993

[58] Akira Ishimaru, Wave Propagation and Scattering in Random Media, Vol. 1-2, Academic Press, Inc., 1978.

CHAPTER 3

Design and Construction of an Atmospheric Turbulence set up for Studying Scintillation Effects on a Multipath Optical Beam

3.1 Introduction

This chapter presents the design and development of (i) mechanical mounts for optical systems, (ii) electro-optical measurement systems and (iii) computer controlled systems for generation of atmospheric turbulence in laboratory environment to test reliability and availability of optical channel. The system has been designed to create scintillation effects on a propagating optical field and measure the corresponding Rytov variance from the statistical measurement data under weak turbulence. The set up could produce weak to moderate turbulence in atmosphere surrounding the region of the travelling paths of the optical beam.

The propagating optical field was a digitally modulated optical carrier traveling through the artificially generated atmospheric turbulent medium [1-2]. The digital data were generated by a dedicated computer (PC). The PC generated the bit sequences in a standard format according to a program run within the computer for pseudo-random generation of bits. The serial data bits from the PC were ASK modulated by a sinusoidal carrier before feeding a stabilized laser diode driver circuit.

The optical ASK output from the laser diode was launched into the atmospheric turbulent medium using suitable lenses acting as transmitting antenna. The optical wave traversed the turbulent medium several times in a horizontal plane before reaching the aperture antenna of a photodiode receiver. From the source of light to the detector of light a folded-optic multiple optical ray paths were created using mirrors and prisms for producing prominent atmospheric scintillation effects on the traversing optical beam. Using closed loop feedback arrangements, the demodulated and turbulence affected data bits from the photodiode receiver were sent back to the PC for comparison of transmit and receive data using software program.

This procedure enabled us for instantaneous measurement of bit error rate (BER) performance of a digitally modulated optical carrier propagating through the turbulent medium. All the measurements were made under dynamic equilibrium conditions of air temperature and air flow rate through the use of a microcontroller based data acquisition system and control and multiple sensors mounted at desired locations. The overall automated system worked under the command signals generated by the PC. The MATLAB program supports were utilized to calculate the statistical parameters.

The laser diode sources, the photodiode detectors and associated electronic and photonic systems were specifically designed to study in detail the effects of atmospheric turbulence on the reliability and availability of the communication link. Since we have several different arrangements needed for the design of the overall system of measurements, we segregated the design aspects into two major groups.

The mechanical and optical systems required in the scintillation chamber are presented in section 3A while the design aspects of the electronic, photonic circuits and systems as well as the electronic control system for creating scintillation are presented in section 3B. Thus our overall system is a closed loop system for practical measurement of the performance characteristics of our free-space optical communication link. The schematic diagram of the atmospheric turbulence set up is shown below in Fig. 3.1.1 and described in proceeding section 3A.

Section 3A

Mechanical System Design

3.1 The Prototype laboratory Set up for Studies of the Effect of Atmospheric Turbulence on a Propagating Multiple Path Coherent Optical Beam .

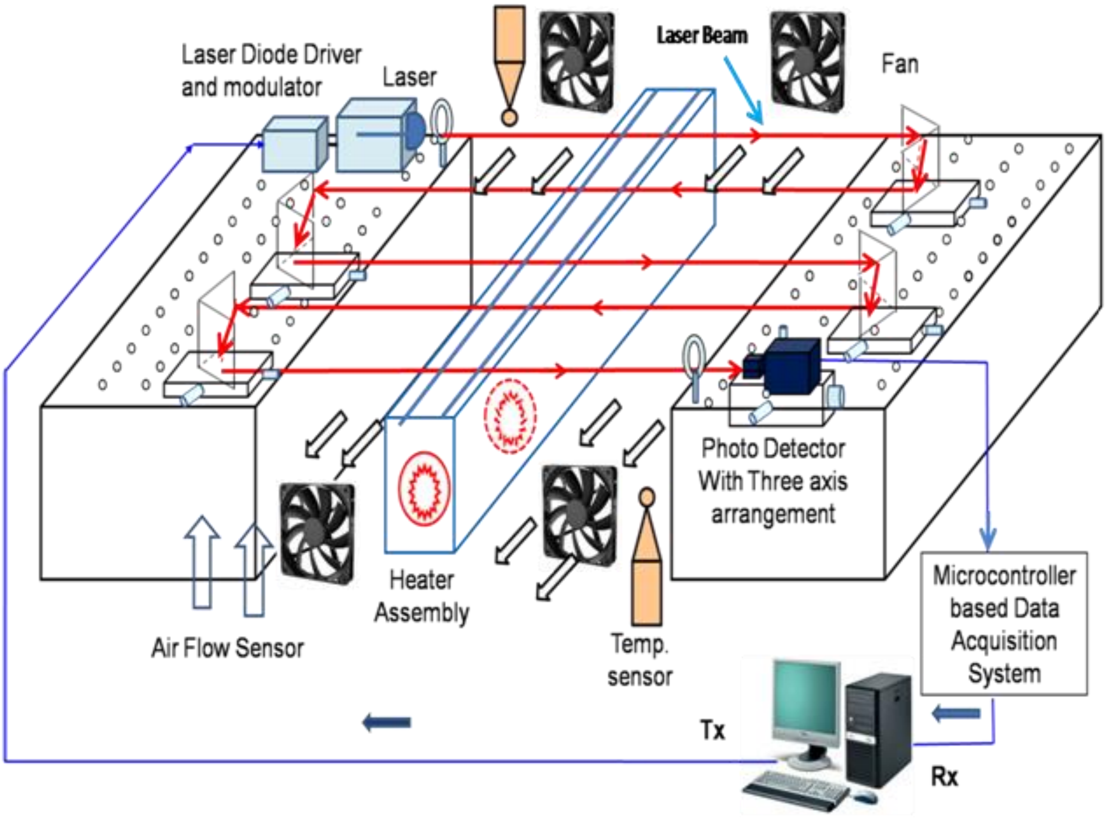

Fig. 3.1.1: Schematic diagram of the design of a laboratory set up for studying scintillation effects on a propagating optical beam in a turbulent medium

Fig.3.1.1 is the schematic diagram of the laboratory type atmospheric turbulence generator designed and developed in our laboratory for studying the atmospheric scintillation effects due to turbulence created by heating and cooling of air in a localized region. Electrical heaters, electric fans and coolers were mounted at appropriate locations with facilities for adjustments of air-flow velocity, air-temperature variations and directions of cold air flow. Flow and temperature of air at different locations were monitored using flow sensor and temperature sensors. The operation of the whole system is controlled by a personal computer and the data acquisition and control algorithms were implemented using a microcontroller PIC18F452. The PC was connected in a closed loop path as shown in Fig.3.1.1, supervising the total operation of the automated system for turbulence generation, control, measurement and finally determining the instantaneous effects of turbulence on the propagating optical beam. It is also dedicated for sending specific digital data bit patterns for modulation of the optical source and simultaneously receiving the corrupted bit patterns as obtained from the receiving photo-detector output.

Design of a Multiple Path Folded Optic System

In our laboratory set up for the transmission of laser beam through an artificially created turbulent medium, we designed and developed a multiple path folded optic system using lenses and high precision mirrors such that the overall optical path length would be longer. The coherent optical beam from a semiconductor laser transmitter traversed through an almost identical atmospheric turbulent medium multiple times until finally it reached the photo-detector receiving aperture mounted at the other end as shown in Fig.3.1.1 If the single optical path length is $\bar{n} \times \mathrm{l}$, then for N number of travel of the optical beam, the overall total optical path length (L) would be

$$\mathrm{L} = \{\textstyle\sum_{\mathrm{n}=0}^{\mathrm{N}}(\bar{\mathrm{n}})\}\mathrm{Nl} \qquad (3.1)$$

Where, $\bar{n}$ is the average value of the refractive index over a single optical path of the medium through which the optical beam traversed and l- is the single path length. Two high precision right angled glass optical mirrors with reflectivity R= 0.988 were mounted to produce 180^0 phase shift of incident optical beams at both ends of optical set up to produce multiple path travel of optical beam in turbulent medium. Collimating lenses were used just after the laser diode transmitter to produce a narrow and parallel optical beam at the transmitter end. All the optical components were mounted on vibration-isolation optical tables and high precision x-y-z positioners were used for alignment of axes of the folded-path optical beam.

The scintillation effect due to atmospheric turbulence is simulated by exploiting the dependence of the channel index of refraction on temperature variations. As shown in Fig 3.1.1 the optical beam is a straight path propagating above hot and cold surfaces.

When the optical beam is passing through a cooler region it experiences turbulence cells having different refractive indices causing variation in the optical beam incident angle. After propagating through this region optical beam enters into hotter region having different refractive indices causing beam fluctuation. The combined effect of cold and hot region with random wind velocity modulates laser beam and causes multipath propagation of optical beam while they arrive at the surface of photo-detector. The addition and subtraction of collected signals generate intensity fluctuation called scintillation. The amplitude and frequency of scintillation depends on the comparative size of the cells to the beam diameter [3-4]. The whole process is well defined in Fig 3.1.2

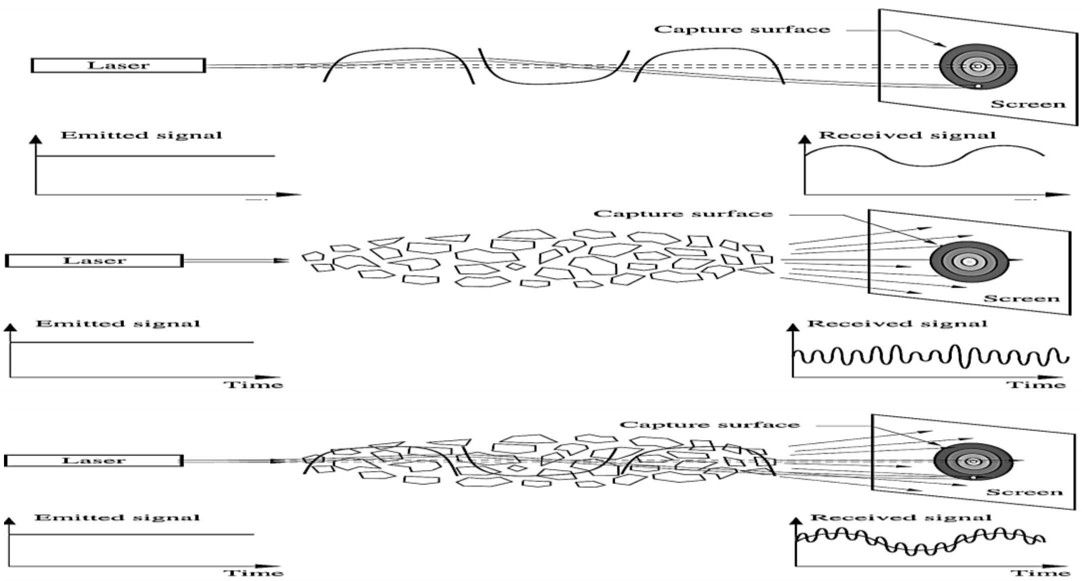

Fig. 3.1.2: Effects of various different sized turbulence cell on a laser beam propagation

3.2 Design of Laser Diode Mount

The visible wavelength and NIR semiconductor DH lasers used in this project were low cost TO-3 mount packaged devices [5]. All the lasers were single-mode lasers and had arrangements for temperature stabilization using thermoelectric cooler. At the room temperature of (25^0C) light-current (L-I) transfer characteristics and electrical I-V characteristics of the devices were supplied by the manufacturer of the devices. The devices had built-in backplane photodiode mounts for monitoring and stabilization of laser light intensity using feedback mechanisms. The room temperature threshold current of the lasers were less than 20 mA. We have used MQW 670 nm, 780 nm, and 1300 nm as well as 1550 nm DFB lasers manufactured by Philips, Hitachi and Mitshubishi which was purchased from china with financial assistance from Jadavpur University.

Fig.3.2.1 (a) **Fig.3.2.1(b)**

Fig.3.2.1 : Laser diode with holder and lens

In order to physically mount the laser on a vibration isolation optical table we used three-axis mechanical positioners for axial alignments of laser diode optical beam along a line-of-sight direction towards the photodiode receiver. We designed and fabricated a laser diode holder (Fig. 3.2.1 (a),(b)) using aluminum having an integral micro-optic lens for fine adjustments and collimation of laser diode optical beam. We used spherical ball lens of 2 mm diameter and focal length of 6 mm available as standard passive optical component in the market. The laser diodes had maximum optical power emission of 10 mW. Then, total 5 laser diode holders are suitably mounted on one plate, such that they can freely move from one position to another to maintain the space diversity among all laser diodes. The photographic view of the same is shown Fig. 3.2.2. The Multi-source holder plate with design specifications shown in fig.3.2.2(a) and Fig3.2.2(b) shows the assembled form of laser diode plate mount having area 15 inch X 15 inch. Total 5 holder are use to mount 5 laser diode. We use multi source mount for MIMO system.

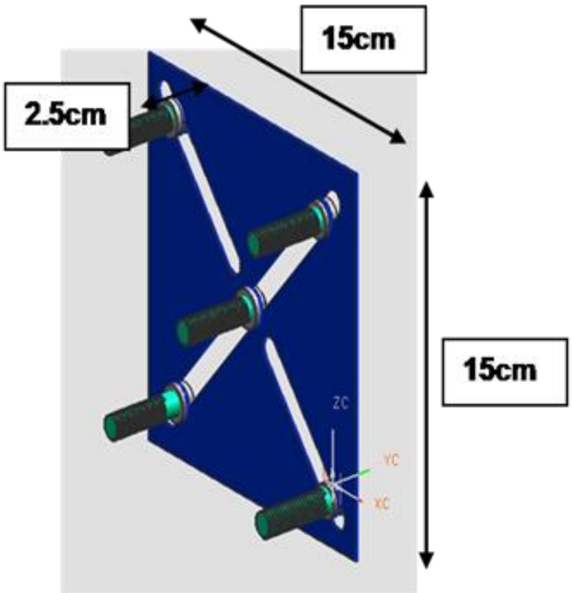

Fig 3.2.2 (a,b): Multiple laser diode mount

3.3 Mount for Glass Reflectors in folded optic light path on Honeycomb optical table

Total 4 glass reflectors are used to fold the laser beam in such a way to make the optical path much longer. The reflecting glass surface is very smooth and 90^0 apart (fig.3.3.1). The reflection that occurs on each side of glass reflector is called regular reflection derived from Fresnel equation. Total 8 reflections are occurring while propagating from source to photo detector.

The incident light ray strikes the interface between two media of refractive indices η_1 and η_2 . The part of the light is reflected and refracted from the surface; the angles that the incident and reflected rays make to the normal of the interface are given by $\theta_{i,}\theta_r$ respectively. The relationship between these angles is given by the law of reflection.

$\theta_i = \theta_r$: Where θ_i - is the incident beam angle θ_r - is the reflected beam angle

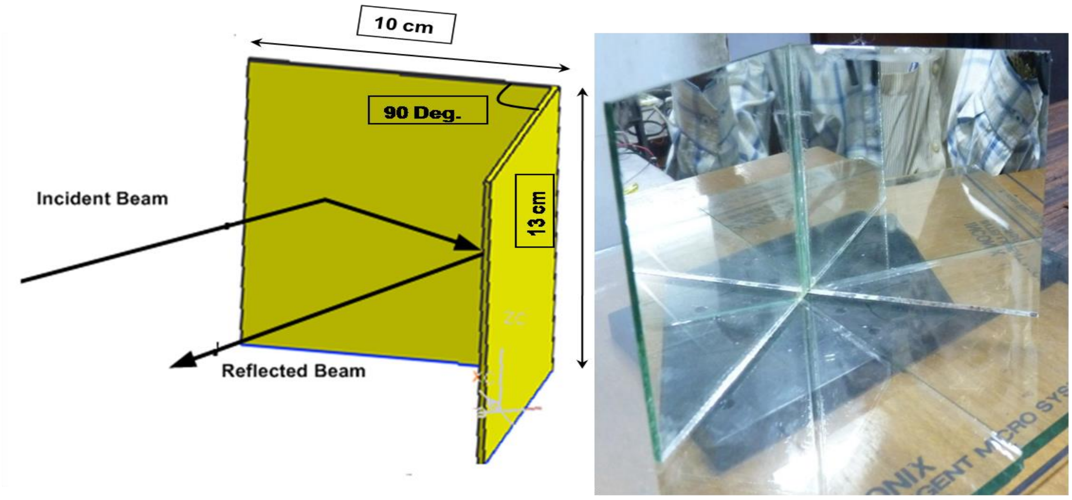

Fig 3.3.1 : Design of glass reflector

Two high precision right angled glass optical mirrors with reflectivity R= 0.988 were mounted to produce 180^0 phase shift of incident optical beams at both ends of optical set up to produce multiple path travel of optical beam in a turbulent medium. Collimating lenses were used just after the laser diode transmitter to produce a narrow and parallel optical beam at the transmitter end. All the optical components were mounted on vibration-isolation optical table with the help of high precision x-y-z positioners for alignment of axes of the folded-path optical beam. The same is depicted in Fig.3.3.1

3.4 Design of Photodiode Mount.

We have used silicon and InGaAs high speed PIN photo-detectors as receiver of light to cover the entire spectral range of visible to near infrared (NIR) of EM spectrum for studies of atmospheric turbulence and its effect on the transmission characteristics of laser beam.

InGaAs worked in the NIR having responsivity in the range 900nm to 1800 nm while silicon has response entirely in the visible region from 360 nm (Near UV) to 1100 nm. [6].

Both the detectors were small area detectors (1mm x 1mm) with double-hetero-junction constructions. The Detectors were mounted on x-y-z positioning systems having arrangements for mounting aperture lenses of variable diameters. A single and multiple photodiode mounting system is shown in Fig.3.4.1 and Fig.3.4.2 The choice of above detectors were dictated by the fact that we have used semiconductor lasers as sources in optical transmitter emitting light at discrete visible wavelengths (650 nm, 680 nm,780 nm) and NIR wavelengths (980 nm, 1300 nm and 1550 nm).

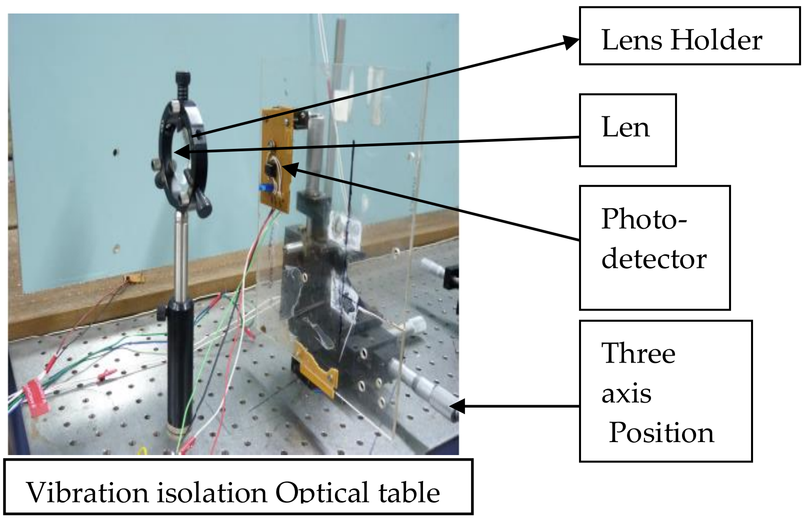

Fig.3.4.1: PIN Photodiode assembly with an aperture lens mounted on a honey-comb table.

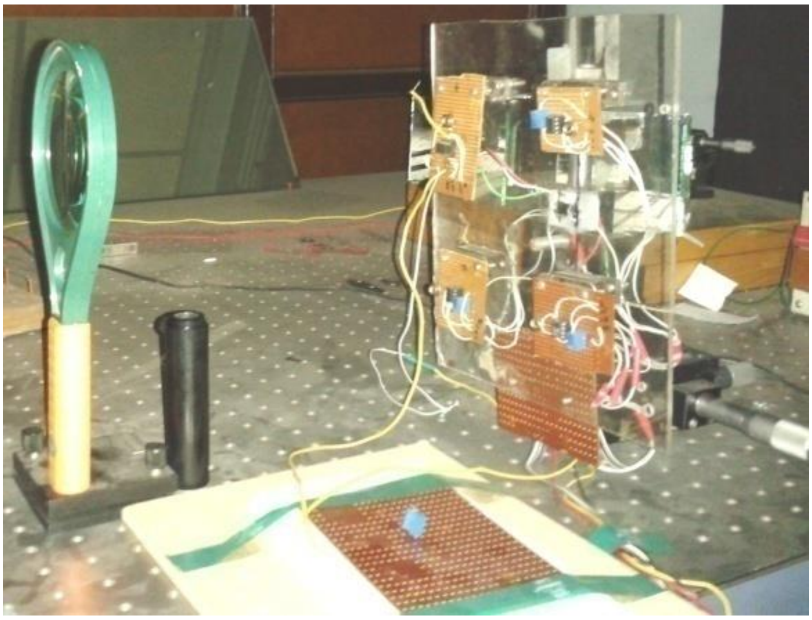

Fig 3.4.2: Design of multi-photodiode receiver optics

3.5 Design of LED Mount

A 5 mm white LED mount is shown in figure 3.5.1. Total 8 white LEDs (3V, 20 mA) are used, connected in parallel configuration. A bread board type base is selected to place the LEDs in one plane and to create well directional optical beam.

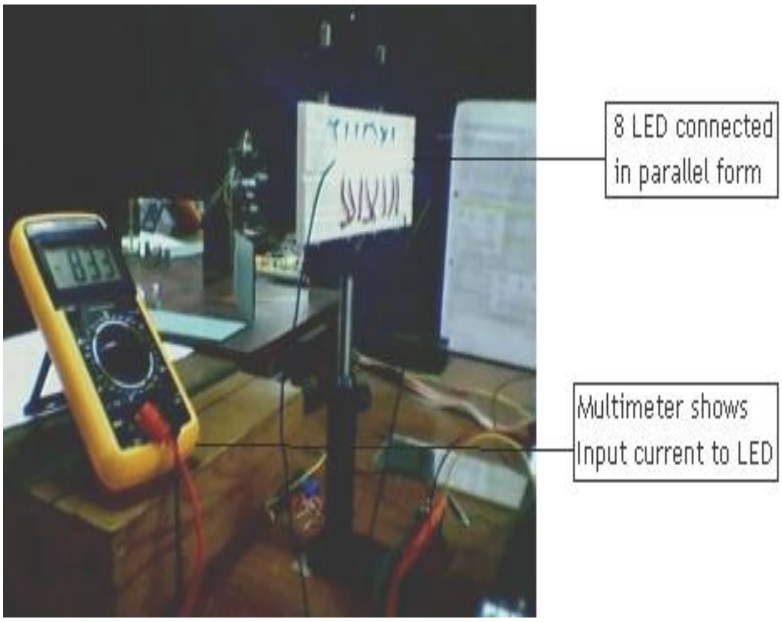

Fig. 3.5.1 : White light LED mount

Section 3B

Electronic and Photonic System

3.6 Design of Stabilized Laser Diode Driver Circuit.

In this work we needed highly stable monochromatic sources of light (single mode) which could be modulated by a high speed external electrical signal. The sources should be able to maintain spatial and temporal coherence and optical output power must remain stable even if the ambient temperature would be varying over a wide range.

We used quantum-well and distributed feedback semiconductor injection lasers for our requirement. Since semiconductor lasers are threshold devices, we needed to bias the lasers using highly stable dc biasing circuits. Again, the laser diodes are highly temperature sensitive devices. The In GaAsP lasers which emit in the NIR region are found to be more temperature sensitive devices compared to GaAlAs lasers emitting in the visible region. The threshold current of In GaAsP lasers increases rapidly with the increase in temperature (Characteristics temperature $=T_0$ ~90 k) while GaAlAs lasers have T_0 ~200 k.

Taking into account of the above facts and requirements, we have designed and developed a stabilized laser diode driver circuit for injecting a combined dc bias current and the digitally modulated ac carrier signals through the laser diodes. The lasers were biased just above threshold current and the modulated sinusoidal carriers were superimposed on it such that stimulated emission of light occurs from the lasers.

For stabilization of optical power output against any variation of ambient temperature or any variations in signal amplitude, a feedback arrangement was made in the laser diode driver circuit using the signal from backplane photodiode of the lasers. The driver circuit has been designed and tested to maintain a constant light output power even if the laser diode threshold current drifted with change in ambient temperature over the range 20^0C to 40^0C.

3.7 Design of Voltage Controlled Current Source [VCCS]

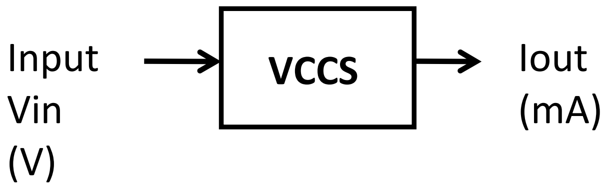

Fig. 3.7.1: Voltage control current source (concept)

A Laser diode or a LED is a PN junction device that converts injected electrons into photons when forward biased. Therefore, we needed a current source to drive a laser for the generation of photons. In our work we designed and developed a voltage controlled current source (VCCS) shown in fig.3.7.1 using BJTs and operational amplifiers having transfer characteristics as:

$$I_{out} = K.V_{in} \tag{3.2}$$

Where, the unit of I_{out} is mA and K (mA/Volt) is the trans-conductance of the VCCS circuit.

The VCCS circuit is shown in Fig. 3.7.2 The analysis of the circuit gives the expression of

$$K = \frac{R_1}{R_2} \times V_{in} \tag{3.3}$$

Thus, the value of K or the slope of output current versus input voltage curve is given by

$$K = \frac{R_1}{R_3 R_2} \tag{3.4}$$

$$I_{out} = \frac{R_1}{R_3 R_2} K.V_{in} \tag{3.5}$$

The expression for I_{out} shows that the current output of VCCS circuit is independent of variations of power supply voltage of the VCCS circuit and therefore a stable current output proportional to the input voltage can be obtained. Again, by choosing a proper ratio of the values of the three resistances R1, R2 and R3 we can vary at ease the change of output current per unit change of the input voltage V_{in}. For our requirement of laser diode biasing current we found that we would need maximum 25 mA to be set for dc biasing of the laser diodes. Taking safety margin we chose 30 mA as the required maximum current. We designed for input voltage V_{in} to be varying in the range 0 to 5 volts, for which the I_{out} would vary from 0 to 30 mA. For such a design we had to choose R_1 = 800 Ω; R_2 =1000 Ω and R_3 = 150 Ω. The transfer characteristic of the VCCS is shown in Fig. 3.7.3. The graph indicates that the circuit would be useful for dc biasing of laser diodes.

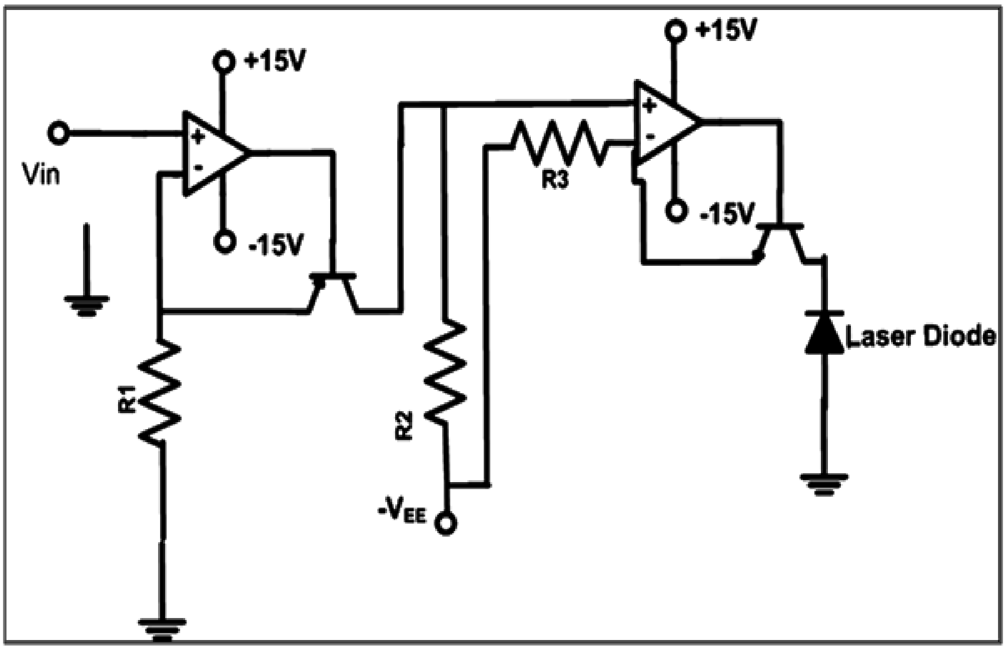

Fig. 3.7.2 : Voltage control current source (circuit)

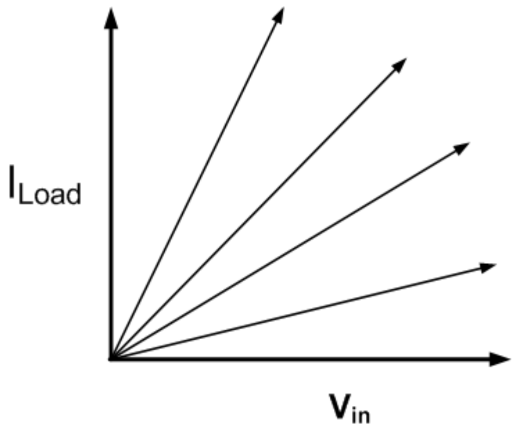

Fig. 3.7.3: Relation between $I_{(load)}$ and V_{in} for different values of k

Then, we design the circuit for generating modulating signal current (I_{MOD}) proportional to the incoming serial bit patterns arriving from computer (PC) serial port. We decided to use Amplitude Shift Keying (ASK) modulation of the arriving bits using a sinusoidal carrier signal from a signal generator and modulating the carrier using a ASK modulator chip- LF 398 as described in section 3B [7].

3.8 Design of Stabilized laser Diode Driver Circuit for Biasing and ASK Modulation of Laser Diodes

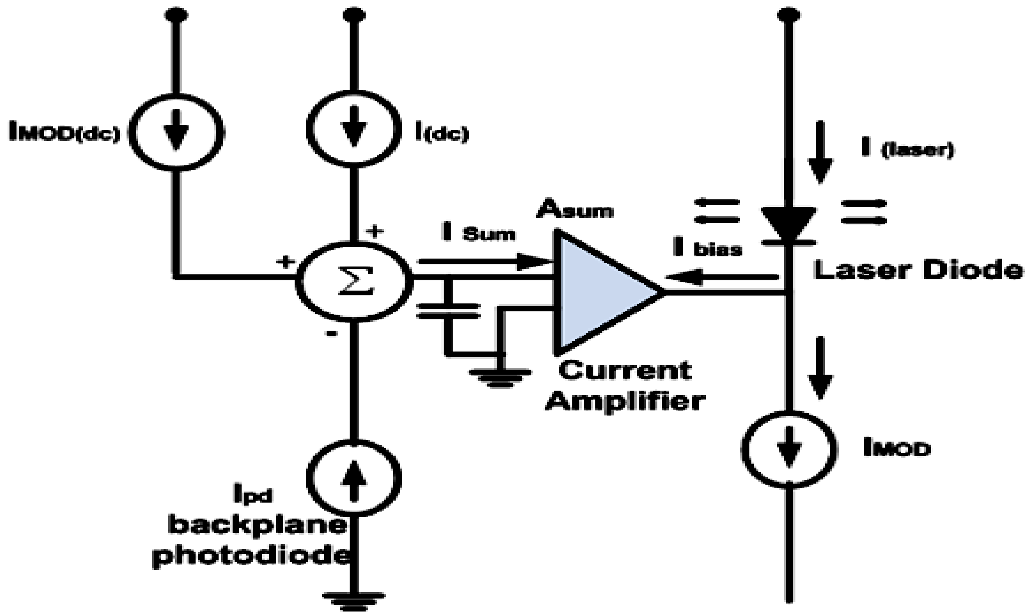

Fig. 3.8.1: Schematic diagram of a feedback stabilized laser diode driver circuit with dc bias current (I_{dc}) and ac digital modulation current (I_{MOD}) control.

We have designed our laser diode driver circuit based on the principle of mean feedback control utilizing the power output signal of the backplane mounted photodiode of the laser diode chips. The schematic diagram of the driver circuit is shown in Fig. 3.8.1. Several strategies of varying complexity have been designed [8-9] to provide automatic output optical power level control for optical communication system design using laser diodes. We decided to use the principle of mean feedback control because it is easy to implement and all the laser diodes we used have arrangements to monitor detector at the rear facet.

From the circuit in Fig. 3.8.1 we see that the current through the laser diode I_{LASER} has two components of current that is:

$$I_{LASER} = I_{BIAS} + I_{MOD} \tag{3.6}$$

Where, I_{BIAS} is the laser diode dc bias current and I_{MOD} is the laser diode modulation current.

The dc bias current I_{BIAS} is the summation of three dc current components [I_{dc}, I_{pd} and $I_{MOD(DC)}$]. The summation is obtained at the summing amplifier A_{SUM} as shown in Fig. 3.8.1 The output of the summing amplifier i.e., I_{BIAS} varies whenever the laser diode power varies due to temperature effects. As for example, if the light output power falls, then the current I_{pd} generated by the backplane photodiode of the laser diode decreases causing the resultant current I_{SUM} to increase. Thus I_{BIAS} increases to automatically increase the laser diode power output. The I_{dc} component of current is regulated to bias the laser just above its threshold current, such that stimulated emission occurs when the data bit is 1. The I_{DC} component of current is generated by our VCCS circuit a shown in Fig. 3.7.2

The current component $I_{MOD(dc)}$ is the current generated by the dc or average value of the modulating ac signal. Thus any variations of the average value of data bit patterns would be compensated by this current such that the dc bias for threshold operation of the laser is not affected.

The I_{MOD} component of current is the ac carrier modulation current generated according to the serial data bit pattern obtained from the computer. Thus:

$$I_{MOD} = K.A\cos(2\pi f_c t + \varphi) \;;\ \text{for data bit} = 1$$
$$= 0 \;;\ \text{for data bit} = 0 \qquad (3.7)$$

Where,

K is a constant and A is the amplitude of carrier signal f_c is the carrier frequency .The I_{MOD} component of current is generated by the ASK modulator circuit

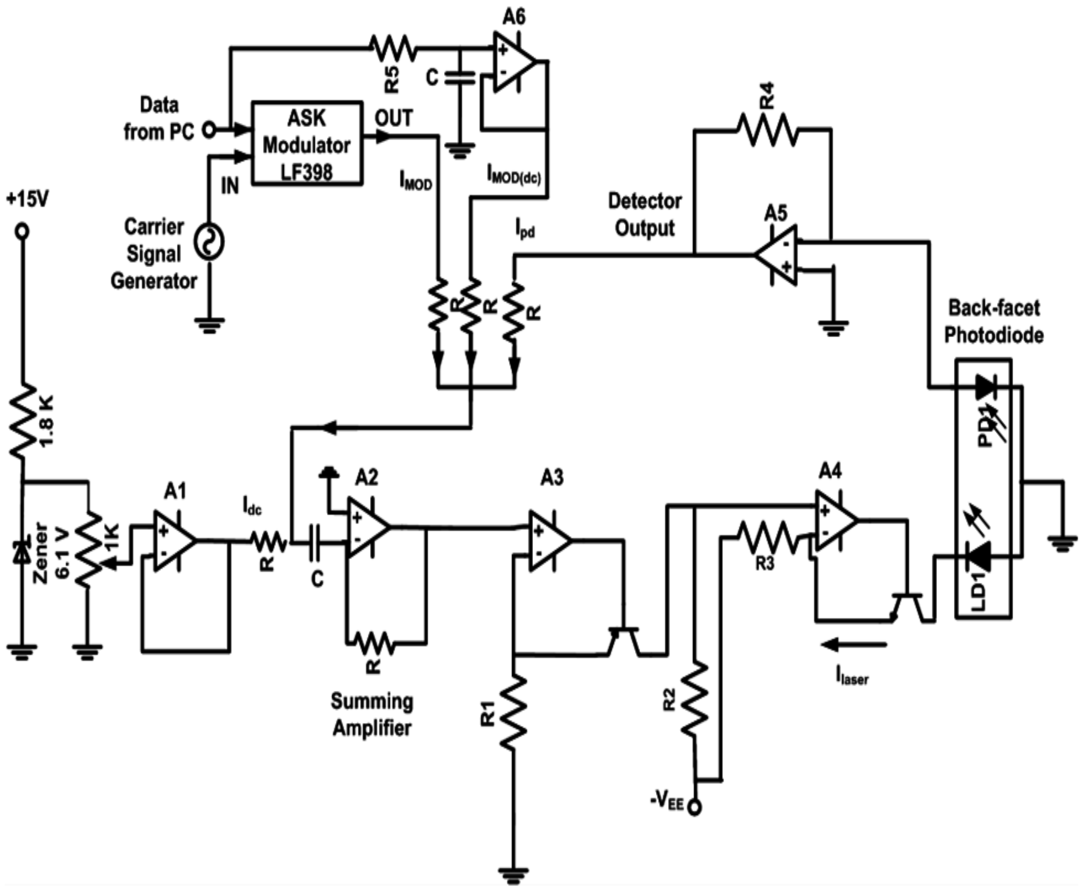

Fig. 3.8.2 : A feedback stabilized laser diode biasing and ASK modulation circuit

One of the major objectives of our work was to study the effect of atmospheric turbulence on the propagation of a modulated optical beam in laboratory environment. The modulated optical beam was obtained from a semiconductor laser biased above threshold and modulated by sinusoidal carrier with on-off keying i.e., ASK modulation. The turbulence was created by heaters, blowers and fans.

We have designed and developed a feedback stabilized dc biasing and ASK modulation circuit for injecting current through semiconductor injection lasers for our above purpose. The detailed circuit is shown in Fig. 3.8.2**.** The light versus temperature characteristics of laser diodes shows that the threshold current of laser diodes are highly temperature sensitive. The threshold current increases with increase in temperature of the laser. This is very prominent in case of In GaAsP lasers emitting at 1300 nm and 1550 nm. Thus, to obtain constant light output power from a laser diode, we had two options in hand.

In one method, we generally keep the laser diode temperature constant, mounting it on a controlled thermoelectric cooler. We would therefore need a temperature sensor to monitor the laser diode heat sink temperature and an electronic temperature controller to keep the laser diode temperature precisely constant during its operation for a specific application. The laser could then be used by injecting a constant dc biasing current I_{DC} through the laser to fix its operating point just above threshold. Then the ASK modulating ac current I_{MOD} have to be superimposed on the dc biasing current I_{DC} to produce constant modulated light output optical power. This is widely used method for very long time (for several years) operation of lasers but more costly. For our requirement, we therefore, chose the low-cost alternative as discussed below.

In this method, we have to continuously monitor the laser diode optical output power and automatically adjust the laser biasing current to keep the dc light output power of laser always constant irrespective of the temperature of the laser. Most advantageously, we have monitor photodiodes mounted at the back facet of all the lasers we have used in this work. The photodiode output can be used as an instantaneous signal proportional to the laser diode power output from its front facet-- the useful laser light for our application. Thus, additionally we need a negative feedback arrangement in our laser diode driver circuit such that a constant dc output power is always available from the laser. We used this method in our work because all of our laser diodes have back-facet photodiodes but no integral thermoelectric cooler.

The schematic diagram of the laser driver circuit is shown Fig. 3.8.2 where all the current components are shown to explain how we achieved the stability in the optical power output against temperature variations of laser diode mount. A summing current amplifier along with a RC low-pass filter have been used to get the sum total average or dc values of the current components labeled as I_{BIAS}, where,

$$I_{BIAS} = I_{PD} + I_{DC} + I_{MOD(DC)} \tag{3.8}$$

I_{PD} is the photodiode current. Since, this current includes the effect of the ac modulating current I_{MOD}, we have to average out the ac variations in summing amplifier. Further, the modulating current I_{MOD} contains the effect of transmitted bit patterns causing its average value changing. Thus, to compensate the effects of such bit pattern variations, we have added the current component $I_{MOD(DC)}$ to get the resultant dc drive current I_{BIAS} for the laser. Finally, the laser diode instantaneous drive current I_{LASER} is given by

$$I_{LASER} = I_{BIAS} + I_{MOD} \tag{3.9}$$

I_{MOD} is the modulation current generated by the ASK modulator circuit.

The complete circuit diagram is shown in Fig.3.8.2 . Here op-amp A_2 acts as the summing current amplifier for all the four current components

$$I_{LASER} = I_{BIAS} + I_{MOD}$$

$$= I_{PD} + I_{DC} + I_{MOD(DC)} + I_{MOD} \tag{3.10}$$

In the circuit of Fig. 3.8.2, the op-amp A_1 along with a zener diode develops a reference voltage for the generation of the dc bias current I_{DC} for the laser. I_{DC} is set according to the threshold current of laser at room temperature. Since this current varies from one laser to another, a provision is there for adjusting the current using the 1-kΩ potentiometer in A_1. The op-amps A_3 and A_4 together form the voltage controlled current source (VCCS) circuit as described in section- 3.7 The op-amp A_5 acts as the photodiode amplifier for the integral backplane mounted photodiode as shown in Fig. 3.8.2. The output voltage of amplifier A_5 generates the feedback current I_{PD} needed for feedback stabilization of optical power. The opamp A_6 acts as an unity gain buffer for feeding the digital bit patterns from PC to generate the $I_{MOD(DC)}$ current at the summing current amplifier A_2. The ASK modulating voltage for the generation of modulation current I_{MOD} is obtained from the IC-LF398. The ASK modulator is driven from a sinusoidal signal generator and the serial digital bit patterns from computer.

The dc conditions of the circuit were tested on a 680 nm laser used as a source over a wide temperature range starting from 25 ^{0}C to 35 ^{0}C. Highly stable light output was obtained using the circuit in Fig. 3.8.2. A variation in optical power output within (± 1%) were obtained in repeated test and measurements.

3.9 Driver Circuit to Measure Laser Characteristics:

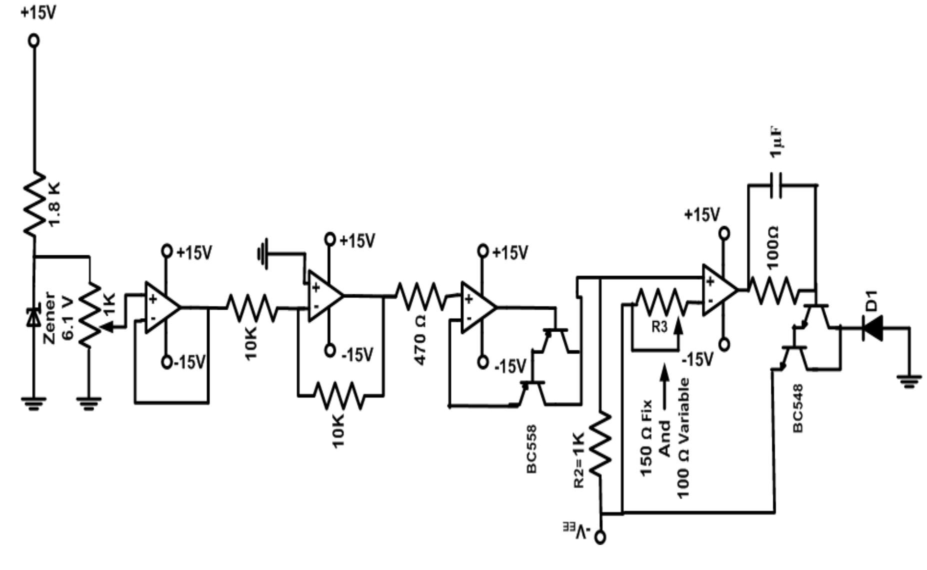

Fig 3.9.1 : Current driver circuit for laser

Precise current source is required to operate the laser in liner region. First the current is set at minimum value ≈0 by adjusting input supplied D.C. voltage and then gradually increases by very small fraction. We designed a current source with modified values of R_1, R_2 and R_3 with addition of Darlington pair in the last stage as shown in above fig 3.9.1. Using this pair the current amplified by the first NPN transistor (BC548) is again applied to collector of second one. This configuration gives a much higher common/ emitter current gain compare to each transistor taken separately. All L-I characteristics are measured at constant room temperature 28^0C.

3.10 Driver Circuit to Measure LED Characteristics:

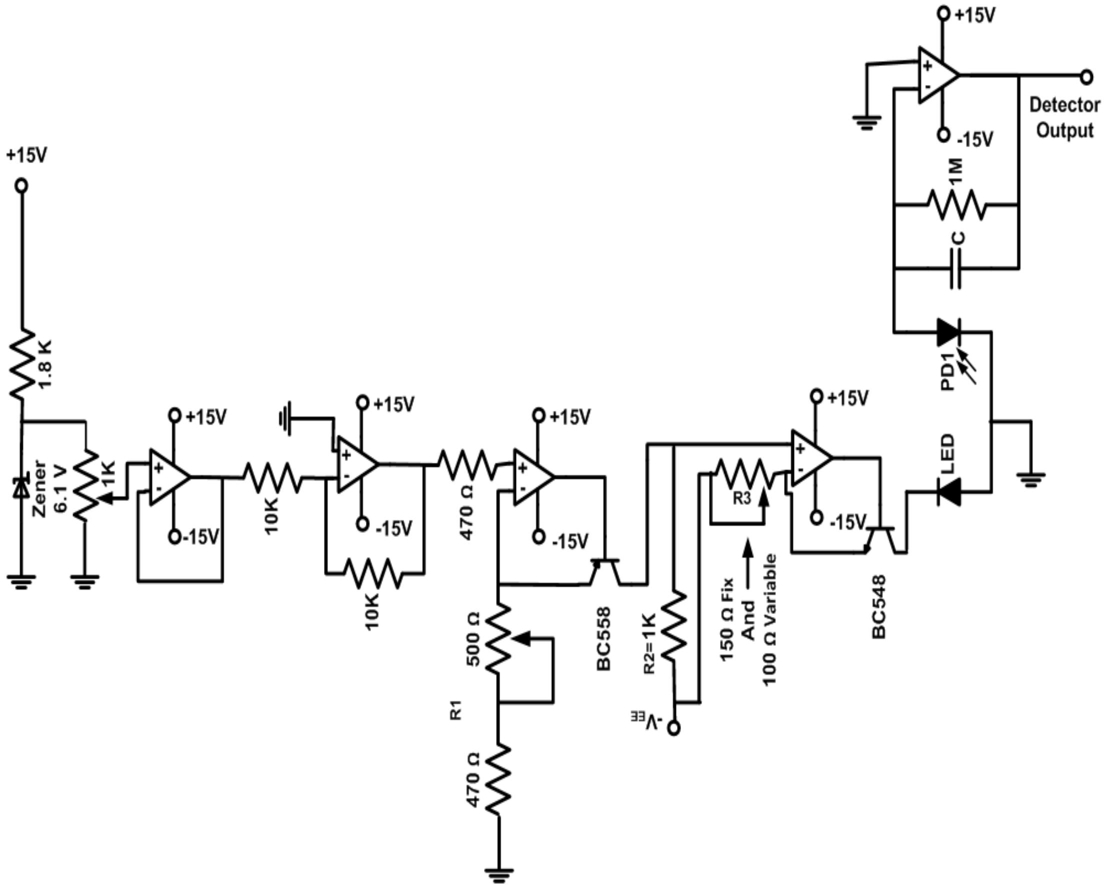

Fig. 3.10.1 : Current driver circuit for LED

A current driver circuit is designed and developed for LED is shown in Fig.3.10.1. VCCS and summing amplifier stage is same as described in laser driver circuit.

3.11 The Photodiode Receiver Design

In intensity modulated/direct detection (IM/DD) free-space optical communication link, we have used two photo-detectors to cover the entire visible and near-infrared (NIR) wavelength ranges for turbulence studies. One was a Silicon PIN photodiode and the other was InGaAs PIN photodiode. The detailed electrical and spectral characteristics of the photodiodes are given in [6]. We have used both the photo-detectors with high performance operational amplifiers with additional signal processing circuit as and when necessary. It was important that the detectors perform efficiently with the following amplifying and signal processing circuits. Inherent to this process was the separation of the information originally contained in the optical signal from the noise generated within the rest of the system and in the receiver itself as well as any limitations on the detectors response imposed by the circuits.

In order to design the receiver circuit we have considered the limit to the performance of the system set by the signal to noise ratio (SNR) at the receiver. The possible sources of noise in our system were found to be: (i) The thermal noise, (ii) the dark current noise (iii) the digital signaling quantum noise and most importantly (iv) turbulence-induced scintillation noise. All of these noise mechanisms can significantly impair the performance of free-space optical links.

The dark current noise and quantum noise, both of which can be regarded as shot noise on the photocurrent. The expressions for these noise sources including the background noise are represented as combined total shot noise given by:

$$i^2_{TS} = 2eB\,(I_p + I_d + I_b) \qquad (3.11)$$

where I_p is the quantum noise photocurrent , I_d is the dark current noise, I_b is the background radiation (such as ambient light) induced photocurrent. The thermal noise from the detector load resistor is very important in the design of the photodiode amplifier. Higher is the value of load resistor less is the bandwidth of the photodiode amplifier and more is the thermal noise. This is especially the case for wideband systems operating in NIR wavelength band because the dark currents in well-designed silicon photodiodes were found to be very small. The thermal noise i^2_t due to the load resistance R_L is given by

$$i^2_t = 4KTB/R_L \tag{3.12}$$

and the receiver bandwidth is given by

$$B = 1/\ 2\pi\ R_L Cd \tag{3.13}$$

Where, C_d is the photodiode junction capacitance.

3.12 The Turbulence-Induced Scintillation Noise

Atmospheric turbulence-induced intensity fluctuations can significantly impair the performance of free-space optical links. These intensity fluctuations often referred to as scintillation noise, can degrade the performance of links using intensity modulation with direct detection (IM/DD), particularly over ranges of several hundred meters or longer.

Two useful parameters describing turbulence-induced scintillation are d_0, the correlation length of intensity fluctuations and τ_0, the correlation time of intensity fluctuations. In typical terrestrial links with wind-driven turbulence, the correlation length is of the order of 1–10 cm, while the correlation time is of the order of 1–10 ms or longer. When the receiver aperture can be made much larger than the correlation length, scintillation noise can be reduced by aperture averaging. Likewise, when the receiver observation time during each bit interval can be made larger than the correlation time, scintillation noise can be reduced via time averaging. However, it is not always possible to rely upon aperture averaging to reduce scintillation noise to an acceptable level because of receiver size constraints. Also at the bit rates of interest in most applications, $T_0 \ll \tau_0$, and time averaging is not a viable means to combat scintillation noise.

Kahn [10] have studied detection techniques to mitigate scintillation noise in the regime when aperture averaging or time averaging cannot be relied upon to completely alleviate scintillation noise. These detection techniques were applicable to links employing ON–OFF keying (OOK) with DD. They were based on the statistical properties of turbulence-induced intensity fluctuations, as functions of both spatial and temporal coordinates. The techniques were divided into two categories: spatial-domain and temporal-domain. Temporal-domain detection techniques could be applied to mitigate these intensity fluctuations [10-12]. If the receiver has knowledge of the joint temporal statistics of intensity fluctuations, maximum-likelihood sequence detection (MLSD) or pilot-symbol assisted detection (PSAD) can be employed.

3.13 The Photodiode Amplifier

Three basic amplifier configurations are used in optical communication receiver circuits. These are (i) low impedance front end voltage amplifier (ii) high input impedance amplifier together with a large detector bias resistor to reduce the effect of thermal noise and (iii) the trans-impedance front end amplifier [13].

The trans-impedance amplifier is widely used in system design because it overcomes the drawbacks of high impedance front end by utilizing a low noise, high input impedance amplifier with negative feedback. An equivalent circuit for an optical receiver incorporating a trans-impedance front end structure is shown in Fig. 3.13.1 below. In this equivalent circuit the parallel resistances and capacitances are combined into R_{TL} and C_T respectively. When the feedback is applied, the closed loop current to voltage transfer function $H_{CL}(\omega)$ for the trans-impedance configuration is given by:

$$H_{CL}(\omega) = -R_f / (1 + j\omega R_f C_T / G) \quad (VA^{-1}) \qquad (3.14)$$

Where R_f is the value of the feedback resistor. In this case the bandwidth B is given by:

$$B \leq G / 2\pi R_f C_T \qquad (3.15)$$

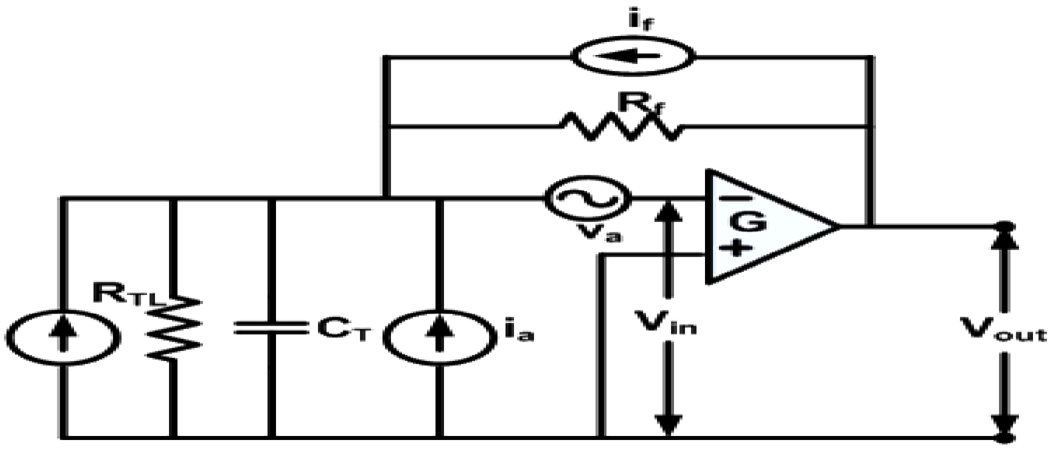

Fig. 3.13.1 : An equivalent circuit for optical receiver incorporating a trans-impedance preamplifier

The trans-impedance amplifier thus gives much greater bandwidth than do the amplifiers without feedback. Again, the noise performance of this amplifier improves with higher values of the feedback resistance R_f. Unfortunately, the value of R_f could not be increased indefinitely due to problems of stability with closed loop design. As seen from eqn. (3.15) that increasing R_f would reduce the bandwidth of trans impedance configuration. This problem could be alleviated by making open loop gain G of op amp as large as the stability of the closed loop would allow.

3.14 Design of ASK Modulator Circuit

In the wireless digital communication, it is not easy to transmit the digital data directly. This is because it needs to pass through the modulator and modulate the carrier signal in order to send the signal effectively. One of the easiest ways is to use the different data stream to change the amplitude of carrier, this kind of modulation is called amplitude modulation, and we call it as amplitude shift keying (ASK) modulation in digital communication.

With an ASK modulating signal, the digital signal value is either -1 or +1, and when it is changed to 0 and +1 it is called OOK. With OOK, the amplitude direction of the modulated wave is indicated by the presence or absence of a carrier wave. In other words, when the signal is 0, there is no carrier wave and when it is 1, there is a carrier wave. The spectrum of the ASK modulated wave is centered on the carrier frequency and the square wave spectrum which is the modulating signal takes a spread-out form as shown in Fig 3.14.1

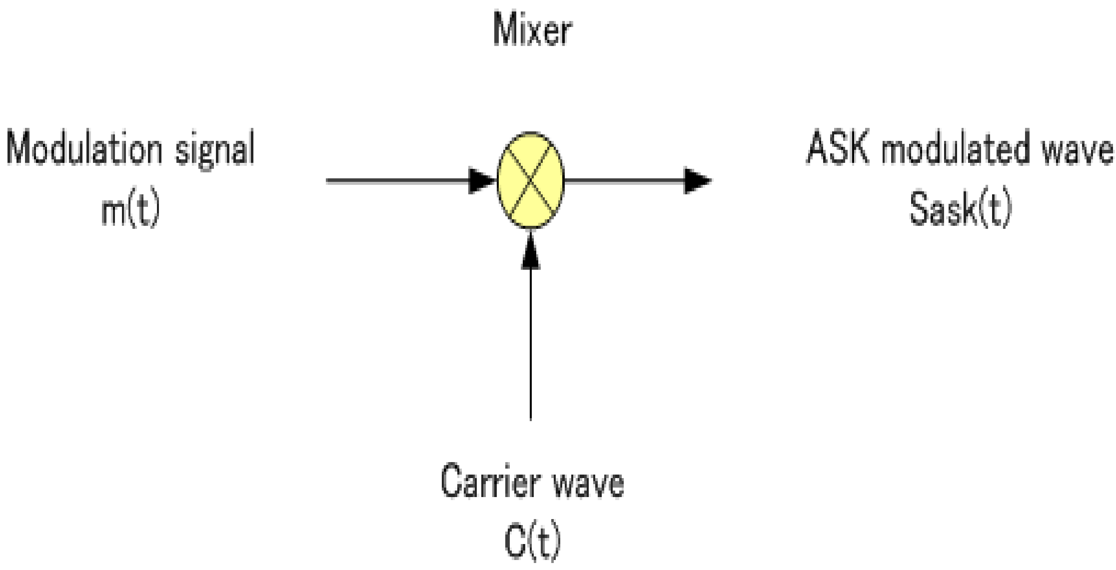

Fig.3.14.1: Basic principle of ASK modulation

Expressed as a formula, carrier wave C(t) takes the following form.

$$C(t) = A_c \times \cos(2\pi.F_c.t)$$

Where, A_c is the Carrier amplitude and F_c Carrier frequency

The ASK modulated wave is modulating signal m(t) multiplied by carrier wave C(t), and is expressed as a modulated signal formula as follows.

$$\begin{aligned} S_{ask}(t) &= m(t).C(t) \\ &= m(t).A_c.\cos(2\pi F_c.t) \end{aligned} \quad (3.16)$$

3.15 ASK Constellation

ASK can also be expressed as the constellation in the figure below, with the information at amplitude point 0 and 1 at phase 0 (rad) corresponding to 0 and 1. 0 rad means that even if the information signal changes, there is no phase shift as shown in fig.3.15.1 and complete ASK modulation w/f is shown in fig 3.15.2

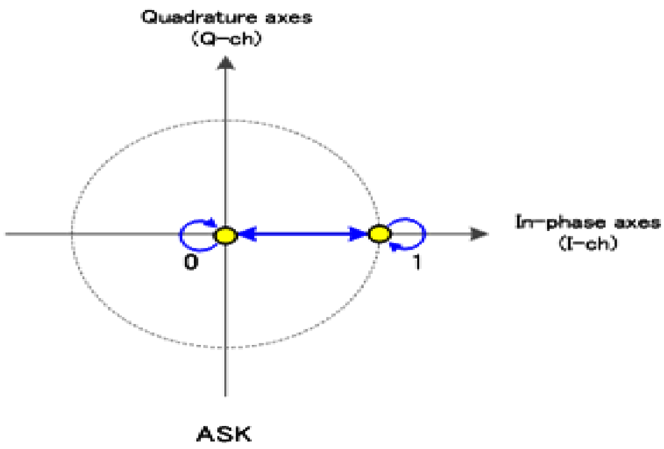

Fig.3.15.1 : ASK constellation Diagram

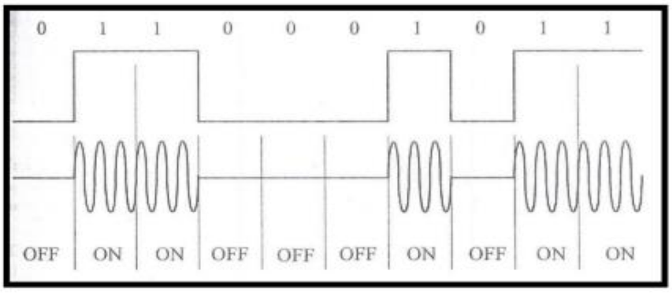

Fig.3.15.2 : ASK modulation signal waveform

3.16 Design of ASK Demodulation

The transmitted ASK signal has an inconstant but well defined envelop. Thus it is possible to demodulate it by envelope detection, to simplify structure and reduced cost a type of synchronous detection is appropriate. Envelope detection is a detection method that can only perform demodulation when the envelope of the modulated signal indicates a modulating signal (Fig. 3.16.1)

The synchronous demodulation requires a phase lock local carrier and carrier acquisition circuitry. The demodulation is a two-stage process: recovery of the band limited bit stream, and regeneration of the binary stream

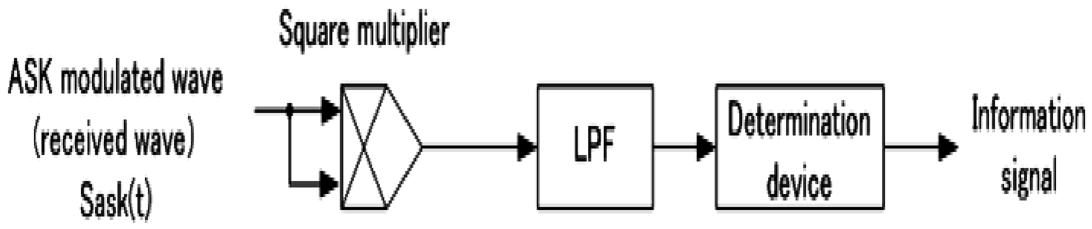

Fig.3.16.1 : The principles of synchronous detection

The ASK modulated wave is multiplied by a squarer as follows.

$$S_{ask}^2(t) = m^2(t).A_c^2.\cos^2(2\pi.F_c.t)$$
$$= m^2(t).A_c^2.\frac{1}{2}\left\{1+\cos\left(4.\pi.F_c.t\right)\right\} \quad (3.17)$$

The second term in the braces is an unwanted component, so only the LPF signal component is added.

$$\left\langle S_{ask}^2(t)\right\rangle_{LPF} = \frac{A_c^2}{2}m^2(t) \quad (3.18)$$

The determination device determines the level of the signal and the transmitting end information signal is obtained.

3.17 Practical Implementation of ASK Modulator

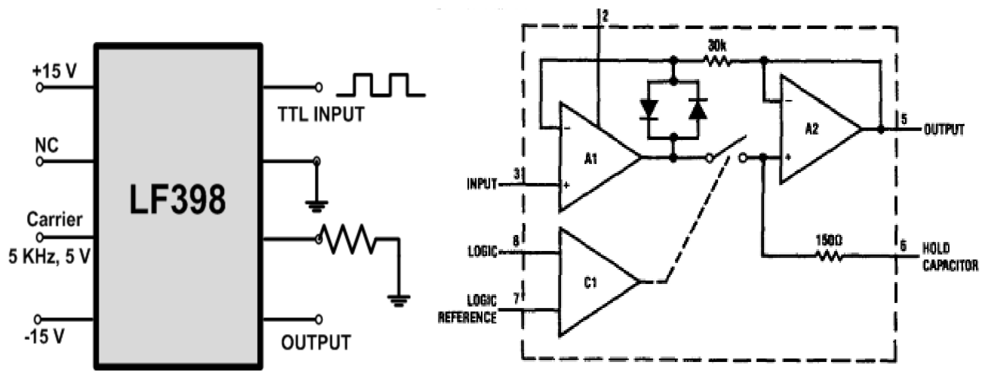

Fig. 3.17.1 : Design of ASK Modulator circuit using IC LF398 (Carrier is 5 KHz)

We have designed a ASK modulator circuit using the precision sample and hold amplifier IC LF398 as shown in Fig.3.17.1. The amplifier uses a combination of bipolar and junction FET transistors to provide precision, high speed and long hold times. It has typical offset voltage of 1 mV and gain error of 0.002% and it has unity gain with 10^{10} input impedance independent of sample/hold mode. The logic inputs are high impedance differential to allow easy interfacing to any logic family without ground loop problems.

For fast sample and hold applications, the size of the hold capacitor is critical. A low value will give fast acquisition, but will also increase errors due to hold step, and droop caused by amplifier bias current. The capacitor should be made as large as possible, consistent with dynamic sampling error requirements. Capacitors larger than 0.1 μF have an additional problem. They are not available in the low loss dielectrics like Teflon, Polystrene. Dielectric absorption in the hold capacitor can often be the major source of error in a sample and hold. The equivalent circuit of a typical capacitor is shown in [URL-3]. We see that rapid changes in capacitor voltage will not be tracked by the internal parasitic capacitors because of the resistance in series with them. This leads to a “sag” effect in the hold capacitor after a sudden change in voltage followed by rapid switch to the hold mode. Considering all these facts we have ultimately chosen a 0.1 μF hold capacitor for our work.

3.18 Temperature Measurement Using Semiconductor Temperature Sensor IC LM35.

In our laboratory set up for creating atmospheric turbulence in the path of an optical beam, we have used multiple numbers of electrical heaters and heaters with fans and blowers surrounding the experimental set up as shown in Fig. 3.1.1 . As the temperature of the air got hot weak turbulence was observed in air. The scintillation produced due to turbulence is a function of the temperature of the atmosphere. Therefore, we had to arrange for a temperature measurement system using multiple temperature sensors mounted at specific locations within the set up. Since we arranged for heaters to produce controlled temperature variations within the range

20^{0}C to 60^{0}C, we therefore, decided to use standard semiconductor diode temperature sensors LM-35 available from the National Semiconductors [14] giving good linearity, accuracy and acceptable response over the above desired temperature range. The schematic diagram of LM-35 with temperature Sensor IC internal Circuit diagram is shown in Fig. 3.18.1.

Variable current is injected through a diode to maintain a constant voltage across when the diode temperature is changing. The current variations are converted to variations in voltage at the output. An output voltage of 10 mV/^{0}C is obtained at the output following a linear law over the temperature range 2^{0}C to 150 ^{0}C.

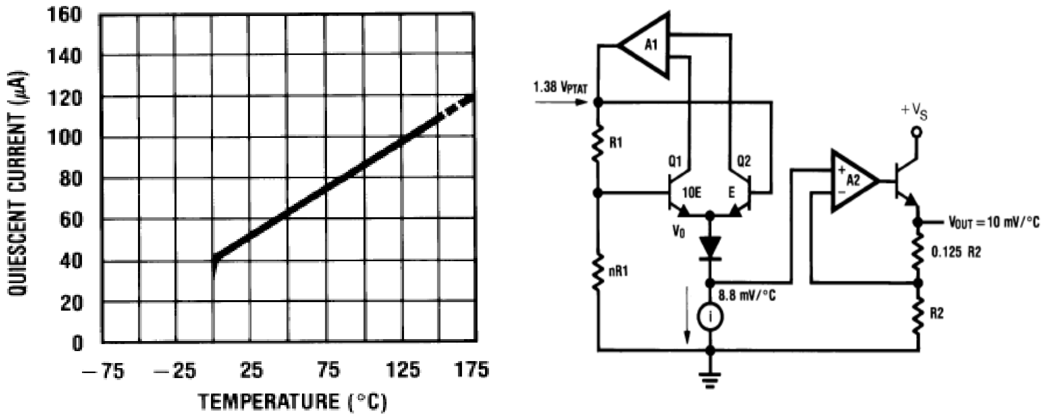

Fig.3.18.1 : LM35 response with internal circuit

The outputs of the temperature sensors were fed to the input of the 10-bit analog-to-digital (A/D) converter of the Microcontroller system 18FC548 as shown in Fig.3.18.2. Since the A/D converter input voltage range was 0 to 5V, an amplifier with the required gain of 5 was connected at the output of the LM35 to calibrate the temperature measurement system to produce an output voltage variation of 0 to 5 volt for the temperature range 0 ^{0}C to 100^{0}C.

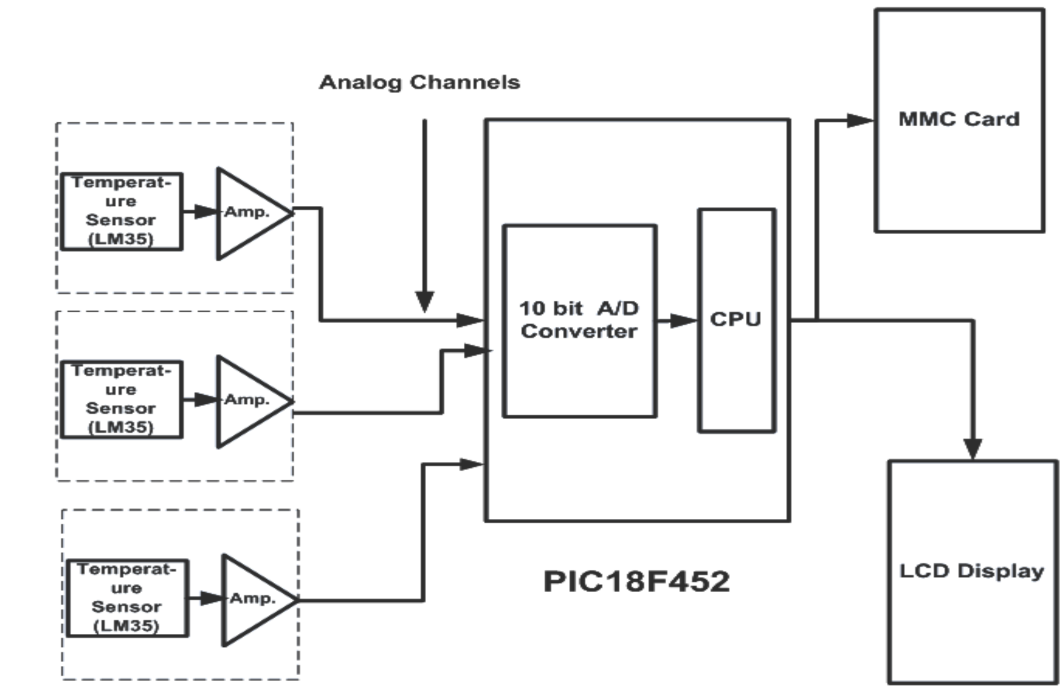

Fig. 3.18.2 : Microcontroller system 18FC548 with temperature sensor LM35

3.19 Design of Photo-Diode Receiver Circuit

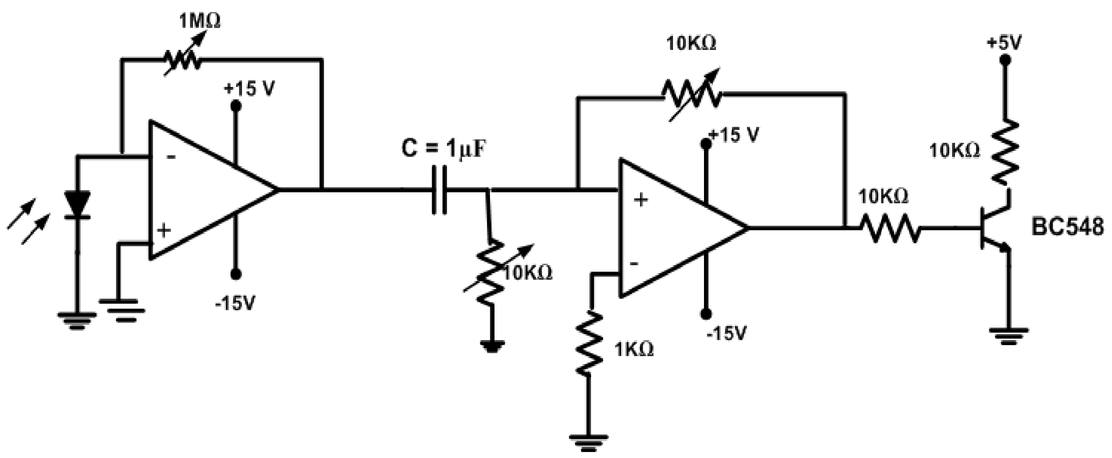

Fig 3.19.1 : Design of photo-diode receiver circuit

A PIN photodiode is used as a photo-detector to detect the light signal followed by preamplifier to amplify weak signals as shown in fig 3.19.1 . A variable feedback resistance 1MΩ is used to adjust the gain of the preamplifier TLO81. A signal collected by photodiode includes carrier and digital data. To filter a carrier signal low pass filter is used.

Now, the gain G is given by

$$G = \frac{V_{out}}{V_{in}} = \left(1 + \frac{R_F}{R_1}\right) \tag{3.19}$$

Where R_F is the feedback resistance, R1 is the diode resistance. Here we adjust the gain of the preamplifier using variable 1MΩ pot. The analog output of photo-detector is store in data acquisition system using microcontroller and interfacing circuit shown in Fig 3.19.2.

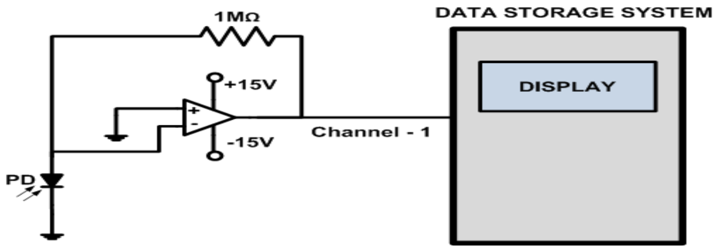

Fig. 3.19.2 : Receiver with data storage system

3.20 Design of Micro-Controller Based Data Acquisition system and PC Interface Electronics

For the studies of atmospheric scintillation effects on optical beam in a controlled laboratory environment we had to measure and control several atmospheric parameters surrounding the laboratory set up using typical sensors, transducers and associated measurement circuits. For automatic control of temperature, and flow velocity of air, we took the support of software based digital control algorithms. For this, we had the requirement of digitization of all analog measurement signals from the sensors just for taking control actions and display purposes.

Since we had several parameters for measurement and control we decided to use a standalone Microcontroller based data acquisition system PIC18F452. It is an 8-bit microcontroller system with analog 4-channel multiplexers for 10 bit analog-to-digital conversion. A schematic diagram of the microcontroller PIC18F452 is shown in Fig. 3.20.1.

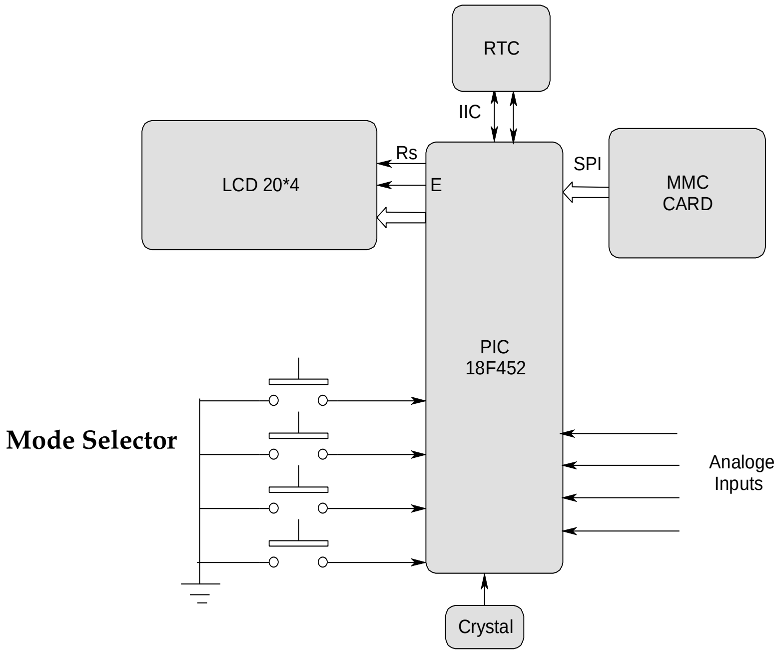

Fig.3.20.1 : Schematic block diagram of MCROCHIP--PIC18F452 Microcontroller

The PIC18F452 microcontroller has the following features: 32 KB of flash memory; 1,536 bytes of RAM and 256 bytes of EEPROM.

A LCD display with 4 lines 16 characters driven in 4 bit mode , make it possible to visualize the various data such as data storage time, recording file number, as well as the value of the input analog channel in terms of sample value varies from 0 to 1024 . The sample value 1024 represents maximum input analog voltage 5V given that the A/D converter having resolution of 10 bits.

Four pushbutton switches S1, S2, S3 and S4 as shown in Fig. 3.20.1 are used to select the operating modes of the microcontroller as given in detail in [15].

Fig.3.20.2 further shows that external memory cards (MMC) can be attached to the system for storage and collections of measurement data and for subsequent analyses in the PC. A photograph of the microcontroller is shown in Fig. 3.20.2. The sequence of instruction to display and store the data in memory card is shown in flowchart Fig. 3.20.3.

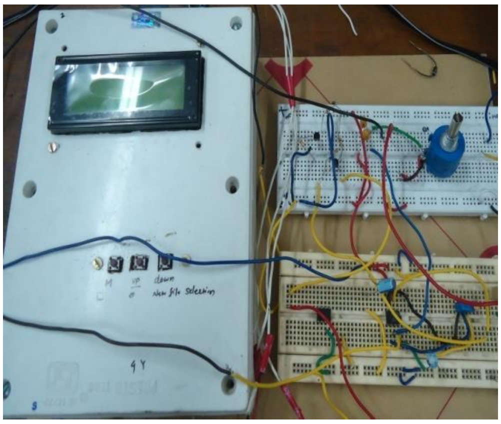

Fig 3.20.2 : Photograph of the microcontroller board used in laboratory base atmospheric turbulence measurement set up

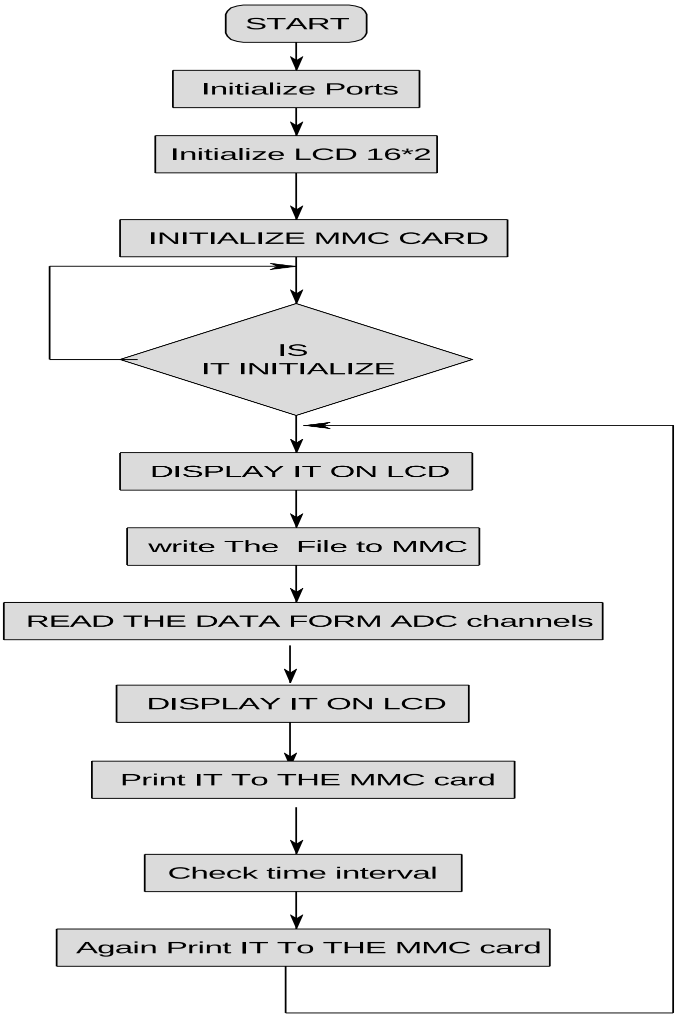

Fig 3.20.3 : Flowchart of signal processing

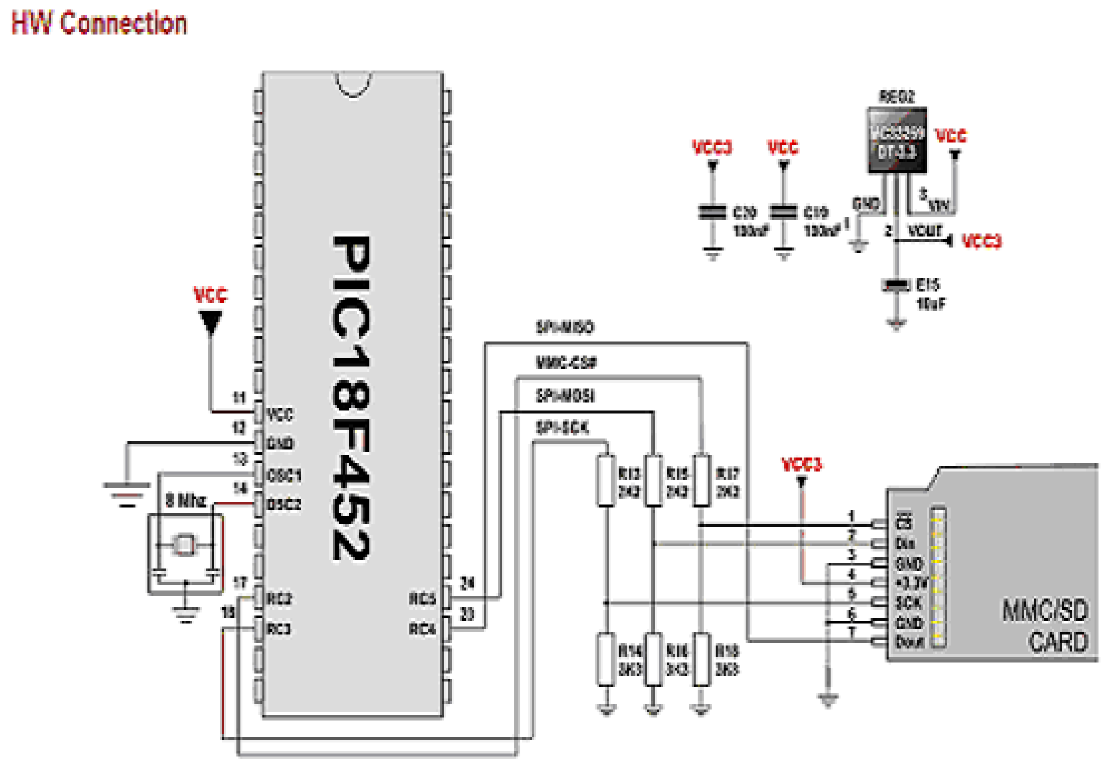

Fig.3.20.4 : Connection diagram of microcontroller PIC452 and SD card

Above fig 3.20.4 shows connection diagram of microcontroller and SD card given in reference PIC18FXX2 (microcontroller with 10-bit A/D) data sheet [15]. Pin 17 and 18 is asynchronous transmit and receive pins through which data is transfer from microcontroller to SD card.

PC Interface Circuit

As shown in Fig 3.1.1, we used a computer system to transmit and receive the digital data from optical channel affected by turbulence. Now to transmit data, we select serial port where RS-232 voltage levels are present. To covert RS-232 data into TTL standard levels (+5V and 0V) we designed PC interface circuit using IC MAX232. This interface circuit uses 5 capacitors having value 10µF. The IC diagram and photographic view is shown in Fig. 3.20.5. A 9 pin "D" serial port connector is used to transmit or receive the data from computer.

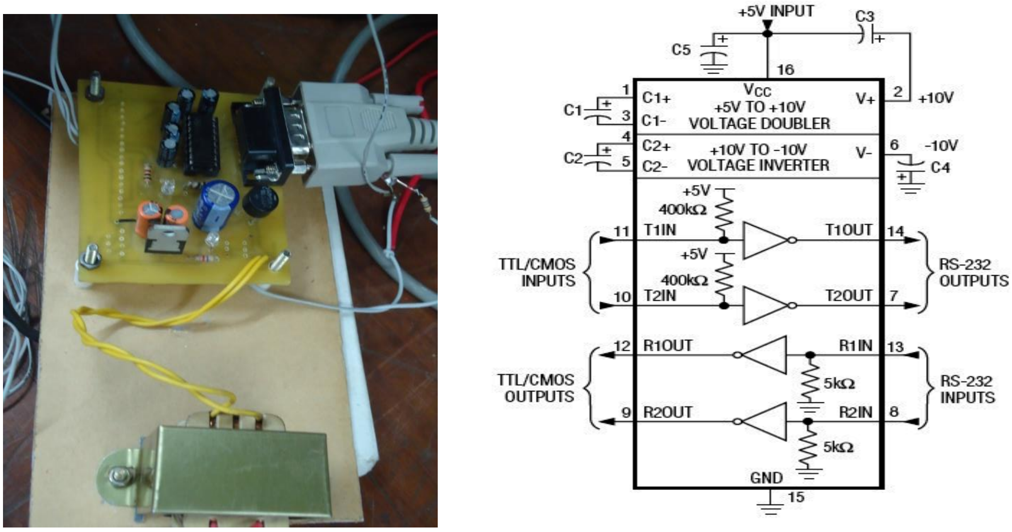

Fig.3.20.5 : Design of serial port interface circuit (line driver)

The Tx pin output of MAX232 is given to the next stage i.e. laser driver circuit and the output of ASK demodulator is again given to Rx pin MAX232 Datasheet.[16]

3.21 PC Software Development, Calibration and Measurement procedure of the Overall Free- Space Optoelectronic System.

The active window of terminal software is shown in following Fig. 3.21.1(a) and 3.21.1(b) [11].The bottom side bar is used to send the data from Tx pin of serial port and upper side bar is use to see the received data directly from Rx pin of serial port. Using scanning option software selects any input - output serial port which is free to transmit and receive the data. Baud rate select data rate as 600,1200,2400,4800 etc.

A serial port using voltage shifter (TTL) MAX232 created compatible voltage levels circuit is used to send the digital data to next stage. The advantage of the MAX232 is that it has faster response times, and allows faster data rates. A standard DB-9 serial connector is used to connect signal to transmitter and receiver respectively.

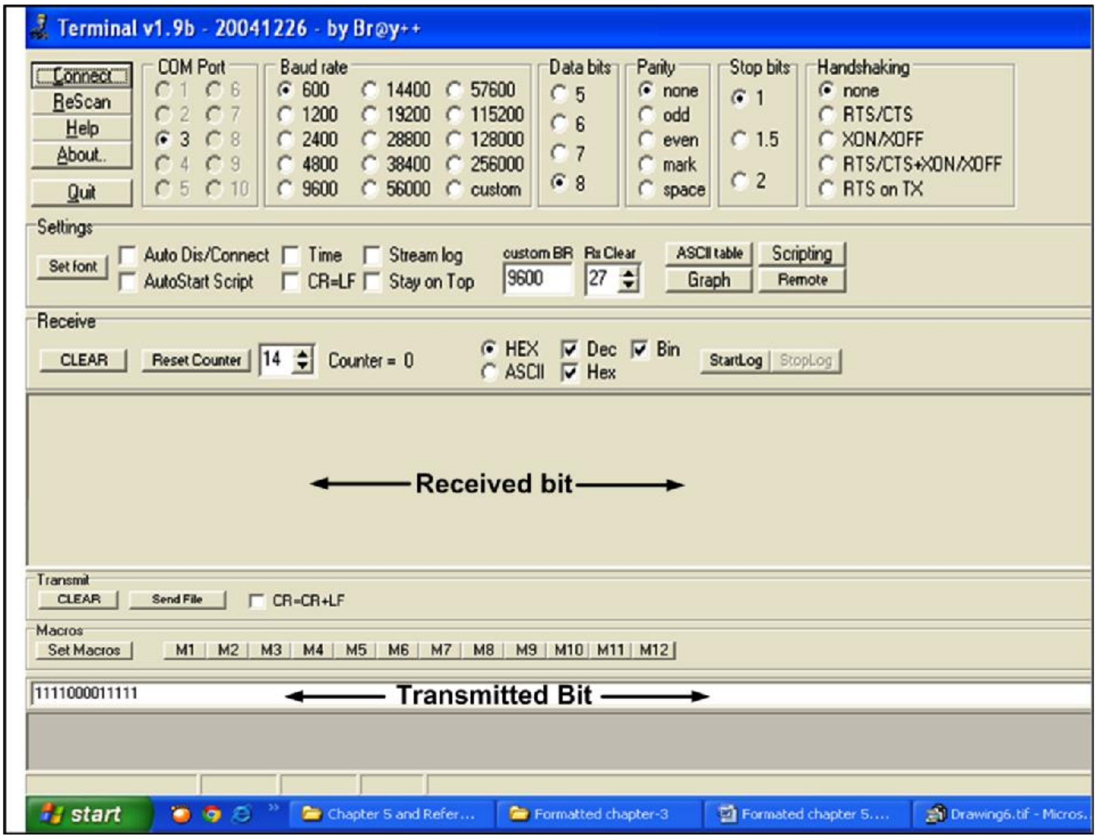

Fig. 3.21.1 (a)

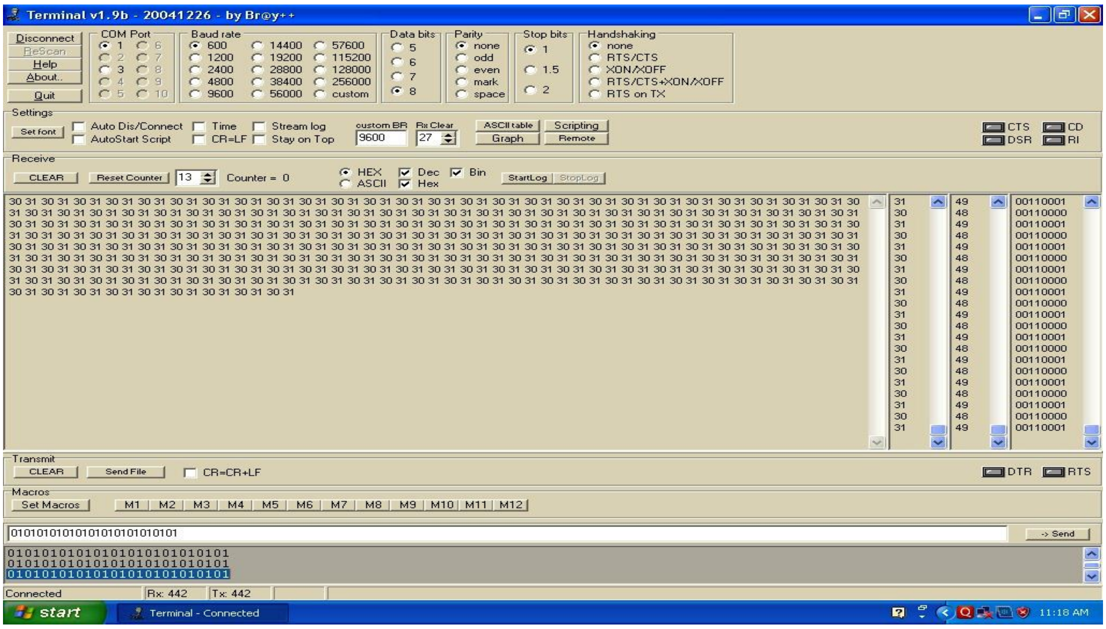

Fig.3.21.1 (b): PC Window showing the status of the FSO comm. Link Tx and Rx status under dynamic operating conditions.

In above Fig. 3.21.1 first window shows transmitter and receiver data slot along with serial port selection menu. It also shows selected baud rate, data bits, parity bit etc. All the received data is display in ASCII code i.e. digital '1' is represent by 31 and digital '0' is represent 30. In second window we display both transmitted and received data bits i.e. when we send '10101010', the receive data slot shows 31 30 31 30 31 30…….

A serial data is transmitted from serial port using transmitter pin of DB-9 socket with specific bit rate. This series of binary bits is applied to input of voltage shifter circuit to converts these bits into TTL voltage levels (+5v, 0v). ASK modulator LF398 with 5 KHz carrier frequency is used to carry these binary bits and given to laser driver circuit for intensity modulation. The intensity modulated signal travel through multipath folded optics system and reach at receiver photo-detector section. The received signal is filtered through low pass filter and separate 5 KHz carrier signal. The data signal is then applied to receiver pin of DB-9 socket such that it will display in the same window. The transmit and receive bits are simultaneously stored as Matlab files to calculate the performance of optical link in terms of BER.

3.22 Complete circuit Diagram to measure the Performance of optical link

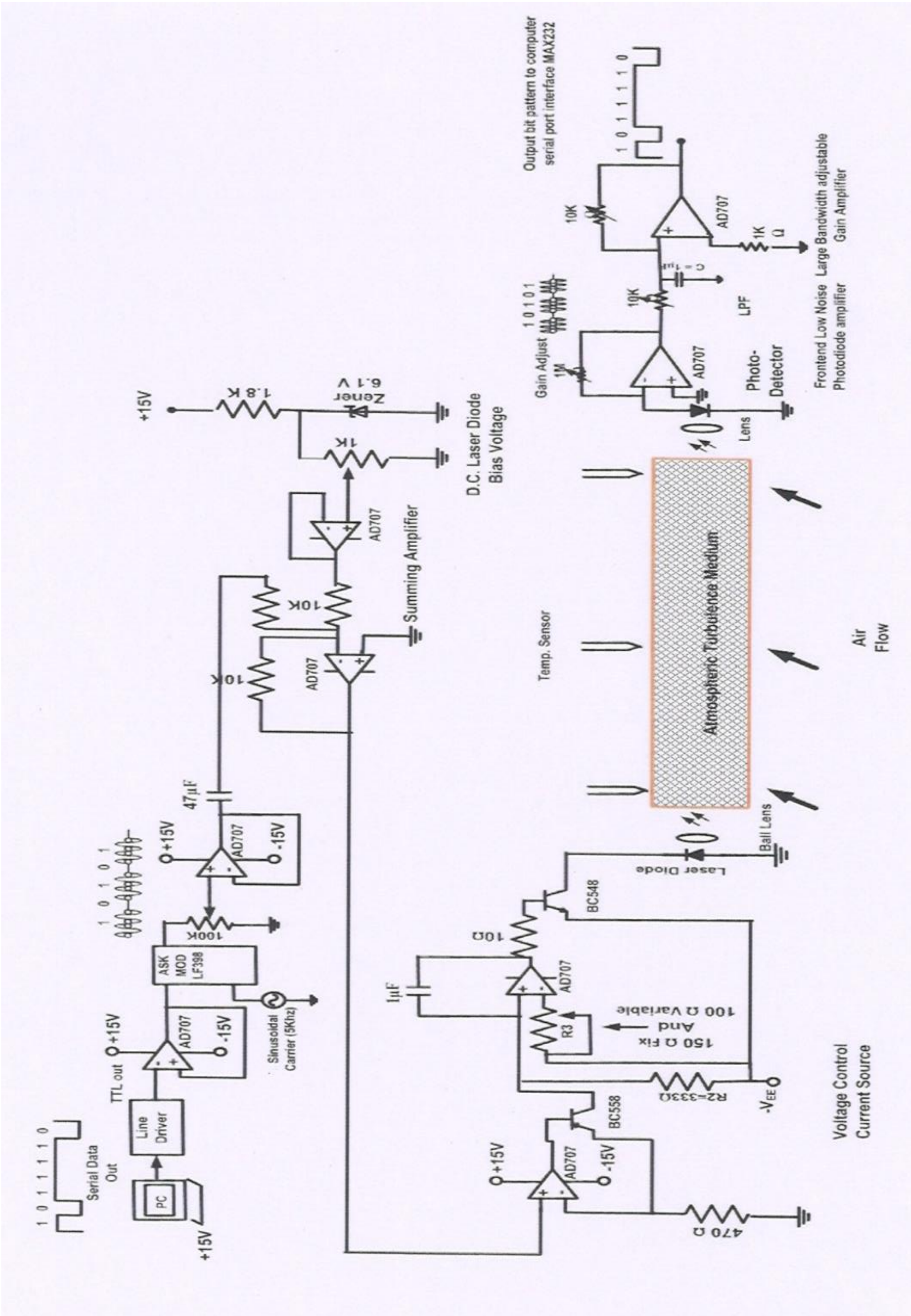

Fig.3.22.1 : Circuit and system for laboratory turbulence measurement

The overall circuit and system developed inside our laboratory for the generation of atmospheric turbulence and measurements of the effects of turbulence on the propagation of a monochromatic beam of light from a semiconductor laser is shown in Fig.3.22.1

This arrangement has been made to perform detailed studies of the effects of (i) variations of transmitting source parameters, such as : intensity and wavelength of light, variations in the characteristics of the electronic modulation scheme , single or multiple sources for space diversity studies, secondly – to study the effects of variations of the atmospheric channel parameters, such as, refractive index variations through temp effects , effects of flow velocity of air , effects of smoke in the path of light beam, effects of rain on the propagating light beam.

Finally to study the aperture averaging effects through the variations of aperture dimensions, effects of multiple detectors for space diversity and angle diversity measurements (MIMO system). The overall system operation and management for measurement and control is done using a microcontroller interfaced PC based system as depicted in Fig.3.1.1

The arbitrary bit patterns, bit rate and baud rate variations are all set by commands from the PC to the microcontroller. The process of digital modulation of the bits generated by the computer and subsequent operations are described below.

The overall system as described in Fig 3.22.1 can be divided into three blocks for their operations as given below.

1. The transmitter circuits and systems
2. The atmospheric turbulence generation system.
3. The receiver system for detection of data analysis.

The transmitter circuit and system block again consists of PC and transmitter interface circuit for transferring serial data from PC to the transmitter unit comprises an arrangement for stabilize laser diode biasing circuit and an ASK modulator circuit.

The modulated carrier along with the biasing signal drives the voltage control current source for generating the laser diode modulation and biasing current $[I_{mod} + I_{bias(D.C)}$].The VCCS (Voltage Control Current Source) generate the required laser modulation and bias current to drive semiconductor laser.

The current modulated light output from the laser is coupled to atmospheric turbulence medium by using an aperture lens as shown in Fig.3.22.1. A dual trace oscilloscope have been continuously used to see the transmitter, receiver performance by measuring the strength and quality of the signal.

The turbulence medium is the available free space in the lab where multiple path optical transmission has been made through the use of multiple reflectors manufacture by fine high quality glass materials. This design has been displayed in section A of chapter 3.

In order to produce artificial turbulence we have used several fans and electric heaters all through the region were the multiple path rays travels in the turbulence medium. Solid state temperature sensor has been mounted at prime location to measure the temperature variations over the whole turbulence region. An arrangement for air flow velocity has been made by mounting an air flow meter (Anemometer type).

The light from the transmitter after having multiple reflections in the turbulence region ultimately reaches the photodiode receiver system. The photodiode system is described below.

The Receiver System:-

The receiver system comprises of a receiver aperture in front of the photodiode receiver. The photodiode is mounted on three axis (x-y-z) high precision positioned system. The arriving optical beam is finally positioned such that the receiver aperture creates an image of the source on the surface of the photo detector.

The photo-detector –an Si PIN photodiode working over the spectrum rang 400 to 1100nm having a surface area of 2mm × 2mm is used for detecting output of laser modulated signal for the wavelength region 400 nm to 1100 nm. To work in the range 1300 nm to 1550 nm we have used an InGaAs PIN photo-detector replacing Si photodiode.

The photodiode mount has built in amplifier designed using op-amp that has low bias current and large bandwidth. The output from the photo-detector is the ASK modulated signal received from the transmitter and corrupted by artificial atmospheric turbulence.

After demodulating the received ASK modulated optical carrier, the demodulated electrical signal is now the bit pattern transmitted by the computer at the transmitter side. These bits patterns are sent back to the same computer for comparison with transmitted bits. Any bit error produced is immediately detected by computer, which are actually the bits in error produced by the atmospheric turbulence medium.

Measurement Techniques:

From the above description of the complete free space optical system with turbulence created by the optical path , we have several possibilities of studying the characteristics of the optical beam travelling in a turbulent medium by changing the different parameter of the transmitter system and turbulence generation system, as for example we can vary bit/baud rate of the data, we can change the carrier amplitude and frequency, we can vary the temperature, air flow rate of the turbulence medium and finally we can change the diameters of the aperture of transmitter as well as the receiver to study the detail link performance of a free space optical communication in a atmospheric turbulence medium .

We have also the option to change the wavelength of the laser by selecting different laser and corresponding photo-detector to study how performance of the system varies with variation in the wavelength of the light sources.

Since the computer can be controlled by software program, from the baud rate of the serial data bit patterns we can easily verify, How the BER performance of the system is changing

1. With the increase or decreases of the signal strength.
2. With the increase or decreases of the temperature.
3. With the increase or decreases of the flow rate.
4. With the increase or decreases of the baud rate in the overall total system.

We have taken all this procedure for measurement sequentially to extract the effect of turbulence on BER performance of the system as shown in Fig.3.22.2. We have calculated as given in the sections of chapter 3 the refractive index structure parameter C_n^2 as a function of bit rate and temperature fluctuations. From experimental outcome, the results are plotted and given in next chapter.

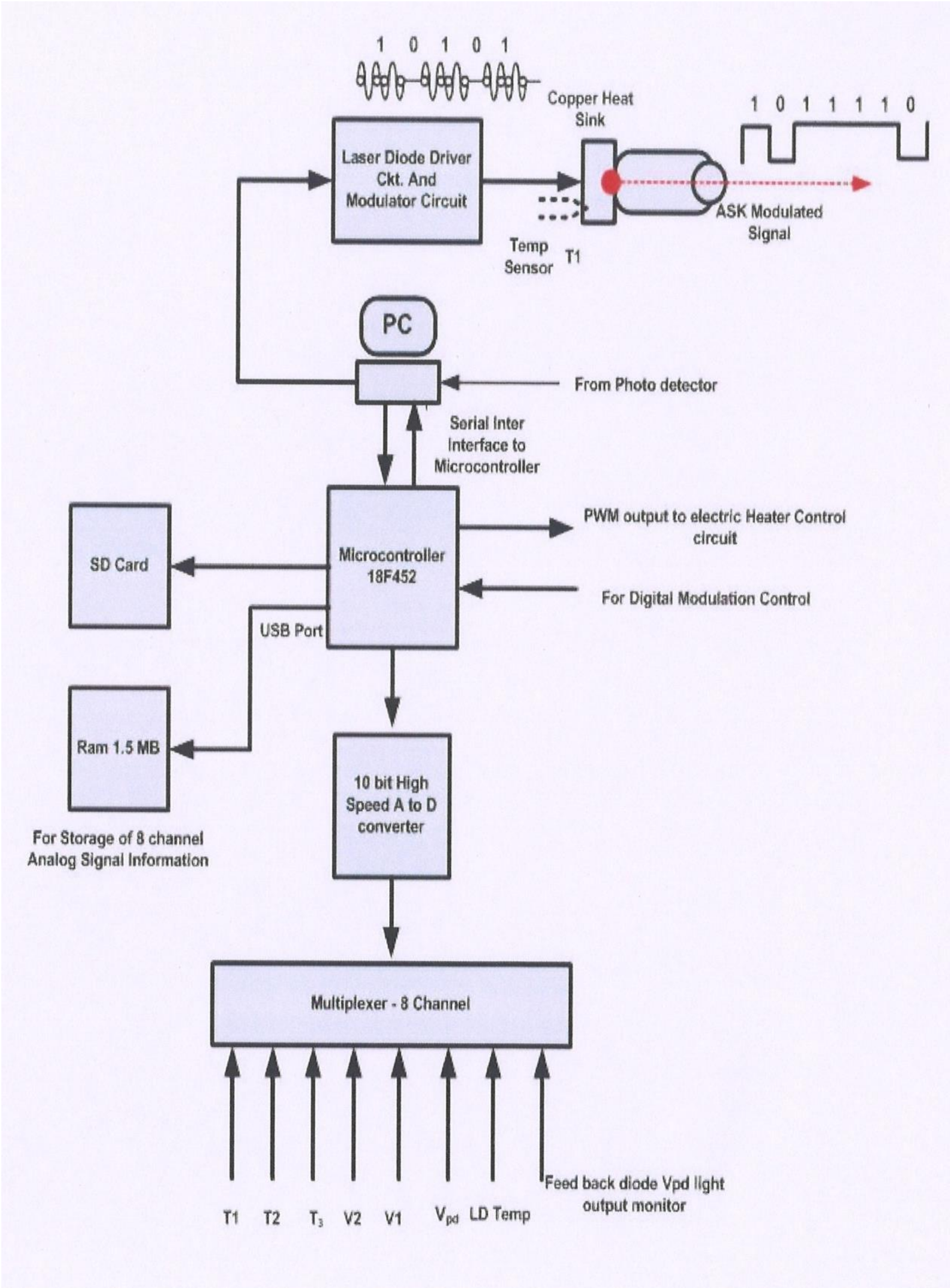

Fig.3.22.2 : Electronic and optical experimental arrangement

3.23 Conclusion :

The proposed folded optics multipath measurement set up for studies of the effects of atmospheric turbulence (scintillation) on short haul optical link is designed and developed. The multipath folded optics system is used to measure the effects of turbulence on an optical beam which carry digital data from one computer to another separated by 27 m distance.

A stabilized current driver circuit and modulator circuit is developed to inject proper current into optical laser source to measure the effects of atmospheric turbulence. Photo-detector circuits with front end low noise preamplifier is designed and developed on a three-axis positional system to collect maximum signal radiated from optical transmitter. A Data logger system based on PIC18F452 is designed to store transmitted and received turbulence affected data and displayed in one window. This laboratory standard artificial atmospheric turbulence set up is helpful to measure the transmitted and corrupted bits using the closed loop computer system.

References:

[1] Carnevel M. , Crosignani B. and Porto P.,” Influence of laboratory generated turbulence on phase fluctuations of a laser beam”, Applied Optics , vol-7, issue 6, pp 1121-1123, 1968.

[2] Majumdar Arun, Gamo H. ,” Atmospheric turbulence chamber for optical transmission experiment : Characterization by thermal method”, Applied Optics , vol- 17, issue 23, pp-3755-3762, 1968.

[3] Richard A. Elliott, J. Richard Kerr ,” Optical propagation in laboratory – generated turbulence “, Applied Optics , vol-18,issue 19, pp-3315-3323, 1979.

[4] Ibrahim M. M. and Ibrahim A.M. ,” Performance analysis of optical receiver with space diversity reception “, Proc. IEEE comm.. vol-143,no-6, pp-369-372, Dec 1996.

[5] Laser diode : L780P010 Thorlabs
https://www.thorlabs.com/thorproduct.cfm?partnumber=L780P010
Laser diode: L980P010
https://www.thorlabs.com/thorproduct.cfm?partnumber=L980P010
Laser diode : ML7XX11 Mitsubishi
https://www.mitsubishielectric-mesh.com/products/pdf/ml7xx11.pdf
http://www.princetel.com/datasheets/1550%20nm%20ML925B45F-01.pdf

[6] Photo diode : FDS010 Thorlabs
https://www.thorlabs.com/thorproduct.cfm?partnumber=FDS010

[7] Sample and hold: LF198 National semiconductor
https://www.alldatasheet.com/datasheet-pdf/pdf/8575/NSC/LF198.html

[8] Theodoros A. Tsiftsis, Sandalidis H.G. ," Optical wireless link with spatial diversity over strong atmospheric turbulence channels", IEEE Transaction on wireless communication vol 8, no-2, pp-951-957 Feb 2009

[9] Senior."OpticalFiber Communication Principles and Practice ", Second Edition , Prentice –Hall, 1999.

[10] Xiaoming Zhu and Joseph M. Khan," Free Space Optical Communication Through Atmospheric Turbulence Channels", IEEE Transactions on Communications, Vol. 50, No.8, August 2002.

[11] Terminal software for serial data communication v1.9b, http://bray.velenje.cx/avr/terminal Accessed on 20 May 2013.

[12] Sevincer A., Bilgi M., Yuksel M., and Pala N., "Prototyping Multi-Transceiver Free-Space-Optical Communication Structures." Accessed on 20 May 2012.

[13] Miyamoto W. Ni, Wakamori Y., and K. Kazaura, "Experimental Study of Atmospheric Turbulence Effects on RoFSO Communication Systems," vol. 1, pp. 65–70, 2009.

[14] Temperature Sensors: LM35 National semiconductor
https://www.alldatasheet.com/datasheet-pdf/pdf/8866/NSC/LM35.html

[15] Microcontroller with 10 bit A/D : PIC18FXX2 Microchip
https://ww1.microchip.com/downloads/en/DeviceDoc/39564c.pdf

[16] RS232 Specifications and standard
http://www.lammertbies.nl/comm/info/RS-232_specs.html

CHAPTER 4

Experimental Studies of Scintillation and Beam Wander Effects on a Free Space Optical Communication Link

4.1 Introduction

In this work, two separate measurements are observed for detailed investigations of the performance of free space optical communication links under (a) scintillation and (b) beam wonder effect for operation in laboratory environments. Both the systems comprised light wave transmitter-receiver systems and the necessary passive optical arrangements for coupling unguided light through the air from the transmitters to the receiver. All operations for a measurement of turbulence effects and its control was made using a computer controlled digital electronic circuit and system as presented in Chapter-3.

The performance of an optical communication link for 27 m distance using laser diode was studied in detail to see how the atmospheric temperature affects their operation as well as how to make simultaneous control of the illumination and communication in outdoor environment. The experimental study has been done to characterize the variation of beam wander displacement for various turbulence conditions at 698 nm operating wavelength. This study helped to analyze the fluctuations in the received irradiance due to beam wander effect.

4.2 Measurement of Electro-Optics Characteristics of Laser Diode and LED used in FSO Link Design.

We have used several laser diodes emitting light in the visible (550 nm, 670 nm, 680 nm) and NIR (860 nm, 1300 nm and 1550 nm.) regions. All the devices were single mode lasers with room temperature threshold currents below 15 mA. We used silicon PIN photodiodes and InGaAs photodiode for detecting visible and NIR wavelength photons respectively.

For studies on the performance of indoor optical wireless communication link, multiple white light LED modules were designed and used simultaneously as illuminating sources and optical transmitters of broadband signals in indoor environment. Each LED Module has a cluster of five white LEDs for illumination and communication purposes.

Since the energy band-gap of the materials for semiconductor lasers, LEDs and the photodiodes were different, the spectral emission and absorption behaviors were also different. The corresponding electrical current-voltage (I-V) characteristics temperature characteristics and spectral behaviors were also very different. Since the manufacturers of the devices did not provide the relevant characteristics of the devices for their applications in our measurement set up, we had to measure the above characteristics of the devices before we used them in our laser and LED driver circuits and photodiode amplifier circuit design. The measured electro-optical characteristics of the devices are graphically presented below.

4.2.1 L-I Characteristics of Laser diode:

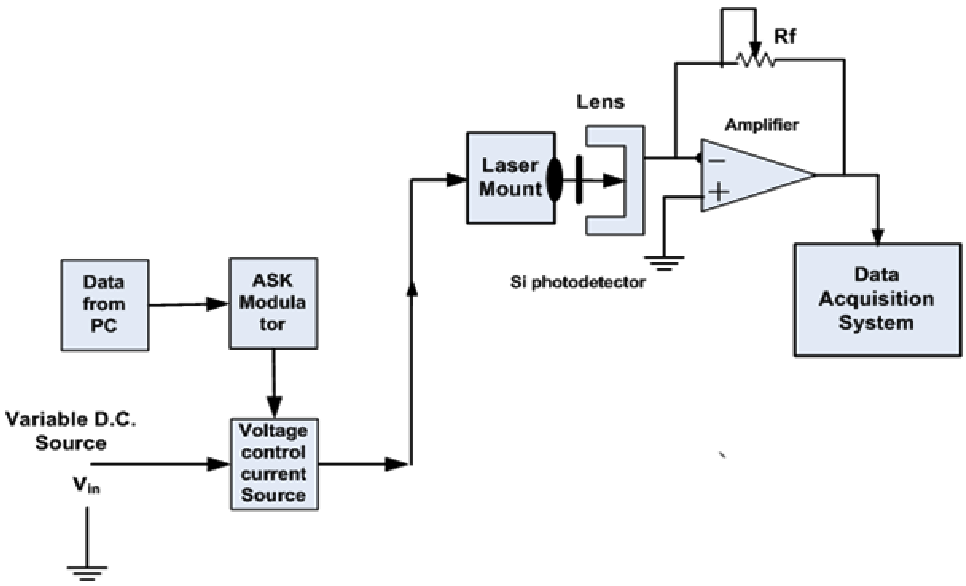

Fig.4.2.1 : Experimental setup for L-I char. of 698.9 nm, 780 nm,980 nm,1310 nm,1550 nm wavelength laser diode. (V_{in} is DC Voltage)

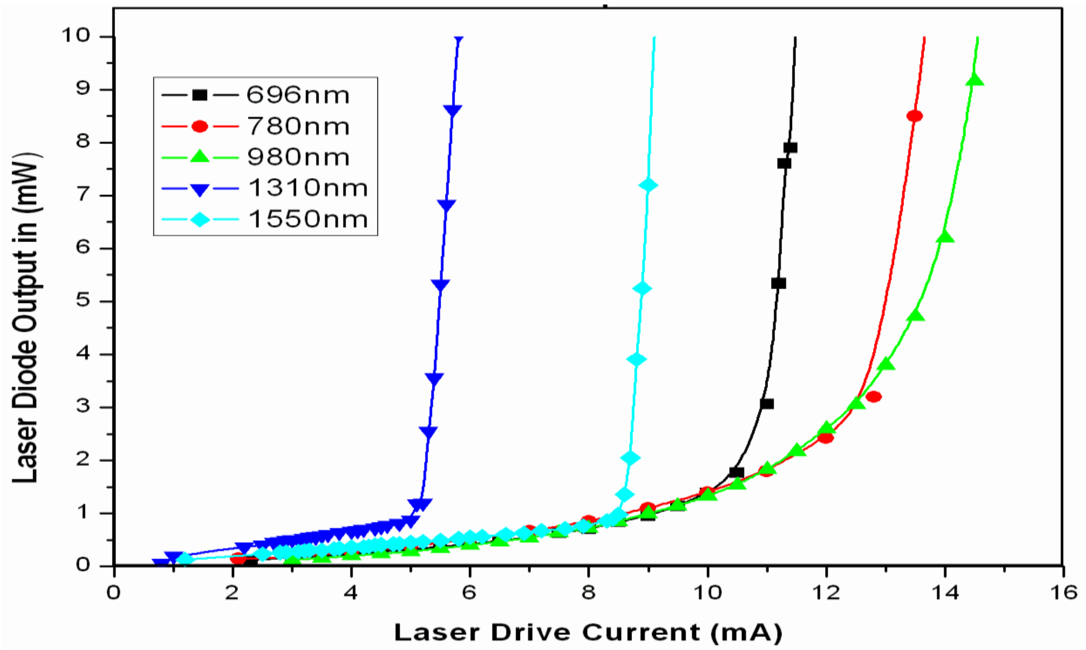

Fig.4.2.2 : Characteristics of laser diodes (696 nm,780 nm,980 nm, 1310 nm, 1550 nm) at room temperature

The experimental arrangement for measurement of L-I characteristics is shown in Fig.4.2.1 and L-I char of laser diodes shown in Fig. 4.2.2, we observe that at low values of the input current, the device acts as a normal diode, producing a small amount of light. At a threshold value, where the population inversion is large enough such that gain is increases by stimulated phenomenon, the coherent light is emitted. As current increases above the threshold value, the light output increases much more rapidly than in the LED region. Ideally, the light output should increase linearly with current. Here we tabulated all lasers with their observed threshold current and voltage across laser at threshold level. Room temp =28^{0}C. R_F= 844kΩ.

Table 4.1Observed threshold current and voltage at Room Temp =28^{0}C

Device Specification	Wavelength (λ) In nm	Threshold Current I_{th}(mA)	Voltage across laser at threshold (V)
China Laser L1 (AlGaAs)	696 nm	10 mA	2.07
China Laser L2(AlGaAs)	696 nm,10 mw	11.2 mA	2.10
AlGaAs	780 nm,10 mw	13.9 mA	1.82
GaAs	980 nm,10 mw	14.5 mA	1.43
InGaAsP	1310 nm,10 mw	5.43 mA	1.05
InGaAsP	1550 nm, 5 mw	8.9 mA	0.92

From above table 4.1 we observe that, Voltage across laser at threshold level decreases because the band gap of the material decreases for longer wavelength. The I-V and power spectrum characteristic is shown in Fig.4.2.3 and Fig.4.2.4 respectively.

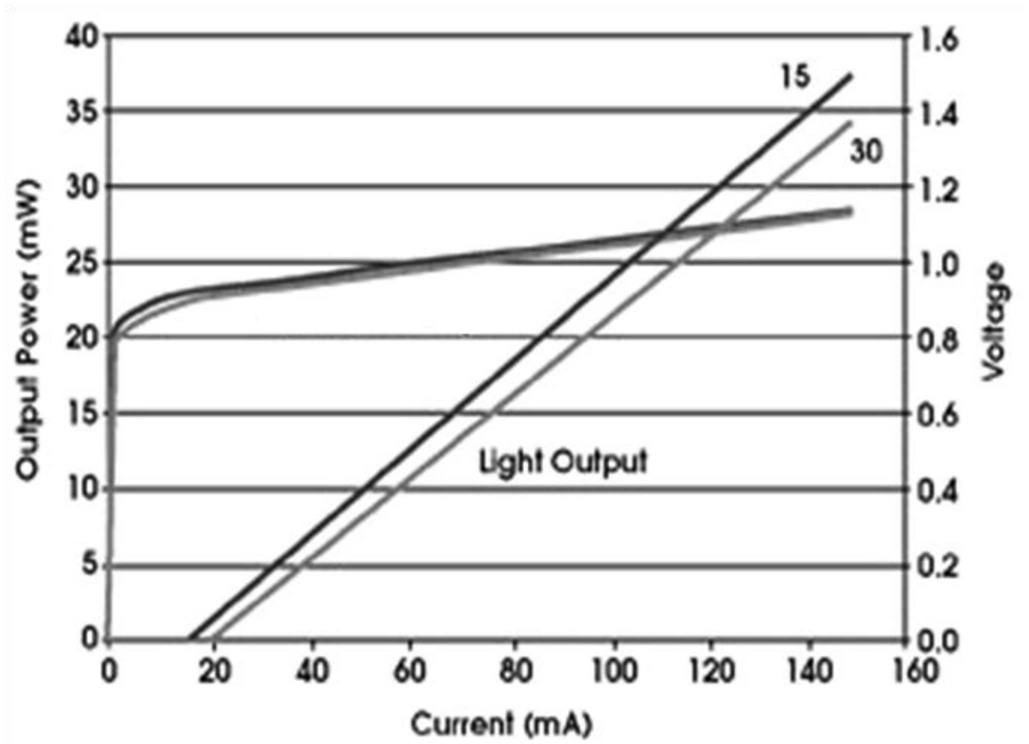

Fig.4.2.3 : I-V Characteristics laser diode

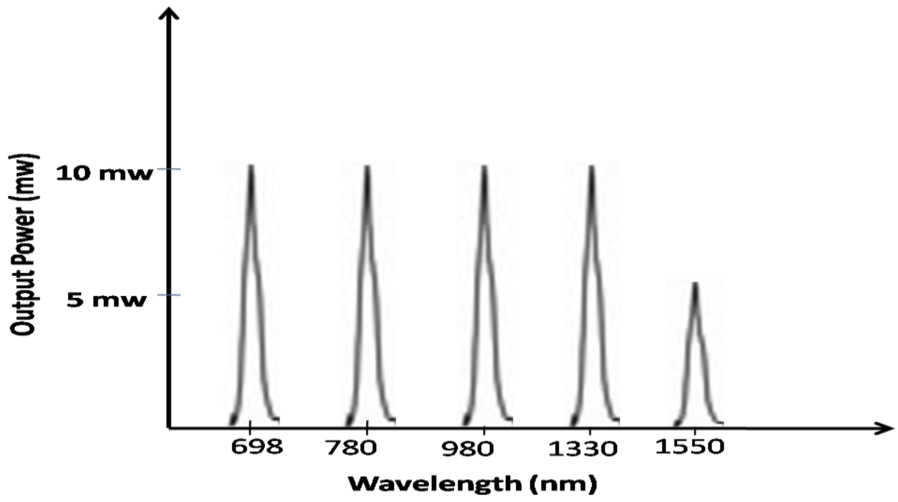

Fig. 4.2.4 : Spectrum characteristics of laser used for experimentation

4.2.2 L-I Characteristics of White Light LED.

Experimental arrangement for L-I and I-V characteristics of LED is shown in following Fig.4.2.5. LED is placed very near to photodetector. Variable current is injected to diode and simultaneously voltage is measured across diode and photo-detector. Measured values are plotted and shown in fig.4.2.6 and fig.4.2.7.

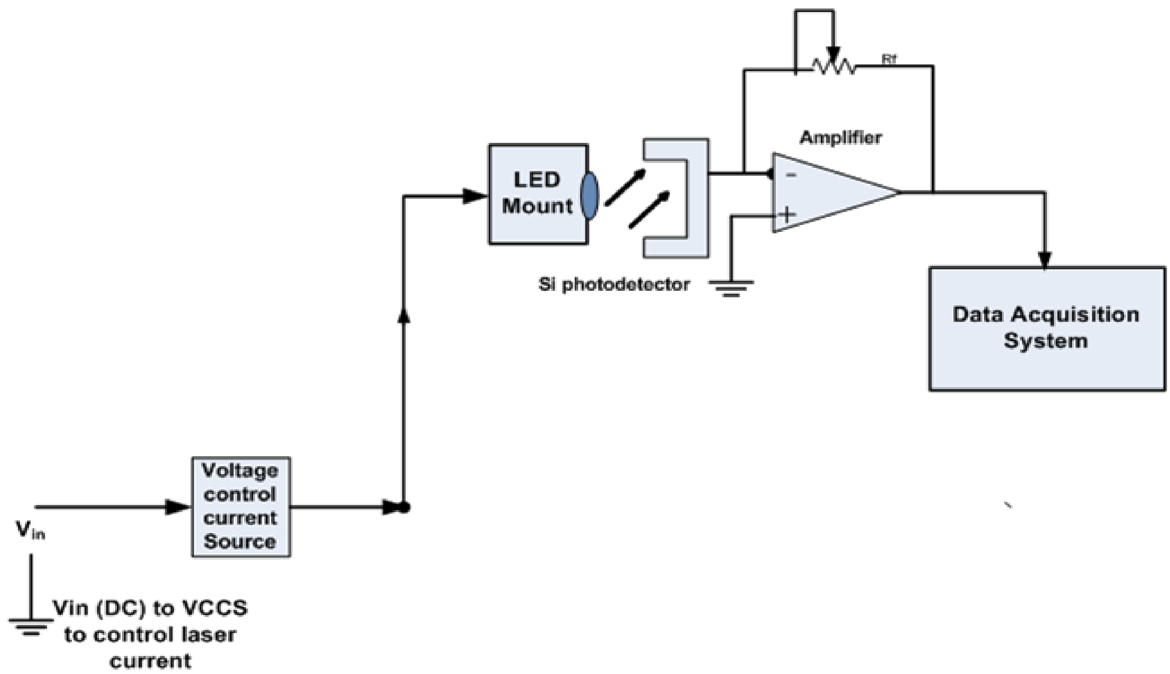

Fig 4.2.5 : Experimental arrangement for measurement of LED characteristics.

We perform this experiment with following parameter.

Color of LED optical beam - White, Number of LED- 01, Input D.C. Voltage - 0 to 5V Room Temp=29^{0}C Constant. Distance between Tx and Rx is ≈Zero; Rf = 10 KΩ ; R2=100Ω; R3=1 KΩ

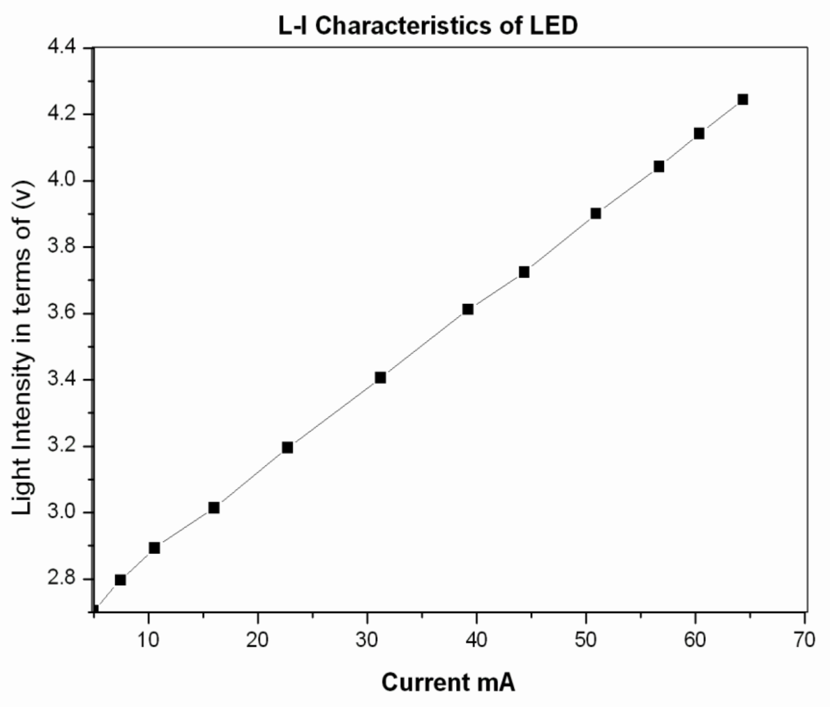

Fig. 4.2.6 : L-I Characteristics of LED

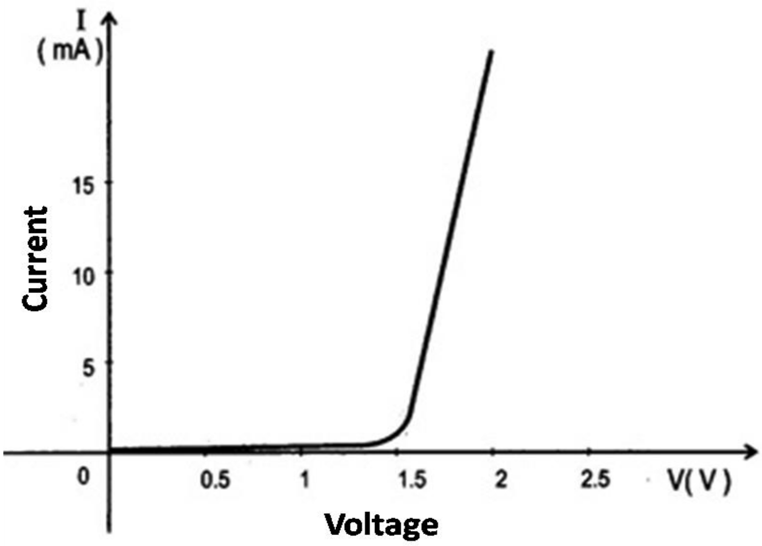

Fig. 4.2.7 : V-I Characteristics of LED

4.3 Tuning and Calibration of Equipments in Computerized Feedback Controlled Atmospheric Turbulence Set Up and Data Acquisition System.

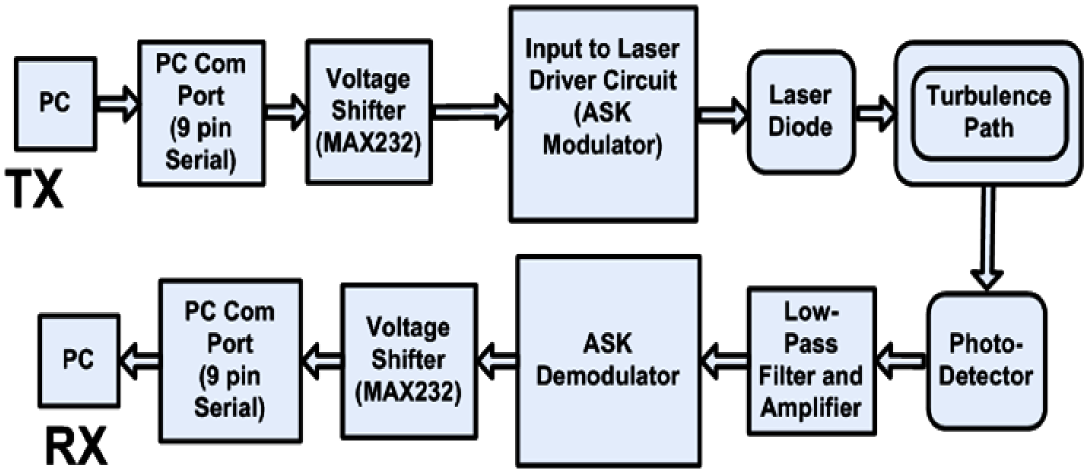

Fig. 4.3.1 : Schematic diagram of the PC based measurement set up for studies of effect of atmospheric turbulence on optical beam propagation

The L-I and V-I characteristics of laser diode and LED are studied in last section to know the behavior of light intensity with injected biasing current. For measurement purpose we select 698 nm laser having threshold current 11.2 mA and output power is 10 mW. Fig 4.3.1 shows the overall setup to measure the effects of turbulence on optical beam which carry a digital data from one computer to another computer separated by 27 meter distance. Transmitting and receiving side consist of computer system installed with terminal software, which is use to generate and accept the serial data bits in ASCII, Binary and Hexadecimal code form.

Component Selection

Following component are used to set up optical link

Transmitter section (Laser Source)

1. GaAlAs696 nm, 10 mW laser diode with threshold current =11.2 mA

Receiver section (Photodiode)

1. Si Photodiode, 10 ns Rise Time,

   Responsivity 350 - 1100 nm, 3.6 mm x 3.6 mm Active Area

We started with testing of transmitter and receiver system. The whole experiment was conducted in a dark room to reduce the effect of ambient light to a minimum as shown in fig 4.3.2. The transmitter receives a digital data from data source and produce appropriate amount of current to drive a laser diode and emitting visible red light of 696.8 nm wavelength into free space.

Following parameters are selected to perform the experiment.

Laser wave-length =696 nm; Room Temp=25^{0}C ; Total Number of reflectors - 04;Modulation type ASK , Carrier Frequency – 5 KHz; Distance between Tx and Rx-27 meter; Lens Diameter=5 cm ;

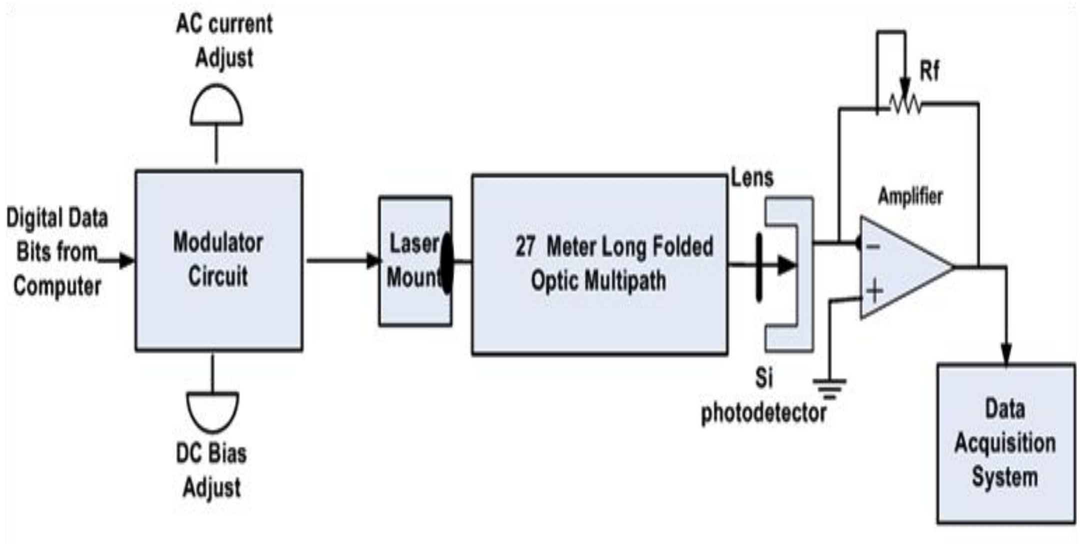

Fig. 4.3.2 : Experimental arrangement to test transmitter and receiver signal under No turbulence Condition

To test analog signal, we select 5 KHz, 3V carrier analog signal (Without Modulation) applied to the laser diode biasing circuit, where it is converted into optical beam through intensity modulation. The laser beam then travel through multiple optical paths covers 27 meter distance with no turbulence and room temp is 25^{o}C.

At the receiver side the signal is converted back into analog signal through PIN photo-detector. The following Fig. 4.3.3 shows display of CRO , the transmitted signal which is applied to laser diode (Channel -1) and received signal (Channel 2) at the output of photo-detector with no temperature variation or turbulence in the Lab.

To performed experiments using some specific TEST digital signals in our turbulence set up, we used a computer software entitled "Terminal" [see chapter 3] for generating and transmitting continuous bits for modulation of the laser source. The laser diode transmitter produced identical light wave signals to pass through the atmospheric turbulence medium. ", As the light passed through the atmosphere, they were corrupted by the turbulent medium depending on the strength of turbulence and these corrupted pulses are finally received at the receiver photodiode",. The received pulses are then forwarded to the computer port for bit-by-bit comparison within the computer using the same Terminal software.

To test digital signal, we used terminal software window for sending and receiving the bits traveling through folded multipath optical link. Digital data is first modulated by ASK modulator and then applied to the laser driver circuit. A continuous train of 10101…..bits are transmitted and simultaneously receive at the input serial port of computer. Display of terminal software window for the complete process is given in fig. 4.3.4.

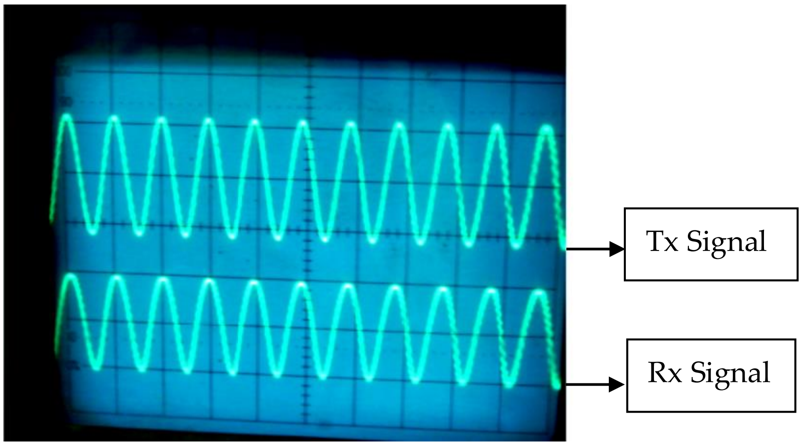

Fig.4.3.3 : CRO Display for Tx and Rx analog signal (without turbulence)

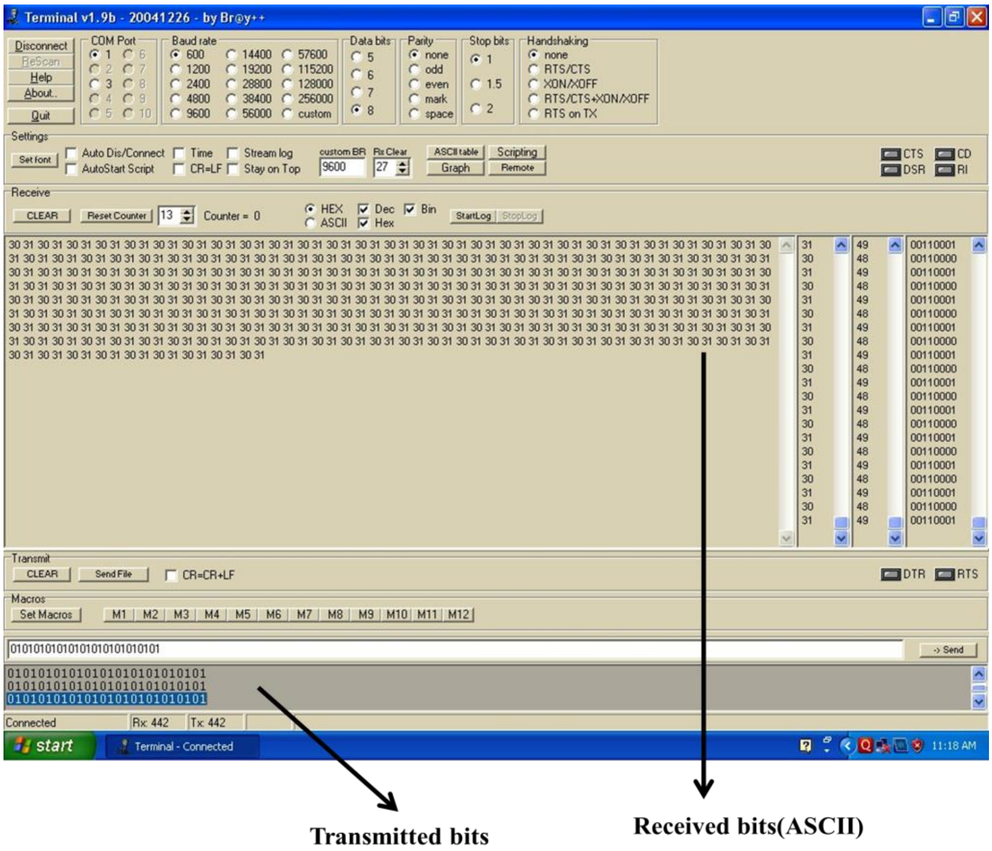

Fig. 4.3.4 : Computer display for Tx and Rx digital signal

4.4 Studies on the Thermally Induced Random Fluctuations of Intensity of Multipath Optical Beam Using the Measurement and Test up.

4.4.1 Case I: Effects of Turbulence on the Varying Lengths of Optical Path

Here we measured turbulence effects with varying path length using the experimental set up as shown in Fig. 4.4.1 , we take the observations for 16 meter and 27 meter optical path with following experimental parameters.

Laser wave-length =698.9 nm; Total Number of reflectors -04 ; Total number of reflections of laser beam-08 ; Number of passes of optical beam between Tx and Rx -05; Distance between Tx and Rx-27 meter; Room temp=Min 25^0C and Max =35^0C; Heater Coil current- 1.8 Amp.; Receiver Aperture Diameter=5 cm Laser Current=13 mA.

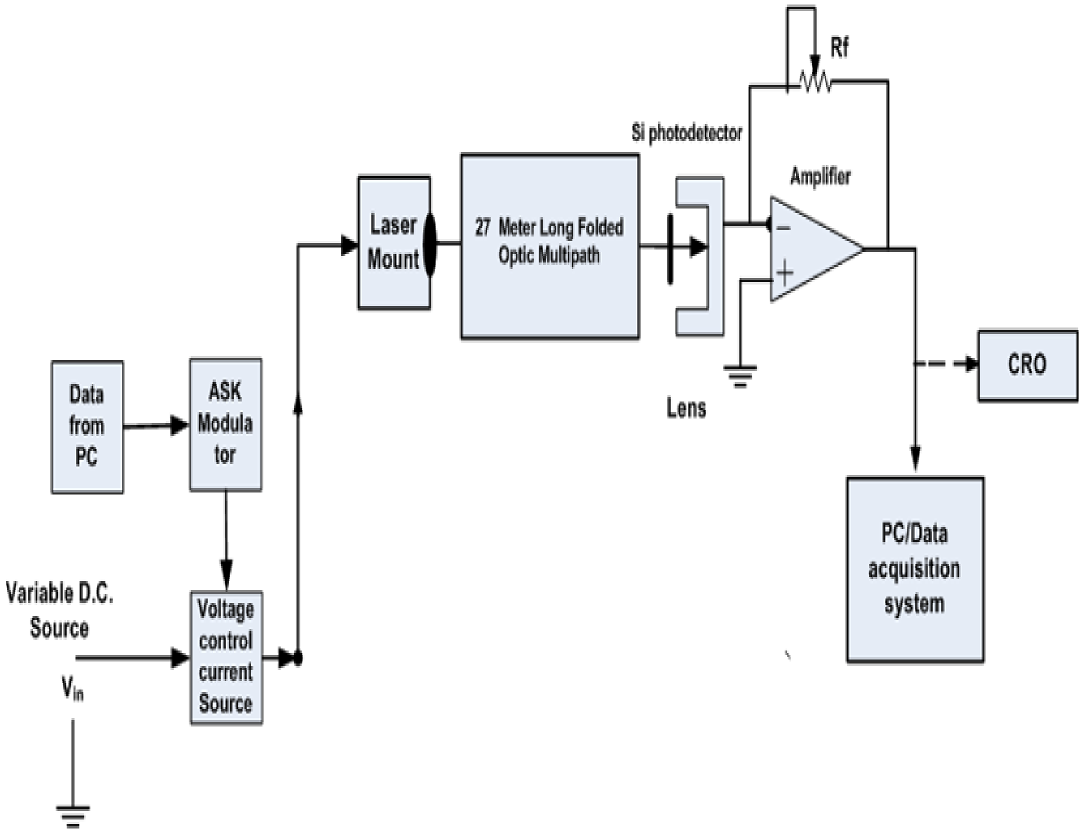

Fig 4.4.1 : Experimental set up for measurement of intensity fluctuations due to temp induced optical turbulence

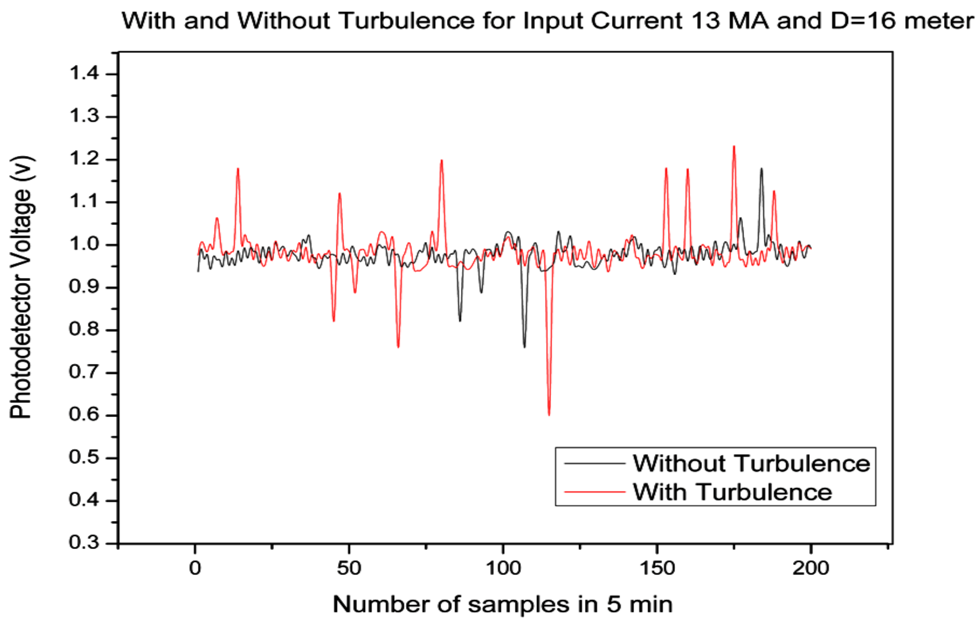

Fig.4.4.2 : Scintillation measurement: with turbulence and distance is 16meter

optical path Length L=16m, Rytov variance =0.0055 For Fig 4.4.2 (Black curve).

optical path length L= 16m, Rytov variance=0.015 For Fig.4.4.2 (Red Curve).

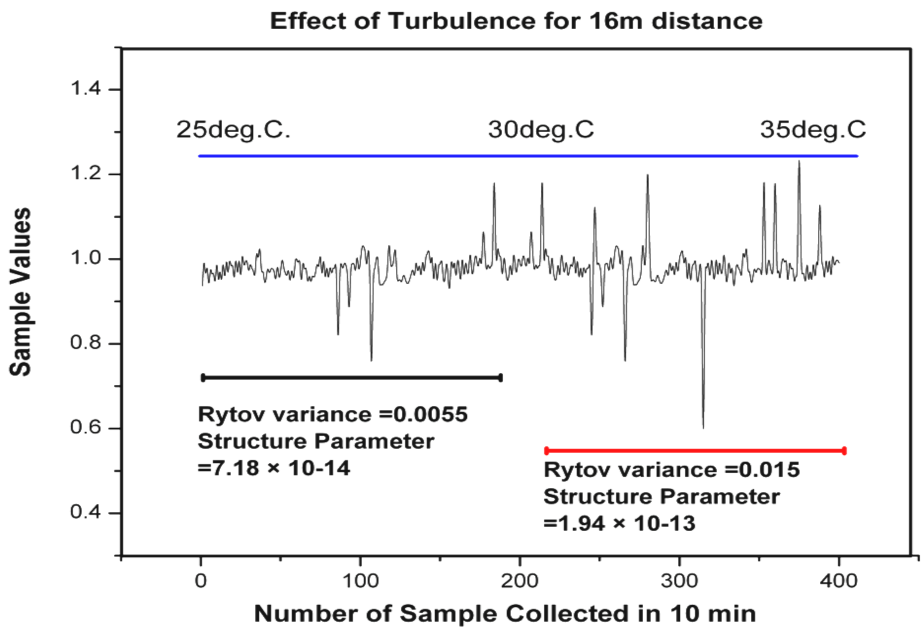

Fig. 4.4.3 : Scintillation effect for 16 meter distance

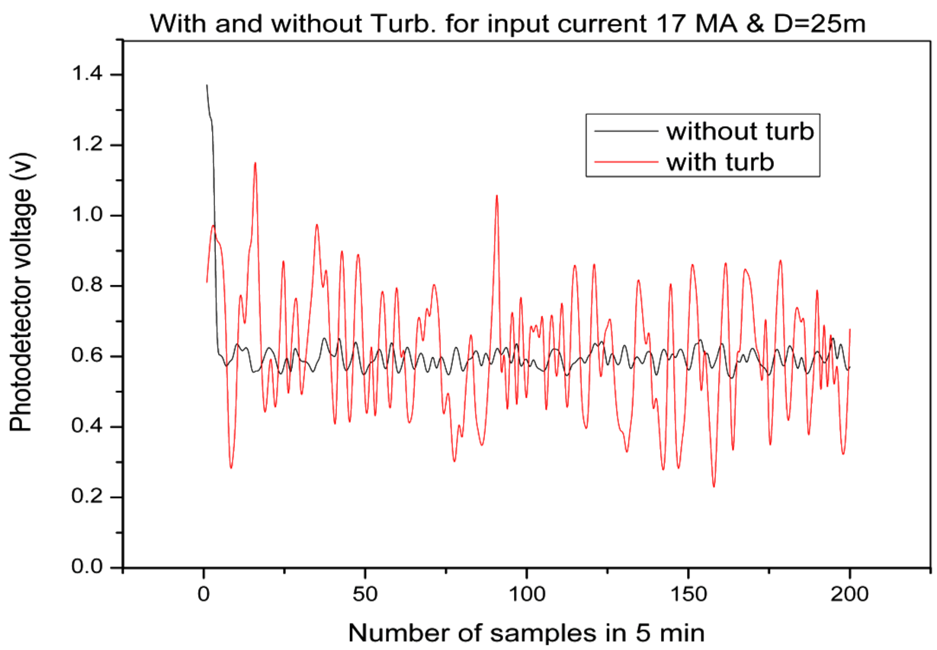

Fig. 4.4.4 : Overall scintillation effect for 25m distance

From above Fig 4.4.2 , 4.4.3 and 4.4.4 it is shows laser radiation propagating through turbulence develops both temporal and spatial fluctuations of irradiance with temperature and optical path distance , which is defined as scintillation (red lines).

A laser-com system generally integrates the signal spatially at the plane of a receiver, but will still see temporal fluctuations in intensity. Scintillation is a serious issue for laser communications for both terrestrial as well as ground-to-space or space-to-ground data links, as it can produce large transient dips in the signal. The fading of the received signal below a prescribed threshold temporarily degrades, or even annihilates, the link performance. Fig 4.4.4 also shows for 27 meter distance (Rytov variance =0.55,0.8) affect more on the quality of signal than 16 meter optical path length as the temperature is changes from 25^0C to 35^0C. As temperature is increases more intensity fluctuation is observed at the output of photo-detector.

4.4.2 Case II: Effects of Turbulence on the Bit Rate Variations of Optical Signal

Table -4.2

Measurement of BER under different room Temp starting from (23 ^{0}C) and Constant Baud Rate Laser Current start from-13.2 mA, λ=698.9 nm, Modulation ASK with carrier amplitude 5V (P-P) and Frequency – 5 KHz. , Output data from PC –TTL.

Sl.No.	Illumination condition	Apertu-re Diame-ter (cm)	Lab Temp	Laser Current mA	Bit Rate bit/sec	Bit period	Bit Se-nt	Run 1	Run 2	Run 3	Run 4	Run 5	Sum	Average BER bit/sec
1	Dark	5	23^{0}C	13.2	11400	87 µs	400	02	02	03	02	04	13	0.0325
2	25W-bulb	5	23^{0}C	13.2	11400	87 µs	400	05	05	02	06	05	23	0.0575
3	200W	5	23^{0}C	13.2	11400	87 µs	400	05	03	05	07	04	24	0.060
4	225W	5	230C	13.2	11400	87 µs	400	10	06	08	05	05	34	0.0875
5	225W & Ton	5	23^{0}C	13.2	11400	87 µs	400	06	06	04	07	02	26	0.068
6	Dark	10	23^{0}C	13.2	11400	87 µs	400	01	02	01	01	02	07	0.0175
7	225W	10	23^{0}C	13.2	11400	87 µs	400	04	04	02	07	03	20	0.050
8	225W &Ton	10	23^{0}C	13.2	11400	87 µs	400	03	01	04	03	08	19	0.0475
9	225W &Ton, SFon	10	23^{0}C	13.2	11400	87 µs	400	0	04	06	05	6	21	0.0525
10	225W&Ton,SFon,ACoff	10	23^{0}C	13.2	11400	87 µs	400	04	07	05	03	12	31	0.0775
11	225W &Ton, SFon,H1	10	26^{0}C	13.2	11400	87 µs	400	03	04	13	55	06	81	0.2025
12	225W &Ton, SFon,H1,H2	10	28^{0}C	13.2	11400	87 µs	400	186	175	203	145	11	720	1.80
13	10cm+225W +Ton+ SFon+H1+H2+H3	10	29^{0}C	13.2	11400	87 µs	400	54	177	190	117	163	701	1.85

Sl.No.	Illumination condition	Apertu-re Diame-ter (cm)	Lab Temp	Laser Current mA	Bit Rate bit/sec	Bit period	Bit Se-nt	Run 1	Run 2	Run 3	Run 4	Run 5	Sum	Average BER bit/sec
14	10cm+225W +Toff+ SFoff+H1+H2+H3	10	29.1^{0}C	13.2	11400	87 µs	400	15	133	196	200	120	664	1.70
15	225Woff &Toff, SFoff,H1,H2,H3	10	29.1^{0}C	13.6	11400	87 µs	400	17	14	10	10	16	65	0.165
16	225Woff &Toff, SFoff,H1,H2,H3	5	29.7^{0}C	13.6	11400	87 µs	400	119	115	187	173	97	691	1.727
17	225Woff &Ton, SFon,H1,H2,H3	5	29.7^{0}C	13.8	11400	87 µs	400	209	170	79	204	80	742	1.855
18	225Woff &Ton, SFon,H1,H2,H3	5	29.7^{0}C	14.0	11400	87 µs	400	20	07	10	04	16	57	0.1425
19	225Woff &Ton, SFon,H1,H2,H3	5	29.7^{0}C	14.2	11400	87 µs	400	07	04	12	04	13	40	0.100
20	225Won &Ton,SFon,H1, H2,H3	5	29.8^{0}C	14.2	11400	87 µs	400	11	16	02	15	07	51	0.1275

Where, T- Tube Light , SF- Small Fan ,H1,H2 and H3- Heater ,25 W and 225 W is the light bulb.

Measurements are taken by sending $(00100001)_2$ '31' as an ideal sample from optical transmitter and simultaneously received using photo detector at receiver under different laboratory conditions. Corrupted samples are collected to measure bit error rate as shown in following fig4.4.5 (a-s)

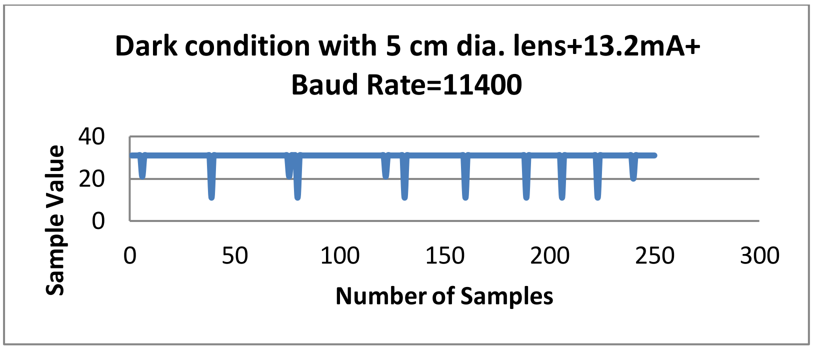

(a) Fluctuation in data sample $(00100001)_2$ due to turbulence-induced irradiance fluctuations at 23°C temperature(scintillation) for 5cm diameter lens: BER=0.035 bit/sec.

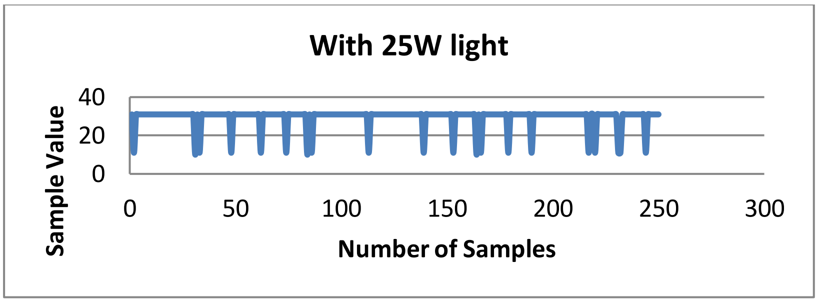

(b) Fluctuation in data sample (00100001)2 due to turbulence-induced irradiance fluctuations and addition of external optical noise radiation due to 25W tungsten light. BER=0.0575 bit/sec.

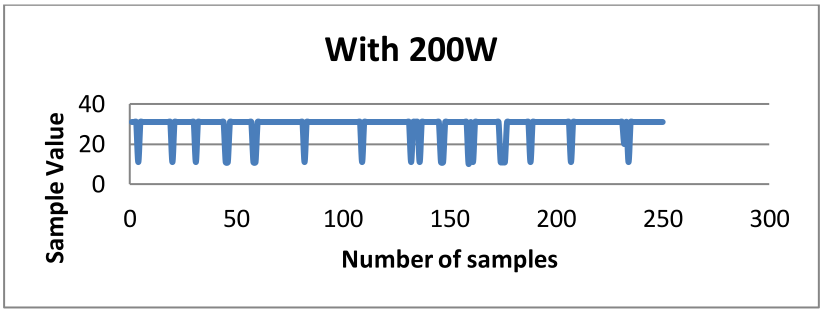

(c) Fluctuation in data sample $(00100001)_2$ due to turbulence-induced irradiance fluctuations and addition of external noise radiation due to 200 W tungsten light. BER=0.060 bit/sec.

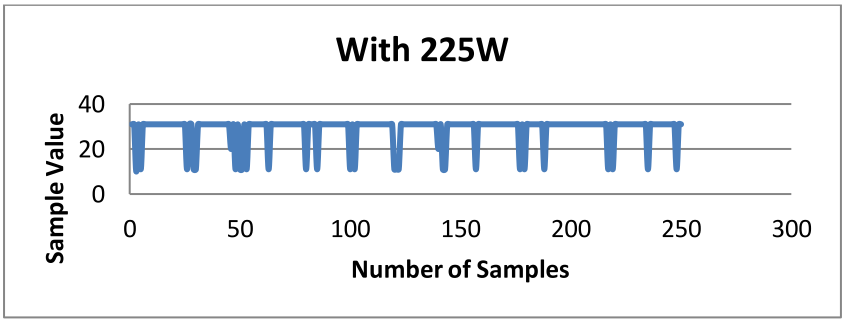

(d) Fluctuation in data sample $(00100001)_2$ due to turbulence-induced irradiance fluctuations and addition of external optical noise radiation of 25 W +200 W tungsten light. BER=0.0825 bit/sec.

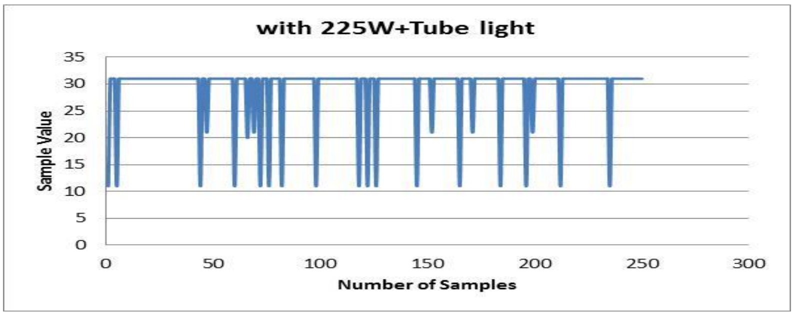

(e) Fluctuation in data sample $(00100001)_2$ due to turbulence-induced irradiance fluctuations and addition of external noise radiation due to 225W tungsten light plus fluorescent tube light (40W). BER=0.065 bit/sec.

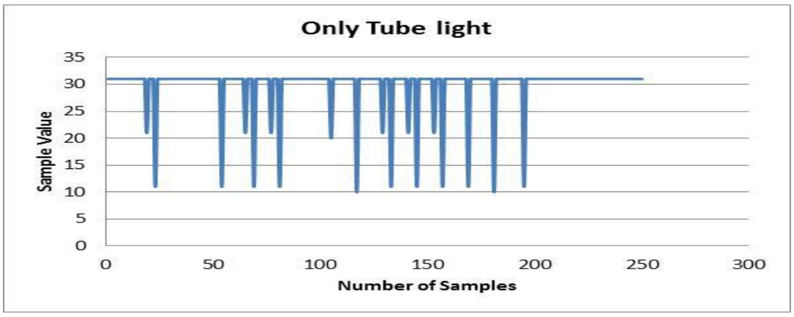

(f) Fluctuation in data sample $(00100001)_2$ due to turbulence-induced irradiance fluctuations and addition of external noise radiation due to only fluorescent tube light (40W): BER=0.053 bit/sec.

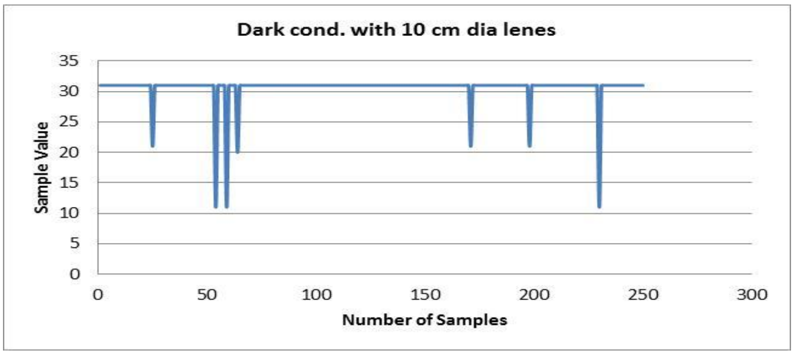

(g) Fluctuation in data sample $(00100001)_2$ due to turbulence-induced irradiance fluctuations is minimise with addition of 10cm diameter lens in dark room condition: BER=0.0175 bit/sec.

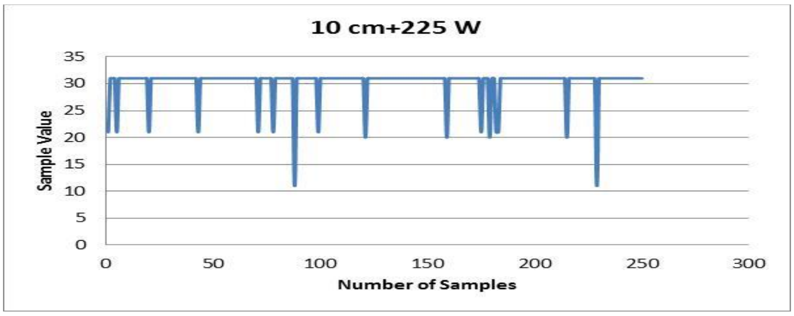

(h) Fluctuation in data sample $(00100001)_2$ due to turbulence-induced irradiance fluctuations plus 225 W external optical noise due to tungsten light is minimise with addition of 10cm diameter lens: BER=0.050 bit/sec.

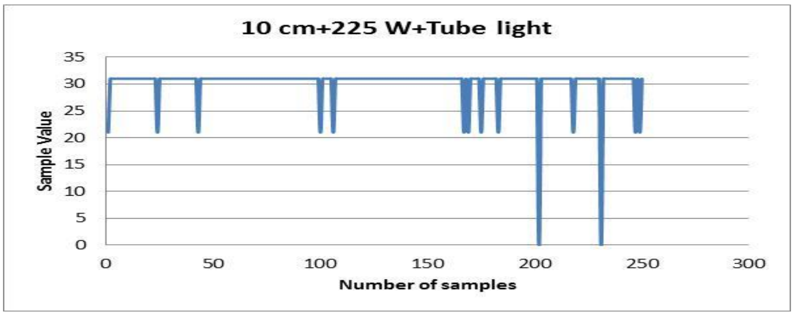

(i) **Fluctuation in data sample (00100001)$_2$ due to turbulence-induced irradiance fluctuations plus 225 W external optical noise due to tungsten light and fluorescent tube light is minimise with addition of 10cm diameter lens : BER=0.0475 bit/sec.**

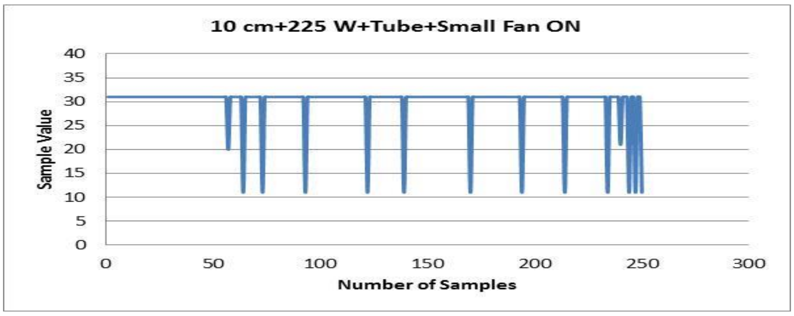

(j) **Fluctuation in data sample (00100001)$_2$ due to turbulence-induced irradiance fluctuations plus 225 W + 40 W external optical noise due to tungsten light and fluorescent tube light with addition of air velocity using small fan for 10cm diameter lens :BER=0.0625 bit/sec.**

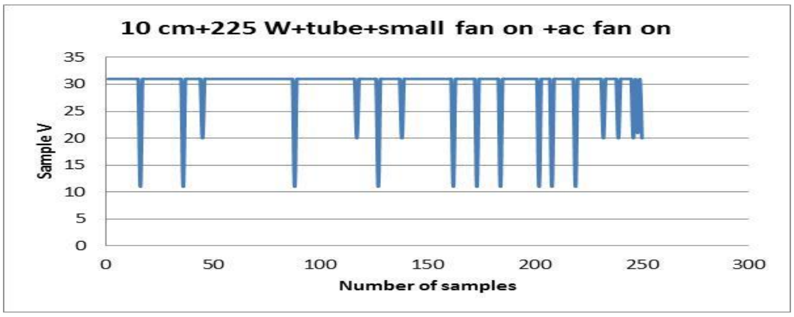

(k) **Fluctuation in data sample (00100001)$_2$ due to turbulence-induced irradiance fluctuations plus 225 W + 40 W external optical noise due to tungsten light and fluorescent tube light with addition of air velocity using small fan and AC fan for 10cm diameter lens :BER=0.0775 bit/sec.**

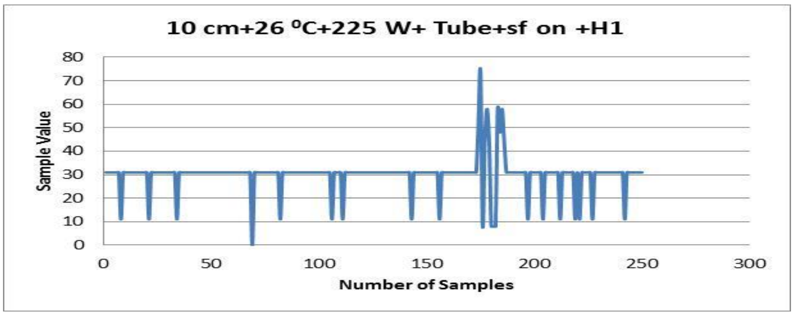

(l) **Fluctuation in data sample (00100001)$_2$ due to turbulence-induced irradiance fluctuations (here temp. is increased by 3^{0}C using room heater H1) plus 225 W + 40 W external optical noise due to tungsten light and fluorescent tube light with addition of air velocity using small fan and AC fan for 10cm diameter lens : BER=0.205 bit/sec.**

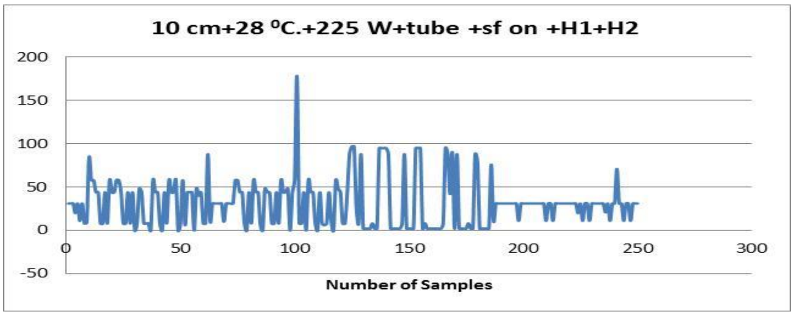

(m) **Fluctuation in data sample $(00100001)_2$ due to turbulence-induced irradiance fluctuations (here temp. is increased by 5 ^{0}C using room heater H1,H2) plus 225 W + 40 W external optical noise due to tungsten light and fluorescent tube light with addition of air velocity using small fan and AC fan for 10cm diameter lens: BER=1.80 bit/sec.**

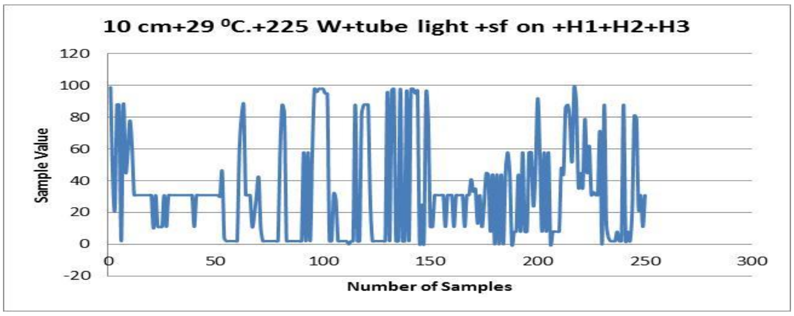

(n) **Fluctuation in data sample $(00100001)_2$ due to turbulence-induced irradiance fluctuations (here temp. is increased by 6^{0}C using room heater H1,H2,H3) plus 225 W + 40 W external optical noise due to tungsten light and fluorescent tube light with addition of air velocity using small fan and AC fan for 10 cm diameter lens :BER=1.85 bit/sec.**

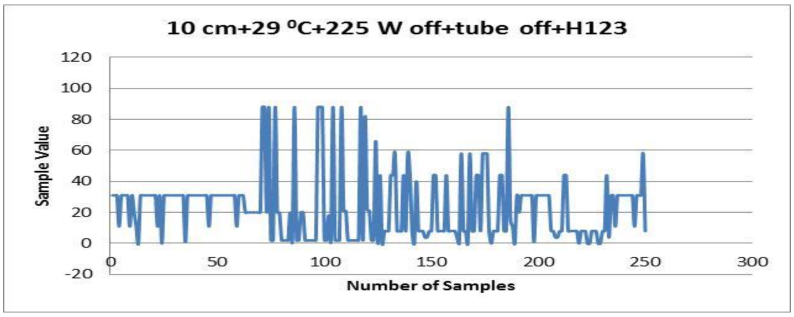

(o) **Fluctuation in data sample $(00100001)_2$ due to turbulence-induced irradiance fluctuations (here temp. is 29^{0}C using room heater H1,H2,H3) and removing 225 W + 40 W external optical noise due to tungsten light and fluorescent tube light for 10cm diameter lens :BER=1.70 bit/sec.**

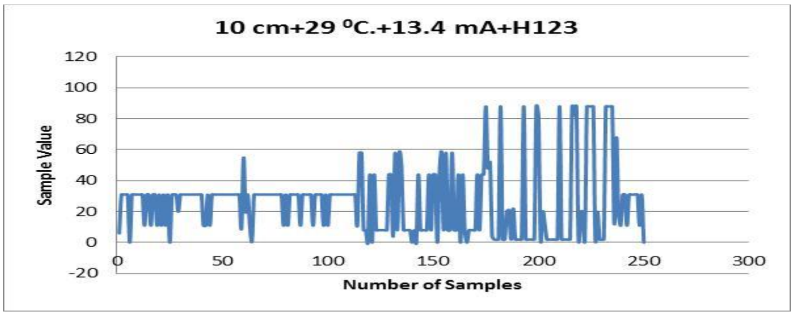

(p) **Fluctuation in data sample $(00100001)_2$ due to turbulence-induced irradiance fluctuations (here temp. is 29^{0}C using room heater H1,H2,H3) is minimizes with increase in laser biasing current by 0.4 mA for 10 cm diameter lens :BER=1.380 bit/sec.**

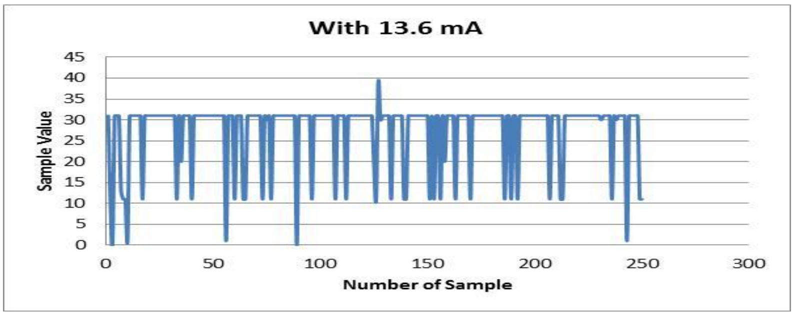

(q) **Fluctuation in data sample (00100001)2 due to turbulence-induced irradiance fluctuations (here temp. is 29⁰C using room heater H1,H2,H3) is minimizes with increase in laser biasing current by 0.6 mA for 10cm diameter lens :BER=0.165 bit/sec.**

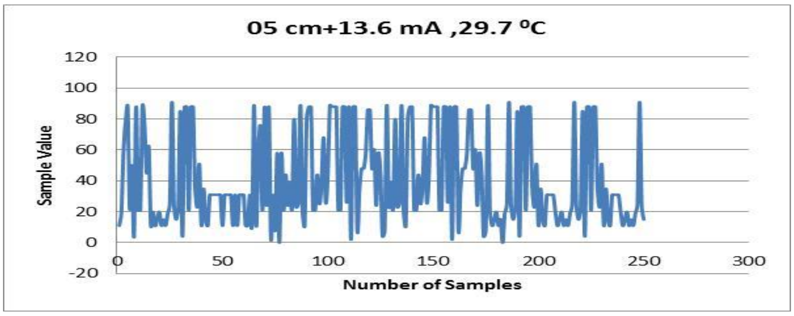

(r) **Fluctuation in data sample (00100001)2 due to turbulence-induced irradiance fluctuations (here temp. is 29.7⁰C using room heater H1,H2,H3) is increase for 5cm diameter lens with 225 W external optical noise and same laser biasing current 13.6 mA :BER=1.727 bit/sec.**

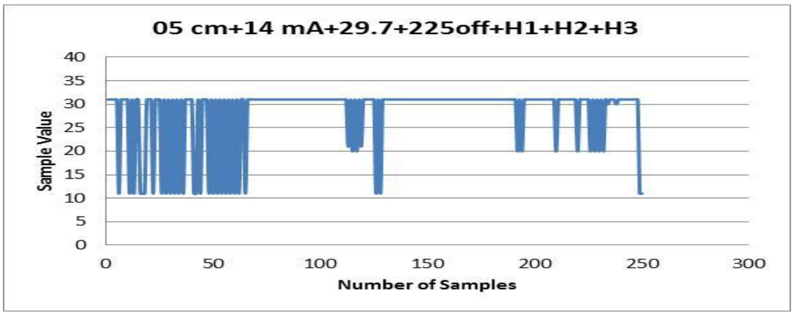

(s) **Fluctuation in data sample (00100001)2 due to turbulence-induced irradiance fluctuations (here temp. is 29.7⁰C using room heater H1,H2,H3) is decrease for 5cm diameter lens with laser biasing current increased by 0.4 mA :BER=0.1425 bit/sec.**

Fig. 4.4.5 : (a-s) Effect of turbulence on BER

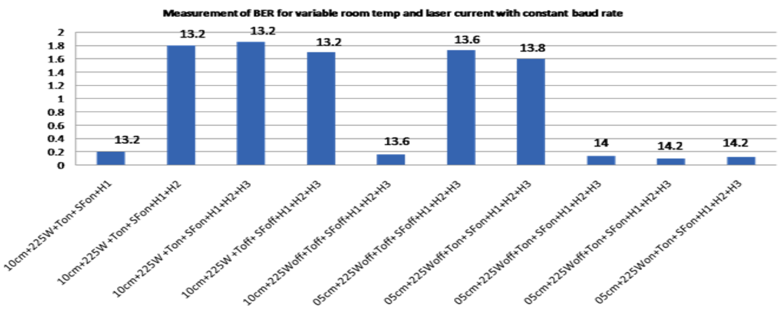

Fig.4.4.6 : BER (Y- axis) variations with laser drive current

Above fig.4.4.6 shows the BER variations for different laboratory conditions. Aperture averaging effects is observed using 5 cm and 10 cm diameter lens at different laser basing current. For 5 cm diameter lens maximum BER shows 1.8 at 13.8 mA laser basing current, however it decreases to 0.2 when laser current increases up to 14 mA.

4.4.3 Case III: Comparison of BER Performance-- with and without turbulence.

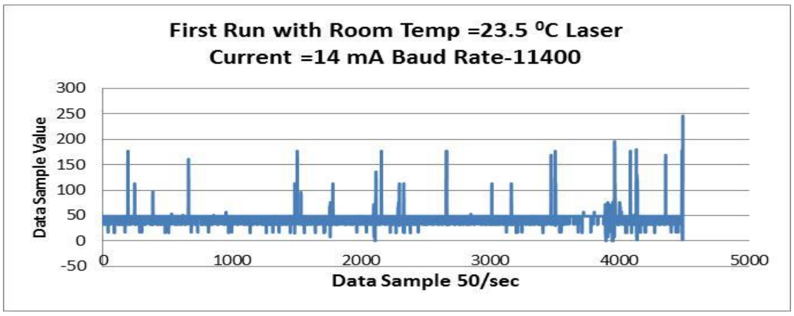

Fig.4.4.7 : Effect of temperature on data samples (without turbulence)

Above figure shows fluctuation in data sample $(00100001)_2$ due to turbulence-induced irradiance fluctuations (here temp. is 23.5 ^{0}C) i.e. No turbulence here total bits are transmitted =3600; bits in Error found =1518; BER=0.0423.

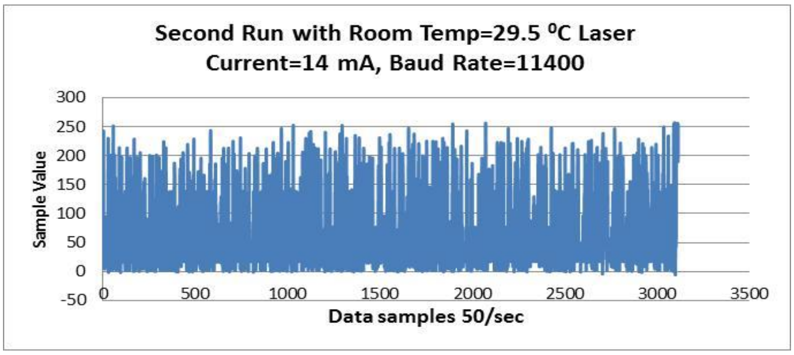

Fig.4.4.8 : Effect of temperature on data samples (with turbulence)

Above figure shows fluctuation in data sample $(00100001)_2$ due to Turbulence-induced irradiance fluctuations (here temp. is 29.5 ^{0}C increased by 6 ^{0}C) i.e. with turbulence here Total Bits transmitted =24920, Bits in Error=11767, BER=0.4723.

The bit rate is the maximum rate of signal transitions that can be supported by a channel. In a channel where noise is present, there is an absolute maximum limit for the bit rate and this limit arises because the difference between two adjacent signal levels become comparable to the noise level when the number of signal levels is increased. Above figures 4.4.7 and 4.4.8 clearly shows that as temperature is increases more fluctuations are occurred and affect the decision level at receiver which will produce more bits in error.

4.5 Studies on the Mitigation of Atmospheric Scintillation Effects on Optical Beam by Controlling Transmitter Optical Output Power and by Data Rate Control.

4.5.1 Case I: Reducing the Bit Error Rate by Controlling Laser dc Drive Current

We have made the experimental arrangement as shown in figure 4.5.1 to study the BER by controlling laser dc Drive Current. we arrange one serial output port for sending a specific bit pattern 250 times (250*8=2000 bits) '31' in BCD code as '00110001' and then measure the corresponding affected bit patterns of the test bit pattern signal at serial input port. By comparing these two sets we calculated total number of corrupted bits to calculate the BER degradation under laboratory generated turbulence conditions.

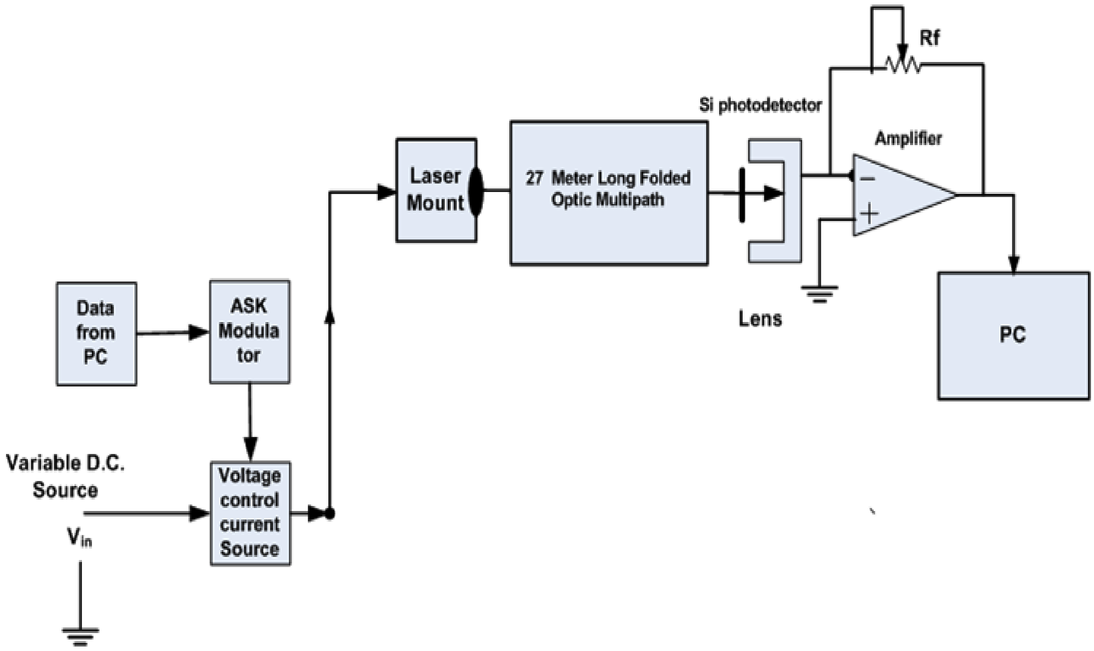

Fig. 4.5.1 : Experimental set up to study the BER by controlling laser dc drive current.

Observations

Table - 4.3 Measurement of BER under constant Room Temp (25 ^{0}C) and Variable Baud Rate

Laser Current-13.2 mA, λ=698.9 nm, Modulation ASK with carrier amplitude 5V (P-P) and Frequency – 5 KHz. ,Output data from PC –TTL

Sr.No.	Laser Current (mA)	Bit Sent	Bit Rate	Run 1	Run 2	Run 3	Run 4	Run 5	Sum	Average BER	Increment in current to make BER=0
1	13.2	50 samples/Run i.e Total 50×8=400 bits sent	600	21	21	22	24	33	121	0.302	0.5 mA
			1200	26	19	24	29	26	124	0.310	
			1800	26	20	23	31	26	126	0.315	
			2400	54	53	52	51	48	206	0.515	
			3000	52	54	45	46	49	246	0.615	
			3500	52	55	53	46	50	256	0.640	
2	13.7	50 samples/Run i.e Total 50×8=400 bits	3500	12	17	17	18	16	80	0.200	0.2 mA
			5900	13	17	12	18	20	81	0.192	
			6000	13	20	13	20	18	82	0.190	

Sr.No.	Laser Current (mA)	Bit Sent	Bit Rate	Run 1	Run 2	Run 3	Run 4	Run 5	Sum	Average BER	Increment in current to make BER=0
		sent	7900	13	18	17	16	17	81	0.210	
			8000	14	15	15	20	19	83	0.207	
3	13.9	50 samples/Run i.e Total 50×8=400 bits sent	7000	0	0	0	0	0	0	0	0.1 mA
			8000	0	0	0	0	0	0	0	
			11400	21	25	26	25	24	120	0.300	
4	14.0	50 samples/Run i.e Total 50×8=400 bits sent	11400	0	0	0	0	0	0	0	0.1 mA
			22500	0	0	0	0	0	0	0	
			22800	26	19	24	29	26	124	0.310	
			22850	163	167	165	174	172	841	2.10	

Here we select different baud rate with ideal data sample ("31"=00110001) . The deviation from ideal sample values is shown by following fig. 4.5.2(a-g)

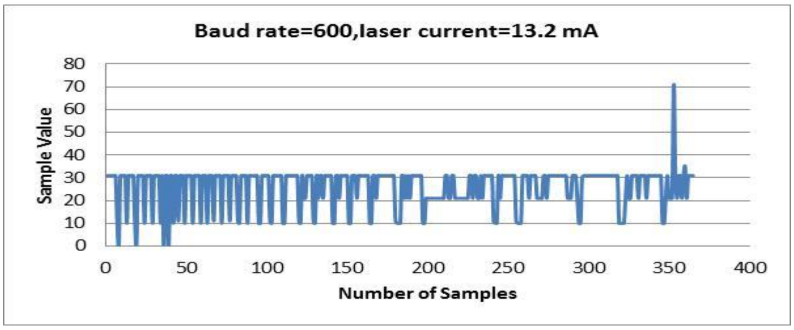

(a) Above figure shows Fluctuation in data sample $(00100001)_2$ due to turbulence-induced irradiance fluctuations (here temp. is 25^0C) with constant baud rate 600 bits/sec and laser biasing current 13.2 mA : Bit Error Rate =0.302 bit/sec.

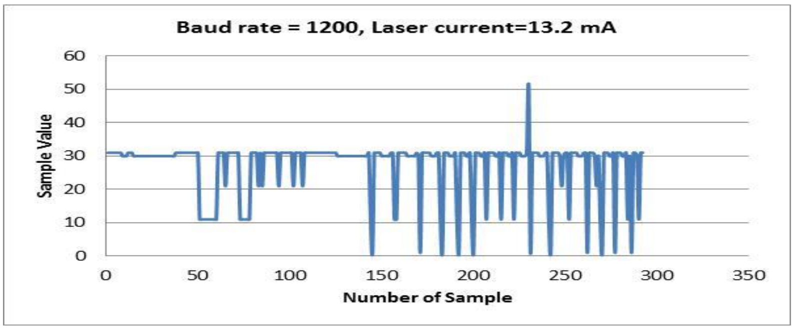

(c) Above figure shows Fluctuation in data sample $(00100001)_2$ due to turbulence induced irradiance fluctuations (here temp. is 25^0C) with constant baud rate 1200 bits/sec and laser biasing current 13.2 mA : BER (increases)=0.310 bit/sec.

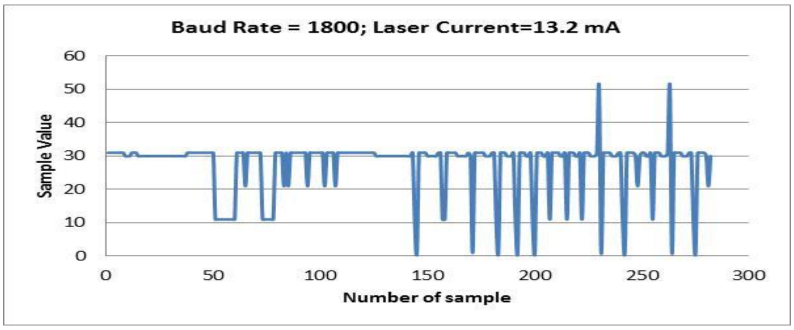

(c) Above figure shows Fluctuation in data sample $(00100001)_2$ due to turbulence induced irradiance fluctuations (here temp. is 25⁰C) with constant baud rate 1800 bits/sec and laser biasing current 13.2 mA : Bit Error Rate (increases by 0.05)=0.315 bit/sec.

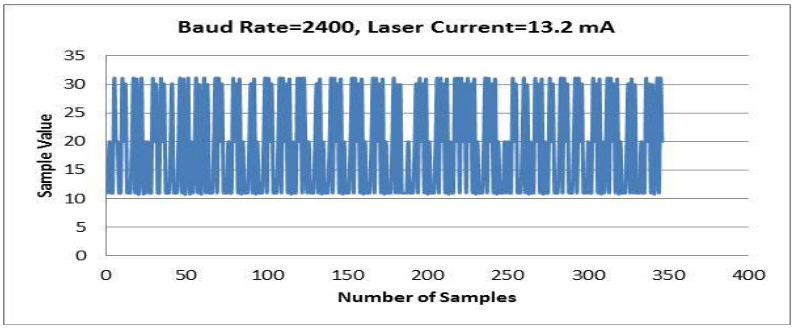

(d) Above figure shows Fluctuation in data sample $(00100001)_2$ due to turbulence-induced irradiance fluctuations (here temp. is 25⁰C) with constant baud rate 2400 bits/sec and laser biasing current 13.2 mA : Bit Error Rate (increases by 0.3)=0.515 bit/sec.

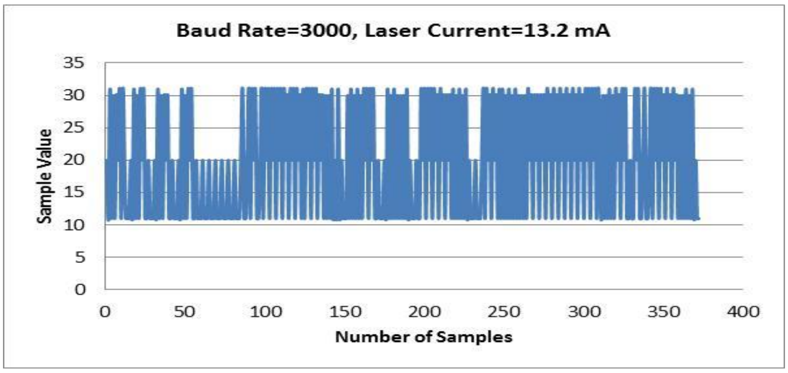

(e) Above figure shows Fluctuation in data sample $(00100001)_2$ due to turbulence-induced irradiance fluctuations (here temp. is 25⁰C) with constant baud rate 3000 bits/sec and laser biasing current 13.2 mA : Bit Error Rate (increases by 0.6)=0.615 bit/sec.

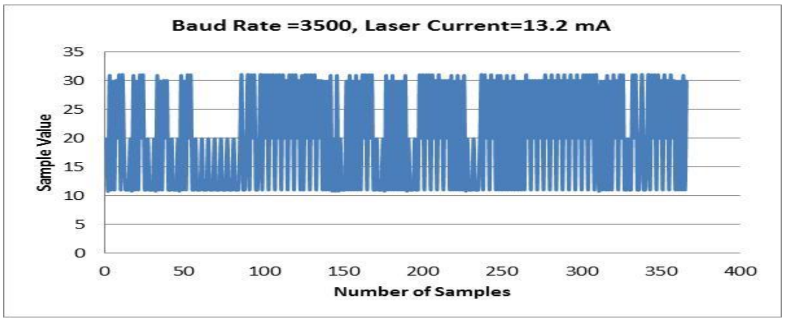

(f) Above figure shows Fluctuation in data sample $(00100001)_2$ due to turbulence-induced irradiance fluctuations (here temp. is 25⁰C) with constant baud rate 3500 bits/sec and laser biasing current 13.2 mA : Bit Error Rate (increases by 0.025)=0.640 bit/sec.

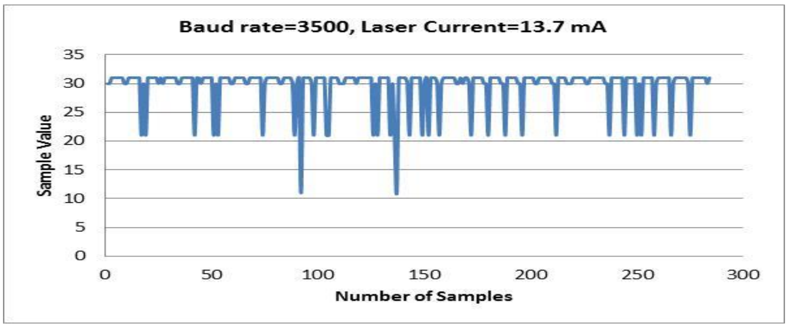

(g) Above figure shows Fluctuation in data sample $(00100001)_2$ due to turbulence-induced irradiance fluctuations (here temp. is 25^{0}C) with constant baud rate 3500 bits/sec and laser biasing current increases by 0.5 mA i.e 13.7 mA : Bit Error Rate (decrease)=0.20 bit/sec.

Fig. 4.5.2(a-g) : Relation between BER and baud rate

From above fig.4.5.2 it shows that for a given line of sight laser communication link as baud rate (bit rate) is increases from 600 to 3500 with constant laser current 13.2 mA , bit error rate (BER) is increases from 0.302 to 0.640. However if laser current increases from 13.2 mA to 13.7 mA (0.5 mA), BER will reduce to 0.20 for baud rate (bit rate) 3500.

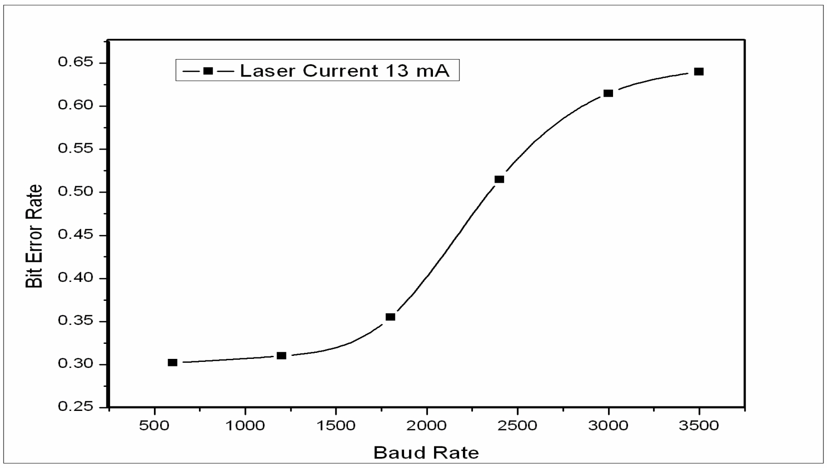

(a) Variation of BER with increasing in baud rate

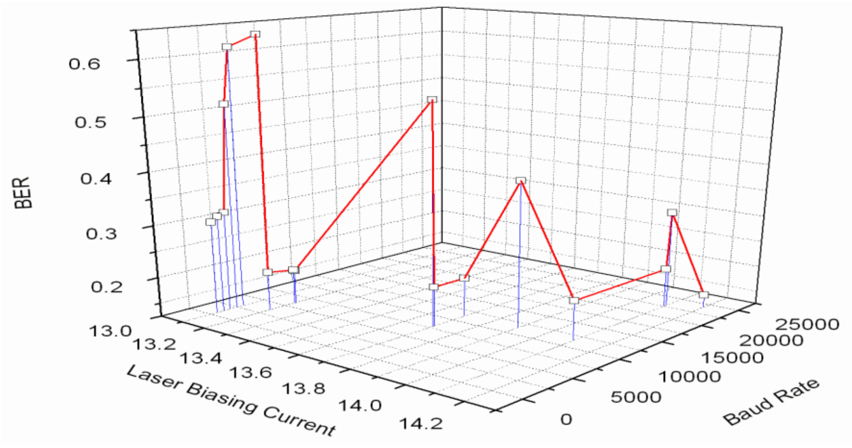

(b) **Variation of baud rate , laser biasing current and BER**

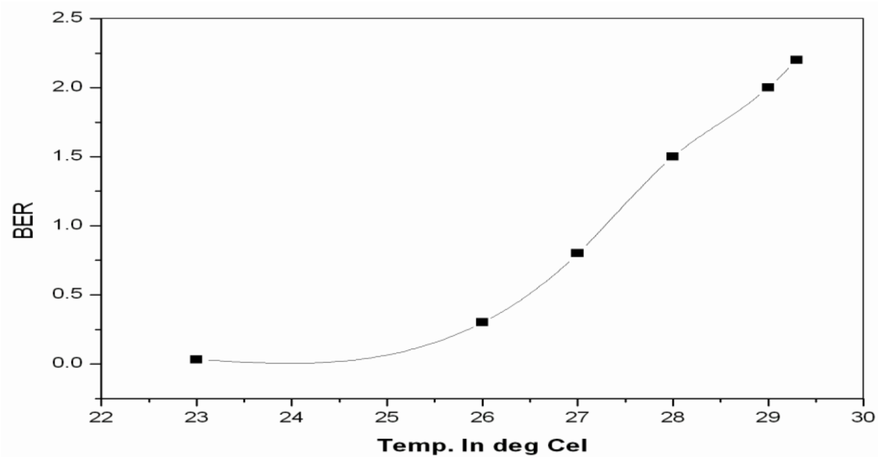

Fig 4.5.3 a) , b) & c) : Shows variation of bit error rate with baud rate and temp.

From above fig.4.5.3 (a,b,c) we observe that for a constant laser bias current the number of bits in error increases when input bit rate is increased beyond a critical value. Second most remarkable thing observed that, when there is certain bits are in error for a particular input bit rate , bit error rate can be reduce gradually , if we increases the laser injected current.

Following table 4.3A shows BER measurements for different laboratory conditions and plotted using bar chart shown in fig 4.5.4. It is observed that for constant bit rate when aperture diameter is changes from 5cm to 10 cm more aperture averaging take place and BER is decreases.

Table 4.3A Measurement of BER under different illumination conditions

Illumination Conditions	BER bit/sec
Dark+ 5 cm lens	0.0325
25 W+5 cm lens	0.0575
200 W+5 cm	0.06
225 W+5 cm	0.0875
225 W++5 cm+ Tube	0.088
Dark+10 cm lens	0.0175
10 cm lens +225W	0.05
10 cm+225 W+Ton	0.0475
10 cm+225 W+Ton+ S-F on	0.0525
10 cm+225 W+Ton+ S-F on	0.0775

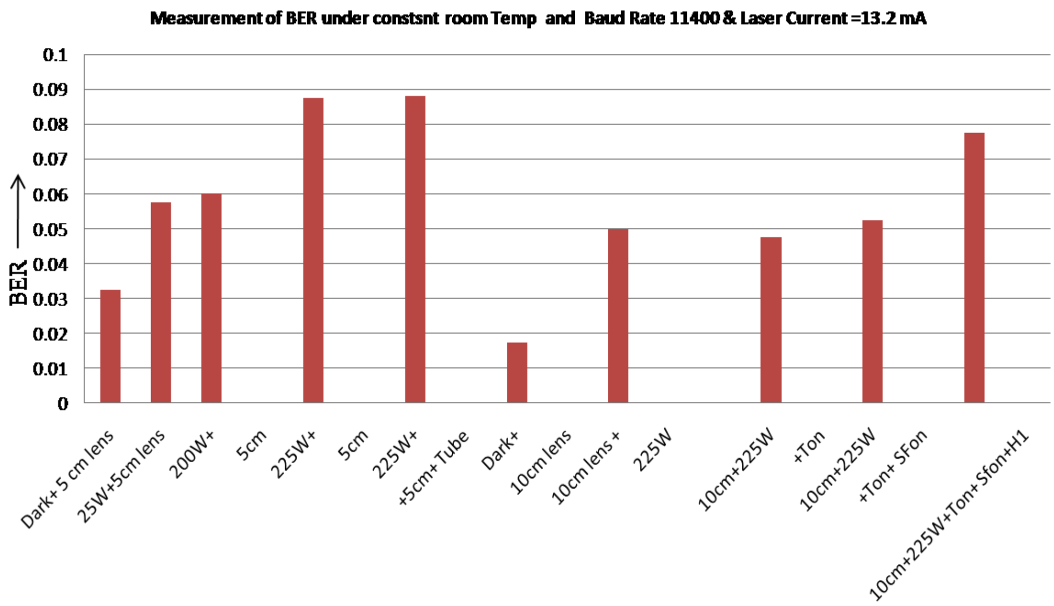

Fig 4.5.4 : Measurement of BER under different laboratory conditions

4.5.2 Case II: Reducing the Bit Error Rate by Controlling Laser Modulating Current

Effects of Change in Amplitude of Carrier on BER

Experimental arrangement is same as described in previous section 4.4 The measured values are given in table 4.4.

Table 4.4 BER Vs Carrier Amplitude

Sr.No	Laser Current mA	Amplitude of Carrier Signal	Photo-detector Voltage (V_{PD})	BER(%)
1	12.8	5	4.02	0%
2	12.8	4.5	3.8	10%
3	12.8	4	3.5	30%
4	12.8	3.5	3.2	50%
5	12.8	3	2.8	100%
6	12.8	2.5	1.8	100%
7	12.8	2	1	100%

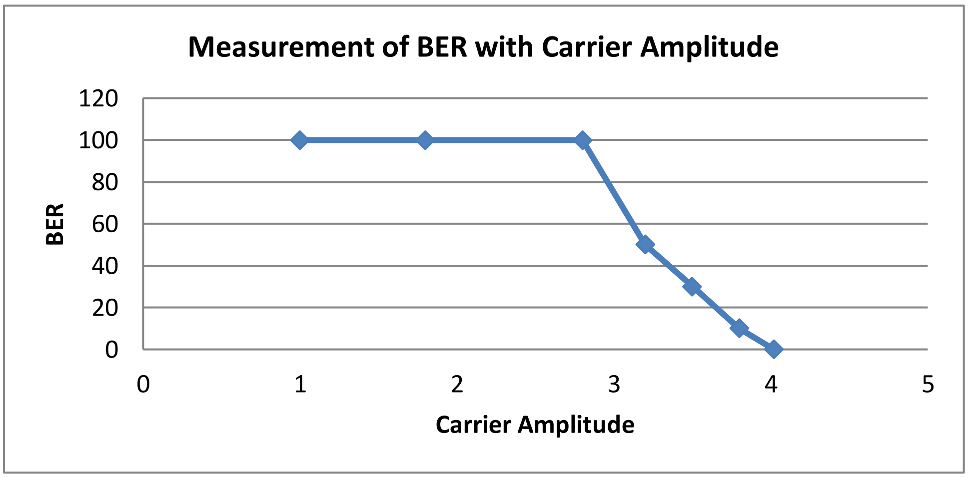

Fig. 4.5.5 : BER as a function of carrier amplitude (v)

Above Fig 4.5.5 shows that amplitude of the carrier signal is inversely preoperational to BER i.e. as signal power decreases to minimum level bit in error increases.

4.6 Measurement of Aperture averaging Effects on the Quality of Received Optical Beam as a Function of Strength of Thermally Induced Turbulence

We performance this experiment to calculate the value of intensity fluctuations with following parameters. We use the same experimental setup as shown in Fig.4.4.1 Laser wave-length =698.9 nm; Total number of reflections of laser beam-08;Number of passes of optical beam between Tx and Rx -05; Distance between Tx and Rx-27 meter; Room temp=Min 25^{0}C and Max =35 ^{0}C; Receiver Aperture Diameter=5 cm, Laser Current=13 mA.

Observations:-   Table 4.5 Measurement of Scintillation Effect

At 25 °C		At 35 °C			At 25 °C		At 35 °C	
Sample no	Sample Value	Sample no	Sample Value		Sample no	Sample Value	Sample no	Sample Value
1	0.4656	1	0.1632		46	0.2832	46	0.6384
2	0.3072	2	0.5712		47	0.2784	47	0.2448
3	0.3408	3	0.1632		48	0.3216	48	0.2064
4	0.2832	4	0.576		49	0.36	49	0.5856
5	0.3504	5	0.6864		50	0.3888	50	0.6288
6	0.312	6	0.528		51	0.312	51	0.6528
7	0.336	7	0.1872		52	0.3744	52	0.6192
8	0.3024	8	0.1872		53	0.3696	53	0.6432
9	0.36	9	0.5376		54	0.3264	54	0.2688
10	0.3072	10	0.6		55	0.288	55	0.4752
11	0.2448	11	0.5712		56	0.2784	56	0.0624
12	0.3744	12	0.6672		57	0.3504	57	0.2688
13	0.3504	13	0.4176		58	0.336	58	0.5184
14	0.3408	14	0.1776		59	0.36	59	0.1104
15	0.3552	15	0.312		60	0.3648	60	0.1872
16	0.3168	16	0.7152		61	0.3264	61	0.6912
17	0.3408	17	0.4848		62	0.312	62	0.648
18	0.3456	18	0.1008		63	0.3216	63	0.0864
19	0.3072	19	0.504		64	0.3408	64	0.504
20	0.3744	20	0.648		65	0.3168	65	0.552
21	0.336	21	0.168		66	0.2976	66	0.3744
22	0.312	22	0.2592		67	0.3648	67	0.1248
23	0.3648	23	0.552		68	0.2976	68	0.2832
24	0.312	24	0.5472		69	0.312	69	0.6288

At 25 °C		At 35 °C	
Sample no	Sample Value	Sample no	Sample Value
25	0.2928	25	0.1824
26	0.3504	26	0.1536
27	0.2688	27	0.6048
28	0.3792	28	0.576
29	0.3312	29	0.216
30	0.312	30	0.3792
31	0.3408	31	0.2448
32	0.3024	32	0.024
33	0.312	33	0.5376
34	0.3792	34	0.648
35	0.312	35	0.216
36	0.3696	36	0.0576
37	0.3312	37	0.5472
38	0.3024	38	0.6336
39	0.3888	39	0.3072
40	0.3312	40	0.1584
41	0.288	41	0.2112
42	0.36	42	0.576
43	0.3792	43	0.2448
44	0.3744	44	0.1632
45	0.3216	45	0.72

At 25 °C		At 35 °C	
Sample no	Sample Value	Sample no	Sample Value
70	0.3744	70	0.6912
71	0.3552	71	0.2688
72	0.3216	72	0.3744
73	0.3744	73	0.1632
74	0.36	74	0.1824
75	0.312	75	0.576
76	0.3648	76	0.3936
77	0.3072	77	0.168
78	0.3504	78	0.0672
79	0.2976	79	0.5136
80	0.3312	80	0.7632
81	0.3552	81	0.4272
82	0.3456	82	0.504
83	0.3408	83	0.168
84	0.3216	84	0.6816
85	0.3024	85	0.5088
86	0.3504	86	0.0912
87	0.3264	87	0.3936
88	0.3792	88	0.5856
89	0.288	89	0.7392
90	0.3792	90	0.2784
91	0.336	91	0.2496

At 25 °C		At 35 °C	
Sample no	Sample Value	Sample no	Sample Value
92	0.3168	92	0.6384
93	0.36	93	0.5568
94	0.3408	94	0.5808
95	0.312	95	0.216
96	0.384	96	0.0192
97	0.312	97	0.4992
98	0.3552	98	0.4944
99	0.312	99	0.192
100	0.3312	100	0
101	0.3888	101	0.5664
102	0.3024	102	0.4704
103	0.3696	103	0.4464
104	0.2976	104	0.1296
105	0.312	105	0.5568
106	0.3408	106	0.24

At 25 °C		At 35 °C	
Sample no	Sample Value	Sample no	Sample Value
138	0.3072	138	0.3744
139	0.3984	139	0.6864
140	0.3168	140	0.264
141	0.3792	141	0.216
142	0.3264	142	0.6384
143	0.2976	143	0.6768
144	0.312	144	0.6192
145	0.3168	145	0.3504
146	0.336	146	0.5424
147	0.384	147	0.8016
148	0.3216	148	0.168
149	0.4032	149	0.1104
150	0.3168	150	0.4944
151	0.312	151	0.5472
152	0.36	152	0.1968

At 25 °C		At 35 °C	
Sample no	Sample Value	Sample no	Sample Value
107	0.3504	107	0.3888
108	0.2928	108	0.648
109	0.3648	109	0.2016
110	0.2736	110	0.3168
111	0.3216	111	0.7296
112	0.3648	112	0.1776
113	0.3504	113	0.576
114	0.3696	114	0.5424
115	0.312	115	0.3888
116	0.3504	116	0.0768
117	0.3552	117	0.672
118	0.288	118	0.192
119	0.3888	119	0.3408
120	0.3504	120	0.624
121	0.3168	121	0.1584
122	0.36	122	0.3456
123	0.3648	123	0.168
124	0.3552	124	0.6048
125	0.3648	125	0.5568
126	0.2688	126	0.4608
127	0.3312	127	0.024
128	0.3264	128	0.4992
129	0.3024	129	0.408
130	0.3552	130	0.0384
131	0.2976	131	0.4656
132	0.3792	132	0.6912
133	0.3792	133	0.3408
134	0.3792	134	0.1728
135	0.2976	135	0.2208
136	0.3696	136	0.672
137	0.36	137	0.2544

At 25 °C		At 35 °C	
Sample no	Sample Value	Sample no	Sample Value
153	0.2736	153	0.1488
154	0.3072	154	0.456
155	0.3168	155	0.5376
156	0.3456	156	0.4992
157	0.312	157	0.192
158	0.36	158	0.3984
159	0.336	159	0.2352
160	0.3504	160	0.4416
161	0.3072	161	0.5616
162	0.3552	162	0.4032
163	0.2544	163	0.0672
164	0.2928	164	0.5424
165	0.3216	165	0.3984
166	0.3648	166	0.5664
167	0.3744	167	0.2352
168	0.3312	168	0.6192
169	0.2928	169	0.5088
170	0.3456	170	0.1344
171	0.2784	171	0.4512
172	0.3024	172	0.6576
173	0.3552	173	0.4176
174	0.2352	174	0.5568
175	0.1152	175	0.1968
176	0.3216	176	0.5856
177	0.3456	177	0.4752
178	0.2208	178	0.1344
179	0.3264	179	0.4848
180	0.3216	180	0.6192
181	0.3648	181	0.144
182	0.3408	182	0.12
183	0.3072	183	0.7104
184	0.36	184	0.3744
185	0.3168	185	0.3744
186	0.3504	186	0.1056
187	0.3264	187	0.5808
188	0.3168	188	0.4128
189	0.3264	189	0.6096
190	0.3648	190	0.2448
191	0.3744	191	0.3552
192	0.2928	192	0.5856
193	0.3648	193	0.504
194	0.3648	194	0.5088

At 25 °C		At 35 °C	
Sample no	Sample Value	Sample no	Sample Value

At 25 °C		At 35 °C	
Sample no	Sample Value	Sample no	Sample Value
195	0.3696	195	0.4896
196	0.3792	196	0.5088
197	0.312	197	0.6336
198	0.3024	198	0.1296
199	0.3696	199	0.2688
200	0.3504	200	0.4944

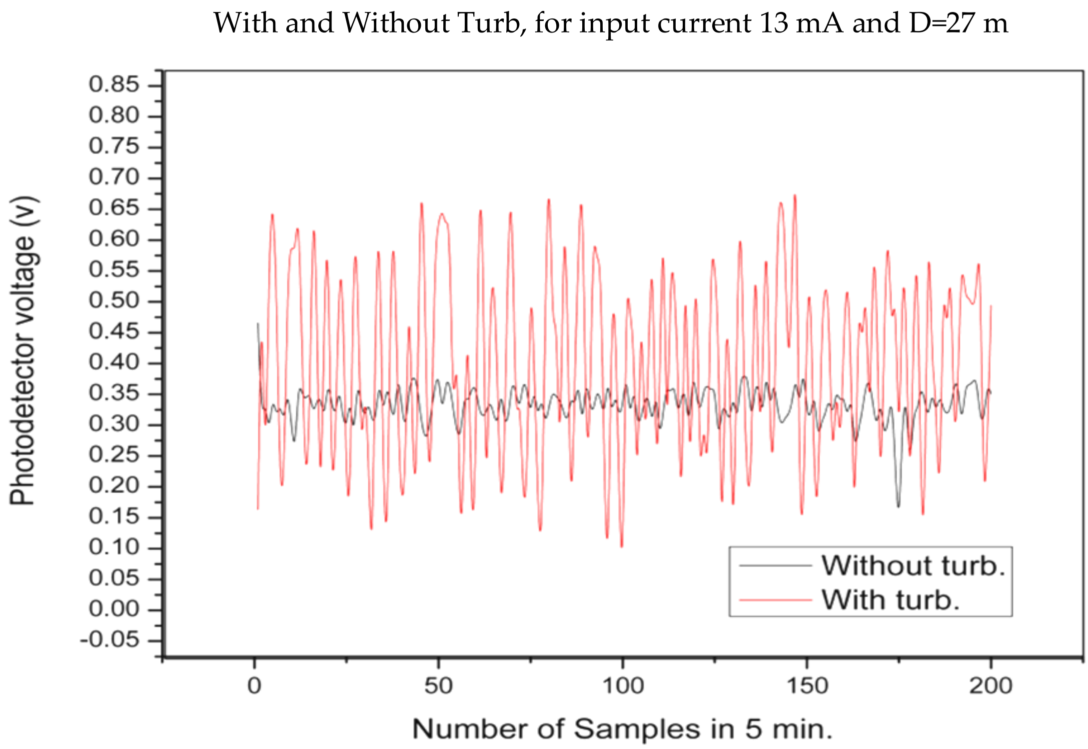

Fig.4.6.1 : Rytov variance measurement : heater is ON for red lines in the graph , turbulence region temp:- 25 ^{0}C, and 35 ^{0}C

Now , from fig.4.6.1 we are able to calculate Rytov variance as,

$$\therefore C_n^2 = \frac{\sigma^2}{1.23k^{\frac{7}{6}}L^{\frac{11}{6}}} \tag{4.1}$$

For Path length L =25 m and Temp = 25 ^{0}C, Rytov variance is 0.006, Therefore we have, Cn= 7.78 × 10^{-14} (From MATLAB program) [A-3] .For temp=35 ^{0}C and L = 25 m, Rytov variance=0.04, Cn= 5.18 × 10^{-13} i.e. if the Rytov variance is increases , C_n^2 is also increases which fulfill the above equation.

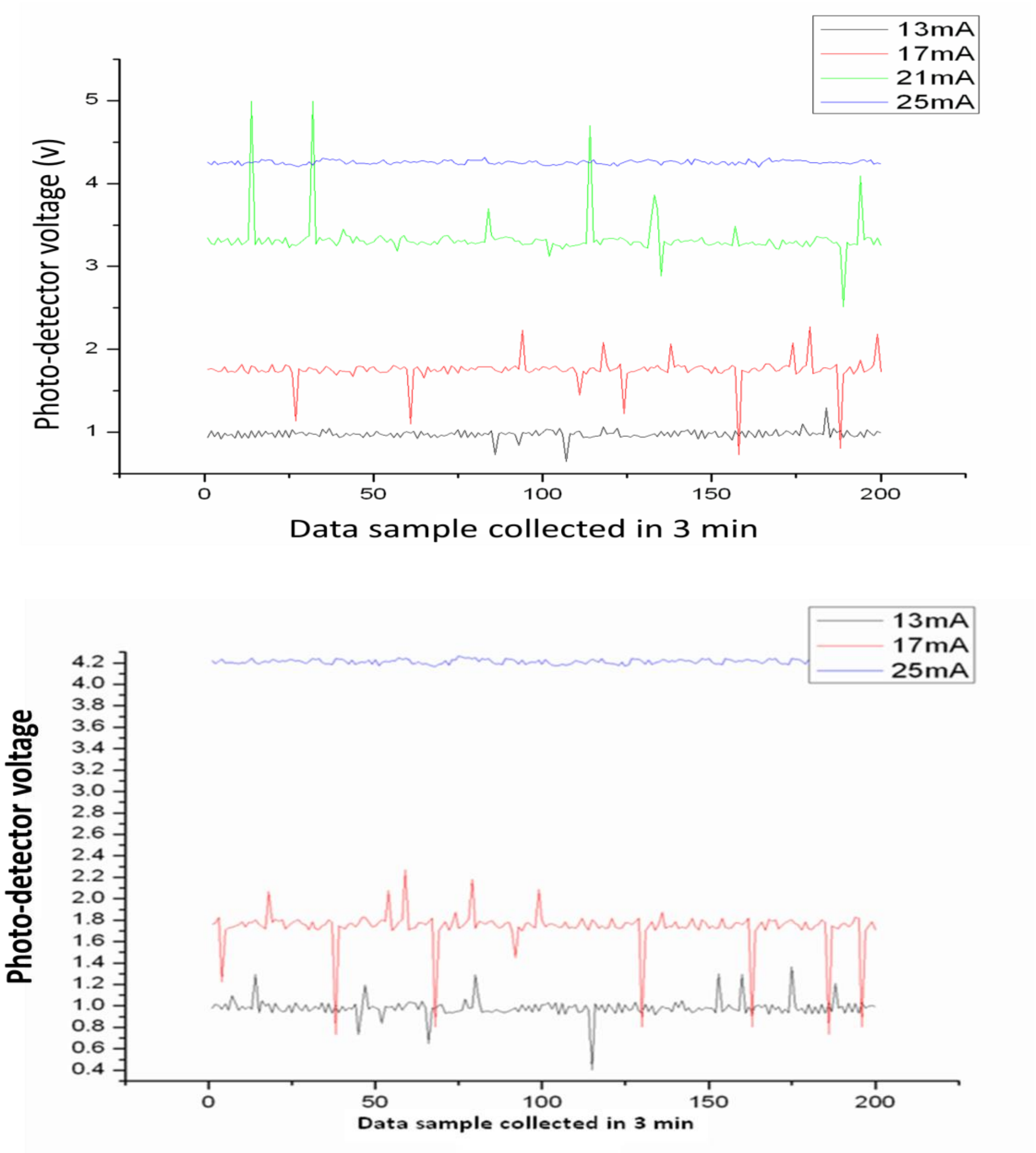

Fig. 4.6.2 : Comparison of laser biasing current vs temp at 25 ⁰C and 35 ⁰C for 16 m distance

Above fig.4.6.2 shows the variations of intensity fluctuations with laser biasing current for two different temperature 25⁰C and 35⁰C (with and without turbulence) and we measured intensity fluctuations for 16m optical path length with 13 mA, 17 mA, 25 mA laser current. From fig. 4.6.2 it is observed that the higher biasing laser current can also help to mitigate turbulence induced fading.

4.7 Measurement of Receiver Photo-detector Output Voltage with Increase in Temperature rise for 27 m distance

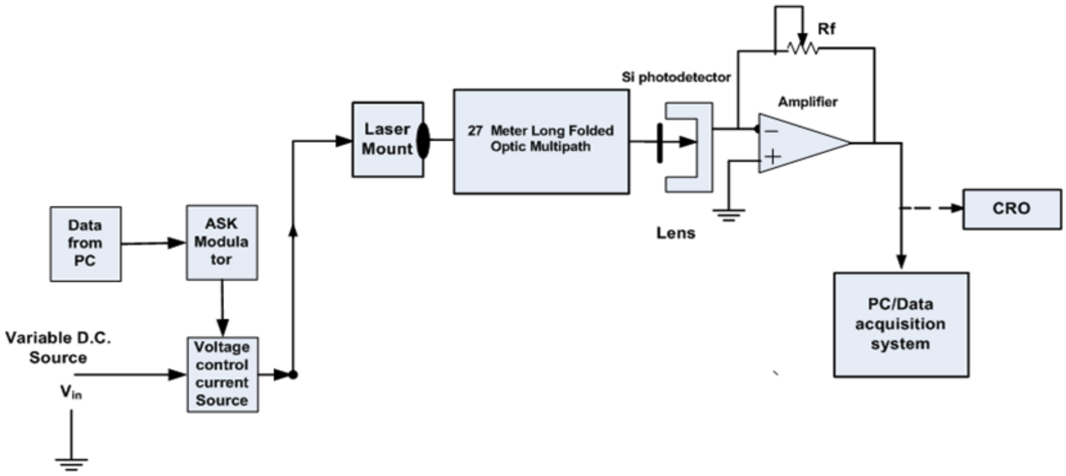

Fig. 4.7.1 : Effect of temp rise on photo –detector output

Fig.4.7.1 shows arrangement for measurement of photo-detector output with temperature rise for optical path distance 27 meter. Following fig. 4.7.2 shows the effect of photo detector output with temperature. It is observed that the surrounding temperature is badly affect the photo-detector output i.e.as the temperature is increases output voltage decreases and vice versa. Therefore we make the suitable arrangement to maintain constant temperature across photo-detector to measure the corrected output of photo detector.

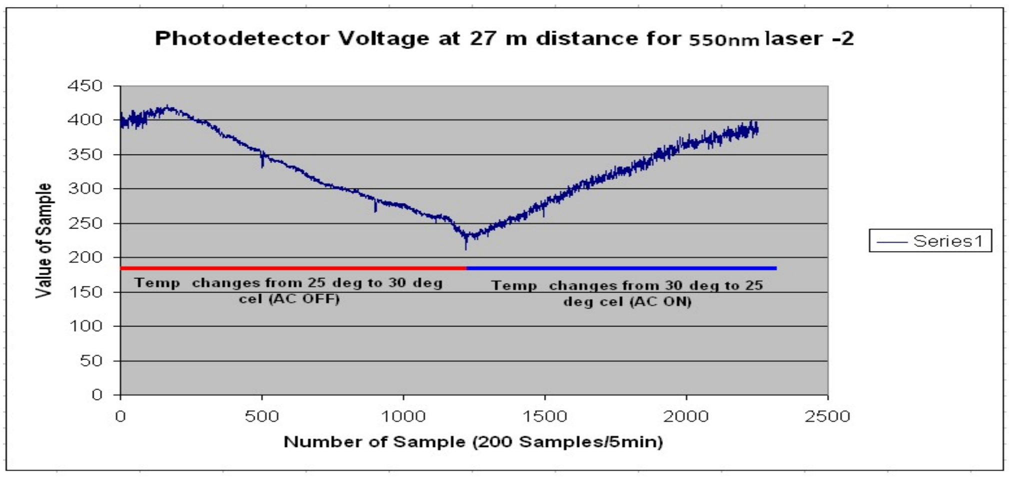

Fig. 4.7.2 : Photo-detector output voltage as function of room temperature.

4.8 Beam Wander Effect

The presence of turbulence in the atmosphere will lead to the formation of eddies of different refractive indices and various sizes. Owing to the smaller size of the transmitter beam relative to the turbulent eddy size near the ground level, the beam will get displaced from its bore-sight and can result in time varying signal fades. This phenomenon is called beam wonder where the instantaneous center of the beam is randomly displaced on the photo-detector plane. This random displacement of the beam centroid and hot spot (the point of maximum irradiance) will result in long term spot size.

This long term spot will represent the average field or irradiance given by [6-7]

$$W_L^2 = W_s^2 + 2\gamma^2 \text{-} \tag{4.2}$$

Where W_L^2, W_s^2 are the long term and short term beam size, respectively and γ^2 is the variance of hot spot displacement of beam centroid given by

$$\langle\gamma^2\rangle = 7.25\, sec^2(\theta)(H-h_0)^2 \left[\frac{1}{W_0}\right]^{\frac{1}{3}} \int_{\eta_0}^{H} C_n^2(h)dh \tag{4.3}$$

Where,

W_0 is the transmitter beam size ,h_0 height above the ground. H is satellite altitude and is given as

$H = h_0 + L\cos(\theta), \theta$ the zenith angle and L is the propagation path.

Equation 6.22 can be rewritten as (for duplex channel)

$$\langle\gamma^2\rangle = 0.54H^2 sec^2(\theta)\left(\frac{\lambda}{2W_0}\right)^2\left(\frac{W_0}{r_0}\right)^{\frac{5}{3}} \tag{4.4}$$

In above equation r_0 is the atmospheric coherence diameter described as

$$r_0 = \left(0.432\int_0^H C_n^2(h)\, dh \times k^2 \sec(\theta)\right)^{-\frac{3}{5}} \tag{4.5}$$

From equation 6.23 it is observed that

Beam wander variance involves the free space diffraction angle $\left(\frac{\lambda}{2W_0}\right)$ and the tilt phase fluctuations averaged over transmitter aperture $2\left(\frac{W_0}{r_0}\right)^{\frac{5}{3}}$.

4.9 Measurement of Atmospheric Turbulence Induced Optical Beam Wander.

When a beam of light propagates through the turbulent atmosphere of the Earth, it experiences random fluctuations in the refractive index. Fluctuations of the refractive index are due to turbulent eddies caused by stochastic variations of the temperature. The characteristic scales of the atmospheric in homogeneities range from millimeters to meters called as small size eddies and large size eddies. Those eddies which are large compared with the diameter of the beam tend to deflect the beam, whereas those eddies which are small compared with the beam diameter tend to broaden the beam but not deflect it significantly. As a result we can observe a broadened laser spot whose centroid randomly moves because of the motion of individual eddies.

Here we investigate the effect of temp on optical beam deflection by considering following cases as shown in fig. 4.9.1 (a) (b). The x-y micrometer of photo-detector mount will be used to measure the change in position of the beam spot and digital thermometer is used to measure the temperature variation while the computer system will be used to determine the BER due to beam deflection when specific turbulence will create in the lab using fan and heater. The amount of shift of the beam spot position due to beam wonder would be manually measured to create a null condition by adjusting the x, y position and by adjusting screw. We also studied beam wonder effect using multiple photo-detector array such as CMOS array as shown in fig 4.9.1 a).

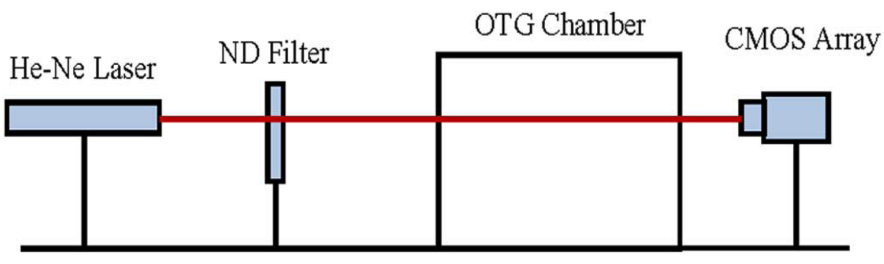

(a)

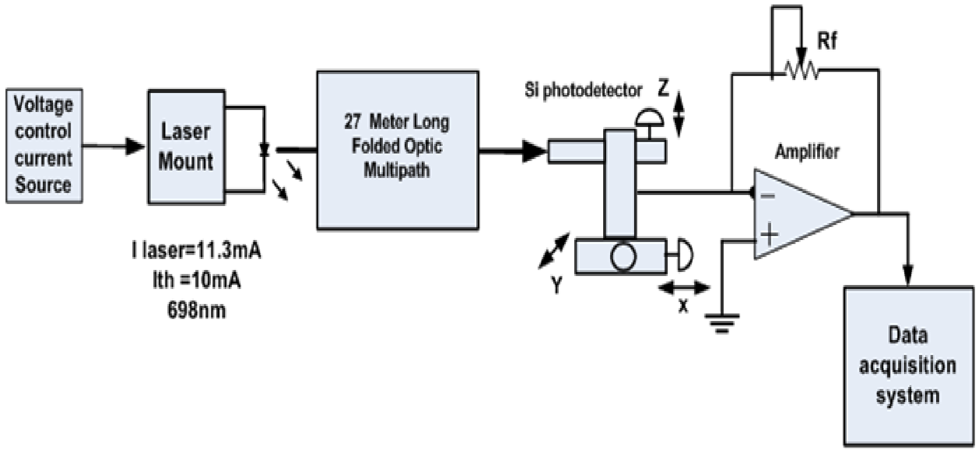

Fig 4.9.1 (a,b): Experimental arrangement for measurement of beam wonder with x-y-z positionier

Parameter used in laboratory experimentation.

Sr.No.	Parameter	Value
1	Laser Power	10 mw
2	Tx Beam Size (W_0)	4 mm
3	Operating Wavelength	698 nm
4	Temp. difference	25 ^{0}C -30^0 C
5	Propagation Length	27 m
6	I_{th}	10 mA

Table 4.6 Measurement of Optical Beam Deflection for increase in Temp.

Temp. in ^{0}C	Photodiode output D.C. Voltage (V)at 27m distance	Time in min.	Distance shifted by optical beam spot in (cm)	Temp. in ^{0}C	Photodiode output D.C. Voltage (V)at 27m distance	Time in min.	Distance shifted by optical beam spot in cm
26.0	1.52	6.40	0	28.0	0.75	7.05	2
26.2	1.50	6.42	0.1	28.2	0.65	7.07	2.1
26.5	1.49	6.44	0.2	28.5	0.45	7.09	2.2
26.8	1.45	6.46	0.3	28.8	0.35	7.12	2.6
26.9	1.37	6.48	0.4	28.9	0.25	7.13	2.8
27.0	1.34	6.50	0.5	29.0	0.19	7.15	3
27.2	1.25	6.52	0.7	29.2	0.18	7.16	3.6
27.5	1.10	6.55	1.2	29.5	0.16	7.17	3.65
27.8	0.96	6.56	1.3	29.8	0.15	7.18	3.7
27.9	0.89	6.58	1.6	29.9	0.12	7.19	3.75
				30	0.11	7.20	4.2

Curves for Beam spot deflection:

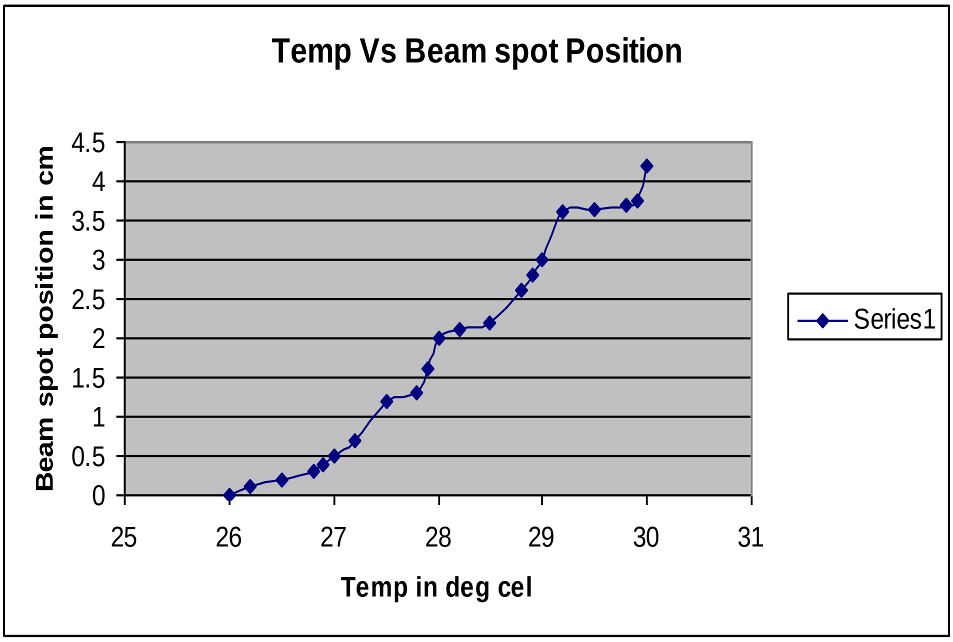

Fig. 4.9.2 : Beam spot deflection measurement: temp vs beam spot position (lab temp. changes from 25⁰C to 30⁰C

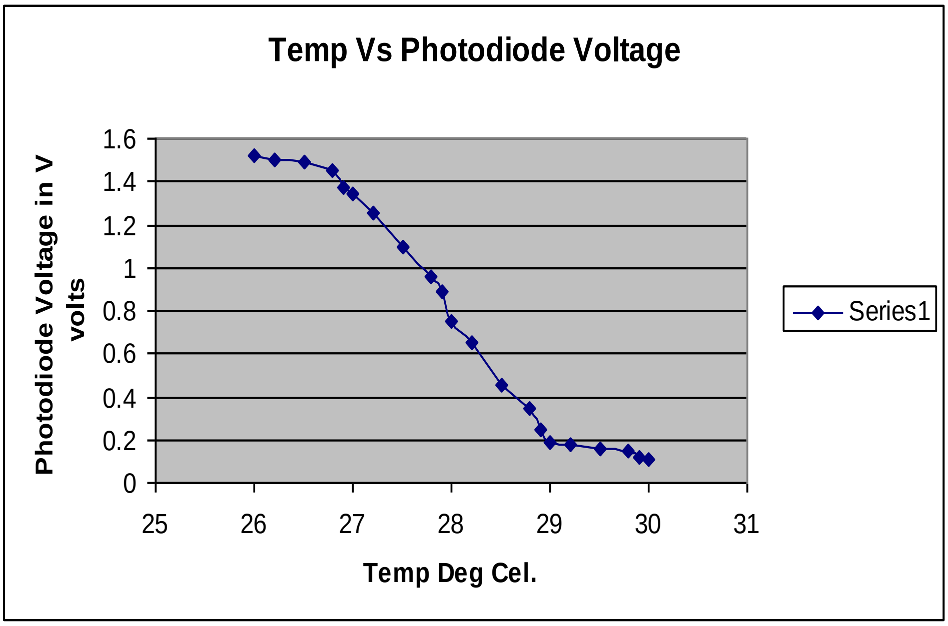

Fig. 4.9.3 : Beam spot deflection measurement : temp vs photodiode voltage

Lab Temp Changes from 30⁰C to 25⁰C

Table 4.7 Measurement of Optical Beam Deflection for decrease in temp

Temp. in ^0C	Photodiode output D.C. Voltage (V)at 27m distance	Time in min.	Distance shifted by optical beam spot in cm	Temp. in ^0C	Photodiode output D.C. Voltage (V)at 27m distance	Time in min.	Distance shifted by optical beam spot in cm
30	0.16	6.21	0	28	0.25	6.40	3
29.9	0.16	6.22	0.3	27.9	0.3	6.41	3.1
29.8	0.16	6.24	0.6	27.8	0.4	6.42	3.2
29.5	0.17	6.25	0.9	27.5	0.58	6.43	3.3
29.2	0.17	6.26	1.2	27.2	0.6	6.45	3.4
29	0.18	6.28	1.4	27	0.64	6.46	3.5
28.9	0.19	6.32	1.7	26.9	0.66	6.47	3.6
28.8	0.19	6.34	2	26.8	0.68	6.48	3.65
28.5	0.2	6.36	2.3	26.5	0.7	6.49	3.7
28.2	0.22	6.38	2.6	26.2	0.71	6.50	3.75
				26	0.75	6.51	3.8

Curves for Beam shifted experiment:-

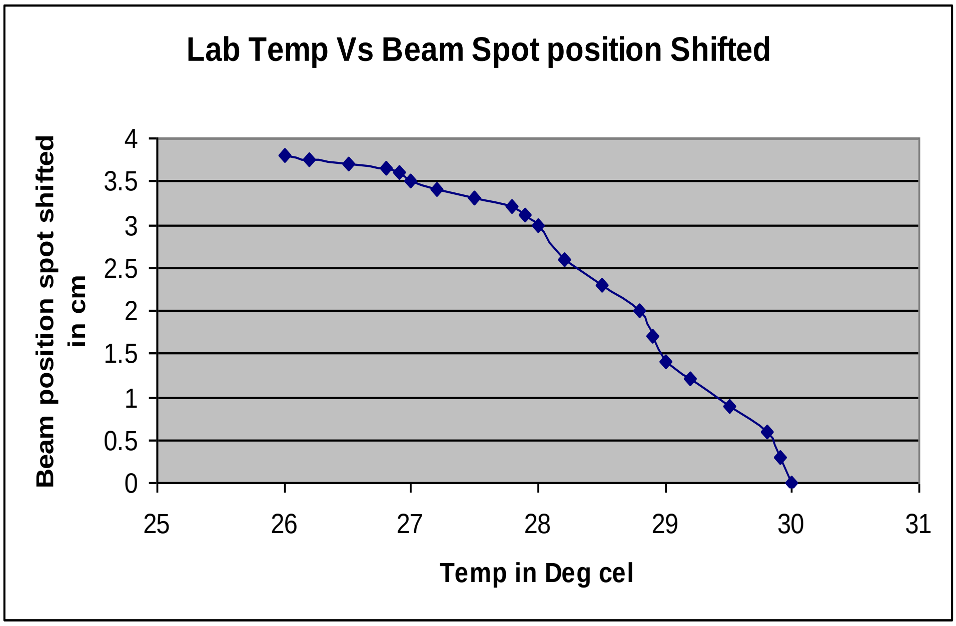

Fig 4.9.4 Beam spot shifted measurement: temp vs beam position (cm)

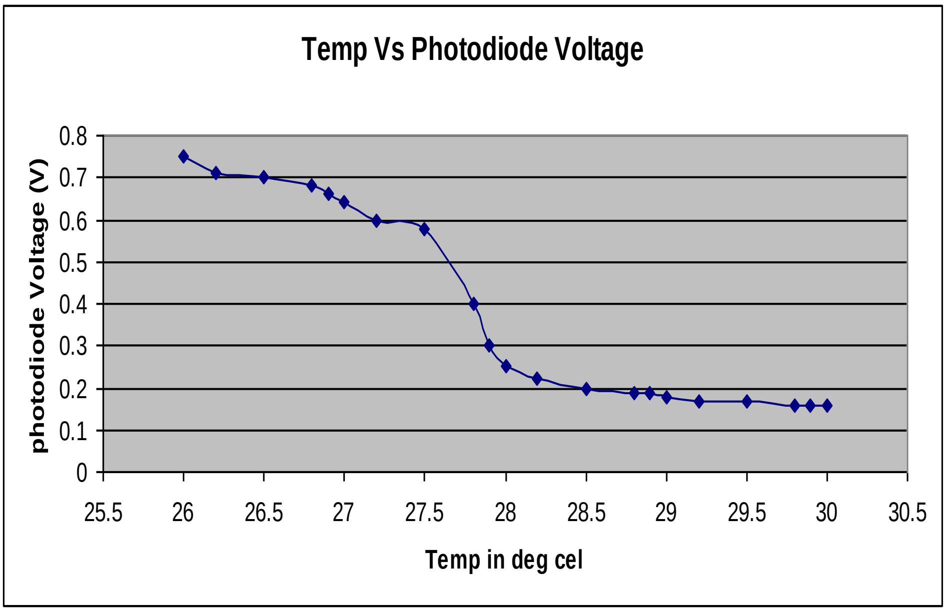

Fig. 4.9.5 : Beam spot shifted measurement: temp vs photodiode voltage (v)

We perform the beam deflection experiment and observe that as the lab temperature increases, laser beam spot position is shifted by 4 cm. vertically from the center of a photo-detector plane (shown in above figure 4.9.5) and hence photo-detector output voltage decreases.

In another case , if lab temp is decreases laser beam will come back to its initial position and photo-detector output voltage gradually increases. Thus lab temperatures changes, refractive index of air changes and deflects the beam position in different direction.

4.10 Conclusion

The Overall circuit and system developed inside our laboratory is used for the generation of atmospheric turbulence and measurements of turbulence on the propagation of laser beam. This arrangement has been made to obtain detail measurements of the effects of atmospheric temperature on digital data bits and also to observe the effects of variations in transmitting source parameters such as intensity, wavelength of laser diode, characteristics of the electronic modulation (ASK). The effect of refractive index variation on the optical beam was experimentally measured by using Rytov variance (equation 3.22 in chapter 3), and based on those results it was revealed that, for optical path length L =27 m and room temperature = 25^0C, Rytov variance was found as 0.006 (section 4.3). The analogous value refractive index structure parameter is calculated, and found as $Cn^2 = 7.78 \times 10\text{-}14$. Applying the same method, we also measured Rytov variance at room temp=35^{0}C (Higher value), and found as 0.04 and $Cn^2 = 5.18 \times 10\text{-}13$, which is greater than that of observed at 25^{0}C. The mitigation of such temperature induce atmospheric turbulence is possible through aperture averaging and by controlling transmitter laser biasing current (13.2 mA to 13.7 mA) or by decreasing transmitter baud rate as shown in Section 4.5. Another important experimental result shows that if optical path length changes (16m to 27m) the scintillation becomes more sever in such cases a probability of minimum bit error rate (10^{-9}) is maintained by controlling transmitter laser biasing current (13.2 mA to 13.7 mA = 0.5 mA) or by decreasing transmitter baud rate (8000 bits/sec to 3500 bits/sec) as shown in Section 4.6.

BER is measured at different temperatures by changing the transmitter data rate to analyze the reliability and availability of the designed optical link. Measurement of BER by producing attenuation using standard attenuators in the optical path is also studied in the same setup [A-2]. Thus, the proposed multipath folded optic closed loop system offers exceptional laboratory standard testing arrangement to measure the effects of atmospheric turbulence on propagating optical field.

CHAPTER 5

Mitigation of Scintillation Effects on Optical Wave Using Aperture Averaging-Simulation and Experiments

5.1 Introduction

The objective of this chapter is to study the aperture averaging techniques to mitigate the effects of scintillation due to the random variations of the refractive index structure parameter. A MATLAB simulation model is developed to analyze and compare scintillation index, S/N ratio and BER for coherent and partially coherent beam for different turbulence conditions.

Random fluctuations of atmospheric refractive index produces random phase variations along with beam wander effect of the traveling optical beam which lead to the displacement of the beam centroid significantly. This random phase variations are simulated using thin optical phase screen model. The turbulence parameters like Rytov variance and refractive index structure parameter due to the turbulence is studied using MATLAB lab simulation programs.

The effect of individual optical beam (Coherent and partially coherent) along with aperture averaging technique at the receiver were compared for different values of the aperture widths. Semiconductor optical sources emitting in the range 780–1550 nm were taken to observe the influence of wavelength in mitigating the scintillation effects using aperture averaging factor 'A'. Performance of the optical communication link was studied using MATLAB simulation programs for the three turbulent situations weak, moderate and strong.

Experimental results for aperture averaging are verified using thermal atmospheric turbulence setup by selecting different receiver aperture diameter varying from 2.5 cm to 10 cm respectively. We measured the effect of aperture averaging to reduce the scintillation effect at 698 nm wavelength. The experimental study has been done to characterize the variation of beam wander displacement for various turbulence conditions at 698 nm operating wavelength. This study will help to analyze the fluctuations in the received irradiance due to beam wander effect.

5.2 Principles in Aperture averaging in Optical scintillation

Atmospheric laser communications using direct-detection systems suffer from severe degradation caused by scintillation. The simplest way of reducing scintillation effect is to increase the receiver size and to take advantage of aperture averaging. Spatial and temporal variations of the received intensity have to be investigated in order to predict the efficiency of aperture averaging.

The aperture averaging factor 'A' is defined by the normalized variance of power fluctuations of the incident optical field on collecting lens. It is the ratio of the irradiance flux variance obtained by a finite-size collecting lens having diameter D to that obtained by a point receiver or on axis flux variance.

Andrews [1] developed a method to predict quantitatively the reduction of scintillation through aperture averaging. This method is based on an ABCD ray matrix formulation of the optical system with one Gaussian lens and enables the computation of the aperture averaging factor 'A'. The aperture averaging factor measures the reduction of the scintillation index relative to a point aperture.

Aperture averaging factor for coherent beam is define as

$$A = \sigma_I^2(D) / \sigma_{I,s}^2\left(0\right) \tag{5.1}$$

Where $\sigma_I^2\left(D\right) \& \sigma_{I,s}^2$ are the scintillation indices for receiver lens of diameter D and a "point receiver" (D≈0) as discuss in section 2.12.

By using aperture averaging technique we average over the relatively fast fluctuations caused by the small-size eddies and thus the frequency content of the irradiance spectrum is shifted to the low spatial frequencies.

5.3Turbulence Mitigation by Aperture averaging in wireless optical system

Under moderate to strong turbulence conditions, only eddies of size smaller than coherence radius ρ_0 or larger than the scattering disk $L/k\rho_0$ contribute effectively to the atmospheric turbulence .To take into account this dependence of the turbulence on coherent and partially coherent beams , consider an aperture averaging factor 'A' to mitigate the effects scintillation by considering the three special cases of weak, moderate and strong turbulence with different wavelengths. The effects of aperture averaging on the received signal is given by

$$\sigma_{I,s}^2 = A \times \sigma_{I,s}^2 \tag{5.2}$$

Where, $\sigma_{I,s}^2$ is aperture-averaged scintillation index.

First, we consider the classical case of plane wave propagation model while neglecting the inner scale i.e. assuming $l_0 = 0$. We have presented the curves of the aperture averaging factor A versus the normalized receiver lens radius d in following chapter. The aperture-averaging factor 'A' begins to decrease effectively for $D \geq \sqrt{\lambda L}$ where $\sqrt{\lambda L}$ is the size of scintillation spot at the receiver. When diameter $D > \sqrt{L\lambda}$, effective aperture averaging take place. But if coherence length $\rho > D$, less effective aperture averaging take place where $\rho = \sqrt{\frac{L}{K}}$. To analyze and compare the effects of scintillation on coherent and partially coherent Gaussian optical beam, we simulate following equation which is used to obtain scintillation index for both type of optical beam as explained in chapter II.

Log irradiance due to large scale eddies is given as

$$\sigma_{\ln,x}^2(D) = \frac{0.49\left(\frac{\Omega - \Lambda_1}{\Omega + \Lambda_1}\right)\sigma_{I,s}^2}{\left[1 + \frac{0.4\left(2 - \bar{\Theta}_1\right)\left(\frac{\sigma_{I,s}}{\sigma}\right)^{\frac{12}{7}}}{\left(\Omega + \Lambda_1\right)\left(\frac{1}{3} - \frac{1}{2}\bar{\Theta}_1 + \frac{1}{5}\bar{\Theta}_1^2\right)^{\frac{6}{7}} + 0.56\left(1 + \Theta_1\right)\sigma_{I,s}^{\frac{12}{5}}}\right]^{\frac{7}{6}}} \tag{5.3}$$

Log irradiance due to small scale eddies is given as

$$\sigma_{\ln,y}^2(D)=\frac{\left(0.51\sigma_{I,s}^2\right)/\left(1+0.69\sigma_{I,w}^{\frac{12}{5}}\right)^{\frac{5}{6}}}{1+\left[1.20\left(\frac{\sigma}{\sigma_{I,s}}\right)^{\frac{12}{5}}+0.83\sigma^{\frac{12}{5}}\right]/\left(\Omega+\Lambda_1\right)} \tag{5.4}$$

Therefore the total scintillation index for coherent optical beam is

$$\sigma_I^2(D)=\exp\left[\sigma_{\ln,x}^2(D)+\sigma_{\ln,y}(D)\right]-1 \tag{5.5}$$

Similarly for partially coherent beam we have,

Log irradiance due to large scale eddies is given as

$$\sigma_{P\ln,x}^2(D)=\frac{0.49\left(\frac{\Omega-\Lambda_{eff}}{\Omega+\Lambda_{eff}}\right)\sigma_{PI,s}^2}{\left[1+\frac{0.4\left(2-\bar{\Theta}_{eff}\right)\left(\frac{\sigma_{PI,s}}{\sigma}\right)^{\frac{12}{7}}}{\left(\Omega+\Lambda_{eff}\right)\left(\frac{1}{3}-\frac{1}{2}\bar{\Theta}_{eff}+\frac{1}{5}\bar{\Theta}_{eff}^2\right)^{\frac{6}{7}}+0.56\left(1+\Theta_1\right)\sigma_{I,s}^{\frac{12}{5}}}\right]^{\frac{7}{6}}} \tag{5.6}$$

& Log irradiance due to small scale eddies is given as

$$\sigma_{P\ln,y}^2(D)=\frac{\left(0.51\sigma_{PI,s}^2\right)/\left(1+0.69\sigma_{PI,w}^{\frac{12}{5}}\right)^{\frac{5}{6}}}{1+\left[1.20\left(\frac{\sigma}{\sigma_{PI,s}}\right)^{\frac{12}{5}}+0.83\sigma^{\frac{12}{5}}\right]/\left(\Omega+\Lambda_{eff1}\right)} \tag{5.7}$$

Therefore the total scintillation index is given by

$$\sigma_{P,I}^2(D)=\exp\left[\sigma_{P\ln,x}^2(D)+\sigma_{P\ln,y}^2(D)\right]-1 \tag{5.8}$$

5.4 Measurement of Aperture Averaging Factor (Simulation Model)

To study the effect of turbulence on optical beam, we consider a lowest order transverse electromagnetic (TEM) Gaussian beam wave. It is assumed that the transmitting aperture located at z=0 and the amplitude distribution is Gaussian with effective beam radius w_0 propagating along positive z axis as shown in Fig.5.4.1.

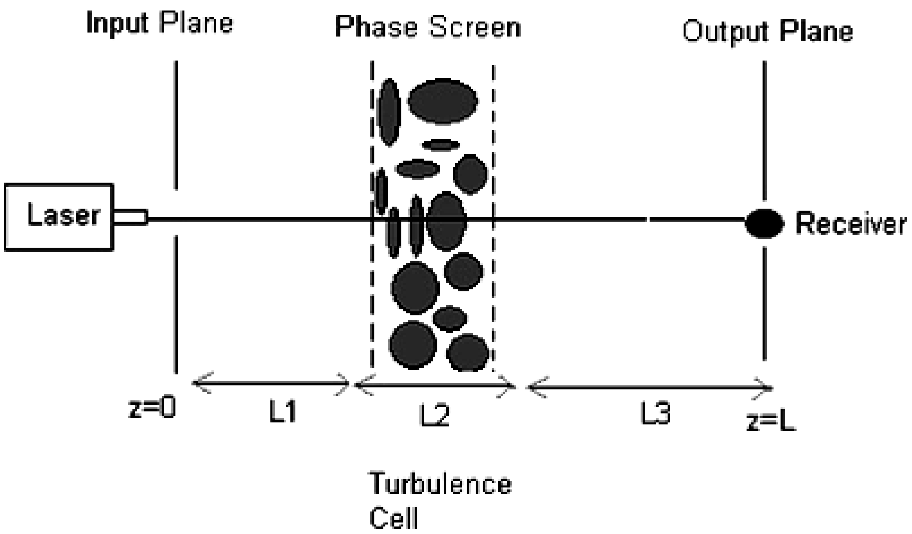

Fig. 5.4.1 Simulated optical channel propagation geometry

From Fig 5.4.1 it is indicated that ",the random medium exists only in between the planes z=L1 and z=L1+L2 and the receiver is located at z=L, where L=L1+L2+L3. A thin turbulent (L2/L3<<1) layer along a propagation path is used to model optical wave propagation through atmosphere, such a turbulent layer is known as a phase screen",.

A Gaussian laser beam propagating through the turbulent atmosphere to a receiver along horizontal path having distance 'L'. The optical field unit amplitude written as,

$$U_0(r,0) = \exp\left(-\frac{r^2}{W_0^2} - i\frac{kr^2}{2F_0} \right) \tag{5.9}$$

Where W_0 and F_0 denotes the spot size radius and phase front radius of curvature, r is the distance in the transverse direction and $k = \frac{2\pi}{\lambda}$ is the optical wave number. If a random medium exists along any part of the propagation path between transmitter and receiver, the optical field at distance z=L under the Rytov approximation is

$$U(r,L) = U_0(r,L)\exp\begin{bmatrix}\psi_1(r,L)+ \\ \psi_2(r,L)+----\end{bmatrix} \tag{5.10}$$

The above equation shows phase perturbations caused by the random medium. Where,

$$\psi = \chi + i\phi \tag{5.11}$$

Real part of the equation χ represents the fluctuations of the logarithm of the amplitude and therefore it is called the log-amplitude fluctuations while the imaginary part ψ represents the fluctuations of phase.

In line of sight problem, the wave experiences amplitude and phase fluctuations as it propagates through the thin layer. We can represent this field as U0U1 , Where U0 is the incident wave and U1 represents the fluctuations. The field U0U1 is incident on the second layer to produce U0U1 U2. In this way the total output of field becomes the product of U0U1 U2U3------- Un as shown in following figure.5.4.2

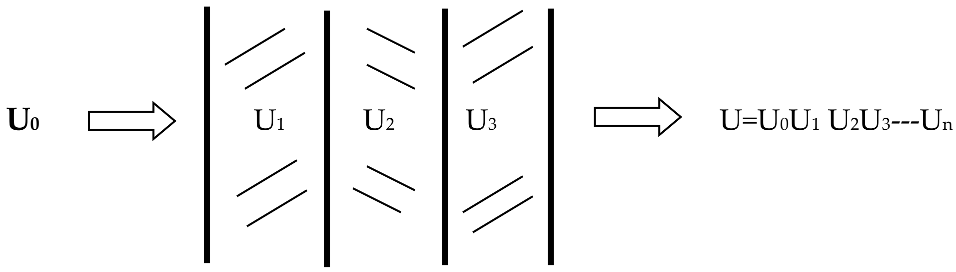

Fig. 5.4.2 : Field distribution

In equation (5.11) χ - is the log-amplitude perturbation and ϕ is the phase perturbation.

To theoretically represent the atmosphere as a phase screen, the above field distribution is represented in terms of effective structure parameter $C_{n_i}^2$, the location along the propagation path and the thickness of the turbulence slab. The typical atmospheric phase screen created using MATLAB simulation is given in Fig.5.4.3 [2-6]

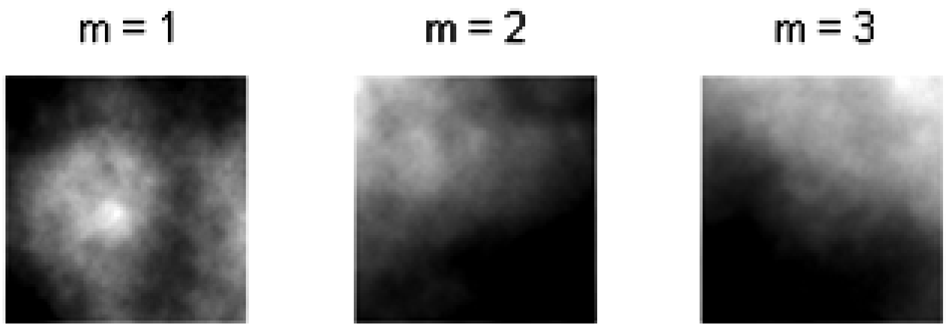

Fig.5.4.3 : MATLAB-lab simulated atmospheric phase screen

Phase screens are created by transforming computer generated random number into two – dimensional arrays of phase values on a grid of sample points that have the same statistics as turbulence –induced phase variations. In above figure dark region represents negative maximum phase while bright region represents maximum positive phase variations. Symbol 'm' represents the number of phase screen.

5.5 Simulation results for Aperture averaging

In this section we compared irradiance of received optical beam for different input parameters propagating through randomly generated atmospheric region. Total number of phase screens here we assume (m=10), with beam parameters considered as follows.

1. Beam Profile: Gaussian optical beam
2. Wavelength $\lambda = 1550\ nm, 1310\ nm, 980\ nm, 780 nm$

3. Distance $L = 2000m$ between source and detector
4. Refractive Index structure parameter

   $C_n = 10^{-12}, 10^{-14} \,\&\, 10^{-16} m^{\frac{-2}{3}}$ for weak strong, moderate turbulence conditions .

The MATLAB simulated results for (m=10) is shown in following fig.5.5.1

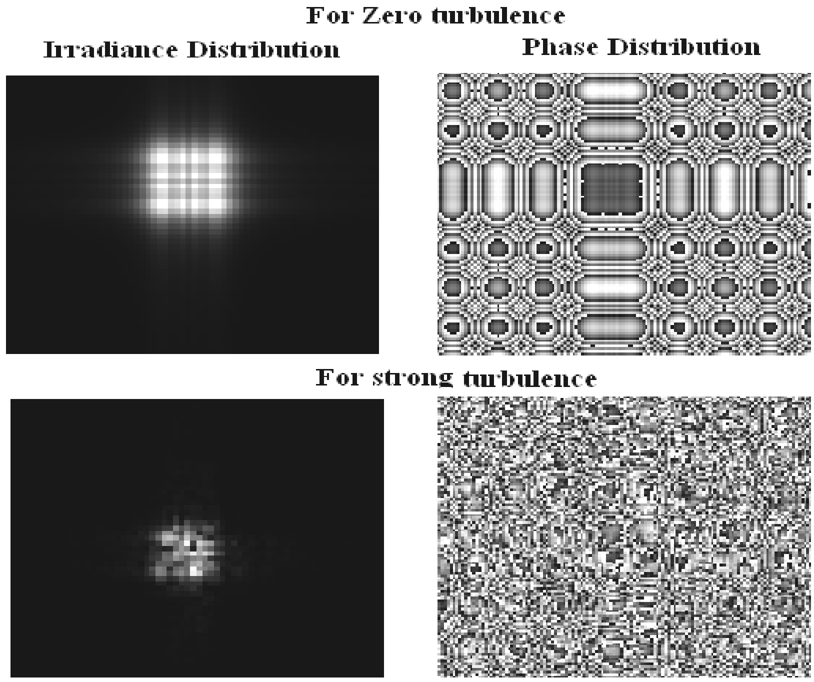

Fig. 5.5.1 : Optical irradiance and phase distributions for two different turbulence conditions

The simulation model output is given in above figure 5.5.1 when zero turbulence is present, irradiance and phase distributions are not disturbed. But when we set the values of refractive index structure parameter C_n^2 as a strong turbulence, the irradiance and phase distributions are completely changed. In addition we calculate scintillation index, aperture averaging factor for different receiver aperture diameters. To compare the performance of coherent and partially coherent optical beam, first, we define the output SNR in the absence of optical turbulence by the ratio of the detector signal current i_s to the root-mean-square (rms) noise current- σ_N, which yields

$$SNR_0 = \frac{i_s}{\sigma_N} = \sqrt{\frac{\eta P_s}{2h\nu B}}, \tag{5.12}$$

$$i_s = \frac{\eta e P_s}{h\nu} \tag{5.13}$$

where i_s - is signal current , P_s is the signal power in watts , B - filter bandwidth , η is the detector quantum efficiency in electrons/photon , e is electric charge in coulombs , h is the Planck's constant ($h = 6.63*10^{-34}$ joule-second) and ν is optical frequency in hertz . In the presence of atmospheric turbulence, the received signal exhibits additional power losses (refraction, diffraction) and random irradiance fluctuations. The output current from the detector is given by

$i = i_S + i_N$ & the variance

$$\sigma_{SN}^2 = \langle i_S^2 \rangle - \langle i_S \rangle^2 + \langle i_N^2 \rangle$$

$$= \left(\frac{\eta e}{h\nu}\right)^2 \langle \Delta P_S^2 \rangle + \frac{2\eta e^2 B \langle P_S \rangle}{h\nu} \tag{5.14}$$

Where, ΔP_S – represents power fluctuations in the signal.

SNR at the output of the detector

$$\langle SNR \rangle = \frac{\langle i_S \rangle}{\sigma_{SN}} = \frac{\langle P_S \rangle}{\sqrt{\langle \Delta P_S^2 \rangle + \frac{2h\nu B \langle P_S \rangle}{\eta}}} \tag{5.15}$$

Rearranged as,

$$\langle SNR \rangle = \frac{SNR_0}{\sqrt{\left(\frac{Pso}{\langle Ps \rangle}\right) + \sigma_I^2(D) SNR_0^2}} \tag{5.16}$$

Where Pso the signal power in the absence of the atmospheric effects, and $\sigma_I^2(D)$ is the irradiance flux variance on the photo detector. Angle bracket $\langle \ \rangle$

represent mean. Signal to noise ratio for strong turbulence condition $\left(C_n = 10^{-13}\right)$ using coherent optical beam. , assume that $\frac{Pso}{\langle Ps \rangle} = 1$, for different values of $SNRo$

$$\langle \mathrm{SNR} \rangle = \frac{\mathrm{SNRo}}{\sqrt{1+\sigma_I^2(D)\mathrm{SNR}_0^2}} \tag{5.17}$$

Now using all above equation we first calculate Rytov variance and then scintillation index and from scintillation index we analyzed aperture averaging factor 'A' for coherent and partially coherent beam. We also studied different cases to know the effect of atmospheric turbulence.

5.6 Simulation Results for Single Source Single Detector

We start with single source and single detector scheme as shown in following figure.5.6.1 .For wavelengths 780nm to 1550nm with aperture diameter 0.08m and Refractive Index structure parameter $C_n = 10^{-13} m^{\frac{-2}{3}}$ for strong turbulence conditions the variations of scintillation index with distance is given.

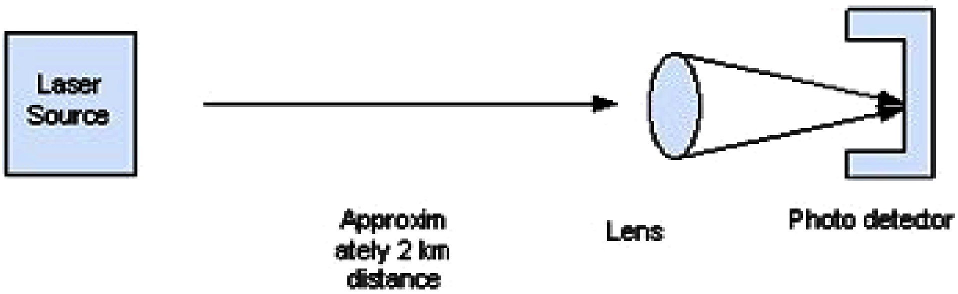

Fig 5.6.1 : Single source single detector scheme

5.6.1 Case-1 (Fix Diameter)

Beam width W and diameter D of receiver aperture for both coherent and partially coherent beam is chosen as 0.025 m and 0.08 m (fix). We compare aperture averaged scintillation index for both the beams using different wavelengths (1550 nm to 780 nm) shown in Fig.5.6.2 and Fig.5.6.3 . From the graph it is observed that using partially coherent beam with aperture averaging for 1550nm wavelength, scintillation index decreases from 0.134 to 0.0302 but for 780nm wavelength saturation region is shifted to non-saturation region with increased scintillation index from 0.060 (i.e. saturation region) to 0.1509.[7]

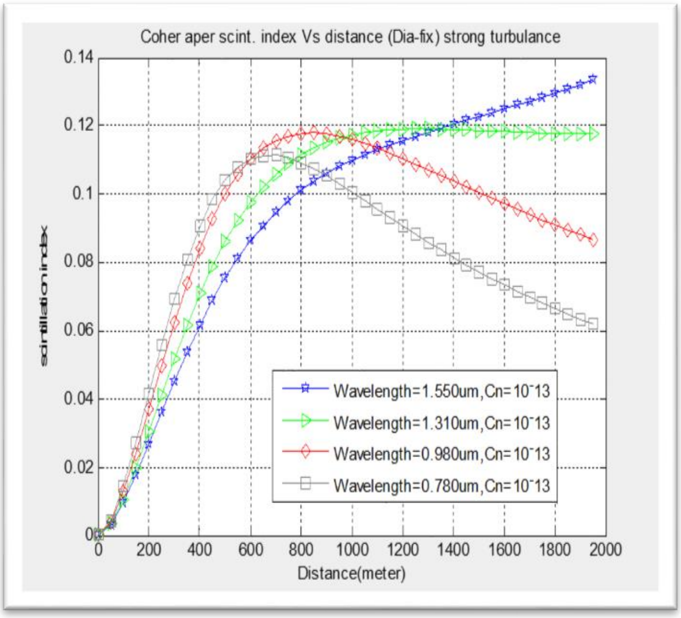

Fig 5.6.2 : Scintillation index for coherent beam vs distance for strong turbulence

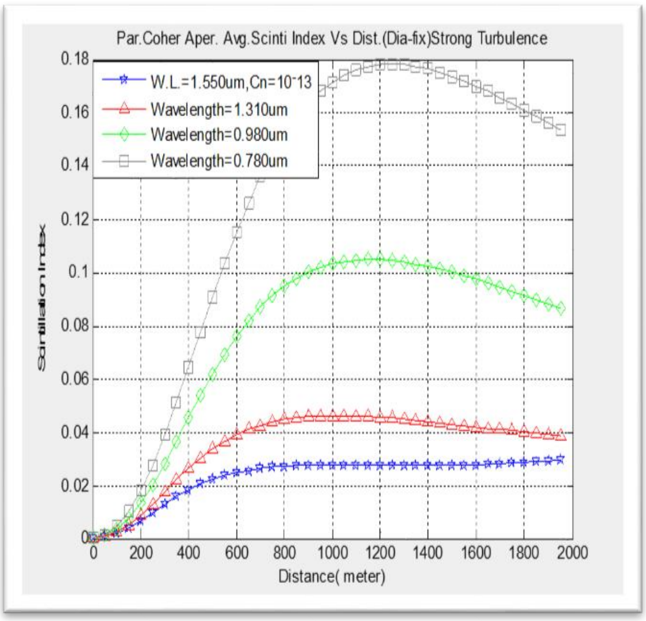

Fig.5.6.3 : Reduced scintillation index vs distance using partially coherent beam.

5.6.2 Case-2 (Variable Diameter)

In another case we consider that the beam width is same but diameter D of receiver aperture is increased 10 times i.e. from 0.08 to 0.8meter for the same distance L=2km. Following fig.5.6.4 and fig.5.6.5 shows the effect of large aperture diameter on scintillation index for strong turbulence conditions using 1550nm and 780nm.

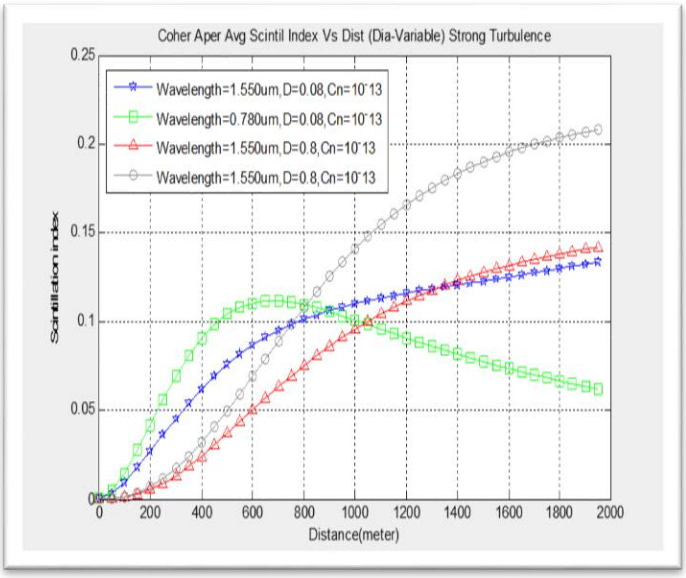

Fig. 5.6.4 : Scintillation index for coherent beam vs distance for strong turbulence with variable aperture diameter

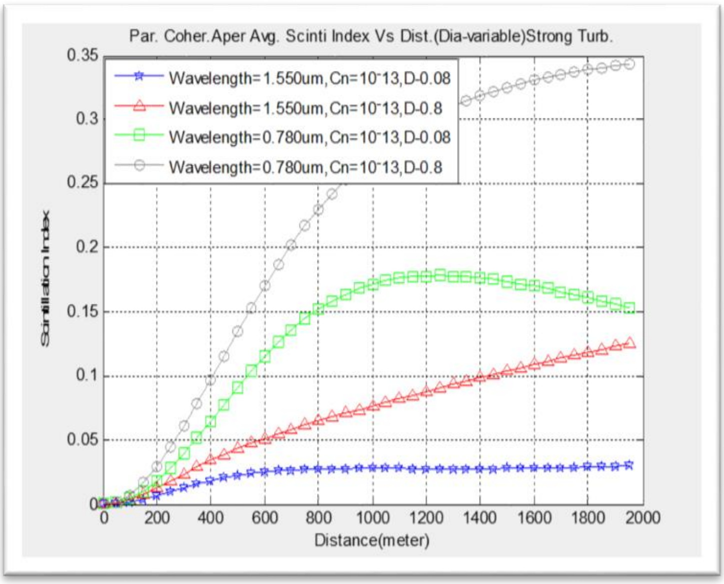

Fig 5.6.5 : Scintillation index vs distance for partially coherent beam with variable aperture diameter

From above graph it clearly shows that using partially coherent beam scintillation index decreases from 0.148 to 0.120 but for 780nm increases from 0.208 to 0.344 respectively.

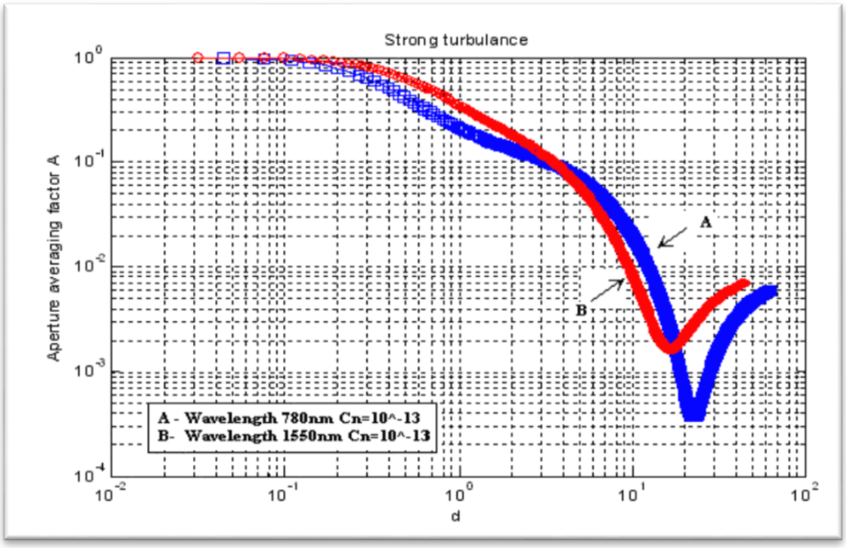

Fig.5.6.6 : Aperture averaging factor vs diameter (scaled by'd') for coherent beam with strong turbulence

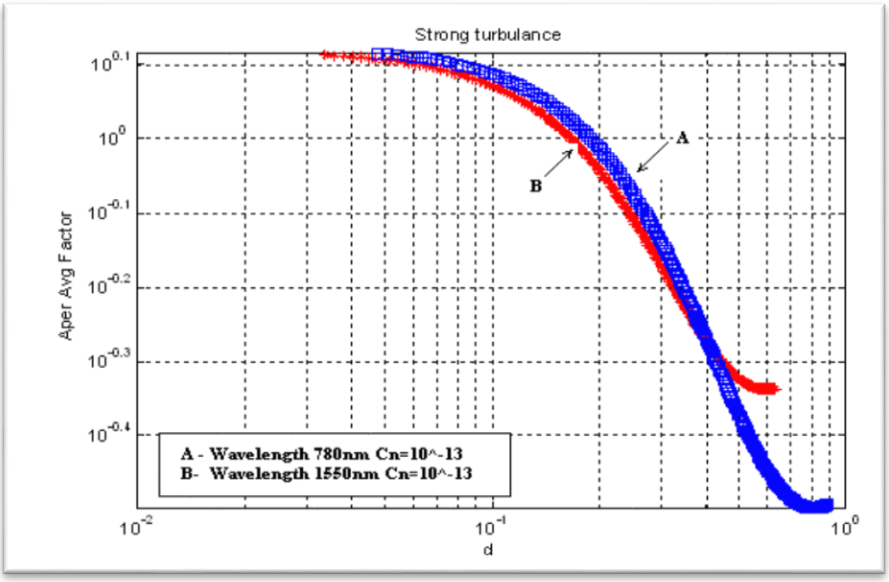

Fig. 5.6.7 : Aperture averaging factor vs diameter (scaled by 'd') for partially coherent beam with strong turbulence

Aperture averaging factor 'A' with aperture diameter is shown in fig 5.6.6 and 5.6.7 respectively. Fig shows that A decreases as aperture diameter increases and in case of partially coherent beam more aperture averaging takes place compared to coherent optical beam.

Table 5.1: Performance Characteristics of different wavelengths in terms of Signal to Noise Ratio

Parameter	Wave length λ1= 780 nm		Wave length λ2= 980 nm		Wave length λ3= 1310 nm		Wave length Λ4= 1550 nm	
Atmos. Turbul.	Weak Turbulence $Cn^2=10^{-16}$	Strong Turbulence $Cn^2=10^{-13}$	Weak Turbulence $Cn^2=10^{-16}$	Strong Turbulence $Cn^2=10^{-13}$	Weak Turbulence $Cn^2=10^{-16}$	Strong Turbulence $Cn^2=10^{-13}$	Weak Turbulence $Cn^2=10^{-16}$	Strong Turbulence $Cn^2=10^{-13}$
Scint. Index	7.1×10^{-4}	0.06 (saturation)	4.9×10^{-4}	0.085 (saturation)	3.2×10^{-4}	0.12	2.9×10^{-4}	0.13
(S/N) db	15.29	6.08	15.92	5.33	16.50	4.34	16.80	5.27

For different values of SNRo, mean SNR is plotted in Fig 5.6.8 and Fig. 5.6.9. This clearly shows 50% improvement in signal to noise ratio for 1550nm wavelength. The simulated parameters are summarized in Tab.5.1 for different wavelengths and atmospheric turbulence conditions with distance L=2 km. It is observed that the scintillation index for 780 nm and 980 nm is less but it goes into to the saturation region after traveling 1 km distance.

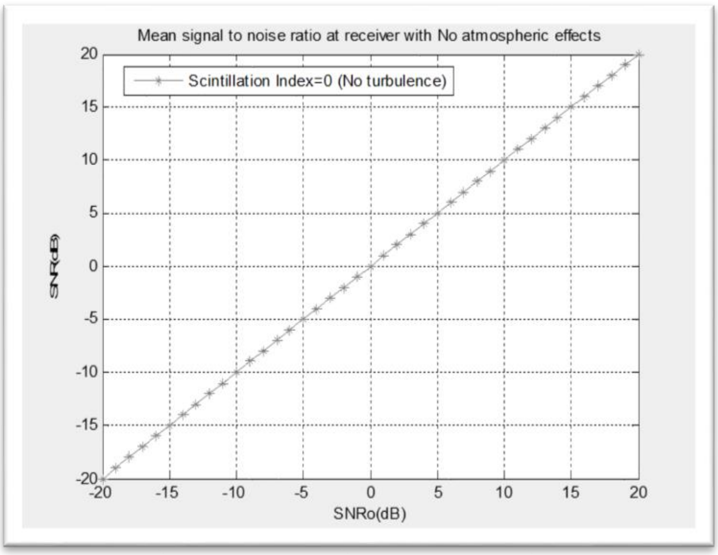

Fig.5.6.8 : Mean SNR Vs SNRo for Zero turbulence

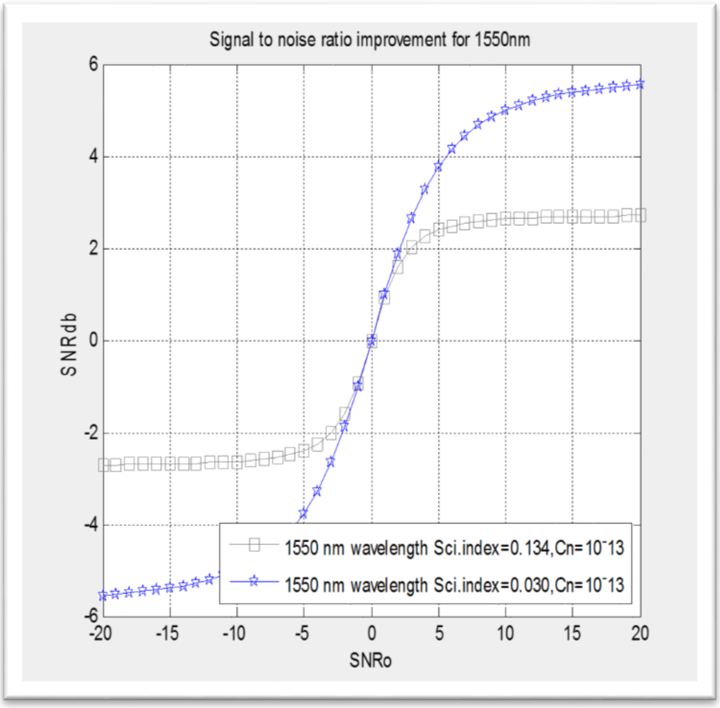

Fig.5.6.9 : Improvement in SNR using aperture averaging of partially coherent beam.

The variation of mean BER with different values of scintillation index and assuming fixed aperture diameter is given in following Fig.5.6.10. The curve shows that as the SNR increases it decreases scintillation index and therefore BER reduces.

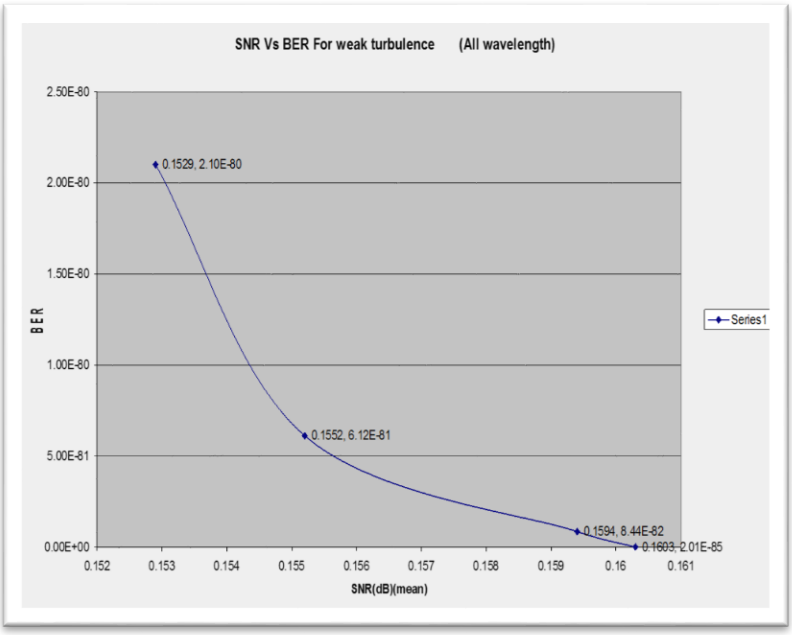

Fig.5.6.10 : Mean BER vs SNR for different wavelength with fix diameter

The proposed aperture averaging technique using partially coherent optical beam for mitigating atmospheric turbulence is studied and simulated for 2 km long FSO link under weak, moderate to strong atmospheric turbulence conditions. The performance of the system was studied at the 780–1550 nm wavelengths by analyzing SNR for various aperture diameters D for strong atmospheric turbulence conditions C_n^{-13}. Results are verified using MATLAB simulation and summarized in Table 5.1. It is observed that scintillation index variations are more pronounced for 780 nm coherent Gaussian beam compared to partially coherent beam.

5.7 Simulation result for Single Source with Multiple Aperture Multiple Detector

We consider a single source multiple detectors with multiple apertures system as shown in Fig.5.7.1. We represent M_d as the number of detectors and M_a as the number of apertures being used in the averaging scheme. We take the diameter D of each aperture as 0.008 m. Now, for M_a =10 then total diameter is $D_t = M_a D^2$, D_t =0.08 m and we take beam width W=0.025 m. The aperture averaging factor A_M for the multiple aperture averaging scheme is then obtained using equation (5.1) as

$$A = \sigma_I^2(D) / \sigma_{I,s}^2(0) \tag{5.18}$$

In above equation by adding the effects of multiple detectors and multiple apertures, the equation becomes

$$A_M = \frac{\sigma_I^2\left(\frac{D_t}{\sqrt{M_a}}\right)}{M_d \sigma_I^2(0)} \tag{5.19}$$

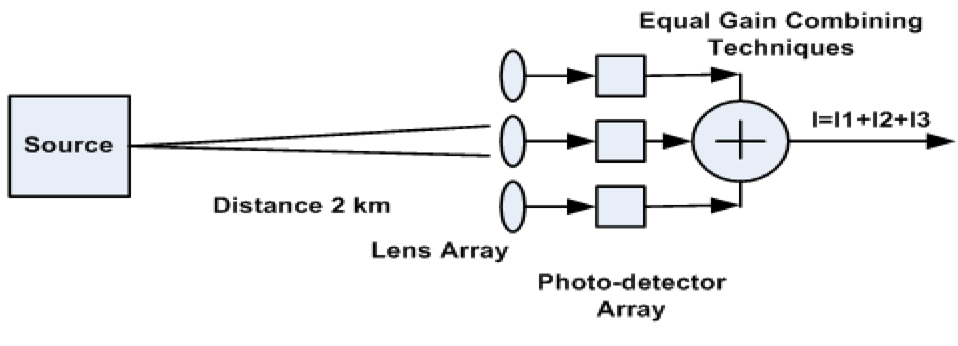

Fig. 5.7.1 : Single source multiple detector scheme

The effect of above factor on total scintillation index is given by

$$\sigma_{I,s}^2 = A_M \times \sigma_{I,s}^2 \tag{5.20}$$

We compare aperture averaged scintillation index using multiple number of photo-detector M with single detector at wavelength 1550nm and shown in following fig 5.7.2. From Figure it is again observed that scintillation index is reduced using SSMDMS scheme with partially coherent beam at 1550nm wavelength.

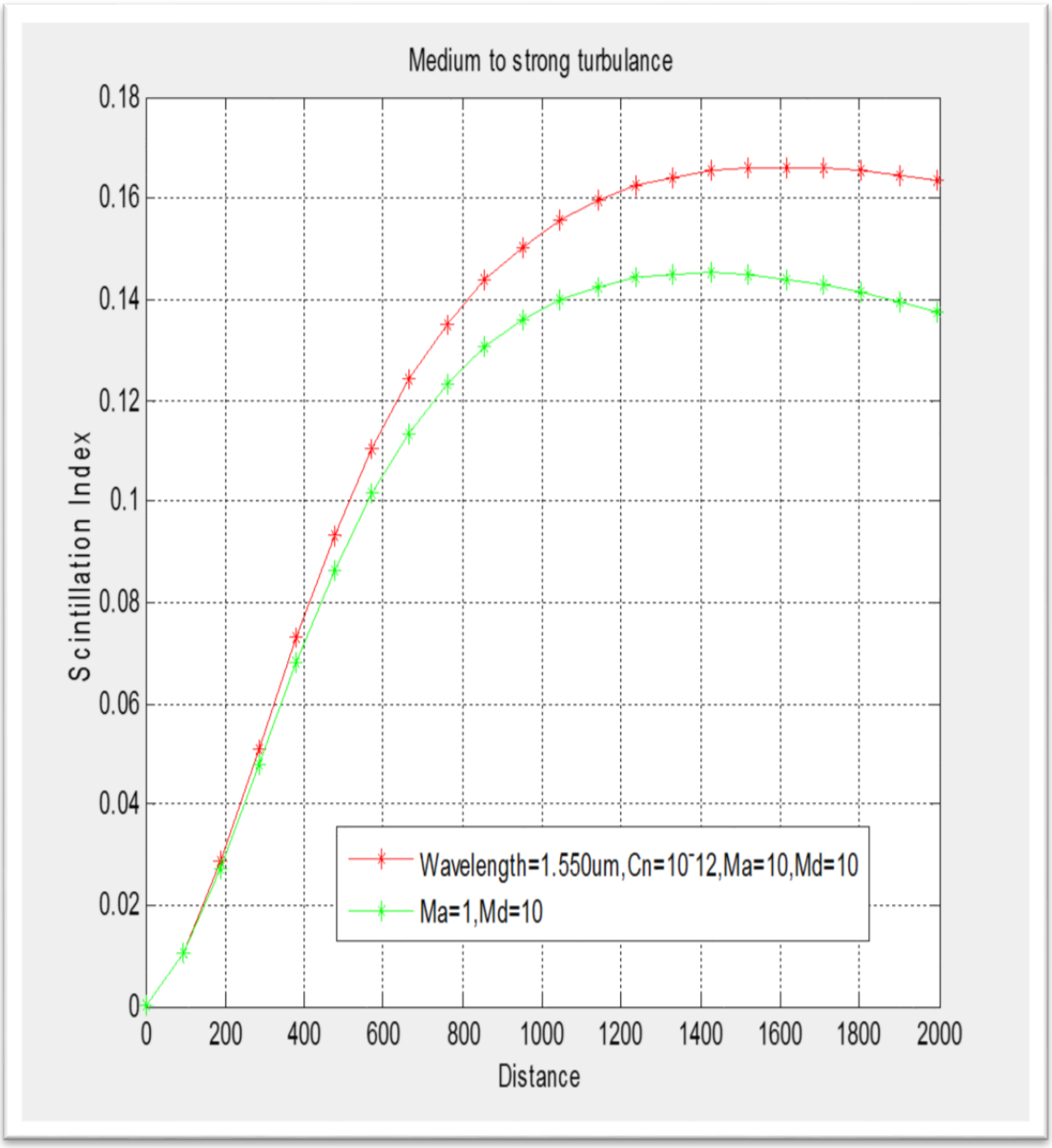

Fig 5.7.2 : Scintillation index comparison for single source single aperture with single source multiple aperture/ detector

5.8 Experimental Measurement of Aperture Averaging Effects on the Performance of FSO system

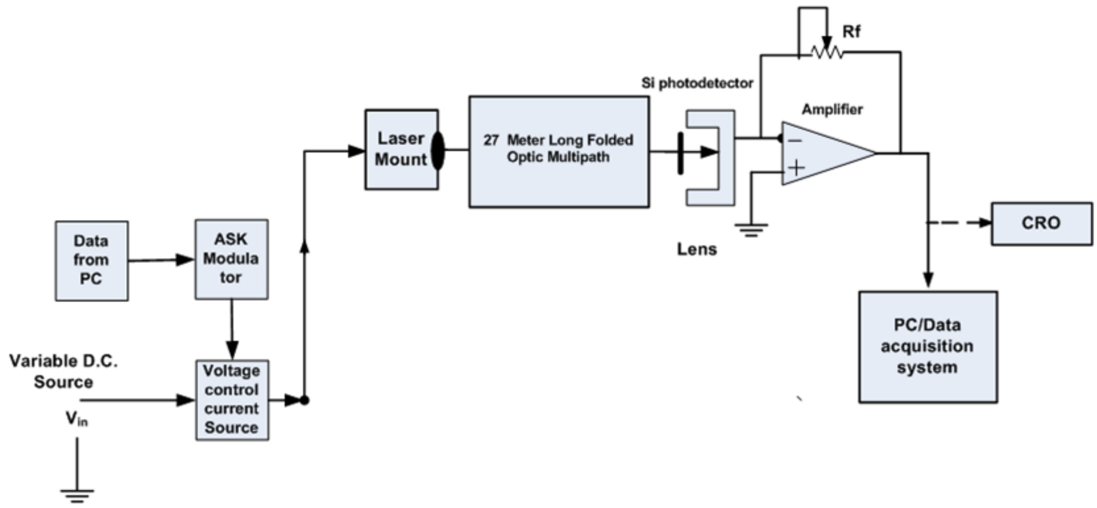

Fig 5.8.1 : Experimental arrangement for aperture averaging effects

Aperture Averaging Effect with Digital Input

The aperture averaging experiment by selecting two lenses having diameters 5 cm and 10 cm respectively with following parameters and experimental arrangement shown in fig.5.8.1

Laser wave-length =698 nm; Modulation - ASK; Laser Current- 12 mA. Carrier frequency for ASK modulation -5Khz and 5V(p-p) sine wave; Room Temp= Min.30^{0}C and Max 40^{0}C ; Total Number of reflectors -04;Distance between Tx and Rx-27 meter; Lens Diameter=5 and 10cm respectively ;

The laser diode transmitter produced identical light wave signals for passing through the atmospheric turbulence medium. As the light passed through the atmosphere, they were corrupted by the turbulent medium depending on the strength of turbulence and these corrupted pulses are finally received at the receiver photodiode. We used LM35 temperature sensor whose conversion factor is 10mv=1^{0}C. We took samples for 15 min. If the sample value is 63 then conversion is 63 * 0.0048= 0.3024 V i.e. 302 mv and hence 30.2 ^{0}C.

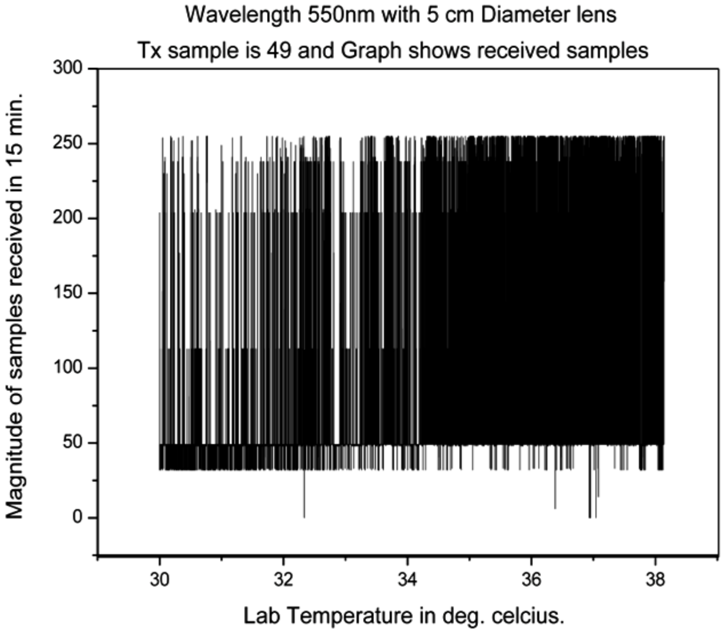

Fig. 5.8.2 : Aperture averaging measurement: for 5 cm lens diameter, number of samples collected in 18 min.

We observe from Fig 5.8.2 and 5.8.3 that when receiver aperture diameter is small, the increasing C_n^2 value with increase in temp of room giving us a more fluctuations in the received data bits, but when the aperture diameter is large the averaging effect remove the fluctuation.

For 5cm diameter it is observed that intensity fluctuation increases rapidly, however for 10 cm diameter it reduces. Data sample values in between 200 to 250 is completely removed when aperture diameter is 10cm.

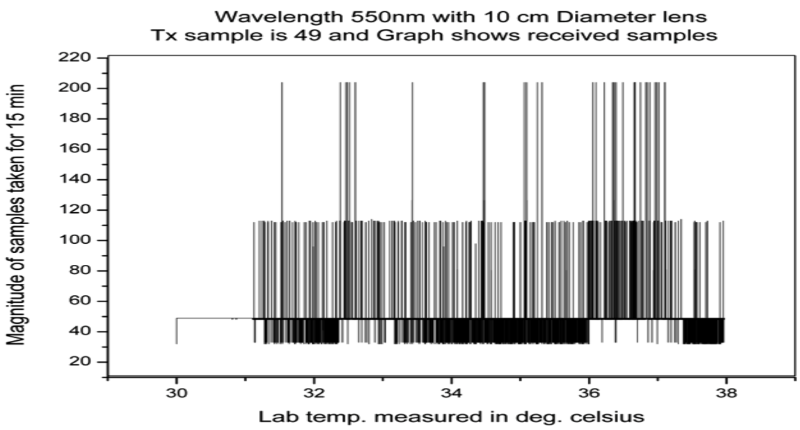

Fig. 5.8.3 : Aperture averaging measurement: for 10 cm lens diameter number of samples collected in 18 min.

Aperture averaging effect with analog input

For Lens diameter Radius R=4 cm (Small), Room Temp- 28^{0}C

Table 5.2 Measurement of Aperture avaraging (Lens Diamater=4 cm)

Sr.No	Output Rx. Photo-Detector	Sr.No	Output Rx. Photo-Detector	Sr.No	Output Rx. Photo-Detector	Sr.No	Output Rx. Photo-Detector
1	124	15	23	29	49	43	25
2	27	16	88	30	28	44	46
3	76	17	22	31	21	45	116
4	20	18	100	32	20	46	122
5	65	19	19	33	23	47	98
6	86	20	122	34	23	48	81
7	25	21	133	35	32	49	40
8	117	22	104	36	103	50	30
9	71	23	111	37	121	51	106
10	32	24	55	38	113	52	68
11	25	25	40	39	24	53	34
12	117	26	126	40	108	54	30
13	107	27	99	41	24	55	94
14	125	28	117	42	64	56	128

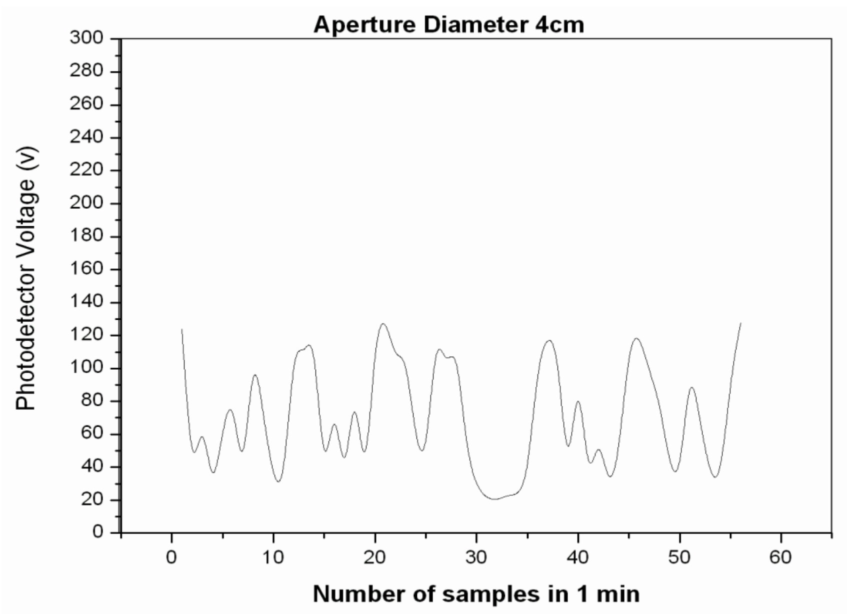

Fig. 5.8.4 : Aperture averaging measurement for 4 cm diameter lens

To calculate photo-detector voltage in terms of sample value we have multiplied sample value with 0.00488 constant.

Rytov variance (practical) = 0.4549 (from fig.5.8.4), Refractive Index structure parameter (using rytov variance) $=5.1*10^{-12}$, Rytov variance theoretically (simulation) =0.4438, Refractive Index structure parameter (using rytov variance) $=5.4*10^{-12}$.

For 5 cm lens Diameter, Room Temp- 28^{0}C

Table 5.3 Measurement of Aperture avaraging (Lens Diamater=5 cm)

Sr.No	Output Rx. Photo-Detector	Sr.No	Output Rx. Photo-Detector	Sr.No	Output Rx. Photo-Detector	Sr.No	Output Rx. Photo-Detector
1	103	17	26	33	76	49	163
2	25	18	233	34	49	50	29
3	144	19	165	35	50	51	32
4	24	20	25	36	26	52	36
5	89	21	92	37	39	53	180
6	60	22	184	38	31	54	54
7	100	23	113	39	27	55	26
8	39	24	27	40	74	56	115
9	98	25	261	41	27	57	117
10	51	26	140	42	113	58	263
11	227	27	27	43	73	59	217
12	46	28	265	44	24	60	75
13	243	29	27	45	32	61	28
14	36	30	39	46	32	62	34
15	213	31	142	47	48		
16	62	32	72	48	25		

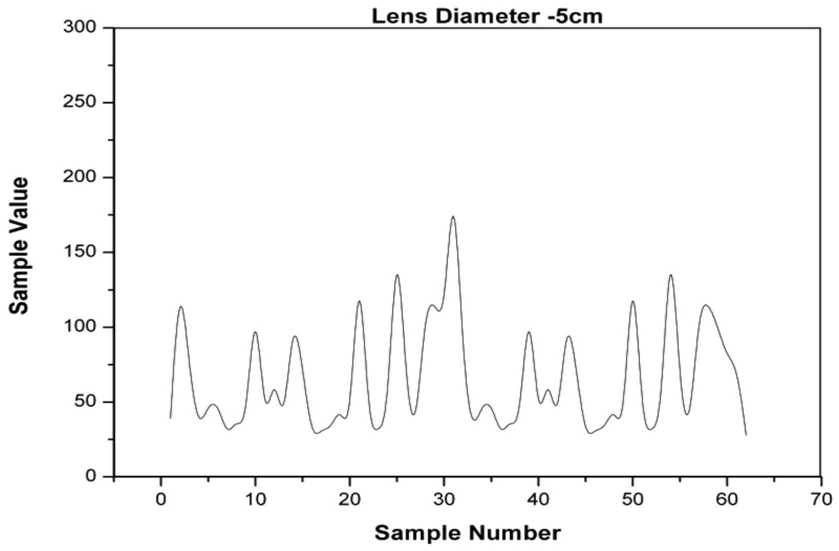

Fig.5.8.5 : Aperture averaging measurement for 5 cm diameter lens

Above graph clearly shows that when lens diameter increases from 4 cm to 5 cm the intensity fluctuations are reducing to 0.34v as shown in figure 5.8.5

5.9 Measurement of Aperture Averaging Factor 'A'.

We use the same experimental setup as described in previous section 5.8 for measurement of aperture averaging factor 'A'. From equation 5.7 we have,

Aperture averaging factor for coherent beam is defined as

$$A = \sigma_I^2(D) / \sigma_{I,s}^2(0)$$

Where $\sigma_I^2(D) \& \sigma_I^2(0)$ are the scintillation index for receiver lens of diameter D and a "point receiver" (D≈0).

Observation Table :

Case-I : We measure the intensity fluctuations (Analog Data) using 4cm and 5cm diameter lens in terms of photo-detector voltage V and calculate the value of $\sigma_I^2(D)$. Fig.5.8.6 shows the relation between aperture diameter and aperture averaging factor 'A'. $\sigma_{I,s}^2(0)$=1.2

Table 5.4 Diameter 'D' Vs Aperture averaging factor 'A'

Aperture Diameter D (cm)	**Wavelength (λ)**	$\sigma_I^2(D)$	$A = \sigma_I^2(D) / \sigma_{I,s}^2(0)$
2.5 cm	698 nm	0.63	0.52
4 cm	698 nm	0.45	0.37
5 cm	698 nm	0.34	0.28
7cm	698 nm	0.25	0.20
10 cm	698nm	0.16	0.13

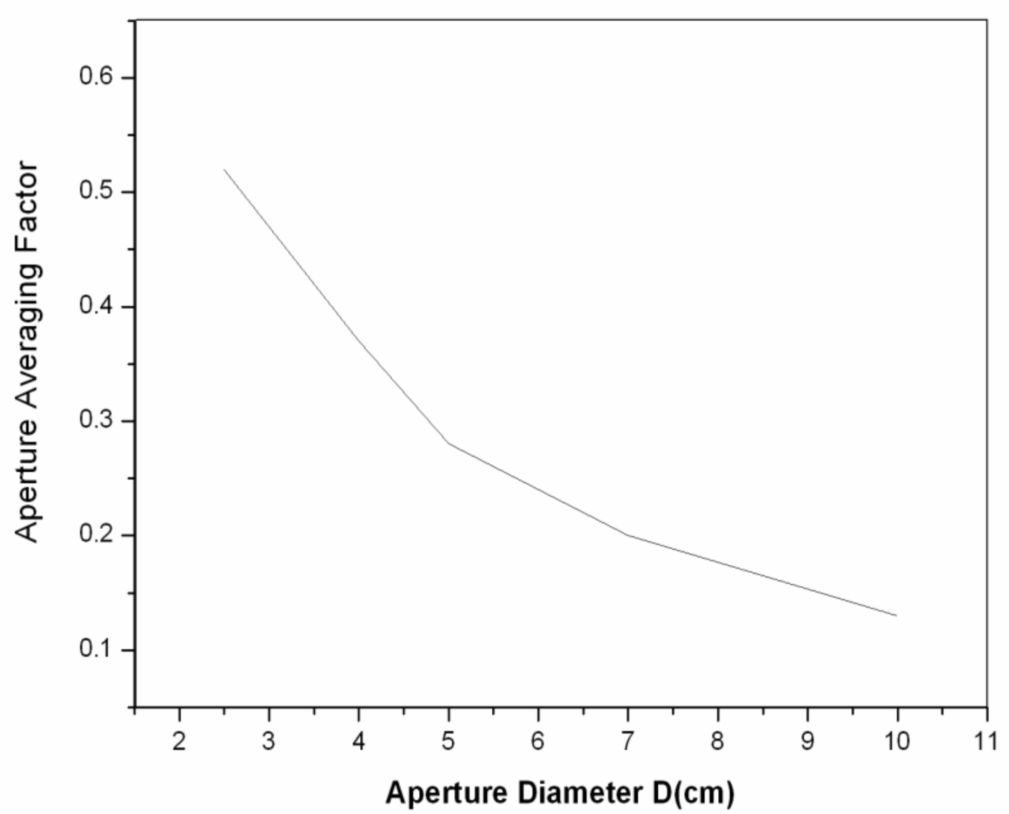

Fig.5.8.6 : Aperture diameter 'D' vs aperture averaging factor 'A'

Case-II : We measure the BER using 5cm and 10cm diameter lens for digital data shown in fig 5.8.7.

To perform this experiment using some digital signals in our turbulence set up, we used a computer software entitled "Terminal" [from chapter 4] for generating and transmitting continuous bits for modulation of the laser source. The laser diode transmitter produced identical light wave signals for passing through the atmospheric turbulence medium. As the light passed through the atmosphere, they were corrupted by the turbulent medium depending on the strength of turbulence and these corrupted pulses are finally received at the receiver photodiode. The received corrupted pulses are then forwarded to the computer port for bit-by-bit comparison within the computer using the same Terminal software.

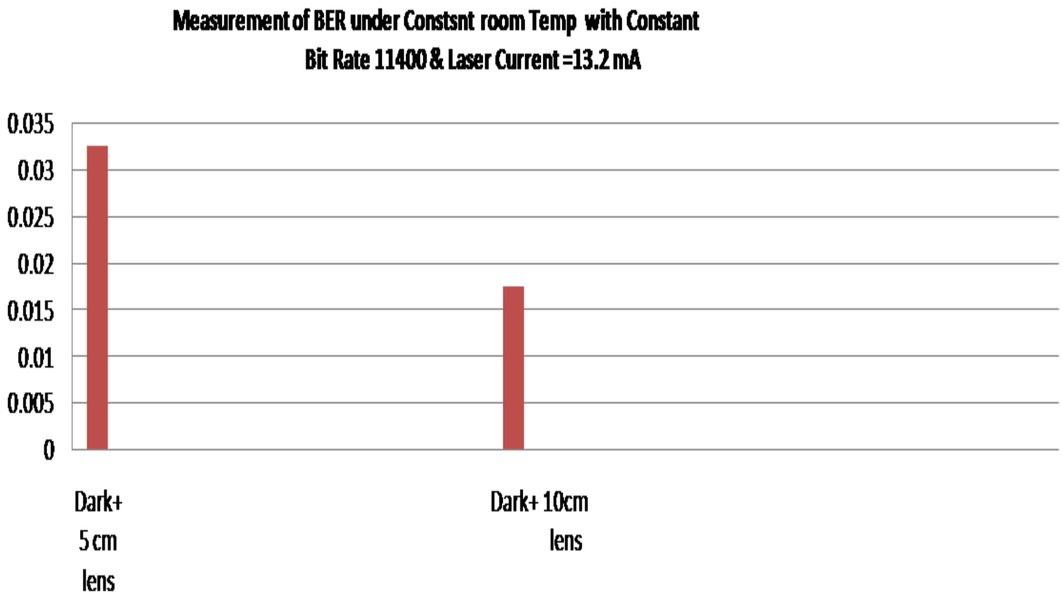

Fig. 5.8.7 : BER for 5cm and 10cm diameter lens

The simulated and experimental measurements show that aperture averaging technique is effective for aperture diameter up to 10cm for 27m optical path length. Also, significant improvement in BER performance is seen from 0.034 to 0.018 with the increase in aperture diameter. However, the aperture diameter cannot be increased indefinitely as it leads to increase in background noise that causes reduction in signal to noise ratio of the system.

The mitigation of scintillation effects is done by increasing laser biasing current at transmitter side as discuss in section 5.3

5.10 Conclusion:

The aperture averaging technique using coherent and partially coherent optical beams for mitigation of atmospheric turbulence is studied and simulated for 2 km long line of sight FSO link under weak, moderate to strong atmospheric turbulence conditions. The performance of the system was studied at the 780–1550 nm wavelengths by analyzing SNR for various aperture diameters varies from 0.8m to 0.08m for strong atmospheric turbulence conditions $Cn=10^{-12}$. Results are verified using MATLAB lab simulation software.

We observe that, if beam width *W* and diameter *D* of receiver aperture for both coherent and partially coherent beam is chosen as 0.025m and 0.08 m (fix)and compare scintillation index for both the beam using different wavelengths (1550nm–780 nm) then using partially coherent beam with 1550 nm wavelength , scintillation index decreases from 0.110 to 0.0302 i.e.(≈30%) but for780 nm it is increases from 0.10 to 0.18 (≈55%). experimental measurements show that aperture averaging technique is effective for aperture diameter up to 10cm for 27m optical path length. Also, significant improvement in BER performance is seen from 0.034 to 0.018 with the increase in aperture diameter.

References

[1] Andrews, L.C. and Phillips, L.R. ,"Laser Beam Propagation through Random Medium", Second Edition, SPIE Press, Bellingham, Washington, USA, 2005.

[2] Hunt B.R., R Lipsman,"A Guide to MATLAB for beginners", Cambridge University Press, New York, 2001.

[3] Jason D. Schmidt ,"Numerical Simulation of optical wave propagation with example in MATLAB", SPIE press, pp 149-183, 2010.

[4] Behlouli A.. Combeau P, Aveneau L, "Efficient Simulation of Optical Wireless Channel Application to WBANs with MISO Link ," Procedia Comput. Sci., vol. 40, pp. 190–197, 2015.

[5] Akira Ishimaru ," Wave propagation and scattering in random media, Multiple scattering , Turbulence , Rough surface and remote sensing , Vol.2 , Academic press, New York, pp. 347-385, 1978.

[6] Mehta N., Kaushal H., Jain V. K., and Kar S., "Experimental Study on Aperture Averaging in Free Space Optical Communication Link," *IEEE Conference*, February, 2013.

[7] Sachin M Kale, Asim Kar, "Mitigation of scintillation in FSO using aperture averaging of partially coherent input Gaussian optical beam", International Journal of Signal and Imaging Systems Engineering, Vol 7: No.1 pp:21–29,.2014.

CHAPTER 6

Studies on LED Based Indoor Optical Wireless Communication System

6.1 Introduction

Full use of the capacity provided by an optical fiber cable delivered to homes will necessitate the use of broad-band links including indoor wireless access technologies capable of operating at Gbit/s. In recent years optical wireless (OW) has emerged as a strong candidate for high speed indoor communications , as a complementary scheme to RF systems. The main advantages of optical wireless communications are unregulated and unlicensed electromagnetic spectrum, high quality data transmission, immunity to electromagnetic interference and highly secured communications. White light LEDs were proposed to replace the laser as the light sources for indoor communications in order to lower the cost while maintaining the high-speed data rate and the security feature that FSO offers.

The purpose of this chapter is to present design and development of laboratory standard line of sight indoor optical communication and illumination system using white light LEDs. The proposed work addresses the need to develop low-power, high speed electronics circuit by means of existing laboratory hardware components for indoor optical communication-cum-lighting systems. A current driver circuit is designed using operational amplifier to drive signal and multiple light emitting diodes (LED) with amplitude shift key (ASK) modulation. A 5 KHz carrier signal is selected to modulate the output of personal computer from serial port using data interfacing circuit to send the signal from transmitter to receiver. A silicon photo detector with preamplifier is used to receive data signal at receiver.

6.2 Impulse Response for Indoor Optical Propagation Channel

RF (Radio Frequency) is the most prevalent technology in wireless communication field at present. However the forthcoming new generation of lighting based on LEDs provides some advantages compared to fluorescent and incandescent technology, such as: significant energy saving, longer lifetime, etc. LEDs' short response time is also the prerequisite for communication with visible light [1-2]. It is sensible that communication with semiconductor lighting could be reckoned as a complementary wireless communication technology of RF, and even can replace RF in some high safety demand and RF pollution awareness situations. The LED could be easily modulated for communication due to its short response time. By quickly switching LED on and off (brighter and dimmer) logical "1" and "0" can be sent out serially.

We present an optical wireless communication system that employs white LEDs for indoor wireless line of sight communication. Now, LED light has two basic properties- luminous intensity and transmitted optical power. The luminous intensity is the unit that indicates the energy flx per a solid angle, and it is related to luminance at an illuminated surface . The luminance intensity is used for expressing the brightness of an LED, while the transmitted optical power indicates the total energy radiated from LED. The luminous intensity is given by,

$$I = \frac{d\phi}{d\Omega} \tag{6.1}$$

Where,

Ω- is the spatial angle ,Φ- is the luminous flux , which can be given from energy flux Φ_e as:

$$\phi = K_m \int_{380}^{780} V(\lambda)\Phi_e(\lambda)d\lambda \tag{6.2}$$

Where, $V(\lambda)$ is the standard luminosity curve , K_m is the maximum visibility and it is 683 lm/W at λ =555 nm . The integral of the energy flux Φ_e in all direction is the transmitted optical power P_t given as

$$P_t = \int_{\Lambda_{min}}^{\Lambda_{max}} \int_0^{2\pi} \Phi_e d\theta d\lambda \tag{6.3}$$

Where $\Lambda_{min}, \Lambda_{max}$ is determine from sensitivity curve of photo diode.

The luminous intensity in angle ϕ is given by [2-3]

$$I(\phi) = I(0)\cos^m(\phi) \tag{6.4}$$

A horizontal illuminance E_{hor} at a point $(\mathbf{x,y})$ is given by

$$E_{hor} = I(0)\cos^m(\phi) / D_d^2 \cos(\Psi) \tag{6.5}$$

Where

$\mathbf{I_0}$ – is the center luminous intensity of an LED, $\boldsymbol{\phi}$ – is the angle of irradiance , $\boldsymbol{\Psi}$ – is the angle of incidence , and $\mathbf{D_d^2}$ – is the distance between an LED and detector surface. The received optical power P_r is derived by the transmitted optical power P_t as follows

$$P_t = H(0).P_t \tag{6.6}$$

Where

$$H(0) = \begin{Bmatrix} \dfrac{(m+1)A}{2\pi D_d^2} \times \cos^m(\phi) T_s(\Psi) g(\Psi) \cos(\Psi) \end{Bmatrix}$$
$$0 \le \Psi \le \Psi_c;$$
$$0;$$
$$\Psi \ge \Psi_c \tag{6.7}$$

Where A- is the physical area of the detector in a PD , D_d – is the distance between transmitter and receiver, $T_s(\Psi)$ – is the gain of an optical filter , $g(\Psi)$ – is the gain of an optical concentrator. Ψ_c – denotes the width of the field of vision at a receiver

The $g(\Psi)$ is given by :

$$= \left\{ n^2 \Big/ \sin^2 \Psi_c \right\} \text{when} - 0 \le \Psi \le \Psi_c;$$
$$0; \text{when}\, 0 \ge \Psi_c \qquad (6.8)$$

Where η denotes refractive index.

6.3 Studies on the Performance of LED Based Optical link.

LEDs produce wider emission beams than laser diodes (LD), which makes them the preferred option of the indoor optical communication. In addition they are generally consider as eye safe, which means that they can be used at higher emission powers than laser diodes [3-6]. Other important feature of LEDs include the simplicity of the driver circuit associated with them. LDs on the other hand require more complex driver circuits and are more sensitive to temperature variations. Despite these limitations, laser diode can be modulated at higher speeds then LEDs gives higher data rate . As the laser diode emits very narrow beam, they can be used over longer distance, which favors their use in directed – LOS (line of sight) outdoor communication.[7-9] The block diagram of indoor optical communication as shown in following Fig.6.3.1 Where optical rays are travelling either in straight path or reflected path to photo-detector.

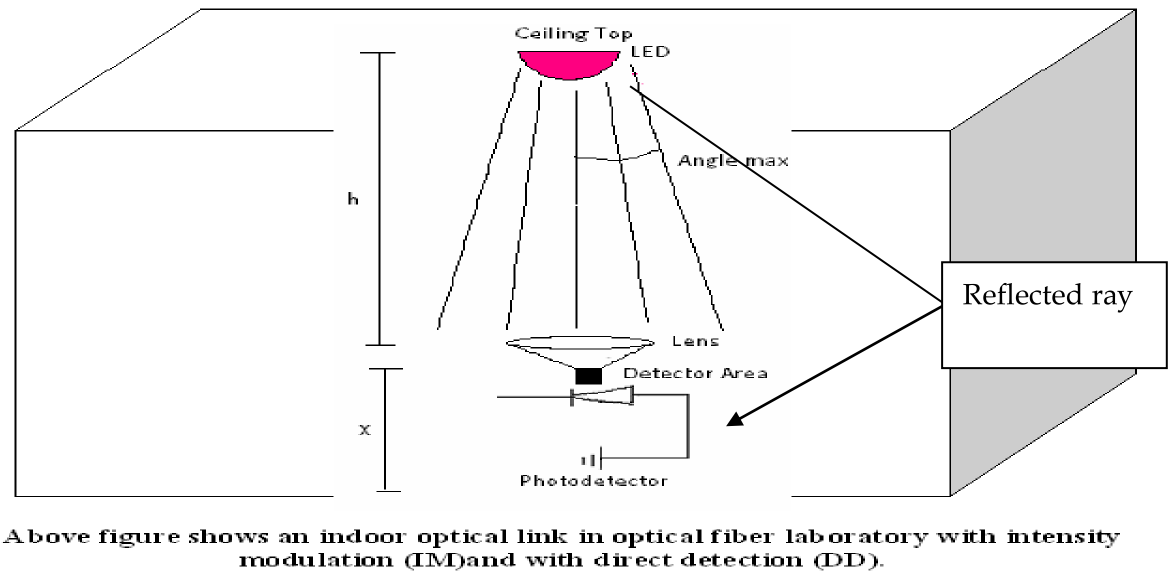

Fig 6.3.1: Block diagram indoor optical communication

The optical transmitter front end consists of a driver circuit along with a light source (LED or Laser diode) as shown in Fig. 6.3.2 in addition to this it consists of two parts; an interface circuit and a source drive circuit, which converts the input signal to an optical signal suitable for transmission [10-12]. The driver circuit of the transmitter transforms the electrical signal to an optical signal by changing the current flow through the light source.

Transmitter Block.

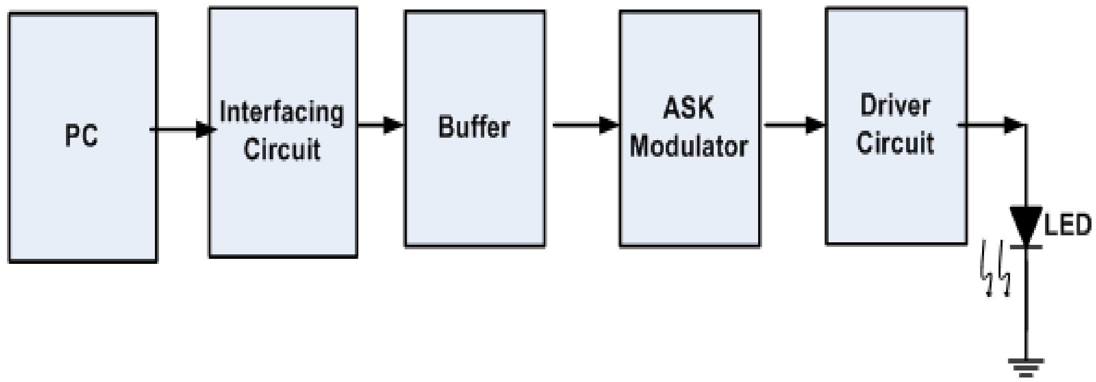

Fig 6.3.2: Design of LED base indoor optical transmitter

6.4 Design and performance studies of an indoor optical wireless link using white light LED.

The performance and design of an indoor visible light communication link using white light LED modules was studied in detail to see how the ambient light affects their operation and how to make simultaneous control of the illumination and communication in indoor environment.

In this system, the optical incident power is detected by a photodiode and converted into an electrical current. In room condition of operation, there is always ambient light that enters the photodiode along with the signal light. The power of the ambient noise, Pamb is determined by the equation.[13]

$$Pamb = Namb \times Bopt \qquad (6.9)$$

Where Namb denotes the ambient radiation, and Bopt denotes the optical bandwidth of the photodiode. Therefore, the resulting electrical current has a DC component (I_{DC}) of,

$$I_{DC} = R \cdot Pamb \tag{6.10}$$

and a signal current of,

$$Is = R \cdot Ps \tag{6.11}$$

Where, R denotes the responsivity of the photodiode (unit of A/W), and Ps is the optical power of the signal [14]. The photodiode also produce a dark current typically on the order of nA and is negligible. Since a trans-impedance is used in the receiver to convert the current generated by the PIN into a voltage signal and can be calculated in terms of incident power as,

$$Vpp = R \cdot Ptot \tag{6.12}$$

Where, Vpp denotes the peak-to-peak voltage generated, and Ptot is the total power that is the sum of Pamb and Ps. Here the responsivity has unit of V/W.

The received optical power P at the receiver is expressed as,

$$P = P_t \frac{(m+1)}{2\pi d^2} cos^m(\phi).T_s(\Psi).g(\Psi).cos(\Psi) \qquad 0 \le \Psi \le \Psi_c \tag{6.13}$$

Where Pt is the transmitted power from an LED, ϕ is the angle of irradiance with respect to the transmitter axis, Ψ is the angle of incidence with respect to the receiver axis, and d is the distance between an LED and a detector's surface. Ts(ψ) is the filter transmission g(ψ) is the concentrator gain. Ψ_c is the concentrator field of view. Semi-angle m is the order of Lambertian emission, and is given by the transmitter half angle (at half power) as

$$m = -l_n\, 2/l_{n(\phi_{1/2})} \tag{6.14}$$

Here we assume, m= 1 from $\Psi_{1/2}$= 60^o (Lambertian transmitter) [15-16].

A white LED/(Dimmer) wireless communication prototype was design and developed. The transmission is based on the assumptions of direct LOS (Line of sight) with simplex channel conditions. A D.C. signal is used to provide the biasing voltage to control the intensity of LED. Amplitude Shift Key (ASK) modulation is used to modulate the data and applied to LED. The tests were carried out in laboratory under normal room temperature conditions. The controlled conditions are defined as the turbulence free environment is maintained within the room. The LED link is designed to transmit a data with fix data rate 2Kbps through free space. A PIN photodiode is employed in the receiver circuit to collect the light sent from the transmitting LED. Total 8 number of LEDs (equal spacing) in parallel connection are used to produce optical link between transmitter to receiver. Photo-detector mount is used to measure the change in optical power of the received beam and digital thermometer is used to measure the temperature variation. A computer controlled feedback system is used to determine the performance of optical link in terms of BER as shown in Fig.6.5.1

6.5 Measurement of BER for Indoor Optical Link

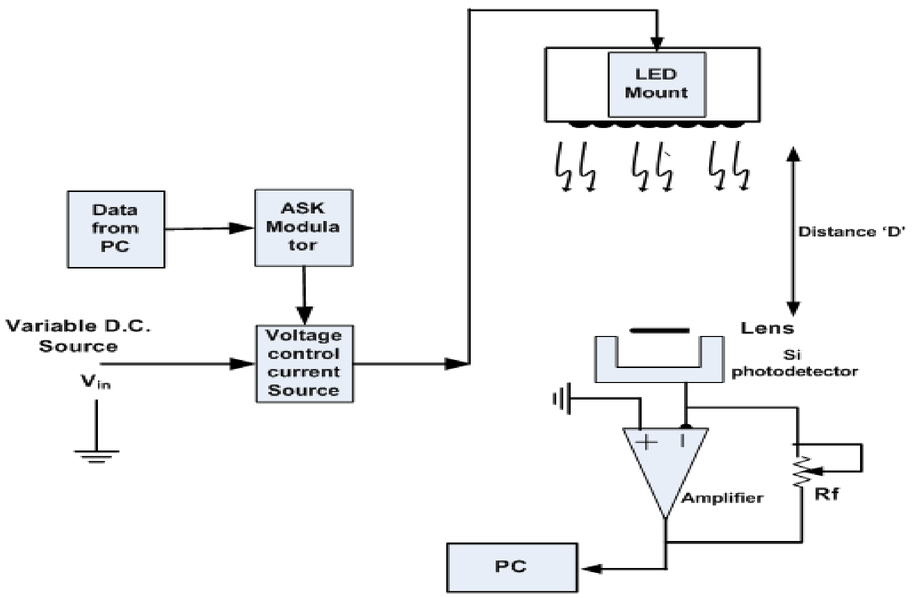

Fig. 6.5.1: Experimental arrangement for measurement of BER (Indoor optical link)

Color of LED optical beam - White, Number of LED= 08 (Parallel connection) Modulation –ASK, Carrier frequency for ASK modulation 5 KHz and 5V (p-p) sine wave. Room Temp=29 ^{0}C, Distance between Tx and Rx-4 meter; Lens Diameter at receiver = 10 cm;

Current Driver Circuit to drive multiple LEDs.

The design of current driver circuit is same as a laser driver circuit explained in Chapter 3 which is designed to provide enough biasing current that turns the LED diode ON and OFF according to the logical value of the data ('0' or '1'). It also allows desired modulation scheme to operate under worst atmospheric or room conditions. It is designed to drive single or multiple LEDs to handle different indoor channel conditions as shown in fig. 6.5.2.

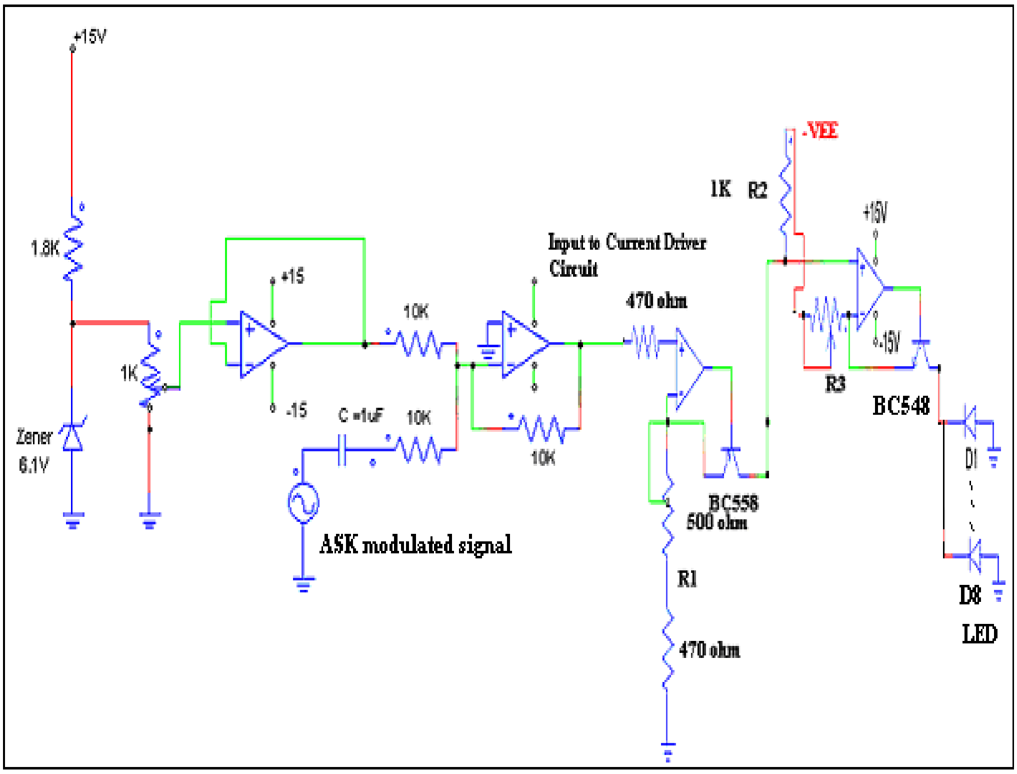

Fig. 6.5.2: Current driver circuit to drive multiple LEDs

Where, R1=470 Ω, R2=1 KΩ, R3= 100 Ω, At 600 bit rate we took reading for 10 seconds. The total count was 250 (for 10 sec) was displayed ; Total number of data points-250 in 10 second (10000 ms) therefore for one data 10000/250 = 40 ms i.e. T=25 Hz.

Following bytes are received (After XOR operation) input current is 10 mA for 8- number of LEDs connected in parallel.

Transmitted Byte is :- 00110001 i.e. 31 (ASCII code) and Received byte after traveling 4 meter is 1 1 1 1 1 0 1 1 , XOR operation of

1 1 1 1 1 0 1 1 $\otimes$ 0 0 1 1 0 0 0 1 = 1 1 0 0 1 0 1 0

As total number of 1's are 4 ; total number of error bit is 4. A Matlab program is developed to compare received bit with transmitted bit to calculate BER.

Received 250 bytes are given below

```
---------------------------------------------------------------------------
 1  1  0  0  1  0  1  0
 1  1  1  0  0  1  1  1
 1  1  1  0  0  1  1  1
 1  1  1  0  0  1  1  1
 1  1  1  0  0  1  1  1
 1  1  1  0  0  1  1  1
 1  1  1  0  0  1  1  1
 1  1  1  0  0  1  1  1
 1  1  1  0  0  1  1  1
 1  1  1  0  0  1  1  1
```

Total Number of bits transmitted 8*250= 2000; Total Number of bits received 8*250= 2000; Bits_in_error = total number of 1's in each received byte (After Ex-or operation). 1270 For 10 mA. Bit_error_rate = bit in error / total number of bits = 0.6350

For 20 mA :Bits_in error =272, Bit_error_rate = 0.1360, For 30 mA. Bits_in error =18. Measured data is given in table 6.1 and relation between LED current and BER shown in fig. 6.5.3.

Table 6.1: LED current vs BER

Input drive current (mA)	BER
8	1.2
8.5	1
8.8	0.9
9	0.8
9.5	0.7
10	0.6
12	0.5
14	0.4
16	0.3
18	0.2
20	0.1
30	0.0

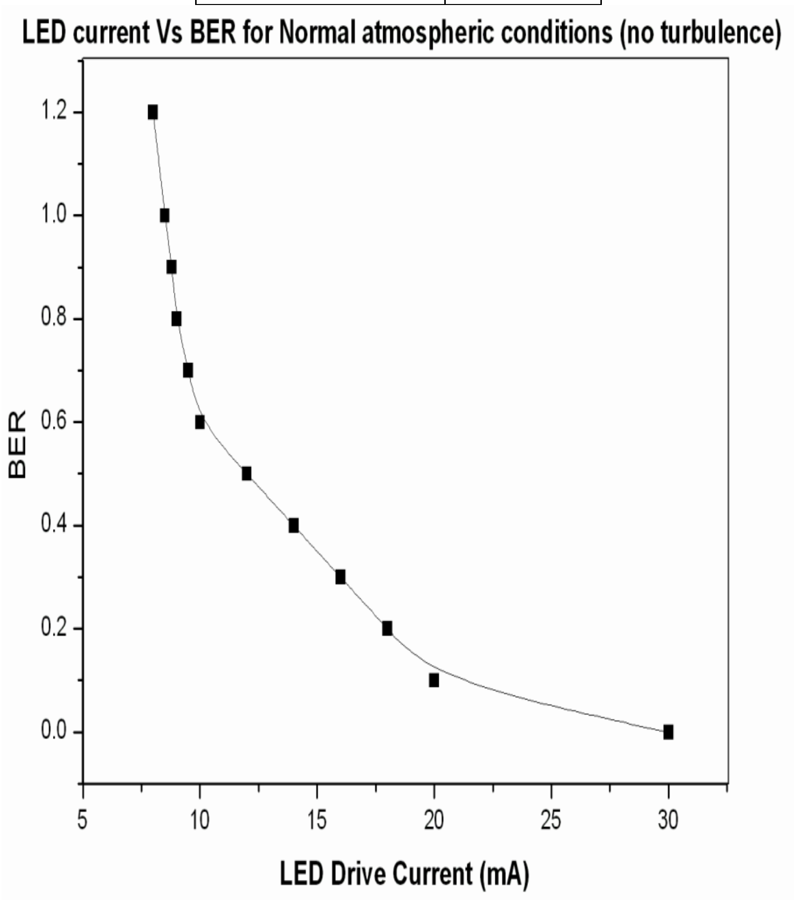

Fig.6.5.3 : LED current vs BER

6.6 Conclusion

In the present chapter we investigate the influence of normal atmospheric conditions on multipath indoor optical links using multiple source white light LED (total=8, parallel configuration) transmitter and single PIN diode photo-detector receiver circuit. In this system the transmitted digital data are divided into several optical channels and transmitted simultaneously. ASK digital modulation is use to modulate NRZ digital data by addition of D.C. biasing voltage. Experimental result shows that parallel transmission using multiple LEDs degrades the effect of ISI (Inter symbol interference) due to multipath propagation by providing constant SNR without decreasing the total data rate. Along with parallel configuration we provide D.C. biasing voltage which is use to maintain constant SNR for continuous illumination and communication purpose within the room.

References

[1] Pang B. Y. G., T. Kwan, H. Liu, and C. Chan, "A novel use of LEDs to transmit audio and digital signals," IEEE Ind. Appl. Mag., vol. 1, FEB 2002, pp. 21–28, 2002.

[2] Komine T., S. Member, and M. Nakagawa, "Fundamental Analysis for Visible-Light Communication System using LED Lights," IEEE Trans. Consum.Electron., vol. 50, no. 1, pp. 100–107, 2004.

[3] Fenq-linJenq., Tang-Jen, "An AC LED Smart Lighting System with Visible Light Time-Division Multiplexing Free Space Optical Communication," IEEE Comput.socity, vol. 7, no. 1, pp. 589–593, 2011.

[4] Rui W., D. Jing-yuan, S. An-cun, W. Yong-jie, and L. Yu-liang, "Indoor Optical Wireless Communication System Utilizing White LED Lights," Proc. Asia-Pacific Conf. Commun., vol. 4, pp. 617–621, 2009.

[5] Grubor J. , S. Randel, K. Langer, and J. W. Walewski, "Broadband Information Broadcasting Using LED-Based Interior Lighting," J. Light. Technol., vol. 26, no. 24, pp. 3883–3892, 2008.

[6] Borogovac T., M. Rahaim, and J. B. Carruthers, "Spotlighting for Visible Light Communications and Illumination," Tech Republlic, 2011.

[7] Pang G., T. Kwan, H. Liu, and C. Chan, "Optical Wireless based on High Brightness Visible LEDs," IEEE Ind. Appl. Society Conf., vol. 7, no. 1, 1999.

[8] "Energy-efficient Visible Light Communication", Engineering for Environmental Sustainability, http://engineering.tufts.edu, Accessed on May 2011.

[9] Elgala H., R. Mesleh, H. Haas, and B. Pricope, "OFDM Visible Light Wireless Communication Based on White LEDs," IEEE Int. Symp., vol. 1, pp. 2185–2189, 2007.

[10] Látal J., P. Koudelka, V. Vašinek, F. Dostál, and K. Sokanský, "Possible use of power LEDs for lighting and communication," Electr.Rev., no. 4, pp. 25–28, 2011.

[11] Wu Z., J. Chau, and T. Little, "Modeling and Designing of a New Indoor Free Space Visible Light Communication System," IEEE Int. Symp., no. 1, pp. 72–75, 2011.

[12] Yang Y., X. Chen, L. Zhu, B. Liu, and H. Chen, "Design of Indoor Wireless Communication System Using LEDs," proceeding of the SPIE-OSA-IEEE, vol. 7632, no. 1, pp. 1–8, 2009.

[13] Suzuki, Tomihiro. "High-Speed 1.3-um LED Transmitter Using GaAs Driver IC".Journal of Lightwave Technology, vol. lt-4, no.7,July 1986.

[14] Otte R., "Low-Power Wireless Optical Transmission," Delft University Press, Delft, Netherlands, 1998.

[15] Lee C. G. , C. S. Park, J. H. Kim, and D. H. Kim, "Experimental verification of optical wireless communication link using high-brightness illumination light-emitting diodes," Journal of Opt. Eng. Vol 46, 2007.

[16] Kahn J. M. and J. R. Barry, "Wireless infrared communications," IEEE Proc, vol. 85, no. 2, pp. 265–298, 1997.

CHAPTER 7

Simulation and Experimental Results, Analyses and Discussions

This dissertation describes the design and development of a laboratory standard set up for studying scintillation effects on a propagating optical beam in indoor and outdoor environments. Since the situations in the two cases (indoor and outdoor) are largely different, we made two separate approaches in measurement set ups to study the performance characteristics of free space communications in indoor and outdoor environments. For studies of the effects of atmospheric turbulence we have designed and developed a laboratory based horizontal multi-pass optical path with arrangements for studying effects of thermally induced weak and medium atmospheric turbulence on a propagating optical beam.

We designed a vertical path optical beam transmission for studying the characteristics of indoor wireless optical system. We designed and fabricated the necessary digital optical transmitter system for dc biasing and signal modulation to produce controlled intensity and wavelength of light from various semiconductor lasers for optical communication. We have used two photodiode receiver systems using silicon and InGaAs photodiodes for detection of light over the entire visible and NIR wavelength regions respectively.

For our detailed studies of atmospheric turbulence effects on free space optical signal, we designed and fabricated a free space multi-pass (5 pass) optical path cell in a horizontal plane over a thermally generated turbulent medium. We have used precision mirrors and lenses with adjustable mounts for transmission of narrow laser beam through the thermally induced atmospheric turbulent medium.

We have experimentally observed that in outdoor situations atmospheric scintillation effects can force to inhibit the operation of a FSO system depending on the strength of turbulence. From our theoretical investigations and simulations using

Matlab programs we perform different experiments in laboratory environment to understand how much we can be successful in mitigation of atmospheric turbulence through the aperture averaging effect at the receivers of FOS systems.

We designed and developed an elaborate arrangement of measurement and control set up for our studies of atmospheric turbulence. The complete turbulence system works under the command and control of a PC based hardware and software support indigenously developed for our application.

Simulation Result

The simulation results on the performance of FSO link at different wavelengths, starting from 780 nm to 1550 nm showed that the scintillation index for three different turbulent conditions (weak, moderate and strong) were found to be decreasing, when the wavelength of the optical beams were longer. For example, for weak turbulence, scintillation index values at 780 nm, 980 nm, 1310 nm and 1550 nm were observed as 7.1×10^{-4}, 4.9×10^{-4}, 3.2×10^{-4} and 2.9×10^{-4} respectively.

The simulation results obtained for receiver diversity using single source multiple aperture multiple detector scheme at 1550 nm wavelength partially coherent beam showed that the scintillation index was reduced from 0.18 to 0.14 for strong atmospheric turbulence condition.

The aperture averaging technique for mitigation of atmospheric turbulence was studied using partially coherent optical beam and simulated for 2 km long FSO link under weak, moderate and strong atmospheric turbulence conditions. The performance of the system (Section-5.6)was studied at 780–980-1310-1550 nm wavelengths by analyzing SNR for various aperture diameters varied from 0.08 m to 0.8 m for $C_n^2 = 10^{-12}$.

We observed that, if beam width and diameter of the receiver aperture were kept constant at 0.025 m(25 mm) and 0.08 m (8 cm)respectively for both coherent and partially coherent beams, at 1550 nm wavelength , scintillation index decreased from 0.110 to 0.0302, but for 780 nm it was increased from 0.10 to 0.18 in case of partially coherent beam. From these results we observe that longer wavelengths are less affected by atmospheric turbulence.

In another case, we kept beam width constant 0.025 m and changed aperture diameter gradually from 0.08 m to 0.8 m. We compared (Section -5.6) the aperture averaged scintillation index for both the beams using different wavelengths and found that for 1550 nm, scintillation index decreased from 0.15 to 0.03, and for 780 nm it increased from 0.22 to 0.35 in case of partially coherent beam. From these results it is observed that partially coherent beam with 1550nm wavelength produced more aperture averaging compared to 780 nm wavelength.

Experimental observations

To measure the effect of atmospheric turbulence on propagating optical field experimentally, we used a feedback stabilized laser diode biasing circuit as described in section 3.B .The (L-I) characteristics of 696.8 nm, 780 nm, 1310 nm and 1550 nm wavelength laser diodes at constant room temperature 28 ^{0}C were obtained to get threshold current I_{th} for biasing and intensity modulation of laser operating them in the stimulated emission region. For example, we found threshold current of 13.9 mA for the 780 nm multiple quantum well laser.

When a beam of light of wavelength 698 nm was propagating through the turbulent path of multiple folded optics system, it experienced random fluctuations due to change in refractive index. We found that, as temperature was increased from 25 ^{0}C to 35 ^{0}C, the optical beam spot position moved vertically up by ~ 4.2 cm from the center of the photo-detector plane. Since the photo-detector area was 1 mm x 1 mm , therefore, the beam spot was outside the sensitive region of photodiode and no signal output of photo-detector was obtained. This produced 100% BER. This observation shows that FSO communication system is critically affected by pointing error and beam wander problems. Thus, mitigation of beam wander is essential for satisfactory operation of a FSO system in outdoor environment.

The effect of refractive index variation on the optical beam was experimentally measured by using Rytov variance and based on those results it was revealed that, for optical path length L =27 m and room temperature = 25 ^{0}C, Rytov variance was found as 0.006 (section 4.4). From this value of Rytov variance, we obtained refractive index structure parameter using Matlab program, and found its value as $Cn^2 = 7.78 \times 10^{-14}$. Applying the same method, we also measured Rytov variance at room temp=35 ^{0}C, which was found as 0.04 and $Cn^2 = 5.18 \times 10^{-13}$, which is greater than that observed at 25 ^{0}C.From above observations we say that turbulence generated in our multipath flooded optic system is weak and follows lognormal distribution.

The effect of aperture averaging on intensity fluctuation was observed for 698.6 nm laser optical link with optical path length 25 m, and we found that when the receiver aperture diameter is 5 cm, the variation in output data samples transform more rapidly with increase in temperature. However, when aperture diameter is selected as 10cm, the averaging effect neutralizes the produced intensity fluctuation.

For example, when 200 samples of photo-detector voltage were collected for 3 minutes, the sample value varied from 1 V to 4 V but with aperture averaging it remains about 3 V. Aperture averaging also improves BER when aperture diameter changes from 5cm to 10cm BER changes from 0.032 to 0.018. For example, when 25,000 samples of digital data were collected for18 minutes, the sample value varied from $(00101001)_2$ changes to any arbitrary value, but with aperture averaging it remains stable at $(00101001)_2$, as describe in chapter 4.

We measured the performance of a 27m distance optical link using artificially generated multipath folded optic system in a controlled environment. At first, we found that when room temp was low i.e. 23^{0}C with constant bit rate of 11400 (b/s) and laser current as 14 mA, for transmission of 36000 bits, only 1518 bits were corrupted, and BER was measured as 0.0423. However, when room temp was increased up to 35 ^{0}C, and 36000(b/s) bits were transmitted, 11767 bits were corrupted, and BER was measured as 0.423. From this outcome, it is revealed that as strength of turbulence increases, BER also increases.

Based on the comparison between the effect of atmospheric turbulence measured for 16m and 27 m distance between transmitter and receiver, it is concluded that as the channel length increases from 16m to 27 m , intensity fluctuation increases from 0.015 to 0.8 (section 4.4) at constant room temperature 28^0C. However the variations in laser basing current (13 mA, 17 mA, 21 mA and 25 mA) shows that addition of laser current reduces intensity fluctuations and improves the link performance.

ASK modulator was designed and developed to know the effects of changes in carrier amplitude on the performance of optical link and we observed that, as the amplitude of carrier signal was decreased from 5 V to 1 V, the photo-detector voltage gradually decreased and hence BER increased.

The 27 m laser optical link was tested under the influence of external optical noise and it was found that the BER increases with the increase in strength of the optical noise. For example, for 225W electrical light bulb (ambient noise) the BER increases from 0.03 to 0.05. Thus the quality of optical link deteriorates as the external optical noise interferes or mix at the photo-detector input .

We measured the absorption coefficient of two glass slab attenuators and obtained the performance of optical link in terms of BER. It was found that, as absorption coefficient was increased from 4.87 to 5.35, BER increased from 10% to 15%. For same conditions, it was also revealed that if gain of an optical antenna was increased, the BER reduced to minimum level i.e. BER=0.

Finally, we investigate the influence of normal atmospheric conditions on multipath indoor optical links using multiple white light LED (total=8, parallel configuration) transmitter source and single PIN diode photo-detector receiver circuit. In this system the transmitted digital data are divided into several optical channels and transmitted simultaneously. ASK digital modulation is use to modulate digital data by using D.C. biasing circuit. Experimental result shows that parallel transmission using multiple LEDs degrades the effect of ISI (Inter symbol interference) due to multipath propagation without decrease the total data rate. Along with parallel configuration we provide D.C. biasing voltage which is use to maintain constant SNR for continuous illumination and communication purpose within the room.

Chapter 8
Conclusion

We began our studies and research with the notion to understand the underlying problems and difficulties in implementing the concept of optical wireless technologies for communications in indoor and outdoor environments. We were able to identify some of the major problems and then we tried for their possible solutions for mitigations. We present our findings in the following sections. The successes made in stage wise developments are also presented below.

The performance of outdoor optical wireless communication system was tested in laboratory environment while for studying scintillation effects on a free-space optical link; we arranged a separate multipath optical beam and studied its characteristic behavior under atmospheric turbulence. Numbers of experiments were performed to understand the effects of atmospheric parameters on the propagation of optical beams and their deleterious effects on the quality of an information transmission signal and system.

Elaborate arrangements were made for experimental studies of the temperature induced atmospheric scintillation on the BER performance of modulated coherent, as well as partially-coherent optical beams from semiconductor injection lasers. We also used LEDs as incoherent source and studied its performance in a turbulent medium. These arrangements were made to get precision results under most suitable conditions for studies of temperature induced scintillation effects. The experimental arrangement also included several mitigation techniques to study the improvement in the quality of performance of optical information transmission systems. Among them, the optical aperture averaging technique was studied in detail both experimentally and through simulation. Both coherent and partially-coherent optical beams were used in these studies to make comparison of their performances. In addition, sources of different wavelengths were used to see how improvement in performance could be obtained by choosing appropriate wavelength for a specific work.

An experimental arrangement for studies of beam divergence was made using single laser source as transmitter and multiple photo-detectors as space diversity receivers. In order to study the optical beam wander under varying atmospheric temperature conditions, separate arrangements were made using single optical source and imaging detector (CCD device) over varying optical path lengths in the laboratory environment. The complete optical set up and its operations were controlled by specially designed dedicated electronic circuits and a computerized automated measurement system.

In our separate indoor optical wireless system design, we have experimented with various off-the shelf LEDs including a high power (10 watt) visible light LED. We studied their electro-optical and spectral characteristics and their frequency response. Using the high-power white light LED and a PIN photodiodes we designed a communication link for digital image transmission over a short distance (~1m).

In all our studies, experiments and simulations as stated above we achieved the following results with improvements in the performances of optical wireless communication systems.

1. Our design of a computerized test-bed for studies of performance of optical wireless communication system is a unique versatile stand-alone unit. The system could be configured to perform variations in studies for optical beam parameters through software and hardware control functions. Arrangements for variations of optical path lengths, optical beam wavelength, beam diameter and optical output power, as well as varying the modulation index of a modulated optical beam can be done by computer control mechanisms. The transmitter optical input data-bits and the corresponding optical receiver output data-bits are directly available at the computer screen for visualization of BER performance improvements/ deterioration when the optical beam suffers from atmospheric scintillation effects. Arrangements for introducing

controlled amount of atmospheric turbulence helped us to make precision studies on the cause of intensity fluctuations, beam wander or beam divergence. The automated system can itself generate an error signal depending on the number of bits in error and accordingly act to mitigate the effect of turbulence using a feedback signal for transmitter intensity control as described in detail in chapter-III (section 3.8). The experimental results obtained under different temperature conditions and for different optical path lengths were analyzed using the theory of Rytov variance given in schapter II. The measured values of Rytov variance were found to be close within 5% of the calculated as well as simulated values as given in chapter-IV and V

2. The studies on the aperture averaging effects for the mitigation of the optical turbulence were one most important aspect of our work in this thesis. Theoretical, experimental and simulation studies were made on aperture averaging effects with the vision of getting improved performance under worst atmospheric turbulence.

   Experimentally we observed that a significant improvement in BER performance can be obtained by using aperture of increasing diameters. In our experiments, we got minimum BER using an aperture of 10 cm diameter. As an example, we observed from our measurement results that the BER changes from 0.032 to 0.018 when the aperture diameter increased from 5cm to 10cm (Chapter 4). Further increase in aperture diameter did not produce any better results due to the fact that unwanted ambient external optical signal increased the noise and as a result the S/N ratio decreased.

3. In our simulation studies for aperture averaging effects using the theory of Andrew & Philips as presented in Chapter-II , we verified that under strong turbulence conditions ($C_n^2 = 10^{-12}$) for a coherent optical beam at 1550 nm wavelength with constant optical beam width, the aperture averaging factor (A) decreased from 0.15 to 0.13 when the aperture diameter was increased from 8 cm to 80 cm. But for a similar situation with partially coherent optical beam, the aperture averaging factor A, decreased from 0.14 to 0.03. Thus it

proved that compared to a coherent optical beam at 1550 nm wavelength, a partially coherent optical beam at the same wavelength can give better aperture averaging effects with improved BER performance. We also carried out simulation studies on aperture averaging effects of coherent as well as partially-coherent optical beams of wavelength 780 nm. Here we found different results on aperture averaging effects. The results showed that at 80 cm diameter, the coherent beam was giving better results compared to the partially-coherent beam in the sense that the value of A was 0.23 for the coherent beam and 0.35 for the partially coherent beam.

Similar simulation using matlab programming was performed for weak turbulence conditions ($C_n^2 = 10^{-16}$) for both coherent and partially coherent beams for 780nm and 1550nm wavelengths. The results shows that in weak turbulence conditions (section 5.6), aperture averaging effects only improve the performance by small amount.

In our experimental set up we have arrangement for fixing different optical path lengths to study the effects of atmospheric turbulence under varying distances from source to detector. We have also arrangements for studies for varying the horizontal optical plane as well as measuring the optical losses in vertical direction. In one such experiment, we measured scintillation parameters at 16m and again at 27 m under identical atmospheric and other conditions. The experimental results showed that the value of scintillation index (σ_I^2) was more at 27 m than at 16m as because refractive index structure parameter remaining the same, a longer optical path was affected more than a smaller path. We verified in the system that by automatic negative feedback arrangement we can adjust the transmitter optical power to maintain a constant receiver output power so as to keep the BER at a constant value as explained in chapter-IV (section-4.4.).

4. The another most important aspect of our work in this thesis is the study of influence of room conditions on multipath indoor optical links using multiple source white light LED (total=8, parallel configuration) transmitter and single

PIN diode photo-detector receiver circuit. Experimental result shows that the effect of ISI (Inter symbol interference) due to multipath propagation is minimise by providing constant SNR without decreasing the total data rate as shown in chapter 6 (section-6.4). Along with parallel configuration we provide D.C. biasing voltage which is use to maintain constant SNR for continuous illumination and communication purpose within the room.

Finally, with our system set up we have extensively measured the atmospheric turbulence effects on different optical beam geometry. We measured the Rytov variance and studied its significance in detail to reveal how an optical wireless communication system should be designed with arrangements for mitigation of the atmospheric turbulence effects. In order to study the physics of optical beam wander and beam divergence in more detail, we have used our controlled turbulence set up to measure these parameters using appropriate detectors and verified that by increasing transmitter optical power these effects are minimize. Interesting results were observed which needed further studies for explanation. We mention here this as one of our future work for theoretical and detailed experimental studies. Such studies would be relevant to designing optical quantum communication systems for the next generation high speed (Terabit) data transmission. As mentioned in Chapter-I, the test set up we have designed would be useful for designing short distance wireless optical links for body area network or underwater optical wireless system design.

APPENDIX A1

Comparative Results of simulation and experiments

Comparison of Simulation Results with Experimental Results

<table>
<tr><th>Parameters</th><th>Simulation</th><th>Experimental</th></tr>
<tr><td>Rytov Variance</td><td>
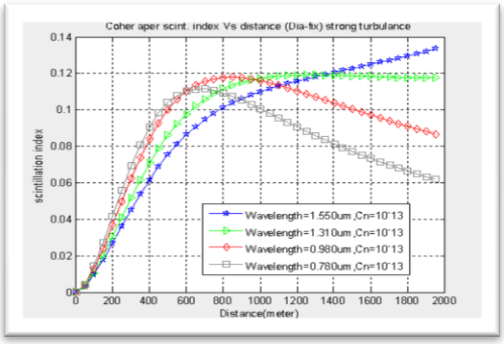

</td><td>for optical path length L =25 m and room temperatur = 25 ^{0}C,wavelength λ =698nm
Rytov variance = 0.006.
Cn = 7.78 × 10^{-14}.

At room temp = 35^{0}C,
Rytov variance =0.04
and Cn = 5.18 × 10^{-13}, which is greater than that of observed at 25^{0}C.</td></tr>
<tr><td>Aperture Averaging effect</td><td>
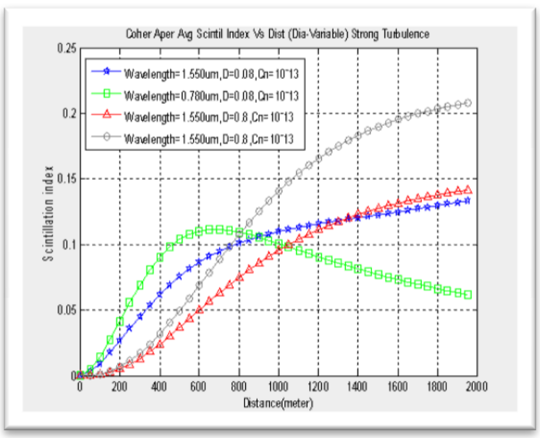

Lens diameter change from 0.08m to 0.8m.

For 27 meter distance
Rytov variance theoretically (simulation) =0.4438
Refractive Index structure parameter (using rytov variance) = $5.4*10^{-12}$</td><td>For 27 m distance
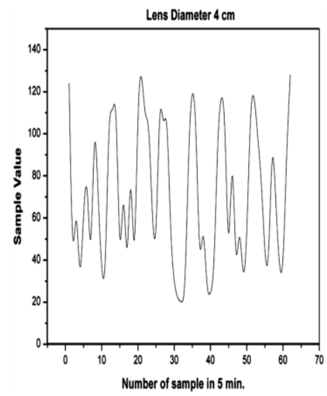

Rytov variance (practical) = 0.4549
Refractive Index structure parameter (using rytov variance) = $5.1*10^{-12}$
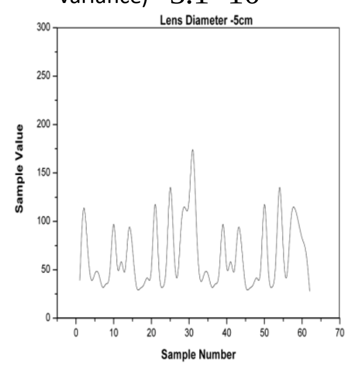

Rytov variance (practical) = 0.04</td></tr>
</table>

<table>
<tr>
<td>Turbulence Effect with distance</td>
<td>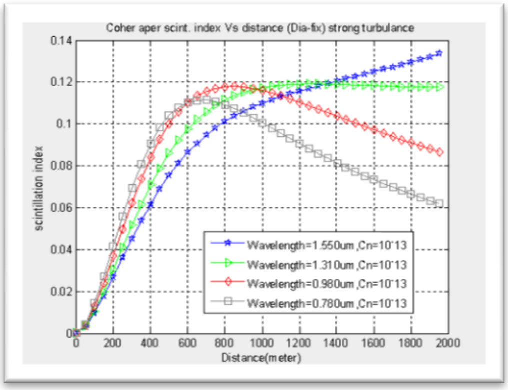
</td>
<td>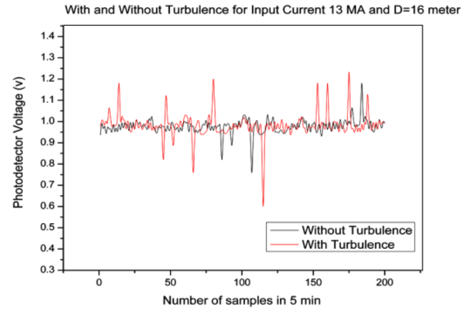

(Black curve)optical path Length L=16m, Cn = 7.18×10^{-14}, Rytov variance =0.0055
(Red Curve)optical path length L= 16m,Cn = 1.94×10^{-13}, Rytov variance=0.015
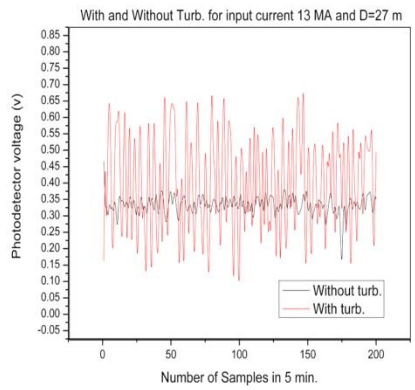

For Path length L =25 and Temp = 25 ^{0}C
Rytov variance is 0.006
Cn = 7.78×10^{-14}
For temp=35^{0}C and L = 25
Rytov variance=0.04,
Cn = 5.18×10^{-13}</td>
</tr>
<tr>
<td>Beam spot position</td>
<td>For 1 km distance, wavelength=1550nm
Beam position is shifted from 1 cm to 7 cm with Rytov variance =1.99.
And $C_n^2=10^{-13}$.</td>
<td>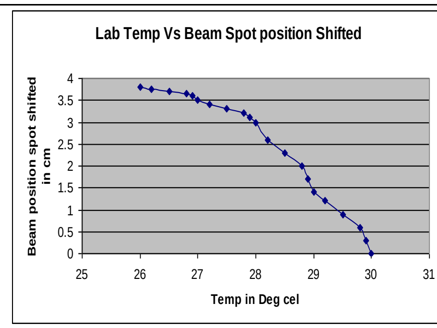

For 27 meter distance for 698nm wavelength beam spot position shifted by 4 cm</td>
</tr>
</table>

<table>
<tr>
<td>Bit error rate
(improvement due to aperture averaging)</td>
<td>
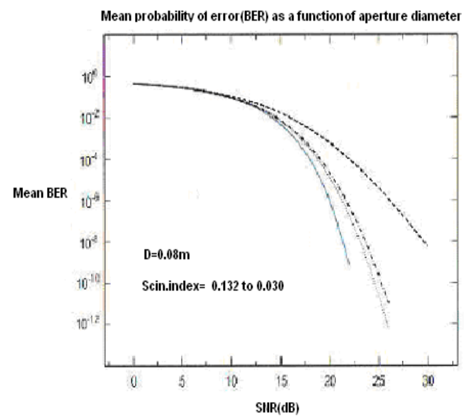

</td>
<td>
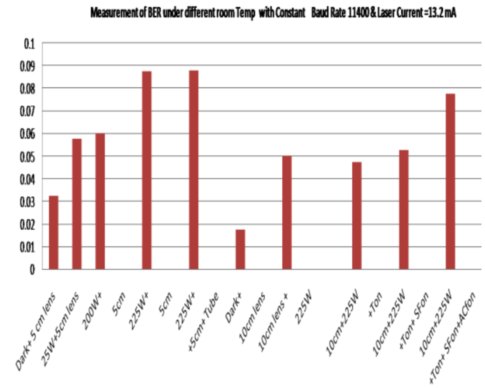

From above graph bit error rate for 5cm diameter lens diameter=0.033
For 10 cm diameter lens =0.015
</td>
</tr>
<tr>
<td>Signal to Noise Ratio (External Noise Interfance)</td>
<td>
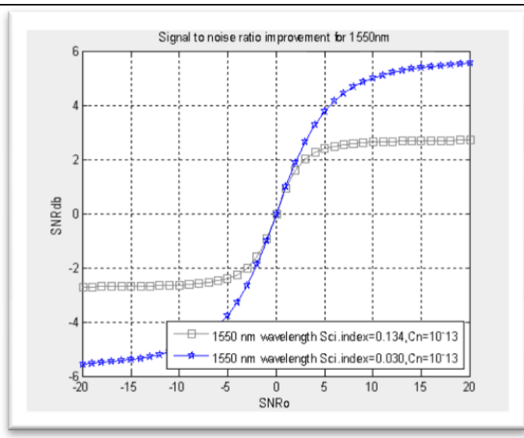

Improvement in Signal to noise ratio due to aperture averaging
</td>
<td>
Power measurement Using Carl-Zeiss (LM1) Power meter.
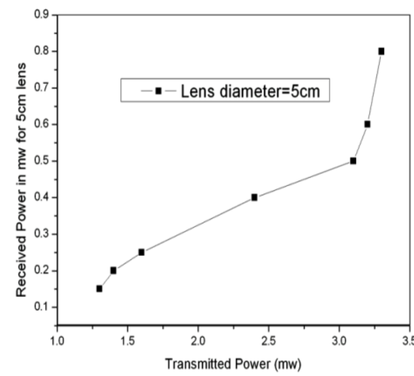

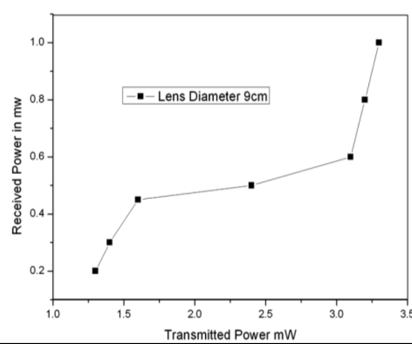

</td>
</tr>
</table>

APPENDIX A2
Measurement Results of Laser Beam Attenuation by Optical Glass Slab

Measurement of Optical attenuation Using Closed Loop Computer Controlled Measurement System.

The atmospheric channel attenuates the optical filed as it navigates through atmosphere. It is an effect of absorption and scattering process. The concentrations of matter like smoke or gases in the atmosphere vary spatially and temporally and depend on the current local weather conditions. Here we simulate these conditions in our optical laboratory and analysis how these conditions affect the quality of optical signal in term of BER.

We start with No turbulence and Sturdy wind flow condition with room temp. 25^0C constant. The experimental arrangement is shown below.

Color of Laser optical beam – Red, $\lambda = 696.8nm$

Input D.C. Voltage: - 0 to 5V

Distance between Tx and power meter is 7inch.We measure I_t (transmitted beam power) and I_0(incident beam power) by standard power meter.

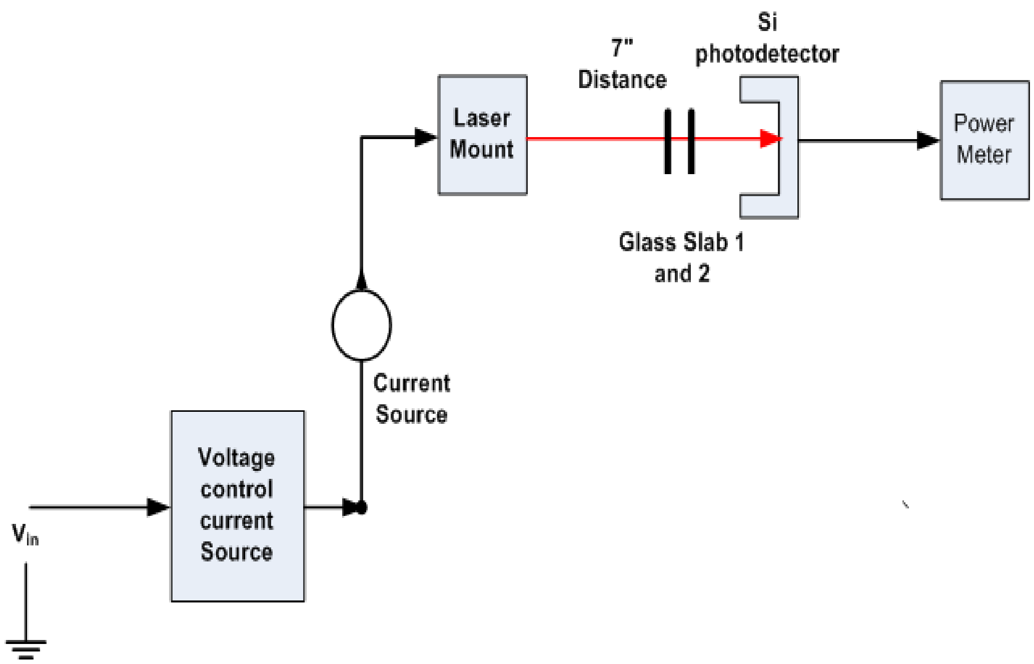

Experimental Arrangement for calibration of optical attenuator and optical transmitter-receiver system

Observations

Table 6.7 Measurement of I_0 and I_t

Sr. No	Laser Current (mA)	Att-1 I_0 (mW)	Att-1 I_t (mW)	Att-2 I_0 (mW)	Att-2 I_t (mW)	Both I_0 (mW)	Both I_t (mW)	$T = \frac{I_T}{I_0}$
1	7.0	0.5	0.3	0.5	0.3	0.5	0.2	0.4
2	8.5	0.7	0.4	0.7	0.5	0.7	0.35	0.5
3	9.4	0.8	0.6	0.8	0.6	0.8	0.4	0.5
4	10.2	1.1	0.7	1.1	0.7	1.1	0.5	0.45
5	10.5	1.3	0.8	1.3	0.9	1.3	0.6	0.46
6	10.8	1.4	0.9	1.4	0.95	1.4	0.65	0.464
7	11	1.6	1.0	1.5	1.1	1.5	0.7	0.466
8	11.2	1.8	1.3	1.8	1.3	1.8	0.8	0.444
9	11.4	2.1	1.5	2.0	1.6	2.1	1.0	0.476
10	11.6	2.4	1.7	2.3	1.75	2.3	1.1	0.478
11	11.8	2.6	2.1	2.6	2.2	2.6	1.3	0.5
12	11.9	2.7	2.2	2.7	2.3	2.7	1.3	0.56
13	12.6	2.8	2.3	2.8	2.4	2.8	1.4	0.5
14	12.7	2.9	2.4	2.9	2.7	2.9	1.5	0.6
15	12.8	3.0	2.8	3.0	2.7	3.0	1.5	0.7
	Average	2.01	1.54	2.01	1.61	2.0	0.97	0.477

Attenuator

The another important purpose of attenuator is that for 27m distance ,when the maximum current is injected into photo-detector , the output of photo-detector is saturated. Now if we use glass slab the laser power will be reduce and current may decreases. In other words beam will travel more distance (>27m) for same input condition and we will see How the turbulence affect the quality of optical signal. We use glass slab Attenuator having 100×60×18 mm size (1.8 cmwidth)

Using Beer's Lambert law

We have,

% Transmittance for First Glass Slab

$$T = \left(\frac{I_t}{I_0}\right) \times 100\%$$

$$\therefore T = \left(\frac{1.54}{2.01}\right) \times 100\%$$

$$\therefore T = 0.766 \times 100\%$$

Now

$$\text{Absorption}\left(A\right) = \ln\frac{1}{T}$$

$$A = \ln\frac{1}{0.00766} = 4.87$$

% Transmittance for Second Glass Slab

$$T = \left(\frac{I_t}{I_0}\right) \times 100\%$$

$$\therefore T = \left(\frac{1.61}{2.01}\right) \times 100\%$$

$$\therefore T = 0.800 \times 100\%$$

Now,

$$\text{Absorption}\left(A\right) = \ln\frac{1}{T}$$

$$A = \ln\frac{1}{0.00800} = 4.82$$

Total % Transmittance for Both Glass Slab

$$T = \left(\frac{I_t}{I_0}\right) \times 100\%$$

$$\therefore T = \left(\frac{0.97}{2.01}\right) \times 100\%$$

$$\therefore T = 0.482 \times 100\%$$

Now

$$\text{Absorption}(A) = \ln\frac{1}{T}$$
$$A = \ln\frac{1}{0.00482} = 5.33$$

BER measurement without attenuator

A closed loop multipath optical communication link setup is used to measure BER without attenuator. Here a serial data bits having baud rate 600/s send to laser biasing circuit with ASL modulation at transmitter side and simultaneously detected by photodiode at receiver.

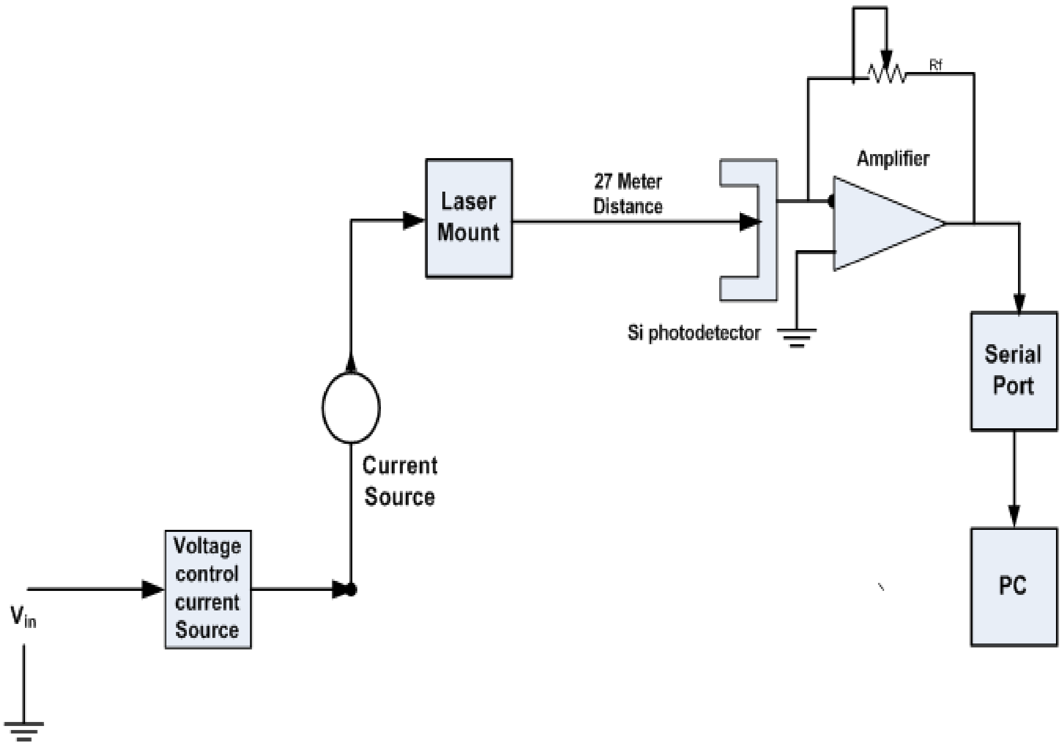

Experimental Arrangement for Measurement of BER without Attenuator

Table 6.8Measurement of BER Without Attenuator

Sr. No.	Input D.C. Voltage (Vdc 0-6v)	Input Current to Laser (mA.)	Output Voltage at phodetector (Vout)	Bit Error Rate $= \frac{Number-of-bits-in-error}{Total-number-of-bits}$
1	2.22	11.8	0.60	100%
2	2.23	11.9	0.61	50%
3	2.26	12	0.68	30%
4	2.29	12.2	0.73	5%
5	2.30	12.3	0.76	3%
6	2.33	12.4	0.78	1%
7	2.34	12.5	0.80	0%

BER measurement with Single attenuator

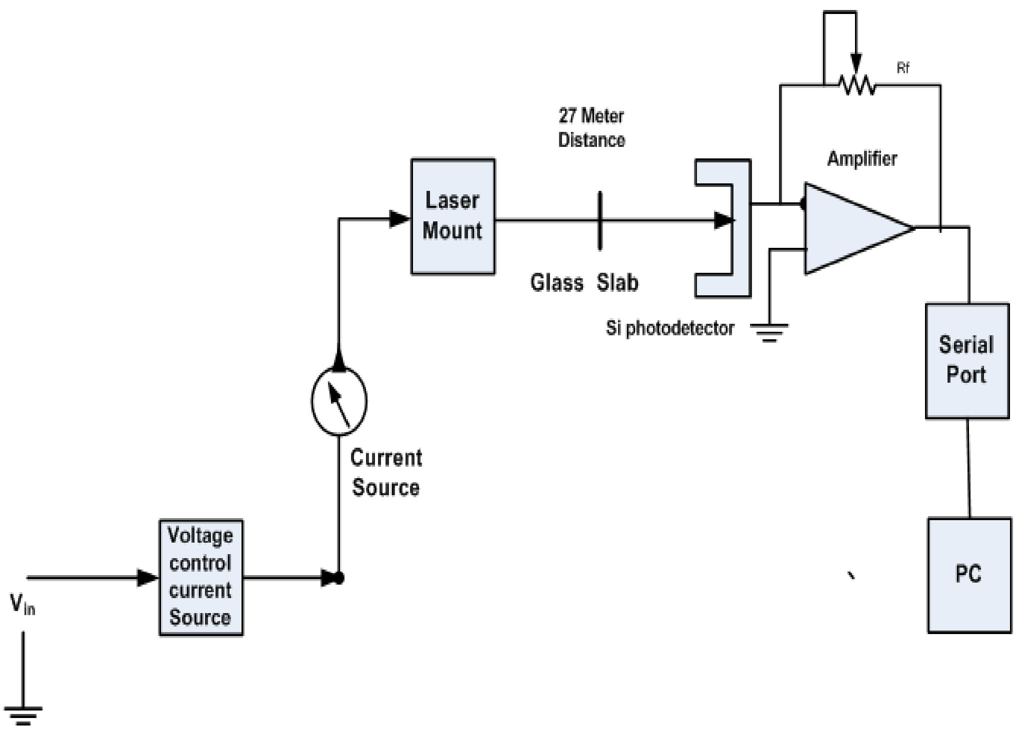

Experiment **Arrangement for measurement of BER with single Attenuator**

Observation for With Single Attenuator

Table 6.9 Measurement of BER with Single Attenuator

Sr. No.	Input D.C. Voltage (Vdc 0-6v)	Input Current to Laser (mA.)	Output Voltage at phodetector (Vout)	Bit Error Rate	Sr. No.	Input D.C. Voltage (Vdc 0-6v)	Input Current to Laser (mA.)	Output Voltage at phodetector (Vout)	Bit Error Rate
1	2.22	11.8	0.60	75%	12	2.54	13.5	0.87	0
2	2.23	11.9	0.61	60%	13	2.56	13.6	0.88	0
3	2.26	12	0.68	20%	14	2.57	13.7	0.89	0
4	2.28	12.1	0.73	5%	15	2.60	13.8	0.90	0
5	2.29	12.2	0.76	2%	16	2.61	13.9	1.00	0
6	2.33	12.4	0.78	0%	17	2.62	14	1.2	0
7	2.34	12.5	0.80	0	18	2.64	14.1	1.4	0
8	2.38	12.7	0.81	0	19	2.66	14.4	1.5	0
9	2.42	12.9	0.83	0	20	2.68	14.5	1.55	0
10	2.45	13.0	0.84	0	21	2.22	11.8	1.65	0
11	2.50	13.3	0.86	0	22	2.23	11.9	1.99	0

BER measurement with Double attenuator

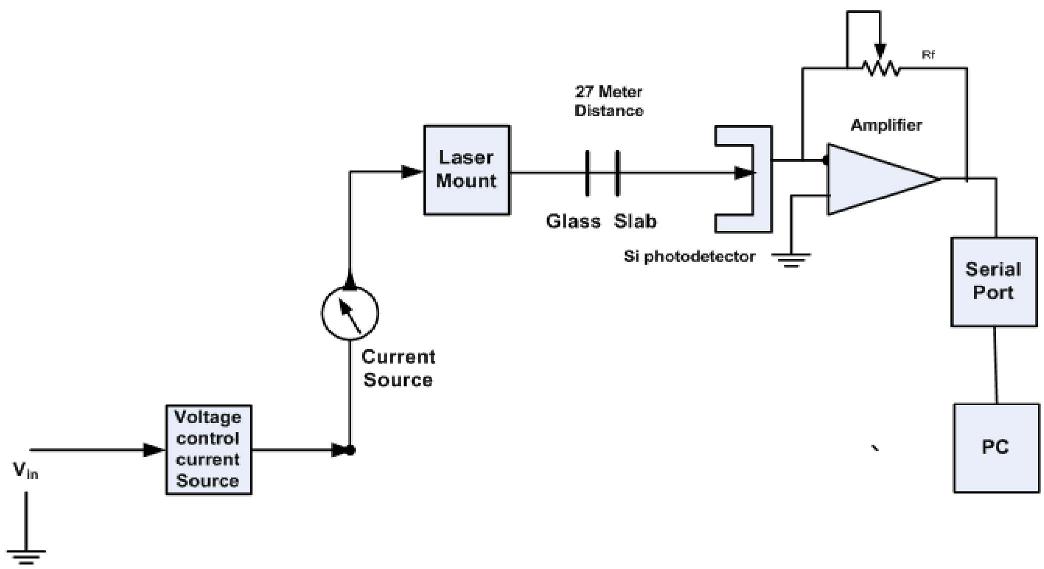

BER Measurement with Double Attenuator

Observations with Double Attenuator: 5 cm diameter lens, room temp 27 deg. cel.

Measurement of BER with Double Attenuator

Sr. No.	Input D.C. Voltage (Vdc 0-6v)	Input Current to Laser (mA.)	Output Voltage at phodetector (Vout)	Bit Error Rate	Sr. No.	Input D.C. Voltage (Vdc 0-6v)	Input Current to Laser (mA.)	Output Voltage at phodetector (Vout)	Bit Error Rate
1	2.22	11.8	0.3	100%	12	2.54	13.5	0.65	50%
2	2.23	11.9	0.3	100%	13	2.56	13.6	0.68	40%
3	2.26	12	0.31	100%	14	2.57	13.7	0.69	30%
4	2.28	12.1	0.33	100%	15	2.60	13.8	0.72	20%
5	2.29	12.2	0.34	100%	16	2.61	13.9	0.72	10%
6	2.33	12.4	0.38	95%	17	2.62	14	0.76	5 %
7	2.34	12.5	0.41	92%	18	2.64	14.1	0.77	4%
8	2.38	12.7	0.45	90%	19	2.66	14.4	0.85	3%
9	2.42	12.9	0.50	90%	20	2.68	14.5	0.90	1%
10	2.45	13.0	0.52	80%	21	2.70	14.7	0.92	0%
11	2.50	13.3	0.59	60%					

BER Analysis

$$\textbf{Bit Error Rate} = \frac{\text{Number} - \text{of} - \text{bits} - \text{in} - \text{error}}{\text{Total} - \text{number} - \text{of} - \text{bits}}$$

We send 2000 bits through serial port of computer system for 10 sec. and modulate these bits by optical carrier using ASK modulator and allow to pass through two attenuators 1 and 2 respectively. When two attenuators are placed, out of 2000 bits 740 bits are corrupted. Therefore BER for two attenuators is 0.3 (30%) which is more than single attenuator and without attenuator.

Attenuator	Absorption Coefficient 'A'	Minimum Photo-Detector voltage for BER=0%
With one Glass Slab	4.87	0.78V
With two Glass Slab	5.35	0.92V

Effect of Aperture averaging on BER with double Attenuator

In above experiment with double attenuator, we assume 5 cm diameter lens as receiver aperture.Now, for identical conditions we use 10cm diameter lens as receiver aperture,

Receiver Aperture	Laser Current (mA)	Photo-detector Voltage (v)	BER in %
5cm Diamter	12.1	0.7	5 %
10 cm Diameter	12.1	1.1	0%

Analysis of effective area of a lens. (D_r=9 cm)

$$A = \frac{\pi \times d^2}{4}; = \frac{\pi \times 81}{4} = \frac{3.14 \times 81}{4} = 63.5\text{cm}^2$$

Optical Beam Diameter measured at the receiver aperture is $D_R = 5$ cm

Hence,

$$A = \frac{\pi \times (5)^2}{4}; = \frac{\pi \times 25}{4} = 19.6\text{cm}^2$$

As effective area is large compare to smaller lens diameter (D_L =5cm) , a few numbers of photon loss and required more current (12.1 mA) to make BER=0. But for identical condition, if the diameter of a lens is increases to 10 cm the required current reduces to 11mA. Thus if effective lens area is increases more and more photons will collect and S/N ratio increase which will definitely affect BER.

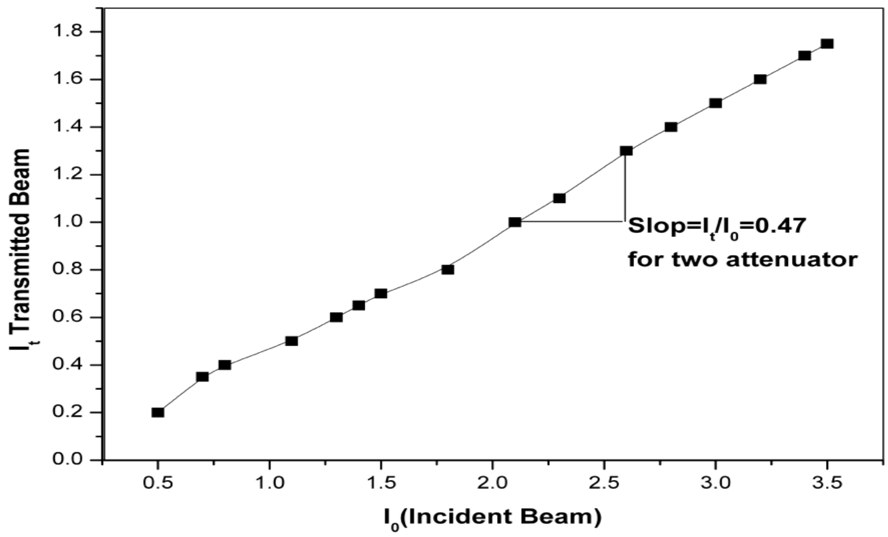

Relation between I0(Incident Beam)and It(Transmitted Beam)

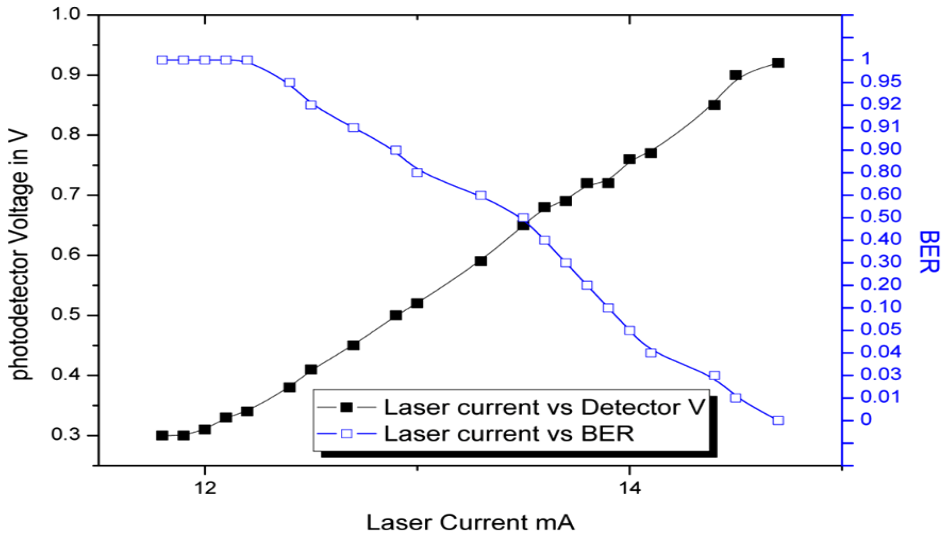

Relation between Laser Current (mA), Photo-detector Voltage(V) and BER(%)

Above curves clearly shows that when laser current is maximum BER will be zero, but when it is less than some threshold value say 10 mA, BER will increases. In atmosphere also if attenuation due to absorption or scattering is occurs then by increasing laser current by small fraction BER will be improve and link performance will be increases.

APPENDIX A3

Mat-lab simulation model and software program for microcontroller

MICRO CONTROLLER PROGRAM

```
SP          EQU     081H
IE          EQU     0A8H
ACC         EQU     0E0H
B           EQU     0F0H
DPL         EQU     082H
DPH         EQU     083H
TMOD        EQU     089H
TCON        EQU     088H
SCON        EQU     098H
TI          BIT     SCON.1
RI          BIT     SCON.0
PCON        EQU     087H
TR1         EQU     TCON.6
SBUF        EQU      099H
TH1         EQU      08DH
TL1         EQU      08BH
P2      EQU     0a0h
P3      EQU          0B0H
P0      EQU          080h

RS          EQU    P3.2
E           EQU    P3.3

FLAGE             EQU      020H
FLAGE0             EQU     FLAGE.0
FLAGE1                     EQU      FLAGE.1
FLAGE2             EQU     FLAGE.2
FLAGE3            EQU      FLAGE.3
FLAGE4             EQU     FLAGE.4
FLAGE_LEVEL        EQU     FLAGE.5
FLAGE_COUNT        EQU     FLAGE.6
FLAGE_VAB          EQU     FLAGE.7

FLAGE_1            EQU    021H
FLAGE_COUNT_READ BIT    FLAGE_1.0


RSELC    EQU    070H
TEMP    EQU    071H
TEMP1    EQU    072H
TEMP2    EQU    073H
COUNTER  EQU    074H


ORG     0000H
LJMP    0060H

ORG     0003H
RETI
```

```
ORG     000BH
RETI

ORG     0013H
RETI
ORG     001BH
RETI
ORG     0023H
LJMP SERIAL
ORG     0060H
 MAINLINE:

                MOV SP,#040H
                CLR TR1
                MOV TH1,#0FAH
                MOV TL1,#0FAH
                ANL TMOD,#0FH
                ORL TMOD,#020H
                SETB TR1
                MOV SCON,#050H
                MOV PCON,#080H
                MOV FLAGE,#00H
                MOV IE,#090H
                SETB  TI
                CLR RI
MAN:


                JNB FLAGE0,SKEEP0 ;      ADC0
                 ACALL READ_ADC0
                 ACALL READ_ADC0
                 ACALL READ_ADC0
                 ACALL READ_ADC0
                 ACALL READ_ADC0
                 ACALL READ_ADC0
                 ACALL READ_ADC0
                 ACALL READ_ADC0
                 MOV SBUF,A
SKEEP0:

                 JNB FLAGE1,SKEEP1 ;     ADC1
                  ACALL READ_ADC1
                  ACALL READ_ADC1
                  ACALL READ_ADC1
                  ACALL READ_ADC1
                  ACALL READ_ADC1
                  ACALL READ_ADC1
                  ACALL READ_ADC1
                  ACALL READ_ADC1
                  MOV SBUF,A

                  SJMP SKEEP0
```

```
SKEEP1:
        JNB FLAGE2,SKEEP2
        ACALL READ_ADC2
        ACALL READ_ADC2
        ACALL READ_ADC2
        ACALL READ_ADC2
        ACALL READ_ADC2
        ACALL READ_ADC2
        ACALL READ_ADC2
        ACALL READ_ADC2
        MOV SBUF,A
        SJMP SKEEP1
SKEEP2:
        JNB FLAGE3,SKEEP3
        ACALL READ_ADC3
        ACALL READ_ADC3
        ACALL READ_ADC3
        ACALL READ_ADC3
        ACALL READ_ADC3
        ACALL READ_ADC3
        ACALL READ_ADC3
        ACALL READ_ADC3
        MOV SBUF,A
        SJMP SKEEP2
SKEEP3:
        JNB FLAGE4,SKEEP4
        MOV SBUF,P0
        ACALL  DELAY
        ACALL  DELAY
        ACALL  DELAY
        ACALL  DELAY
        ACALL  DELAY
        ACALL  DELAY
        ACALL  DELAY
        ACALL  DELAY
        ACALL  DELAY
        ACALL  DELAY
        ACALL  DELAY
        SJMP  SKEEP3
SKEEP4:
        JNB FLAGE_LEVEL,SKEEP5
        MOV A,P1
        MOV SBUF,A
        ACALL  DELAY
        ACALL  DELAY
        ACALL  DELAY
        ACALL  DELAY
        ACALL  DELAY
        ACALL  DELAY
        ACALL  DELAY
        ACALL  DELAY
```

```
                ACALL  DELAY
                ACALL  DELAY
                ACALL  DELAY

                SJMP  SKEEP4
SKEEP5:
                JNB FLAGE_COUNT,SKEEP6
                MOV COUNTER, #00H
                SETB P3.4
        Y1:     JB P3.4, Y2
        Y2:
                JNB FLAGE_COUNT,SKEEP6
                JB P3.4,Y1
        Y3:
                JNB P3.4,Y4
        Y4:
                JNB FLAGE_COUNT, SKEEP6
                JNB P3.4,Y3
                INC COUNTER
                MOV SBUF,COUNTER
                SJMP Y1
KEEP6:
                JNB FLAGE_COUNT_READ, SKEEP7
                MOV SBUF, COUNTER
                LCALL DELAY
                CLR FLAGE_COUNT_READ
                LJMP MAN
 SKEEP7:                LJMP MAN

TRANS:  CLR TI
        RETI

SERIAL:
        JB TI,TRANS
        MOV R5,SBUF
        CLR RI

        CJNE R5,#'A',L1   ; CH1
        LJMP S1
L1:     CJNE R5,#'B',L2   ; CH1
        LJMP S2
L2:     CJNE R5,#'C',L3   ;
        LJMP S3
L3:     CJNE R5,#'D',L4   ;
        LJMP S4
L4:     CJNE R5,#'E',L5   ;
        LJMP S5
L5:     CJNE R5,#'F',L6   ;
        LJMP S6
L6:     CJNE R5,#'G',L7 ; REL2 ON
        LJMP S7
L7:     CJNE R5,#'H',L8 ; REL2 OFF
        LJMP S8
```

```
L8:     CJNE R5,#'K',L9 ; REL3 ON
        LJMP S9
L9:     CJNE R5,#'J',L10 ; REL3 OFF
        LJMP S10
L10:    CJNE R5,#'L',L11 ; LEVLE
        LJMP S11
L11:    CJNE R5,#'S',L12 ; STOP
        LJMP S12
L12:    CJNE R5,#'X',L13 ; COUNTER
        LJMP S13
L13:    CJNE R5,#'Y',L14 ; COUNTER_READ
        LJMP S14
L14:    RETI
S1:
        SETB   P2.5          ;  a=0
        SETB  P2.6           ;  b=0
        SETB  P2.7           ;  c=0
        RETI

S2:
        CLR   P2.5           ;  a=1
        SETB  P2.6           ;  b=0
        SETB  P2.7           ;  c=0
        RETI

S3:
        SETB   P2.5          ;  a=0
        CLR    P2.6          ;  b=1
        SETB   P2.7          ;  c=0
        RETI

S4:
        CLR   P2.5           ;  a=1
        CLR   P2.6           ;  b=1
        SETB  P2.7           ;  c=0

        RETI

S5:     SETB  P2.5           ;  a=0
        SETB  P2.6           ;  b=0
        CLR   P2.7           ;  c=1

        SETB P2.0
        RETI

S6:     CLR    P2.5          ;  a=1
        SETB   P2.6          ;  b=0
        CLR    P2.7          ;  c=1

        RETI

S7:   SETB    P2.5 ;  a=0
        CLR    P2.6          ;  b=1
```

```
        CLR    P2.7         ;  c=1
        RETI

S8:     CLR    P2.5         ;  a=1
        CLR    P2.6         ;  b=1
        CLR    P2.7         ;  c=1

        RETI

S9:     MOV FLAGE,#00H
        SETB FLAGE4
        RETI

S10:    CLR P2.2
        RETI


S11:    MOV FLAGE,#00H
        SETB FLAGE_LEVEL
        RETI

S12:    MOV FLAGE,#00H
        RETI

S13:    MOV FLAGE,#00H
        SETB FLAGE_COUNT
        RETI

S14:    MOV FLAGE,#00H
        SETB FLAGE_COUNT_READ
        RETI
READ_ADC0:
        SETB   P2.5         ;  a=0
        SETB  P2.6          ;  b=0
        SETB  P2.7          ;  c=0

        CLR P2.4            ;  soc=0
        SETB P2.4           ;  soc=1
        NOP
        NOP
        CLR P2.4            ;  soc=0

READ_AGAIN:
        JNB  P2.3,READ_AGAIN ;    scan eoc
        MOV A,P0            ;  a=converted data
        RET


READ_ADC1:
        CLR   P2.5          ;  a=1
        SETB  P2.6          ;  b=0
        SETB  P2.7          ;  c=0
```

```
        CLR P2.4            ;  soc=0
        SETB P2.4           ;  soc=1
        NOP
        NOP
        CLR P2.4            ;  soc=0

READ_AGAIN1:

        JNB  P2.3,READ_AGAIN1 ;          scan eoc
        MOV A,P0            ;  a=converted data
        RET


READ_ADC2:
        SETB   P2.5         ;  a=0
        CLR    P2.6         ;  b=1
        SETB   P2.7         ;  c=0

        CLR P2.4                    ;  soc=0
        SETB P2.4           ;  soc=1
        NOP
        NOP
        CLR P2.4                    ;  soc=0

READ_AGAIN2:
        JNB  P2.3 , READ_AGAIN2 ;        scan eoc
        MOV A,P0                    ;  a=converted data
        RET


READ_ADC3:
        CLR   P2.5          ;  a=1
        CLR   P2.6          ;  b=1
        SETB  P2.7          ;  c=0

        CLR P2.4                    ;  soc=0
        SETB P2.4           ;  soc=1
        NOP
        NOP
        CLR P2.4                    ;  soc=0

READ_AGAIN3:

        JNB  P2.3 , READ_AGAIN3 ;        scan eoc
        MOV A,P0                    ;  a=converted data
        RET



READ_ADC4:
        SETB  P2.5          ;  a=0
        SETB  P2.6          ;  b=0
        CLR   P2.7          ;  c=1
```

```
        CLR P2.4                ;  soc=0
        SETB P2.4        ;  soc=1
        NOP
        NOP
        CLR P2.4                ;  soc=0

READ_AGAIN4:
        JNB  P2.3,READ_AGAIN4 ;         scan eoc
        MOV A,P0                ;  a=converted data
        RET


READ_ADC5:
        CLR    P2.5      ;  a=1
        SETB   P2.6      ;  b=0
        CLR    P2.7      ;  c=1

        CLR P2.4                ;  soc=0
        SETB P2.4        ;  soc=1
        NOP
        NOP
        CLR P2.4                ;  soc=0

READ_AGAIN5:

        JNB  P2.3,READ_AGAIN5 ;         scan eoc
        MOV A,P0                        ;  a=converted data
        RET

DELAY:
                MOV     R7,#0FFH
DLAYX:          MOV     R6,#0B0H
DLAYXY:                 DJNZ    R6,DLAYXY
                DJNZ    R7,DLAYX
                RET

DELAY1:
                MOV     R7,#020H
DLAYX1:                 MOV     R6,#040H
DLAYXY1:        DJNZ    R6,DLAYXY1
                DJNZ    R7,DLAYX1
                RET

END
```

MATLAB PROGRAM

```
% program of calculation of scintillation index for weak and strong
turbulance using
% Rytov varience ( coherent beam )
%------------------------------------------------------------------------------
clc;
Cn=(10^-12);                    %refractive index parameter for moderate
fluctuations
k1=((1.550)*(10^(-6)));
K=(2*pi)/ k1;                        %wave number
W=0.011;                             %1.25*0.0254   %beam width in meter
aaa=[];
bbb=[];
ccc=[];
ddd=[];
for L=0:10:1000
F=(2*L)/(K*(W*W));                   %Fresnel Ratio at the input plane
F1=F/(1+F^2);                        %Fresnel Ratio at the output plane
C1=1/(1+F^2);                        %Beam Curvature parameter at output
plane
V=1.23*Cn*(K^(7/6))* (L^(11/6));      %Rytov vzriance
V1=sqrt(V);
aaa=[aaa V];
%------------------------------------------------------------------------------
I=((1+(2*C1))^2+(4*(F1^2)));         %Calculation of scintillation index for
i=0 and L=inf (Weak Turbulance)
I1=0.40 *(I^(5/12));
I6=(1+(2*C1))/(2*F1);
I7=atan(I6);
X=((5/6)* I7);
I2=cos(X);
I8=(F1^(5/6));
I3=((11/16)* I8);
I5= 3.86* V*(I1*I2-I3);
I51=sqrt(I5);
bbb=[bbb I5];
%------------------------------------------------------------------------------

I10=0.49*I5;                        %Calculation of scintillation index for
strong Turbulance
B=I51^(12/5);
B1=(1+C1)*B;
B2=0.56*B1;
B3=1+B2;
B4=I10/(B3^(7/6));
I11=0.51*I5;
B5=0.69*B;
B6=(1+B5);
B61=B6^(5/6);
B7=I11/B61;
B8=B4+B7;
B9=exp(B8);
B10=B9-1;
ccc=[ccc B10]
ddd=[ddd L]
```

```
end;
%----------------------------------------------------------------------------

figure(2);
%plot(aaa,ccc,'-*b');
plot(ddd,ccc,'-*b');
%xlabel('Rytov variance')
xlabel('Distance')
ylabel('Scintillation Index')
title('Medium to strong turbulance')
h=legend('Wavelength=1.55um, Cn=10^-13')
%h=legend('Cn=10^-12')
hold on;
grid on;
%----------------------------------------------------------------------------
%****************************************************************************
```

Observation

Room Temperature -: 28^0 C : Distance :-16 meter without Diffuser and Using reflectors

Time	Detector Output Voltage	Frame Number
1:10 PM	6.5V	Frame1
1:15 PM	7.0V	Frame2
1:20 PM	6.0V	Frame3
1:25 PM	4.5V	Frame4
1:30 PM	3V	Frame5

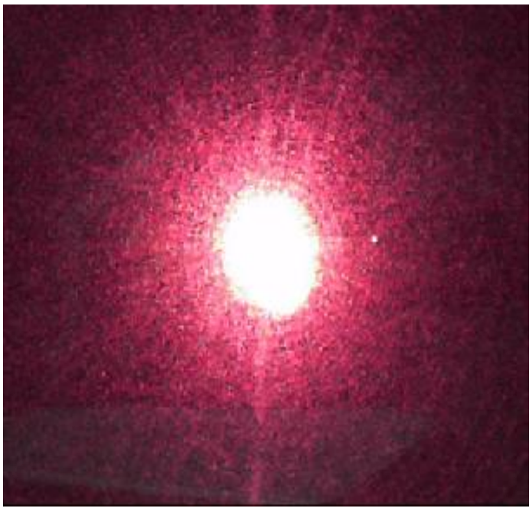

Frame1

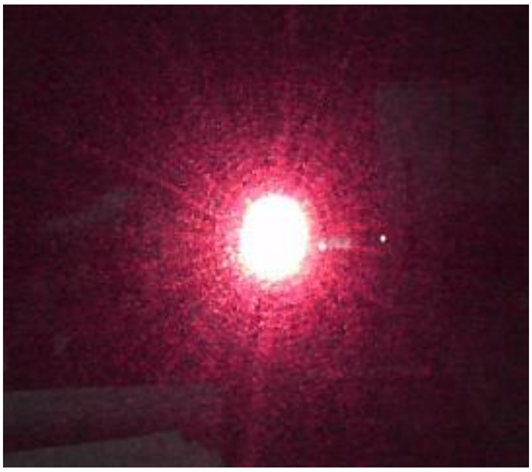

Frame2

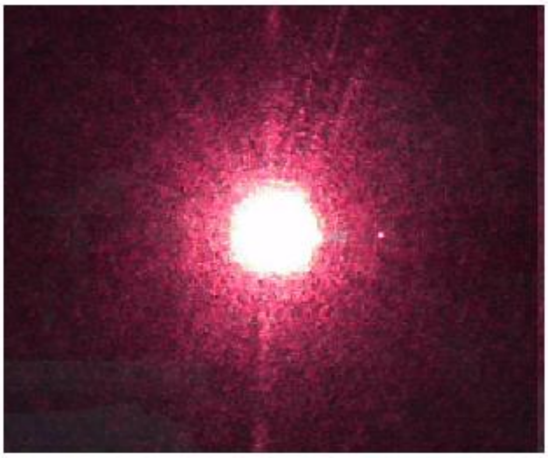

Frame3

Frame4

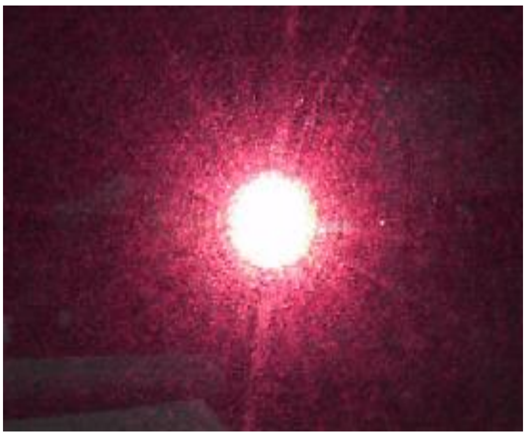

Frame5

Observation

Room Temperature -: 32^0 C : Distance :- 16 meter without Diffuser and Using reflectors

Time	Detector Output Voltage	Frame Number
2:15 PM	3.50V	Frame1
2:20 PM	3.40V	Frame2
2:25 PM	3.60V	Frame3
2:30 PM	4.00V	Frame4
2:35 PM	3.50V	Frame5

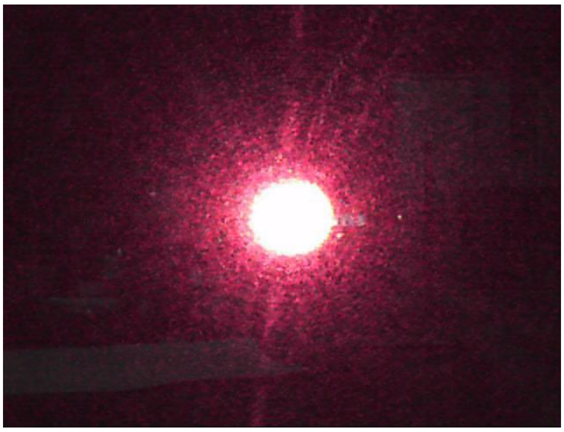

Frame1

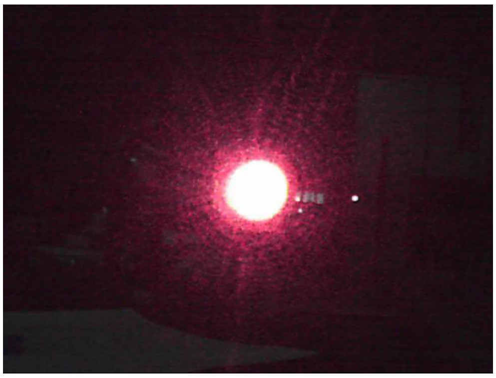

Frame2

Frame3

Frame4

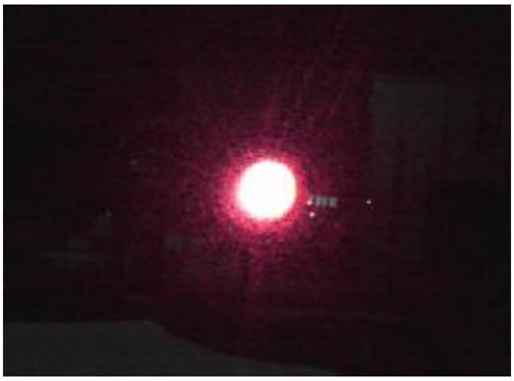

Frame5

APPENDIX A4

Photographic Images of: Beam Profiles of 698nm (Red) Laser Diode ,The laser Driver Circuit, The Laser Transmitter and Aperture Lens Holder

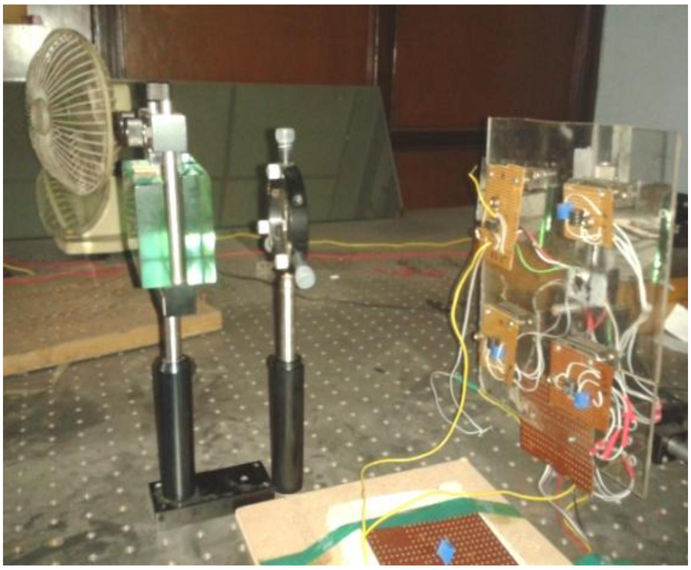
Phtoto Detector with Attenuator

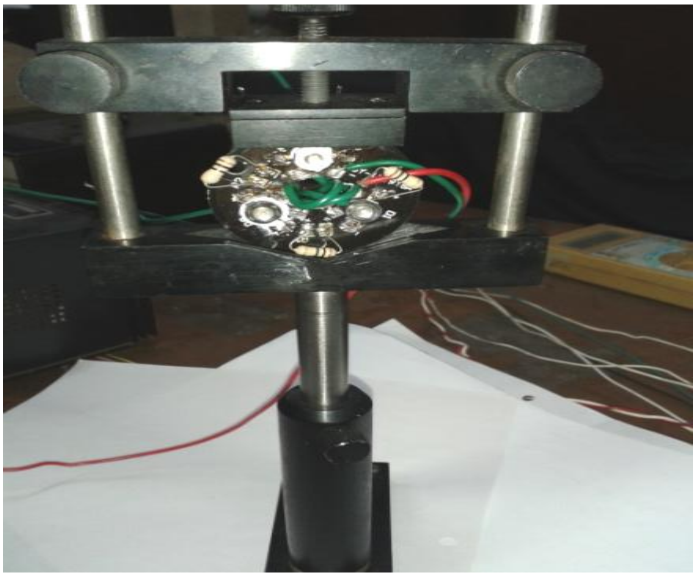

LED Transmitter

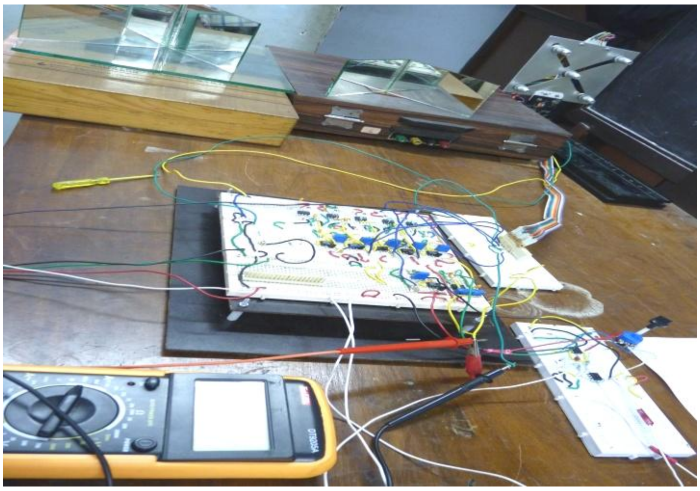
Laser Driver Circuit

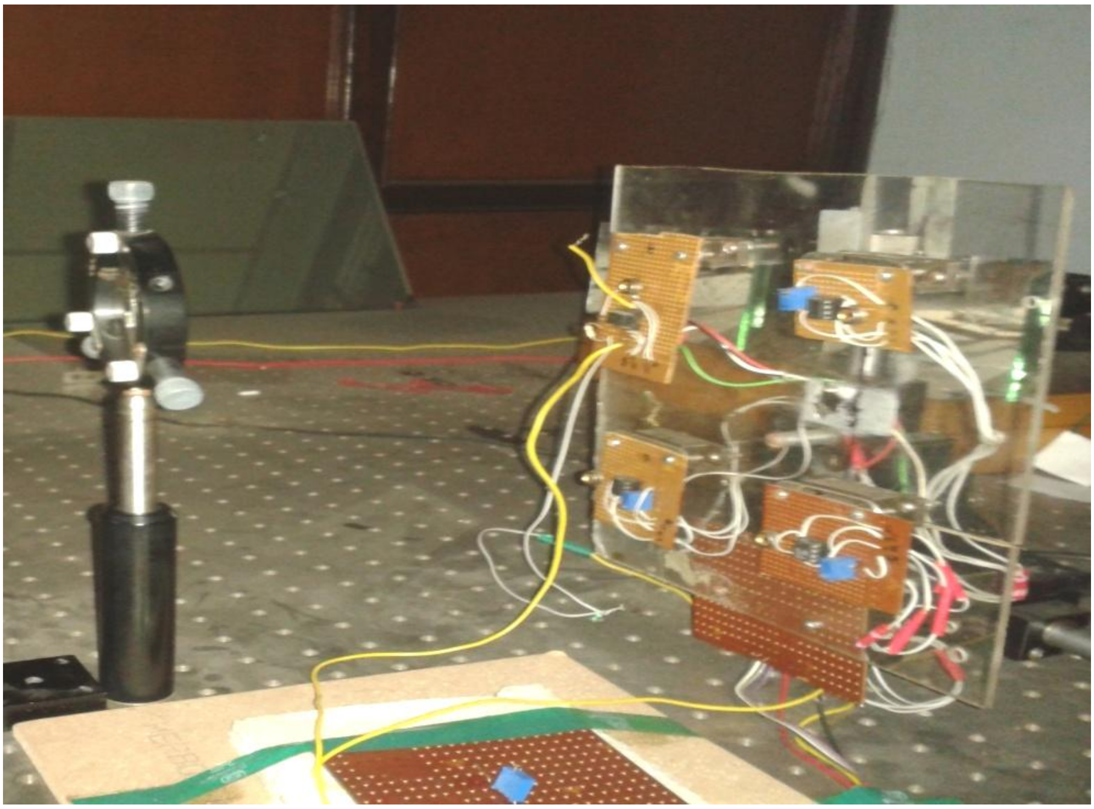

Multiphotodiode Detector

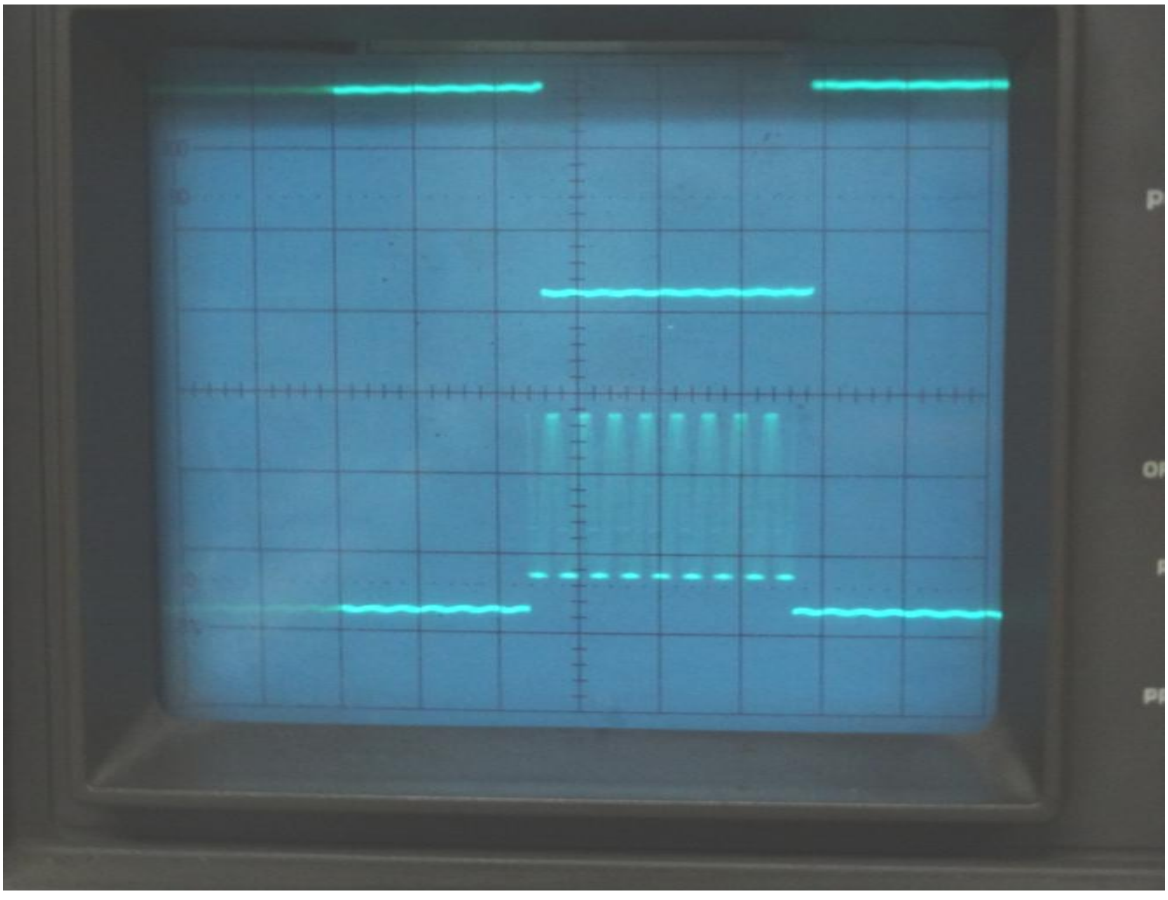

ASK Signal

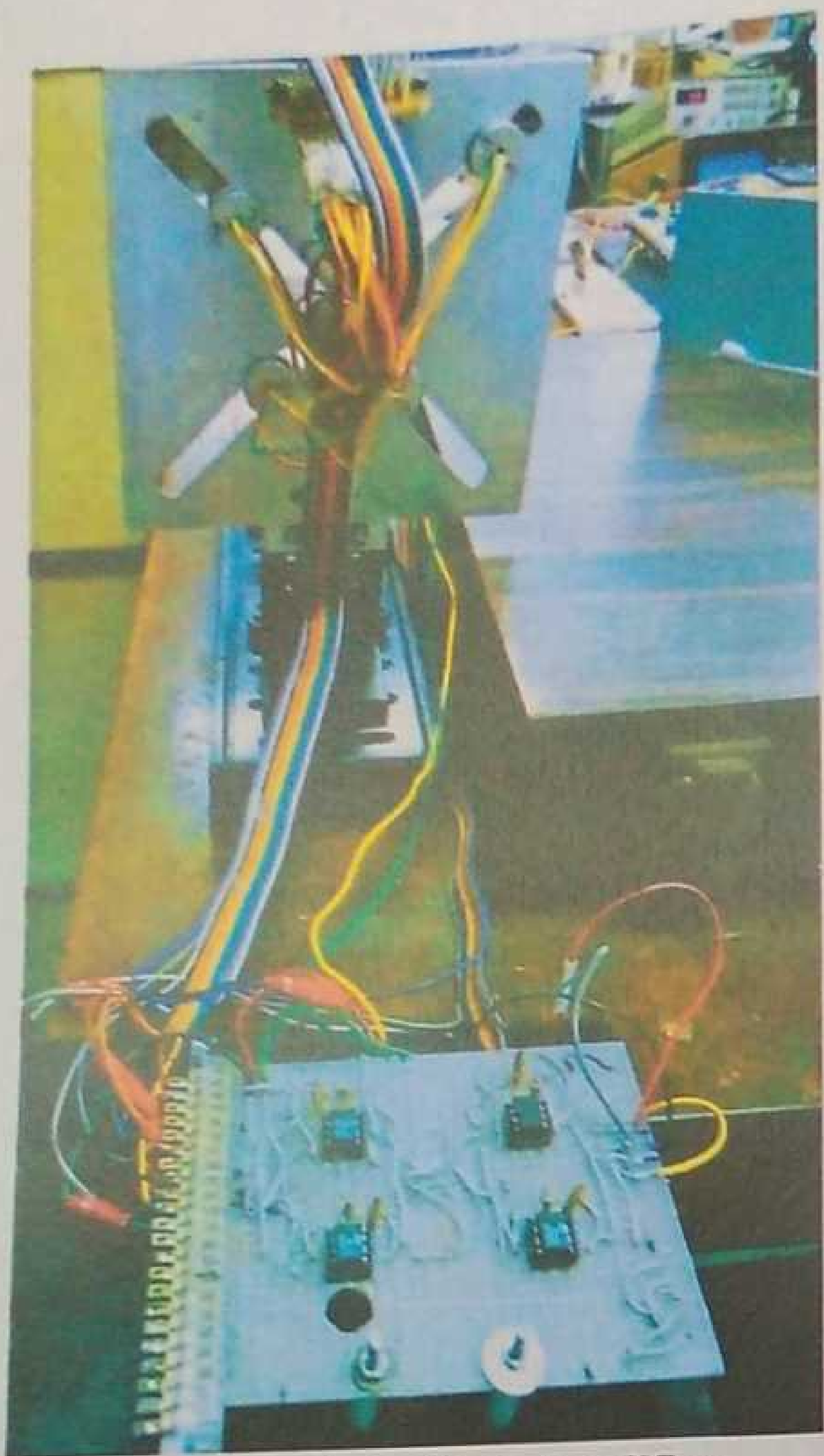

Feedback Photo diode Amplifier

Asim Kar. 15/09/2022

Professor
Electronics & Tele-communication
Engineering Department
Jadavpur University
Kolkata-700 032

Lens Holder

S. M. Kale